Aus dem Adolf-Butenandt-Institut
Lehrstuhl für Stoffwechselbiochemie im Biomedizinischen Centrum der
Ludwig-Maximilians-Universität München
Vorstand: Prof. Dr. rer. nat. Dr. h.c. Christian Haass

Lysosomal dysfunction and microglial hyperactivation in models of progranulin deficiency

Dissertation
zum Erwerb des Doktorgrades der Naturwissenschaften
an der Medizinischen Fakultät der
Ludwig-Maximilians-Universität zu München

vorgelegt von
Anika Reifschneider
aus
Neuss

2022

Mit Genehmigung der Medizinischen Fakultät
der Universität München

Betreuer: Prof. Dr. rer. nat. Dr. h.c. Christian Haass

Zweitgutachterin: Prof. Dr. rer. nat. Magdalena Götz

Dekan: Prof. Dr. med. Thomas Gudermann

Tag der mündlichen Prüfung: 21. Februar 2023

I. Affidavit

LMU LUDWIG-MAXIMILIANS-UNIVERSITÄT MÜNCHEN	Dekanat Medizinische Fakultät Promotionsbüro	

Affidavit

Reifschneider, Anika
_____

Surname, first name

I hereby declare, that the submitted thesis entitled

Lysosomal dysfunction and microglial hyperactivation in models of progranulin deficiency

is my own work. I have only used the sources indicated and have not made unauthorised use of services of a third party. Where the work of others has been quoted or reproduced, the source is always given.

I further declare that the dissertation presented here has not been submitted in the same or similar form to any other institution for the purpose of obtaining an academic degree.

Munich, 25.02.2023
_____
Place, Date

Anika Reifschneider
_____
Signature doctoral candidate

Affidavit   Date: 17.07.2022

# II. Content

III. Abbreviations

AD	Alzheimer´s disease
ADAM10	A disintegrin and metalloproteinase domain-containing protein 10
ALS	Amyotrophic lateral sclerosis
APOE	Apolipoprotein E
Atg	Autophagy-related genes
ATP	Adenosine triphosphate
Aβ	Amyloid-beta
BMP	Bone morphogenetic protein
BNDF	Brain-derived neurotrophic factor
C	Complement component
Cat	Cathepsins
CD	Cluster of differentiation
CHMP2B	Charged multivesicular body protein 2B
CNS	Central nervous system
Cr9orf72	Chromose 9 open reading frame protein 72
CSFR1	Colony stimulation factor 1
CTF	C-terminal fragment
DAM	Disease-associated microglia
DAMPs	Danger-associated molecular patterns
DAP	Adaptor proteins DNAX activation protein
E	Embryonic day
EMP	Erythromyeloid progenitors
ER	Endoplasmatic reticulum
FTLD	Frontotemporal lobar degeneration
FUS	Fused in sarcoma
GCase	Glucocerebrosidase
GRN	Human progranulin gene
Grn	Mus musculus progranulin gene
GWAS	Genome-wide association studies
IL	Interleukin
ITAMs	Immunoreceptor tyrosine-based activation motifs
LAMP	Lysosomal associated membrane protein
LOAD	Late onset AD
LOF	Loss-of-function
LPS	Lipopolysaccharide
M6PR	Mannose 6-phosphate receptor
MAPT	Microtubule-associated protein tau
MGnD	Microglia of neurodegenerative phenotype
mtDNA	Mitochondrial DNA
NCL	Neuronal ceroid lipofuscinoses
NHD	Nasu-Hakola disease
NT-3	Neurotrophins like neutrophin-3

PAMPs	Pathogen-associated patterns
PCD	Programmed cell death
PD	Parkinson´s disease
PET	Positron emission-tomography
PGRN	Progranulin protein
PLCɣ	Phospholipase Cɣ
PR	Dipeptide repeat protein
PRRs	Pattern recognition receptors
PSAP	Prosaposin
SIRP	Signal regulatory protein
SNPs	Single-nucleotide polymorphisms
sTREM2	Soluble triggering receptor expressed on myeloid cells 2
Syk	Spleen tyrosine kinase
TDP-42	TAR DNA-binding protein-43
TGF-β	Transforming growth factor-β
TLRs	Toll-like receptors
TM	Transmembrane
TMEM106B	Transmembrane protein 106B
TNF	Tumor necrosis factor
TREM2	Human triggering receptor expressed on myeloid cells 2 gene
Trem2	Mus musculus triggering receptor expressed on myeloid cells 2 gene
TREM2	Triggering receptor expressed on myeloid cells 2 protein
TSPO	18-kDa translocator protein
UPS	Ubiquitin-proteasome system
VAV	Proto-oncogene vav
VCP	Valosin-containing protein

IV. Abstract

In my thesis I focused on the pivotal role of microglia in neurodegenerative disease, their different activation stages upon progranulin (PGRN) or triggering receptor expressed on myeloid cells 2 (TREM2) deficiency and the connection between lysosomal deficiency and microglial hyperactivation. Microglia majorly contribute to the progression and pathology of neurodegenerative disorders like Alzheimer`s disease (AD) and frontotemporal lobal degeneration (FTLD) and additionally recent advances of genome wide association studies (GWAS) have identified genetic association, as rare variants of genes that are predominantly expressed by microglia increase the risk of developing neurodegenerative disease. Among these risk genes are progranulin (*GRN*) and the triggering receptor expressed on myeloid cells 2 (*TREM2*). While the heterozygous loss of PGRN leads to FTLD, the complete loss of PGRN results in the lysosomal storage disease neuronal ceroid lipofuscinosis, indicating a major role of PGRN in lysosomal protein degradation in the brain. Our laboratory has previously shown, that progranulin knockout mice (*Grn*$^{-/-}$) and *GRN*-associated FTLD patients exhibit increased levels of the lysosomal protein cathepsin (Cat) D, however the exact role of PGRN in lysosomal protein degradation remained unclear. In a collaborative effort with Julia K. Götzl, Alessio-Vittorio Colombo and Kathrin Fellerer, I therefore analyzed microglia and other brain cells regarding changes in expression, maturation and enzymatic activity of lysosomal proteins like Cat D, B and L. We found a striking age-depended increase of lysosomal proteases associated with increased enzymatic activity. Interestingly, we demonstrated that microglia show early lysosomal deficits, even before enhanced Cat transcription levels were observed. Our laboratory has previously shown, that PGRN loss of function (LOF) leads to hyperactivated microglia that exhibit increased phagocytosis, proliferation and migration. The opposite microglial phenotype is found in TREM2 LOF models, where microglia appear to be locked in a homeostatic state, unable to react to pathological insults. In addition to the lysosomal dysfunction discussed above, PGRN LOF microglia also increase TREM2 expression. To test the hypothesis that hyperactivation of microglia in PGRN LOF is TREM2-dependent and that microglia can reversibly switch between activation stages, I used genetic and pharmacological TREM2 antagonistic approaches to prevent the transition of homeostatic microglia to a disease-associated microglia (DAM) state. To further investigate the microglial contribution to disease pathology in PGRN LOF models, I generated *Grn* x *Trem*2 double knockout mice to analyze the expression of DAM genes, lysosomal dysfunction, glucose uptake, lipid metabolism and microglia morphology and activation status. Here, I found that ablating TREM2 in PGRN LOF mice reduces the expression of DAM genes, suggesting that suppression of TREM2 can lower microglia hyperactivation and is likely to be upstream PGRN-mediated microglial transcriptional changes. To further explore whether pharmacological modulation of TREM2 has beneficial functions on microglia states, I used antibodies antagonistic for TREM2, developed at Denali Therapeutics, to treat macrophages isolated from *GRN*-FTLD patients. Treatment of the cells with these antibodies resulted in reduced TREM2 signaling, due to its

enhanced shedding. To confirm these findings, I collaborated with Sophie Robinson, who generated PGRN-deficient microglia derived from human-induced pluripotent stem cells (iPSC). Treatment of these cells with antagonistic TREM2 antibodies resulted in reduced microglia hyperactivation, TREM2 signaling and phagocytic activity. However, we did not observe any effects on lysosomal dysfunction in PGRN deficient iPSC after antibody treatment. In line with this, *Grn* x *Trem*2 double knockout mice not only failed to rescue effects on lysosomal dysfunction, lipid metabolism and microglia morphology, but also further increased synaptic loss and neurofilament light-chain (Nfl) levels, a marker of neuronal damage in the brain. My results suggest that with PGRN deficiency, lysosomal dysfunction is upstream to the microglia hyperactivation. In addition, these findings imply a protective role of TREM2-dependent chronic activation of microglia and show the dynamic nature of microglia kinetics and their ability to reversibly switch between activation stages.
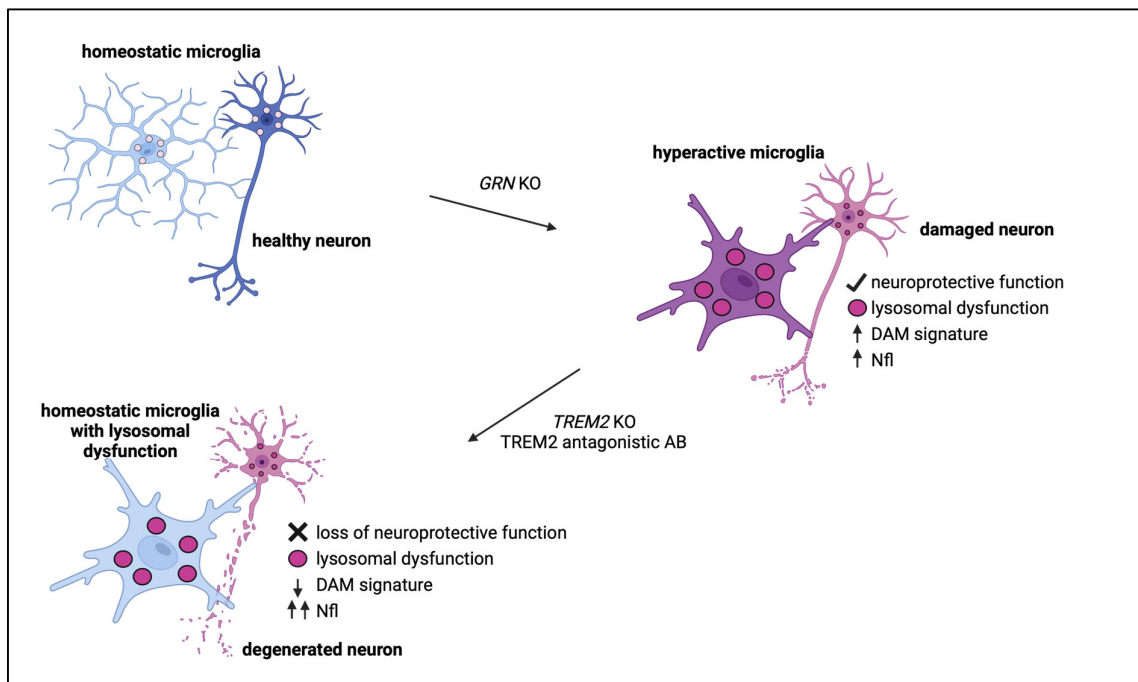

Schematic summary of my thesis findings: PGRN deficiency (*GRN* KO) in the brain leads to lysosomal impairment in microglia, enhanced lysosomal activity in neurons, increased expression of the DAM signature and increased levels of Nfl in the CSF of mice. The genetic (*TREM2* KO) or pharmacological (TREM2 antagonistic AB) inhibition of TREM2 can prevent the transition of microglia to this hyperactivated stage, but does not rescue lysosomal dysfunction. Modified from Reifschneider et al. 2022.

V. Zusammenfassung

In meiner Dissertation konzentrierte ich mich auf die zentrale Rolle der Mikroglia bei neurodegenerativen Erkrankungen, ihre verschiedenen Aktivierungsstadien bei Progranulin (PGRN) oder dem auf myeloischen Zellen exprimierten Triggering Receptor 2 (TREM2) Defizienz und dem Zusammenhang zwischen lysosomaler Dysfunktion und Hyperaktivierung der Mikroglia. Mikroglia tragen wesentlich zur Progression und Pathologie neurodegenerativer Erkrankungen wie der Alzheimer-Krankheit (AD) und der frontotemporalen lobalen Degeneration (FTLD) bei. Darüber hinaus haben jüngste Fortschritte bei genomweiten Assoziationsstudien (GWAS) eine genetische Assoziation aufgezeigt, da seltene Varianten von Genen, die im Gehirn vorwiegend von Mikroglia exprimiert werden, das Risiko der Entwicklung neurodegenerativer Erkrankungen erhöhen. Zu diesen Risikogenen gehören Progranulin (*GRN*) und der Triggering Receptor Expressed in Myeloid Cells 2 (*TREM2*). Während der heterozygote Verlust von PGRN zu FTLD führt, hat der vollständige Verlust von PGRN die lysosomale Speicherkrankheit neuronale Ceroid-Lipofuszinose zur Folge, was auf eine wichtige Rolle von PGRN beim lysosomalen Proteinabbau im Gehirn hinweist. Unser Labor hat zuvor gezeigt, dass Progranulin knockout Mäuse (*Grn$^{-/-}$*) und *GRN*-assoziierte FTLD-Patienten erhöhte Spiegel des lysosomalen Proteins Cathepsin (Cat) D aufweisen, die genaue Rolle von PGRN beim lysosomalen Proteinabbau blieb jedoch unklar. In Zusammenarbeit mit Julia K. Götzl, Alessio-Vittorio Colombo und Kathrin Fellerer untersuchte ich daher Mikroglia und andere Hirnzellen im Hinblick auf Veränderungen in der Expression, Reifung und enzymatischen Aktivität von lysosomalen Proteinen wie Cat D, B und L. Wir fanden einen auffälligen altersabhängigen Anstieg lysosomaler Proteasen, der mit einer erhöhten enzymatischen Aktivität einherging. Interessanterweise konnten wir zeigen, dass Mikroglia schon früh lysosomale Defizite aufweisen, noch bevor erhöhte Cat-Transkriptionswerte beobachtet wurden. Unser Labor hat zuvor gezeigt, dass ein Funktionsverlust von PGRN (LOF) zu hyperaktivierten Mikroglia führt, die eine erhöhte Phagozytose, Proliferation und Migration aufweisen. In TREM2 LOF-Modellen wurde der gegenteilige mikrogliale Phänotyp identifiziert: Mikroglia, die in einem homöostatischen Zustand gefangen zu sein scheinen, unfähig, auf pathologische Insulte zu reagieren. Zusätzlich zu der lysosomalen Dysfunktion weisen PGRN LOF-Mikroglia auch eine erhöhte TREM2-Expression auf. Um zu verstehen, ob die Hyperaktivierung von Mikroglia bei PGRN LOF TREM2-abhängig ist und ob Mikroglia reversibel zwischen Aktivierungsstadien wechseln können, habe ich genetische und pharmakologische TREM2-Antagonisten eingesetzt, um den Übergang von homöostatischen Mikroglia in einen krankheits-assoziierten (DAM) Zustand zu verhindern. Um den Beitrag der Mikroglia zur Krankheitspathologie in PGRN LOF-Modellen besser zu verstehen, habe ich *Grn* x *Trem2* Doppelknockout Mäuse generiert, um die Expression von DAM-Genen, die lysosomale Dysfunktion, die Glukoseaufnahme, den Lipidstoffwechsel sowie die Morphologie und den Aktivierungsstatus der Mikroglia zu analysieren. Ich konnte damit zeigen, dass die Ablation von TREM2 in PGRN LOF-Mäusen

die Expression von DAM-Genen reduziert, was darauf hindeutet, dass die Unterdrückung von TREM2 die Hyperaktivierung von Mikroglia verringern kann. Um weiter zu untersuchen, ob die pharmakologische Modulation von TREM2 positive Auswirkungen auf den Zustand der Mikroglia hat, verwendete ich antagonistische TREM2-Antikörper (entwickelt von Denali Therapeutics) um Makrophagen, isoliert aus *GRN*-FTLD-Patienten, zu behandeln. Die Behandlung der Zellen mit diesen Antikörpern führte zu einer verringerten TREM2-Signalisierung, die auf die verstärkte Spaltung von TREM2 zurückzuführen ist. Um diese Ergebnisse zu bestätigen, arbeitete ich mit Sophie Robinson zusammen, die PGRN-defiziente Mikroglia aus menschlichen induzierten pluripotenten Stammzellen (iPSC) erzeugte. Die Behandlung dieser Zellen mit antagonistischen TREM2-Antikörpern führte zu einer verringerten Hyperaktivierung der Mikroglia, TREM2-Signalisierung und phagozytischen Aktivität. Wir konnten jedoch keine Auswirkungen auf die lysosomale Dysfunktion in PGRN-defizienten iPSC nach der Behandlung mit Antikörpern beobachten. In Übereinstimmung damit zeigten auch *Grn* x *Trem2* Doppelknockout Mäuse keinen rettenden Effekt auf die lysosomale Dysfunktion, den Lipidstoffwechsel und die Morphologie der Mikroglia. Die Werte der Neurofilament-Leichtkette (Nfl) und der synaptische Verlust waren sogar erhöht. Meine Ergebnisse deuten darauf hin, dass bei PGRN-Mangel die lysosomale Dysfunktion primär für die Hyperaktivierung der Mikroglia verantwortlich sein könnte. Darüber hinaus weisen diese Daten auf eine schützende Rolle der TREM2-abhängigen chronischen Aktivierung von Mikroglia hin und zeigen die dynamische Natur der Mikroglia-Kinetik und ihre Fähigkeit, reversibel zwischen den Aktivierungsstufen zu wechseln.
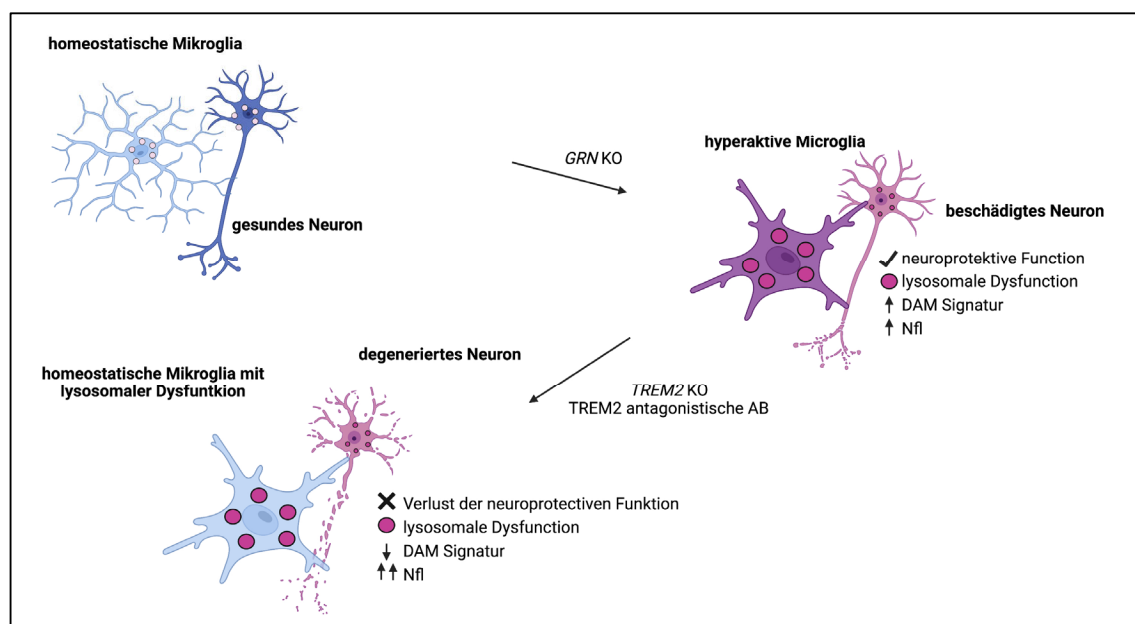
Schematische Zusammenfassung meiner Doktorarbeit: Progranulin-Verlust (*GRN* KO) im Gehirn führt zu einer Beeinträchtigung der lysosomalen Aktivität in Mikroglia, zu einer verstärkten lysosomalen Aktivität in Neuronen, zu einer erhöhten Expression der krankheitsassoziierten Mikroglia-Signatur (DAM) und zu erhöhten Werten der Neurofilament-Leichtkette (Nfl) in der Cerebrospinalflüssigkeit (CSF) von Mäusen. Die genetische (*TREM2* KO) oder pharmakologische (TREM2 antagonistische AB) Hemmung von TREM2 kann den Übergang der Mikroglia in dieses hyperaktivierte Stadium verhindern, aber die lysosomale Dysfunktion nicht retten. Modifiziert aus Reifschneider et al. 2022.

VI. Publications

1. Publications of this thesis

Early lysosomal maturation deficits in microglia triggers enhanced lysosomal activity in other brain cells of progranulin knockout mice

Julia K. Götzl*, Alessio-Vittorio Colombo*, Katrin Fellerer*, **Anika Reifschneider**, Georg Werner, Sabina Tahirovoc, Christian Haass and Anja Capell

* Contributed equally

Loss of TREM2 rescues hyperactivation of microglia, but not lysosomal deficits and neurotoxicity in models of progranulin deficiency

Anika Reifschneider, Sophie Robinson, Bettina van Lengerich, Johannes Gnörich, Todd Logan, Steffanie Heindl, Miriam A Vogt, Endy Weidinger, Lina Riedl, Karin Wind, Artem Zatcepin, Ida Pesämaa, Sophie Haberl, Brigitte Nuscher, Gernot Kleinberger, Julien Klimmt, Julia K. Götzl, Arthur Liesz, Katharina Bürger, Matthias Brendel, Johannes Levin, Janine Diehl-Schmid, Jung Suh, Gilbert Di Paolo, Joseph W Lewcock, Kathryn M Monroe, Dominik Paquet, Anja Capell and Christian Haass

2. Additional publications

The wide genetic landscape of clinical frontotemporal dementia: systematic combined sequencing of 121 consecutive subjects

Corbelis Blauwendraat, Carlo Wilke, Javier Simón-Sanchez, Iris E Jansen, **Anika Reifschneider**, Anja Capell, Christian Haass, Melissa Castillo-Lizardo, Saskia Biskup, Walter Maetzler, Patrizia Rizzu, Peter Heutnik, and Matthis Synofzik

Opposite microglial activation stages upon loss of PGRN or TREM2 result in reduced cerebral glucose metabolism

Julia K. Götzl*, Matthias Brendel*, Georg Werner*, Samira Parhizkar, Laura Sebastian Monasor, Gernot, Kleinberger, Alessio-Vittorio Colombo, Maximilian Deussing, Matias Wagner, Juliane Winkelmann, Janine Diehl-Schmid, Johannes Levin, Katrin Fellerer, **Anika Reifschneider**, Sebastian Bultmann, Peter Bartenstein, Axel Rominger, Sabina Tahirovic, Scott T Smith, Charlotte Madore, Oleg Butovsky, Anja Capell and Christian Haass

* Contributed equally

VII. Introduction

1. Microglia are highly dynamic immune cells of the brain

Microglia, the resident immune cells of the brain, first described in 1919 by del Rio Hortega, constantly surveille the brain and can react within seconds to minutes after brain injuries or inflammatory stimuli (Davalos et al. 2005; Kreutzberg 1996; Rio-Hortega 1919). While in the past microglia activation stages were divided into the proinflammatory M1 stage and the immunosuppressive M2 stage (Tang and Le 2016), the last years of research revealed the highly dynamic nature of microglia and their important function in the molecular and functional regulation of brain homeostasis throughout the lifespan of healthy and diseased individuals (Gosselin et al. 2014; Hammond et al. 2019; Leyns and Holtzman 2017; Madore et al. 2020). One of the attempts to classify this heterogenous population of cells was to describe them by their morphological differences: ramified, with lots of thin, highly branched processes, or amoeboid-like, roundish with few processes. In their role of being the immune cells of the brain, microglia not only constantly surveil the brain parenchyma but also make active contact with synapses (Tremblay, Lowery, and Majewska 2010). To do so, microglia are able to extend and retract their processes within seconds to minutes (Davalos et al. 2005). Although microglia develop from a single-cell type lineage, they diverge into heterogenous populations with different functions. The local environment defines their functionality e.g., by region or damage specific interactions with other cell types like neurons or astrocytes through cell signaling molecules such as chemokines and cytokines. Microglia are equipped with a number of specific cell surface markers to react to these extracellular stimuli (Lynch 2009). In addition they secrete soluble immunomodulatory factors including cytokines, chemokines and complement factors by themselves to communicate with other cells (Lynch 2009).

1.1 Microglia dynamics during development

Although the origin of microglia was in the center of discussion for years, it is now widely accepted that they originate from tissue-resident macrophages in the yolk sac (Ginhoux et al. 2010; Perdiguero et al. 2015; Schulz et al. 2012). These cells derive from $CD45^+cKit^+$ erythromyeloid progenitors (EMPs) that colonize the fetal liver (in mice starting at embryonic day (E)8.5) and mature into CX_3CR1^+ microglia progenitors (Fig. 1). Starting at day E9.5 to E10 before the blood-brain-barrier is formed (E13.5 to E14.5), these progenitor cells migrate into the brain, where they proliferate locally and distribute within the central nervous system (CNS) (Ajami et al. 2007; Bruttger et al. 2015). During the whole lifespan, these progenitor cells are the only source of myeloid cells in the healthy brain (Hashimoto et al. 2013; Sheng, Ruedl, and Karjalainen 2015). Although for a long time, it was not clear how one cell type can adapt the necessary diversity to fulfill the needs throughout the whole lifespan, it is now certain that microglia development follows a stepwise program aligned with the requirements in the developing and adult brain (Matcovitch-Natan et al. 2016). Interestingly, it was shown that each

stage of microglia development is characterized by the differential expression of a large number of genes that are associated with different stimuli and functions (Matcovitch-Natan et al. 2016). Global transcriptional analysis of mouse microglia revealed that this stepwise program can be divided into three temporal stages, classified by specific markers and regulatory factors: early microglia (until E14), pre-microglia (from E14 to a few weeks after birth) and adult microglia (from a few weeks after birth onward) and in each stage microglia fulfill specific roles (Matcovitch-Natan et al. 2016). During the development of the CNS, neurons form far more synapses than ultimately required - the specific elimination program called synaptic pruning is therefore essential to remove unnecessary synapses and by that strengthen the remaining ones (Fig. 1) (Zuchero and Barres 2015). The complement cascade, including the complement component (C) 1q and C3, are essential players in the process of synaptic pruning (Schafer et al. 2012; Stevens et al. 2007). Low-activity synapses get complement-tagged and are thereby marked for the phagocytosis by microglia. When synaptic pruning is disrupted, brain maturation is affected and results in immature synapses and an excess of dendritic spines (Paolicelli et al. 2011). It is estimated that during the early postnatal stage half of all neural cells undergo programmed cell death (PCD), a critical step to form an intact landscape of the nervous system and to regulate proper cell numbers (Yeo and Gautier 2004). As it was observed that microglia not only appear in close proximity to apoptotic neurons but also follow the waves of neural expansion, it became quite evident that they play a key role in PCD (Dailey et al. 2013). Dying or damaged cells express so called "find-me" and "eat-me" signals that allow microglia to recognize them and to initiate phagocytosis (Sierra et al. 2013). Recognition of target cells can happen by the direct contact of microglial cell membrane receptors or in a soluble-manner by opsonins – soluble, extracellular proteins that link the microglia receptor to an "eat-me" signal (Cockram, Puigdellívol, and Brown 2019; Sierra et al. 2013).
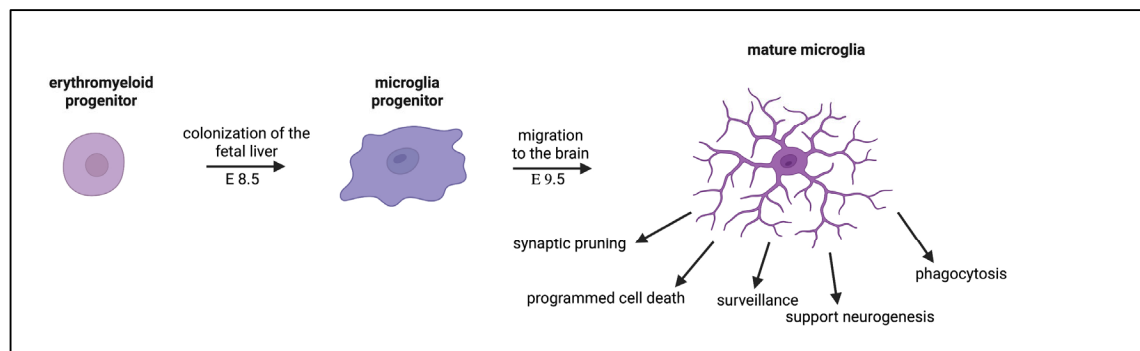

Figure 1. Microglia development and functions: Microglia develop from erythromyeloid progenitor cells into microglia progenitor cells before they colonize the brain and become mature microglia. During development and lifetime, they fulfill a variety of functions including synaptic pruning, supporting neurogenesis, and surveillance of the brain parenchyma.

1.2 Microglia dynamics during lifetime, aging and disease

The surface of microglia is equipped with several specialized pattern recognition receptors (PRRs), including different toll-like-receptors (TLRs) and corresponding co-receptors like

cluster of differentiation (CD) 36, CD14 or CD47. PRRs belong to the innate immune system and are able to sense and get activated by pathogen-associated molecular patterns (PAMPs) and danger-associated molecular patterns (DAMPs) and subsequently activate an immune response to protect the brain against pathogens (Fellner et al. 2013; Udan et al. 2008). PAMPs are conserved molecular patterns, usually associated to invading pathogens, and include lipopolysaccharide (LPS) or double-stranded RNA (Amarante-Mendes et al. 2018). DAMPs can be released by cells that undergo stress or damage and include a variety of different molecules like adenosine triphosphate (ATP) or mitochondrial DNA (mtDNA), but also different cytokines like IL-33 or IL-6 (Amarante-Mendes et al. 2018). In addition to their protective function against pathogens, microglia are also key players in cleaning up unwanted debris like misfolded proteins (Van Acker et al. 2021). Microglia are also affected from the aging process and show age-related morphological and functional effects. Processes from aged microglia lose their speed, leading to decreased surveillance, synaptic contact and reaction to pathological events (Damani et al. 2011; Hart et al. 2012; Hefendehl et al. 2014). The population of microglia during lifetime is sustained by a constant self-renewal mechanism, which is dependent on a transforming growth factor β (TGF-β) signature and involves colony stimulation factor 1 (CSFR1) signaling (Askew et al. 2017; Butovsky et al. 2014; Matcovitch-Natan et al. 2016). This intensive mechanism of coupled apoptosis and proliferation means that microglia undergo hundreds of renewal rounds, suggesting that they may also be negatively influenced and suffer from age-related effects, such as telomere length reductions (Van Acker et al. 2021). These effects may even be enhanced in neurological disorders, and subsequently it was shown that microglia from frontotemporal lobar degeneration (FTLD) and Alzheimer´s disease (AD) patients exhibit an increase of condensed nuclei, a sign for increased turnover and apoptosis (Lewandowska et al. 2004; Sakae et al. 2019). Aging is characterized by brain shrinkage and neuronal loss, while the expression of complement factors, inflammatory mediators and the number of activated microglia increases (Ball 1977; Conde and Streit 2006; Lu et al. 2004; Streit et al. 2008; Syková, Mazel, and Šimonová 1998). These activated microglia exhibit IL-1α expression, and especially enlarged and phagocytic subtypes were found to be increased in an age-dependent manner (Sheng, Mrak, and Griffin 1998).

2. Neurodegenerative disease

The activation of microglia plays a pivotal role in a number of different diseases affecting the CNS, including systemic septic inflammations (Trzeciak et al. 2019), brain tumors (Graeber, Scheithauer, and Kreutzberg 2002), lysosomal storage diseases (Götzl et al. 2018), neurological diseases such as multiple sclerosis (Guerrero and Sicotte 2020), traumatic brain injuries (Donat et al. 2017) and neurodegenerative diseases such as amyotrophic lateral sclerosis (ALS), AD, FTLD and Parkinson's disease (PD) (Kam et al. 2020; Madore et al. 2020; Muzio, Viotti, and Martino 2021). Although activation of the innate immune mechanism is

usually a beneficial effect, microgliosis, the chronic activation of microglia, can also be detrimental, and microglial neurotoxicity appears to be a key player in the development und progression of neurodegenerative disorders (Hickman, Allison, and El Khoury 2008; Lucin and Wyss-Coray 2009).

2.1 Frontotemporal lobar degeneration

The second most abundant form of presenile dementia is FTLD (Rabinovici and Miller 2010). FTLD can occur sporadically, though 40 to 50 % of the cases have a family history (Riedl et al. 2014) and 10 to 30 % of FTLD cases are due to autosomal dominant inheritance with mutations found in genes, encoding the microtubule-associated protein tau (MAPT), chromosome 9 open reading frame protein 72 (Cr9orf72), progranulin (PGRN), charged multivesicular body protein 2B (CHMP2B) and valosin-containing protein (VCP). Based on characteristic protein deposits, FTLD is divided in different pathological subtypes, namely FTLD-tau, FTLD-TDP-43, FTLD-UPS (ubiquitin proteasome system), FTLD-DPR (dipeptide repeat protein) and FTLD-FUS (fused in sarcoma) (Mackenzie, Rademakers, and Neumann 2010). The number of phagocytic and antigen-presenting microglia is increased in FTLD patients, and microglia dystrophy was shown to be even more severe (Woollacott et al. 2020). Several studies also imply, that microglia-mediated synaptic pruning might be enhanced in FTLD patients (Gitler and Tsuiji 2016; Lui et al. 2015). While C3 was found to be increased in the frontal cortex of FTLD patients, the signal regulatory protein (SIRP) and its receptor CD47, which negatively regulate phagocytosis, were reduced (Gitik et al. 2011). The pivotal role of microglia in FTLD also is highlighted by the identification of mutation in the progranulin (*GRN)* gene, leading to FTLD-TDP, as in the brain, PGRN is predominantly expressed by microglia (Götzl et al. 2018; Lui et al. 2015; Zhang et al. 2014).

2.1.1 Progranulin

PGRN is a multifunctional growth factor-like glycoprotein, which is predominantly found in hematopoietic cells and epithelial cells (Bateman and Bennett 1998). The protein can function in its full-length version, but also the proteolytically-derived granulin peptides may play opposite functional roles in various processes. PGRN/granulins have key regulatory functions in inflammatory processes and other cellular pathways, like insulin signaling, wound healing, cell proliferation and as a neurotrophic factor (Bhandari et al. 1996; Kleinberger et al. 2013; Matsubara et al. 2012). The majority of *GRN* mutation carriers exhibit PGRN haploinsufficiency caused by heterozygous nonsense mutations introducing premature termination codons leading to nonsense-mediated mRNA decay (Baker et al. 2006; Cruts et al. 2006). In addition, a number of missense mutations have been identified that reduce PGRN via delayed maturation or processing (Kleinberger et al. 2016; Shankaran et al. 2008; Wang et al. 2010). Although in other neurodegenerative disorders PGRN is usually seen to be increased (most

likely due to microgliosis), *GRN* mutations are reported to have a weak association in AD and PD cases (Brouwers et al. 2007; Kelley et al. 2010).

2.1.2 Lysosomal function of PGRN

The majority of PGRN is secreted, but a minor amount is also directly transported to lysosomes by the sortilin receptor or by forming a complex with prosaposin (PSAP) and subsequently taken up from the extracellular space, mediated by the sortilin receptor or the mannose 6-phosphate receptor (M6PR) and transported to lysosomes (Hu et al. 2010; Zhou et al. 2015) (Fig. 2). Secreted PGRN can be digested into single granulins by elastase. In lysosomes, PGRN is directly or indirectly involved in controlling the activity of different hydrolyses, like cathepsins (Cat), glucocerebrosidase (GCase) and HexA (Arrant et al. 2019; Beel et al. 2017; Butler et al. 2019; Chen et al. 2018; Götzl et al. 2016). It was shown, that PGRN can directly bind GCase and that PGRN deficiency leads to GCase aggregation (Jian et al. 2016), suggesting that one possibility of a direct involvement in the regulation of Cat D and GCase may be a chaperone-like function of PGRN (Beel et al. 2017; Butler et al. 2019; Zhou et al. 2017). Recently, it was shown that the lysosomal phospholipid bone morphogenetic protein (BMP) is stabilized by PGRN (Logan et al. 2021). BMP regulates the degradation of sphingolipids, a process in which GCase and HexA are also involved. In line with a lysosomal function, it was found that a complete loss of PGRN leads to the lysosomal storage disease neuronal ceroid lipofuscinosis (NCL) (Smith et al. 2012). Furthermore, a mouse model for NCL, the Cat D knockout mouse, displays increased levels of PGRN and the transmembrane protein 106B (TMEM106B) (Götzl et al. 2014), a lysosomal protein which has been identified as a genetic modifier for PGRN-associated FTLD (Brady et al. 2013; Lang et al. 2012; Volpicelli-daley et al. 2013). Recent studies surprisingly showed fibrils not made of TDP-43, as expected, but made out of a C-terminal fragment of the transmembrane protein TMEM106B in brains of FTLD-TDP patients (Chang et al. 2022; Jiang et al. 2022; Schweighauser et al. 2022). The same fibrils were also found in aged controls and many other neurogenerative disease (Chang et al. 2022; Jiang et al. 2022; Schweighauser et al. 2022). These studies raise a lot of new questions, for example, it is not clear yet, if these fibrils are directly causative for the disease, associates to the disease or exist without causing any harm. Answering these questions will open a new path of research on the relation between TMEM106B and FTLD. Interestingly, TMEM106B is predominantly located in late endosomes and lysosomes and was shown to be increased in models of PGRN deficiency (Götzl et al. 2014; Lang et al. 2012). This points towards the hypothesis that TMEM106B deposits could be an essential player in the lysosomal dysfunction in FTLD. In PGRN deficiency models, an accumulation of ubiquitin and p62 was observed, suggesting major deficits in the autophagy-lysosomal protein degradation pathway (Chang et al. 2017; Tanaka et al. 2014). PGRN knockout (*Grn*^{-/-}) mice also exhibit accumulation of other lysosomal proteins including lysosomal associated membrane protein (LAMP)1 and Cat D (Götzl et al. 2014, 2018). Moreover, these mice show elevated levels of phosphorylated

TDP-43 (Götzl et al. 2014), a pathological hallmark for FTLD-TDP (Neumann et al. 2006). Additionally, *GRN* gene expression is transcriptionally co-regulated with lysosomal genes (Belcastro et al. 2011). The fact that a complete loss of PGRN leads to the lysosomal storage disorder NCL and that *GRN*-associated FTLD-TDP and NCL share common pathological features supports lysosomal dysfunction as at least one cause for disease onset and progression (Götzl et al. 2016). Besides the apparent lysosomal dysfunction, models of *GRN*-FTLD-associated haploinsufficiency exhibit increased phagocytosis, chemotaxis and clustering around amyloid plaques (Götzl et al. 2018, 2019).
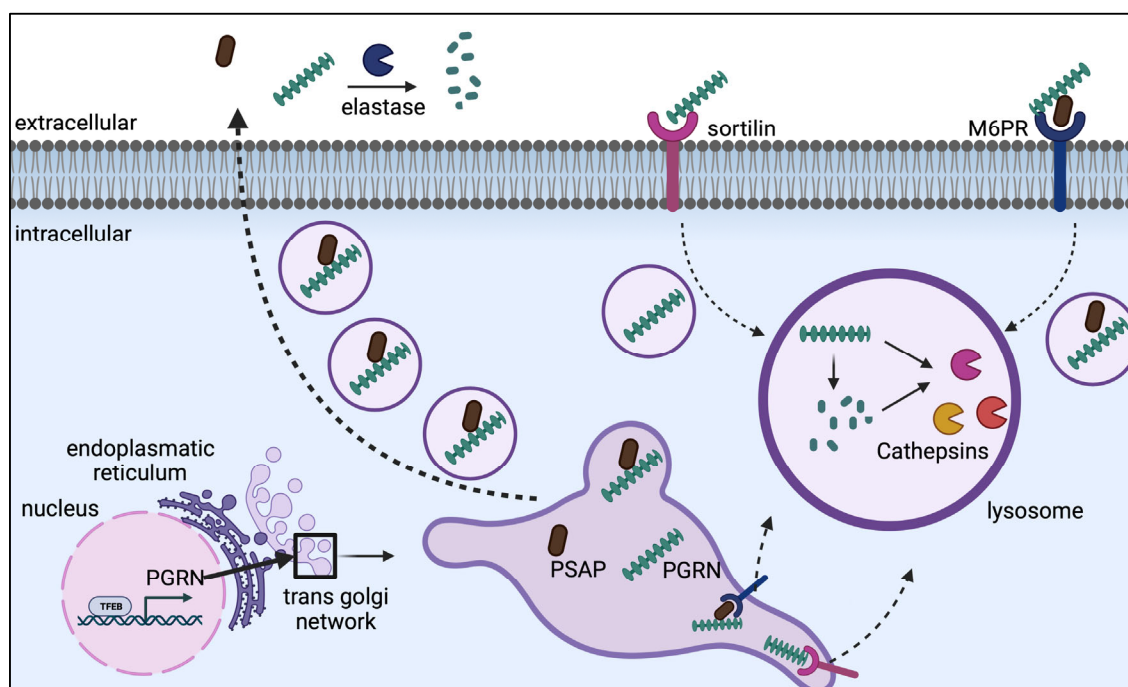

Figure 2. PGRN localization, function and processing: PGRN is a secreted protein, that can be transported to lysosomes involving the sortilin receptor or by forming a complex with PSAP. In lysosomes, PGRN is proteolytically processed into seven and a half granulin peptides. Both, full length PGRN and single granulins have key regulatory functions, including regulation of lysosomal activity. Modified from Holler et al. 2017.

2.2 Alzheimer`s Disease

AD, the most common form of dementia, is a major cause of death in our current increasingly aging society (Campbell-Taylor 2014; Weuve et al. 2014). Pathologically, AD is characterized by the formation of neurofibrillary tau tangles, extracellular amyloid-beta (Aβ) deposits and the loss of neurons and synapses. The central contribution of microglia to the disease pathology is indisputably clear, but if it is detrimental or protective still remains inconclusive (Hansen, Hanson, and Sheng 2014). Each option has been demonstrated in several studies, and it is hypothesized that the role of microglia may be dependent on the disease stage (Long and Holtzman 2019). The strongest genetic risk factor for developing late onset AD (LOAD) is the apolipoprotein E (APOE) ε4 allele (Corder et al. 1993; Guerreiro et al. 2013b; Jonsson et al. 2013). During the past years the triggering receptor expressed on myeloid cells 2 (TREM2)

has become the center of microglia-AD research as whole-genome sequencing studies confirmed that TREM2 mutations increase the risk for LOAD about 2-4 fold, a similar risk as being hemizygous for the APOE ε4 allele (Guerreiro et al. 2013b; Jonsson et al. 2013; Ulland and Colonna 2018). Loss-of-function (LOF) mutations in the triggering receptor expressed on myeloid cells 2 gene (*TREM2)* were first identified in the context of Nasu-Hakola disease (NHD), a form of presenile dementia with recurrent bone lesions (Paloneva et al. 2002). Rare mutations in *TREM2* were also associated with the FTLD-like syndrome without any bone involvement (Guerreiro et al. 2013a).

2.2.1 The triggering receptor expressed on myeloid cells 2

The cell surface transmembrane glycoprotein TREM2 consists of a V-immunoglobulin extra-cellular domain, an ectodomain, a single transmembrane (TM) helix and a short cytoplasmic tail (Fig. 3) (Allcock et al. 2003).
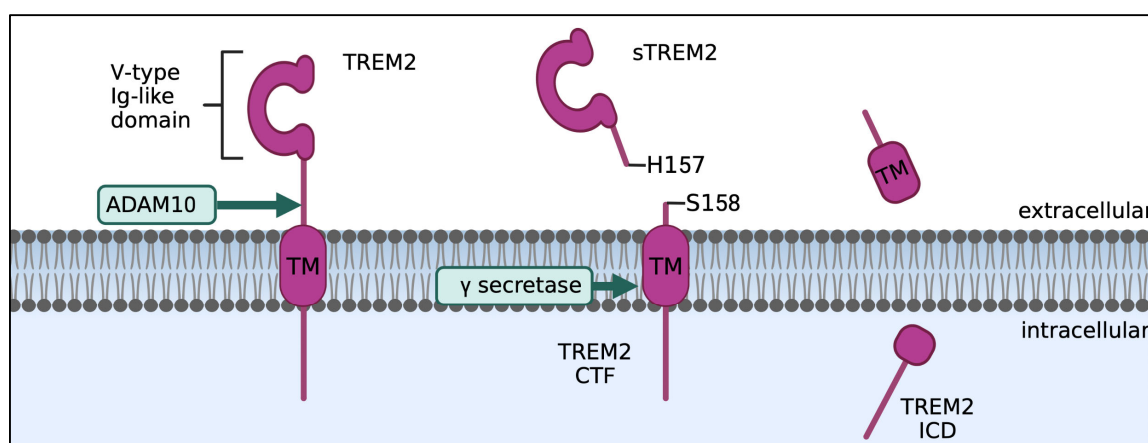

Figure 3. TREM2 structure and processing: The immune receptor TREM2 consists of a short cytoplasmic tail, a single TM helix and a V-type Ig-like extracellular domain. Signaling of TREM2 is initiated by binding of negatively charged ligands (see Figure 4). Shedding of the TREM2 ectodomain terminates signaling and releases sTREM2 into the extracellular space. The remaining CTF can be further cleaved by γ-secretase.

The protein itself does not contain any signal transduction motifs, but was shown to associate in a heteromeric complex and signals through the adaptor proteins DNAX activation protein (DAP) 12 and DAP10 (Fig. 4) (Peng et al. 2010). Upon binding to one out of several proposed ligands, including DNA, lipoproteins, phospholipids or other anionic molecules, downstream signaling of TREM2 is initiated by tyrosine phosphorylation of the co-receptor DAP12/10 within its immunoreceptor tyrosine-based activation motifs (ITAMs) by Src family kinases (Gratuze, Leyns, and Holtzman 2018; Neumann, Linnartz, and Wang 2010), following the recruitment and activation of the spleen tyrosine kinase (Syk) (Colonna and Wang 2016) (Fig. 4). Syk then further activates TREM2 downstream signaling molecules including phospholipase Cγ (PLCγ), several proto-oncogene vav (VAV) guanine nucleotide exchange factors and the nonreceptor tyrosine kinase Pyk2. These signaling cascades then affect a variety of microglia functions including phagocytosis, apoptosis, proliferation, autophagy and transcriptional regulation of

pro-inflammatory cytokines (Fig. 4). Signaling is terminated by shedding of the TREM2 ectodomain C-terminal at histidine 157 by a disintegrin and metalloproteinase domain-containing protein 10 (ADAM10), releasing soluble TREM2 (sTREM2) into the extracellular space (Fig. 3) (Kleinberger et al. 2014; Schlepckow et al. 2017; Wunderlich et al. 2013). sTREM2 levels were shown to be a potential biomarker for microglia activation in early-stage AD and positively correlate with the levels of tau (Suárez-Calvet, Kleinberger, et al. 2016). Furthermore, it was described that sTREM2 is functionally active and increases microglial cell viability and the expression of inflammatory cytokines (Zhong et al. 2017, 2019). The remaining C-terminal fragment (CTF) can be further cleaved by γ-secretase (Fig. 3) (Wunderlich et al. 2013).
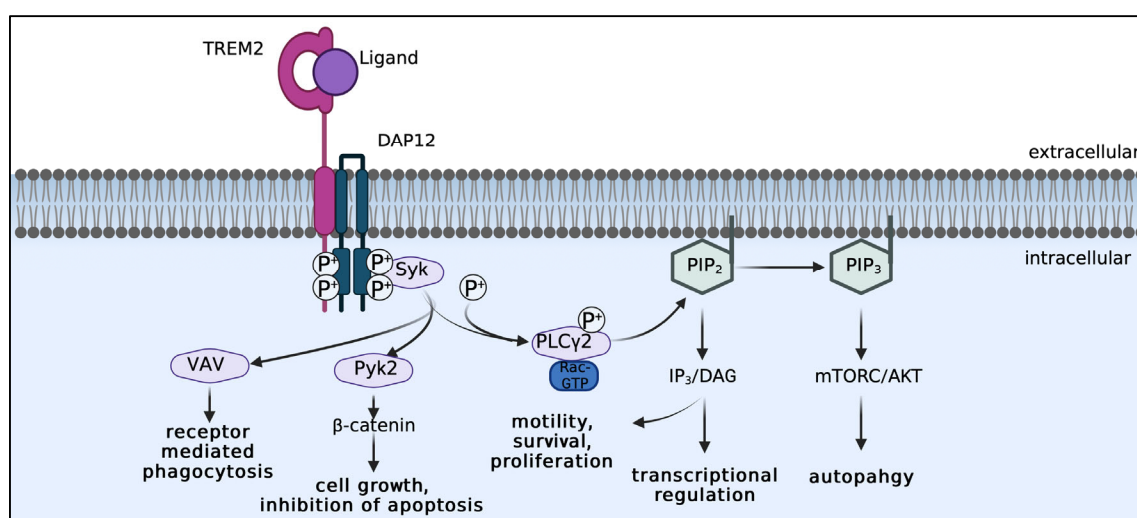

Figure 4. TREM2 signaling and function: Upon binding of extracellular ligands such as Aβ, downstream signaling of TREM2 is initiated by the phosphorylation of DAP12. TREM2 signaling influences various important microglia functions including cell growth, phagocytosis and autophagy. Modified from Lewcock et al., 2020.

2.2.2 TREM2 functions in physiology and pathology

TREM2 is involved in various functions in the healthy and diseased brain (Deczkowska, Weiner, and Amit 2020). Single-cell analysis confirmed that TREM2 is selectively expressed under physiological conditions in tissue-specific macrophages, namely microglia, adipose tissue, adrenal gland and placenta (Han et al. 2020). TREM2 was shown to be an essential player in phagocytic clearance: In mice, the LOF of TREM2 leads to reduced phagocytic ability, including less phagocytosis of apoptotic cells, cellular debris, bacteria, Aβ, lipoproteins and bacteria (Kleinberger et al. 2016; Mazaheri et al. 2017; Takahashi, Rochford, and Neumann 2005; Yeh et al. 2016), and it was shown that TREM2 expression directly associates with the phagocytic rate of the cells (Hsieh et al. 2009). Phagocytosis of debritic material is a beneficial process of microglia to avoid secondary necrosis and inflammation. TREM2 further supports this process by promoting phagocytosis and limiting immune activation (Hamerman et al. 2006; Ito and Hamerman 2012). In line with enhanced phagocytosis, microglia express a number of known anti-inflammatory genes in a TREM2-dependent manner (Jaitin et al. 2019; Keren-

Shaul et al. 2017). TREM2 signaling further promotes microglial chemotaxis, proliferation and survival (Kleinberger et al. 2014; Mazaheri et al. 2017; Takahashi et al. 2005). Additionally TREM2 regulates cholesterol transport and metabolism and is essential in maintaing the microglial energy metabolism (Nugent et al. 2020; Ulland et al. 2017). At this point, several mutations in the *TREM2* gene have been linked to AD. The most common one results in the R47H amino acid exchange, though others like R62H or H157Y have also been thoroughly analyzed (Kober et al. 2016; Lewcock et al. 2020; Song et al. 2017). The AD-associated TREM2 variants are surface exposed and were shown to lead to enhanced shedding or reduced ligand affinity (Gratuze et al. 2018; Lewcock et al. 2020) and thereby reduce essential microglia functions overall (Deczkowska et al. 2020; Lewcock et al. 2020). Binding assays confirmed reduced or impaired affinity to lipoprotein ligands like ApoE for the R47H and R62H variants and thereby reduced uptake into the cells (Kober et al. 2016; Yeh et al. 2016). The R47H variant was in addition shown to have a reduced phagocytic ability, reduced secretion of sTREM2 and is generally expressed at a weaker level (Kleinberger et al. 2014). Only the R47H and R62H TREM2 variants were shown to have a relatively decreased stability compared to the common variant (Kober et al. 2016). While TREM2 mutations associated with AD mostly affect cell signaling and general microglia function, mutations linked to other neurodegenerative disease like FTLD, such as p.T66M, p.Q33X and p.Y38C (Guerreiro et al. 2013a), show impaired glycosylation, cell surface trafficking and maturation of TREM2 (Guerreiro et al. 2013a; Kleinberger et al. 2014, 2017). NHD associated variants mostly affect the folding, expression, stability or structure of TREM2 (Kober et al. 2016). This indicates, that TREM2 mutations contribute to a multitude of neurodegenerative diseases by LOF mechanisms (Kober et al. 2016).

3. Protective and detrimental roles of microglia in neurodegenerative disease

Neuroinflammation and microgliosis are hallmarks of neurodegenerative disorders, including AD and FTLD, and the last years of research have conclusively demonstrated that microglia play an active role in the development and pathogenesis of these diseases (Kwon and Koh 2020; Leyns and Holtzman 2017; Zhang et al. 2021). While for a long time it was thought that inflammation in the brain can only occur by a direct infection following an infiltration of peripheral immune cells, it is now known that also other cells in the brain, including microglia, can trigger inflammation. Microgliosis was thought to be a secondary, detrimental event in the cascade of neurodegenerative disorders with activated microglia promoting neuronal cell death and synaptic pruning (Heneka et al. 2013; Hong et al. 2016). However, increasing evidence strongly suggests that microglia are active players in neuronal damage as their dysregulation results in progressive neurotoxic consequences (Block, Zecca, and Hong 2007; Hickman et al. 2018; Lewcock et al. 2020; Madore et al. 2020). In contrast, microglia may also exhibit neuroprotective functions (Chen and Trapp 2016; Lee and Choi 2022). Active microglia were shown to secrete neurotrophins like neutrophin-3 (NT-3) and brain-derived neurotrophic

factor (BNDF), which support neuronal survival and function (Huang and Reichardt 2001; Kerschensteiner et al. 2003). Microglia support neurogenesis and in the context of neurodegenerative disease, they exhibit further neuroprotective functions, like clearing Aβ deposits as described below. In addition, genetic studies have identified several risk factors associated with neurodegenerative disease that are exclusively expressed by microglia, highlighting their pivotal role (Efthymiou and Goate 2017; Marioni et al. 2018; Villegas-Llerena et al. 2016). Microglia are equipped with a number of receptors that can bind Aβ and become chronically activated due to constant stimulation (Heneka et al. 2013; Heneka, Golenbock, and Latz 2015; El Khoury et al. 2003; Maezawa et al. 2011). Activation is marked by an increase of proinflammatory cytokines, such as interleukin (IL) -6, tumor necrosis factor (TNF) -α, IL-8, and complement factors, such as C3 and C1qB (Shen et al. 1997; Strohmeyer, Shen, and Rogers 2000; Walker, Lue, and Beach 2001). The number of activated microglia, defined by their morphological phenotype, directly associates with the number of plaques and total Aβ load (Felsky et al. 2019). Phagocytic microglia are important to reduce amyloid seeding and tau spreading (Long and Holtzman 2019; Parhizkar et al. 2019; Leyns et al. 2019), by enhanced phagocytosis of Aβ and tau (Doens and Fernández 2014; Lee and Landreth 2010). Several studies have shown that impaired microglia lose their ability to cluster around plaques, which consequently leads to an increase in dystrophic neurites (Cheryl E.G. Leyns et al. 2019; Leyns and Holtzman 2017; Parhizkar et al. 2019). Microglia can limit neurotoxicity of amyloid deposits by forming a protective barrier around early stage plaques and compact protofibrillary Aβ into dense core plaques (Condello et al. 2015; Yuan et al. 2016; Huang et al. 2021). In tauopathies, including AD and FTLD, microglia take up, degrade and remove tau (Asai et al. 2015; Bolós et al. 2016). Proinflammatory microglia are also active players in tau phosphorylation, propagation and seeding such that microglia take up tau, but are unable to fully degrade it, consequently releasing the partially degraded material into the extracellular space. In attempt to clear the partially degraded debris, other cells like neurons could ingest the oligomeric tau, which inherently further induces tau propagation (Hickman et al. 2018; Hopp et al. 2018). In addition, microglia seem to have a pivotal role in complement-mediated synapse loss in AD. For example, in AD mouse models, it was shown that C1q and C3 proteins specifically tag synapses, leading to increased engulfment and phagocytosis by microglia (Hong et al. 2016; Stephan, Barres, and Stevens 2012).

3.1 Genetic association of microglia with neurodegenerative disease

The first two identified single-nucleotide polymorphisms (SNPs) associated with AD that pointed towards a major role for microglia in neurodegenerative disease were *CR1* and *CD33* (Bertram et al. 2008). Additionally, the discovery of a rare coding variant in the triggering *TREM2* gene that increases the risk for late onset AD by four to five fold further supported a crucial role of microglia in neurodegeneration (Guerreiro et al. 2013b; Jonsson et al. 2013). Lastly, the pivotal role of these diverse cells became quite obvious when genome-wide

association studies (GWAS) identified a number of LOAD risk variants in genes that are predominantly expressed by microglia (Efthymiou and Goate 2017; Villegas-Llerena et al. 2016). The identified LOAD risk genes can be clustered in a handful of pathways, like membrane trafficking (*SORL1*, *BIN1*), lipid metabolism (*APOE*, *ABCA7*) or inflammatory processes (*TREM2*, *CD33*, *PLCγ2*), suggesting that they contribute to AD pathology through common pathways (Penadés et al. 2019). Mutations in the *GRN* were also among the identified LOAD risk genes.

3.2 Disease-associated microglia versus homeostatic microglia

Comprehensive single-cell RNA sequencing of various disease and aging models illustrated that the previously used nomenclature of proinflammatory/active M1 versus immunosuppressive/resting M2 is not sufficient to describe the various states of microglia during disease and aging (Hammond et al. 2019; Kang et al. 2018; Keren-Shaul et al. 2017; Krasemann et al. 2017) as microglia exist in dynamic and microenvironment-dependent diverse states that orchestrate specific functions. In the context of AD, ALS and aging, microglia show a distinct profile of mRNA expression with an upregulation of genes like *Clec7a*, *Cd68* and *Cst3* and a downregulation of genes like *P2ry12* and *Cx3cr1*. Since then, this specific population of microglia is generally called disease-associated microglia (DAM) (Keren-Shaul et al. 2017) or microglia of neurodegenerative phenotype (MGnD) (Krasemann et al. 2017), and the typically upregulated genes are considered to be DAM markers. Many of the DAM markers include the expression of genes that are linked to neurodegenerative disease, including TREM2, and are conserved in mice and humans (Deczkowska et al. 2018; Keren-Shaul et al. 2017). In line with their pivotal role in the reaction to neuropathology, DAM markers primarily include genes that are involved in phagocytosis, migration, chemotaxis and lipid metabolism (Hammond et al. 2019; Keren-Shaul et al. 2017; Krasemann et al. 2017; Masuda et al. 2019; Mazaheri et al. 2017). In AD mouse models, it was found that DAM markers are primarily located in the near proximity to Aβ plaques and consequently only found in the brain regions, which are affected by the disease (Keren-Shaul et al. 2017; Mrdjen et al. 2018). Analysis of amyloid mouse models also revealed, that the differentiation of microglia into DAM is a two-stage process, in which stage one is essential to acquire the full activation of stage two (Fig. 5) (Friedman et al. 2018; Keren-Shaul et al. 2017). Interestingly, microglia require TREM2 signaling to acquire the DAM stage two, while transition into stage one is TREM2-independent, and the required factors are still unknown (Deczkowska et al. 2018). In DAM stage one, homeostatic genes (*Cx3cr1, P2ry12, Cd33, Tmem119*) are downregulated and TREM2 regulators like *Tyrobp or Apoe* are upregulated (Fig. 5) (Deczkowska et al. 2018). DAM stage 2 is characterized by an upregulation of genes like *Lpl*, *Cst7* or *Axl* - all genes that are associated to lysosomal, phagocytic and lipid metabolism pathways (Fig. 5) (Deczkowska et al. 2018). TREM2 LOF locks microglia in a homeostatic state, in which they are dysfunctional and unable to react to pathological exposure (Götzl et al. 2019; Keren-Shaul et al. 2017;

Krasemann et al. 2017; Mazaheri et al. 2017). Transcriptional analysis revealed that TREM2-deficient microglia are not able to induce the full DAM mRNA signature, which is essential for the microglial response to amyloid pathology, for compacting amyloid plaques (Ulrich et al. 2014; Wang et al. 2016; Yuan et al. 2016) and for reducing *de novo* seeding of amyloid plaques (Parhizkar et al. 2019). Instead, microglia with TREM2 LOF upregulate a homeostatic mRNA signature (Götzl et al. 2019; Mazaheri et al. 2017). Interestingly, LOF of PGRN results in the opposite phenotype of microglia activation with an increase in DAM signature expression (Reifschneider et al).
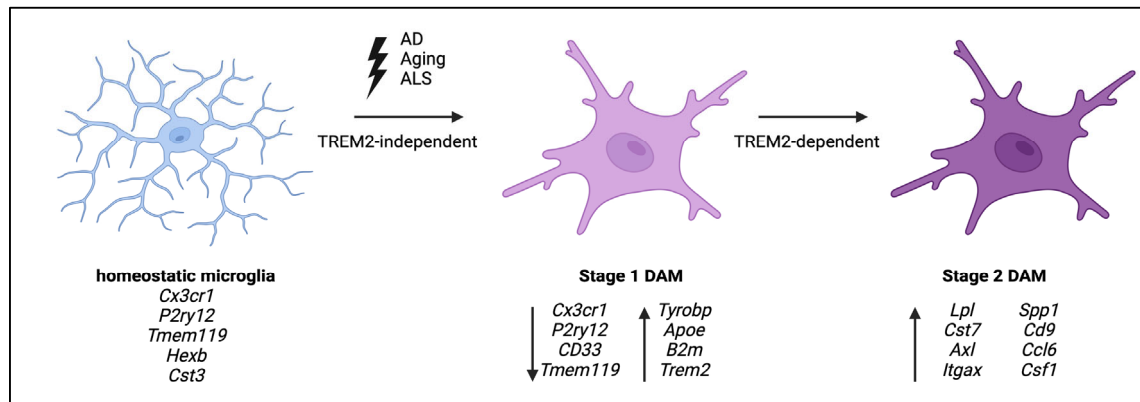

Figure 5. Microglia activation stages: In the context of AD, aging or ALS microglia show a distinct DAM mRNA signature. While transition to stage 1 DAM is TREM2-independent, induction of stage 2 DAM requires TREM2 signaling. Modified from Deczkowska et al. 2018.

4. Microglia as a therapeutic target in neurodegenerative diseases

Although neurodegenerative diseases are one of the major causes of death in our rapidly aging society, there is no disease-curing therapy available. In the past, the amyloid cascade has been the center of focus for new AD treatment strategies, but, so far, with limited success (Haass and Selkoe 2022). Most clinical trials have involved anti-Aβ antibodies or small-molecule inhibitors of β-secretase or γ-secretase, but most of them have not convincingly shown to reduce the cognitive decline (Oxford, Stewart, and Rohn 2020). The FDA very recently approved the anti-Aβ antibody aducanumab as a treatment for AD patients. Aducanumab was shown to reduce the plaque load, but a beneficial impact on cognitive decline could not be fully reproduced during the clinical trials (Sevigny et al. 2016). This is an important step towards better treatment strategies, but more research is needed. In addition to find the right treatment strategy, it is also difficult to assess the right timing of treatment for a disease affecting mostly the elderly, but which has its origin decades before symptoms occur. It is now widely accepted that an effective treatment would need to be applied even before the patients show any symptoms (Bateman et al. 2017; Gómez-Isla et al. 1996; Long and Holtzman 2019). Recent studies have now shown that the therapeutic potential of microglia in neurodegenerative disease has been tremendously underrated, and diverse efforts have been made to target microglia activation stages and thereby slow the cognitive decline in AD (Lewcock et al. 2020). One of the first attempts to study microglia as a therapeutic target was

the usage of microglia depletion models. In these models, microglia were either genetically or pharmacologically depleted (Elmore et al. 2015; Huang et al. 2018; Varvel et al. 2012), but the results were controversial. While some of the studies showed a beneficial effect (Dagher et al. 2015; Elmore et al. 2015), others could not confirm these findings (Grathwohl et al. 2009). In conclusion, microglia depletion as a therapeutic target in AD remains to be further analyzed due to the complex behaviour of these multifunctioning cells. Another approach to therapeutically target microglia in neurodegeneration is to inhibit their inflammatory response. As an emerging target to specifically inhibit the pro-inflammatory response of microglia and thereby limiting their deletterious effects in AD is the NLRP3 pathway (Heneka, McManus, and Latz 2018). Several neurodegenerative disease models exhibit NLRP3 inflammasome activation (Heneka et al. 2018), which was shown to lead to synaptic dysfunction, cognitive deficits and enhanced Aβ seeding (Ising et al. 2019; Venegas et al. 2017). Therefore, several drugs, including small-molecule approaches and antibodies, were developed to target the NLRP3 inflammasome (Lewcock et al. 2020; Venegas et al. 2017; Zahid et al. 2019), though additional clinical studies are necessary to evaluate the efficacy and safety of these drugs. Recently, TREM2 has emerged as a potential therapeutic target to modulate microglia as LOF variants of TREM2 are a risk factor for AD and TREM2 is essential for several microglia functions , including but not limited to efficient phagocytosis and compaction of plaque pathology (Meilandt et al. 2020; Ulrich et al. 2014; Wang et al. 2016). sTREM2 levels, a potential biomarker for TREM2 mediated signaling, were found to be increased very early in the disease and shown to correlate with total tau/phospho tau levels (Lewcock et al. 2020; Suárez-Calvet, Caballero, et al. 2016; Suárez-Calvet, Kleinberger, et al. 2016). Additionally, it was shown that high baseline sTREM2 levels measured in symptomatic sporadic AD patients have a beneficial effect on cognitive function as well as decreased hippocampal volume loss (Morenas-Rodríguez et al. 2022). Therefore, promoting TREM2 signaling by using TREM2 agonist antibodies appears to be a promising treatment strategy in neurodegenerative disease (Cheng et al. 2018; Cignarella et al. 2020; Price et al. 2020; Schlepckow et al. 2020; Wang et al. 2020). These antibodies target epitopes in the stalk region of TREM2 and were shown to increase TREM2 expression and decrease TREM2 shedding (Schlepckow et al. 2020), decrease plaque load and fibrillar plaques (Cignarella et al. 2020; Price et al. 2020; Schlepckow et al. 2020; Wang et al. 2020). The mechanisms of action of these antibodies include stimulation of TREM2 via crosslinking and decreasing TREM2 shedding and thereby increasing signaling competent full-length TREM2 on the cell surface (Cheng et al. 2018; Cignarella et al. 2020; Price et al. 2020; Schlepckow et al. 2020; Wang et al. 2020). When targeting microglia function as a therapeutic treatment strategy, it has to be kept in mind that microglial overactivation may also be detrimental as observed in PGRN LOF (Fig. 6). As described above, PGRN LOF leads to overactivated microglia with increased DAM marker expression, phagocytic and chemotactic activity, increased TSPO-PET signals and lysosomal dysfunction. Although LOF of TREM2 results in similar neurodegenerative disorders and

reduced glucose uptake in the brain, and microglia have shown to play a central role in the development of these disease, TREM2 LOF microglia are in the complete opposite stage of activation (Fig. 6) (Götzl et al. 2019). Locked in a homeostatic stage, they are not able to start their defense program and get activated in order to protect the brain against toxic aggregates. This indicates that both, the constant activation of microglia, but also the inability to be activated, is detrimental and it has to be kept in mind, that a possible therapeutic window for using microglia as a therapeutic target in neurodegenerative disease is rather small and probably disease-stage dependent.
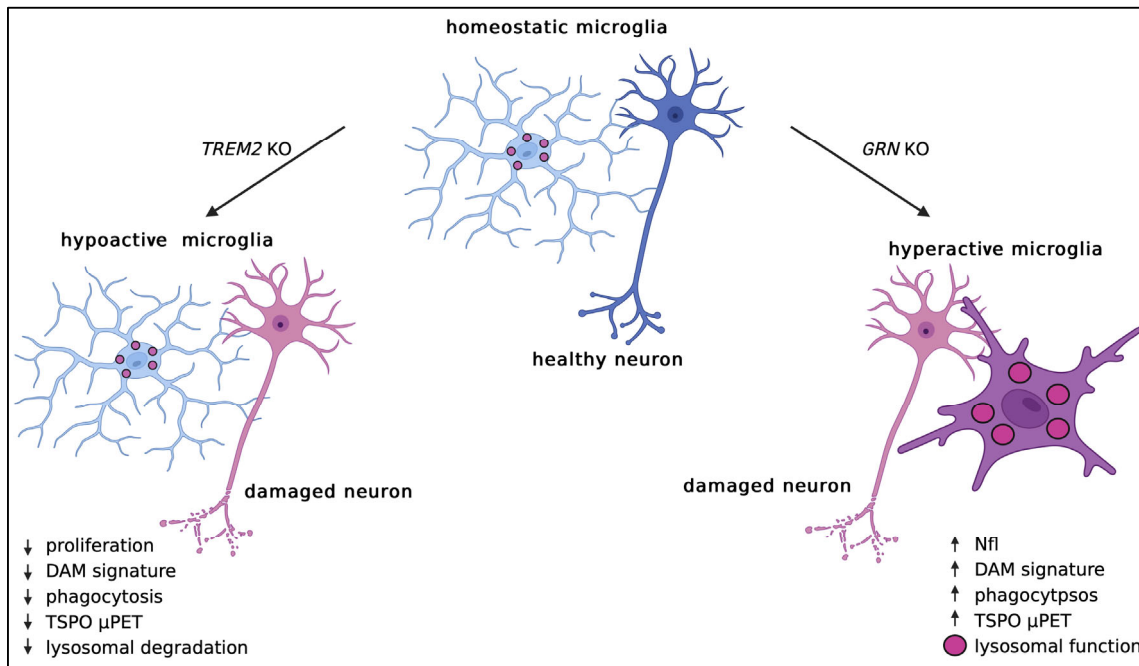
Figure 6. Opposite microglia activation stages upon loss of TREM2 or PGRN: Loss of TREM2 or PGRN leads to opposite microglial phenotypes. TREM2 KO locks microglia in a homeostatic stage with decreased expression of the DAM signature, reduced phagocytosis and reduced proliferation. In contrast, PGRN KO microglia are hyperactivated and exhibit increased expression of the DAM signature, increases phagocytosis and lysosomal dysfunction.

VIII. Aims of the study

How does the loss of PGRN lead to lysosomal dysfunction in *GRN*-FTLD?

As the homozygous loss of PGRN leads to the lysosomal storage disorder NCL, it was hypothesized that PGRN may have an important role in lysosomal biology and may directly influence lysosomal proteins and thereby protein degradation. However, the mechanism was unknown. Therefore, I collaborated with Julia Götzl and colleagues to elucidate the lysosomal function of PGRN and its influence on lysosomal proteases like Cat D, B and L. We wanted to investigate what influences the loss of PGRN has on lysosomal enzyme levels. Additionally, we aimed to not only to understand whether PGRN has a cell autonomous function, but also further characterize which cell types of the brain are involved in the lysosomal dysfunction in PGRN LOF models. Therefore, I isolated microglia and performed biochemical assays on the activity of lysosomal proteases. To elucidate if single granulins may also affect lysosomal activity, I analyzed the effects of PGRN, elastase-digested PGRN and recombinant GRN E on the activity of Cat B, D and L.

Are hyperactivated microglia in PGRN LOF detrimental and is the hyperactivation of microglia reversible?

When I started my PhD, the laboratory of Prof. Christian Haass was studying the opposing activation stages of microglia in TREM2 and PGRN deficiency models, including their mRNA signature, corresponding protein levels, phagocytic, migratory and clustering ability. We found that although mutations in both genes lead to similar diseases and decreased glucose metabolism in the brain, PGRN and TREM2 LOF microglia show opposite phenotypes. Though many questions regarding the possible underlying mechanisms and the connection between the hyperactivated phenotype in PGRN deficiency and TREM2 signaling still remained: **Is the hyperactivation of microglia in models of PGRN deficiency TREM2-dependent?** To answer this question, I generated *Grn* x *Trem2* double KO mice and analyzed the expression of DAM genes, microglia activation stages and morphology, lysosomal function and synapse loss. Mainly, I also wanted to elucidate the long-lasting question in microglia research: **Can microglia reversibly switch between the homeostatic and DAM stage?** This is an important question in regards to the potential of microglia as a therapeutic target in neurodegenerative diseases. It is essential to understand the dynamics between the different activation stages of microglia, to elucidate their therapeutic value. **Can the genetic or pharmacological suppression of TREM2 prevent the transition of homeostatic microglia to DAM and rescue abnormal lysosomal activity in PGRN LOF models?** As the results suggested that antagonistic modulation of TREM2 could be used to lower microglia activation, I also wanted to explore if pharmacological suppression of TREM2 may be beneficial in PGRN deficiency. Therefore, our laboratory collaborated with Denali Therapeutics to generate human antagonistic TREM2 antibodies that block TREM2 signaling and decrease signaling-

competent TREM2. As a first step, I used these antibodies to treat *GRN*-FTLD patient-derived macrophages and examined TREM2 levels, sTREM2 levels and TREM2 signaling. Next, I collaborated with Sophie Robinson (Paquet laboratory), who generated iPSC-derived microglia lacking PGRN. In line with the previous study, these cells were treated with antagonistic antibodies, and we analyzed TREM2 levels, TREM2 signaling, lysosomal status and the expression of DAM genes.

IX. Results
1. Publication I

Early lysosomal maturation deficits in microglia triggers enhanced lysosomal activity in other brain cells of progranulin knockout mice

Julia K. Götzl*, Alessio-Vittorio Colombo*, Katrin Fellerer*, **Anika Reifschneider**, Georg Werner, Sabina Tahirovoc, Christian Haass and Anja Capell

* Contributed equally

Molecular Neurodegeneration

RESEARCH ARTICLE

Open Access

Early lysosomal maturation deficits in microglia triggers enhanced lysosomal activity in other brain cells of progranulin knockout mice

Julia K. Götzl[1†], Alessio-Vittorio Colombo[2†], Katrin Fellerer[1†], Anika Reifschneider[1], Georg Werner[1], Sabina Tahirovic[2], Christian Haass[1,2,3*] and Anja Capell[1*]

Abstract

Background: Heterozygous loss-of-function mutations in the progranulin gene (GRN) lead to frontotemporal lobar degeneration (FTLD) while the complete loss of progranulin (PGRN) function results in neuronal ceroid lipofuscinosis (NCL), a lysosomal storage disease. Thus the growth factor-like protein PGRN may play an important role in lysosomal degradation. In line with a potential lysosomal function, PGRN is partially localized and processed in lysosomes. In the central nervous system (CNS), PGRN is like other lysosomal proteins highly expressed in microglia, further supporting an important role in protein degradation. We have previously reported that cathepsin (Cat) D is elevated in GRN-associated FTLD patients and Grn knockout mice. However, the primary mechanism that causes impaired protein degradation and elevated CatD levels upon PGRN deficiency in NCL and FTLD remains unclear.

Methods: mRNA expression analysis of selected lysosomal hydrolases, lysosomal membrane proteins and autophagy-related genes was performed by NanoString nCounter panel. Protein expression, maturation and in vitro activity of Cat D, B and L in mouse embryonic fibroblasts (MEF) and brains of Grn knockout mice were investigated. To selectively characterize microglial and non-microglial brain cells, an acutely isolated microglia fraction using MACS microbeads (Miltenyi Biotec) conjugated with CD11b antibody and a microglia-depleted fraction were analyzed for protein expression and maturation of selected cathepsins.

Results: We demonstrate that loss of PGRN results in enhanced expression, maturation and in vitro activity of Cat D, B and L in mouse embryonic fibroblasts and brain extracts of aged Grn knockout mice. Consistent with an overall enhanced expression and activity of lysosomal proteases in brain of Grn knockout mice, we observed an age-dependent transcriptional upregulation of certain lysosomal proteases. Thus, lysosomal dysfunction is not reflected by transcriptional downregulation of lysosomal proteases but rather by the upregulation of certain lysosomal proteases in an age-dependent manner. Surprisingly, cell specific analyses identified early lysosomal deficits in microglia before enhanced cathepsin levels could be detected in other brain cells, suggesting different functional consequences on lysosomal homeostasis in microglia and other brain cells upon lack of PGRN.

(Continued on next page)

* Correspondence: christian.haass@mail03.med.uni-muenchen.de;
anja.capell@mail03.med.uni-muenchen.de
†Julia K. Götzl, Alessio-Vittorio Colombo and Katrin Fellerer contributed equally to this work.
[1]Chair of Metabolic Biochemistry, Biomedical Center (BMC), Faculty of Medicine, Ludwig-Maximilians-Universität München, 81377 Munich, Germany
Full list of author information is available at the end of the article

Götzl *et al. Molecular Neurodegeneration* (2018) 13:48

Page 2 of 16

(Continued from previous page)

Conclusions: The present study uncovers early and selective lysosomal dysfunctions in *Grn* knockout microglia/macrophages. Dysregulated lysosomal homeostasis in microglia might trigger compensatory lysosomal changes in other brain cells.

Keywords: Frontotemporal lobar degeneration, Microglia, Neurodegeneration, Progranulin, Lysosome, Cathepsin

Background

Pathogenic mutations in the progranulin gene (*GRN*) are genetically linked to frontotemporal lobar degeneration (FTLD) and a rare adult-onset form of neuronal ceroid lipofuscinosis (NCL) [1–4]. Haploinsufficiency caused by non-sense and a few missense mutations result in *GRN*-associated FTLD (FTLD/*GRN*) [1, 2, 5–7] while homozygous loss-of-function *GRN* mutation carriers, who completely loose progranulin (PGRN) expression, develop NCL [3, 4]. Gene mutations causative for the different NCL forms are mostly associated with the lysosomal degradation pathway [8], indicating that PGRN may also be involved in lysosomal function. Indeed, *Grn* knockout mice are characterized by an increase of lysosomal proteins, NCL-like storage material, lipofuscinosis and an accumulation of the autophagy markers ubiquitin and p62 [3, 9–14]. Beside the genetic link between PGRN and lysosomal disorders [3, 4], there is also increasing evidence supporting lysosomal dysfunction in FTLD [15]. Hallmarks of all FTLD/*GRN* patients are cytoplasmic inclusions of hyperphosphorylated TAR DNA binding protein (TDP)-43 co-localizing with ubiquitin and p62 [16, 17]. Furthermore, FTLD/*GRN* patients show symptoms typically associated with NCL, like retinal thinning, lipofuscin and NCL-like storage material deposits [18–21]. Finally, challenging lysosomes by starvation, sucrose treatment, inhibition of vacuolar ATPase or alkalizing drugs causes an increase in PGRN production [21–23]. PGRN is a multifunctional complex glycosylated protein, which can be secreted as a growth factor into the extracellular space [24–26]. Secreted PGRN is also processed to granulin peptides by several different proteases including matrix metalloproteinases – 9 and – 14 [27, 28], a disintegrin and metalloproteinase with thrombospondin motif 7 (ADAMTS-7) [29], neutrophil elastase, proteinase 3 [25, 30], and intracellular by cathepsin L (Cat L) [31, 32]. Additionally, PGRN can be transported to lysosomes using two distinct transport pathways; one mediated by the sortilin receptor [33] and the other one via complex formation with prosaposin. Prosaposin is then transported to lysosomes by binding to the mannose-6-phosphate receptor or the low density lipoprotein receptor-related protein 1 [34]. Recent evidence indicates that lysosomal localized PGRN [33, 35–37] may function in lysosomal homeostasis and autophagy [38–40]. Additionally, granulin peptides, which are generated within lysosomes [31, 32, 41], might affect the lysosomal function [38].

To further understand if and how the loss of PGRN may cause lysosomal dysfunction we searched for changes in protein expression, maturation and enzymatic activity of a subset of lysosomal cathepsins in microglia and other brain cells. Microglia, which are the main source of PGRN in the brain, showed a severe impairment of lysosomal cathepsin expression and maturation in the absence of PGRN whereas the remaining brain cells showed increased cathepsin processing and maturation. We therefore propose different effects on lysosomal function upon loss of PGRN in microglia and other brain cells like astrocytes and neurons.

Methods

Animal experiments and mouse brain tissue

All animal experiments were performed in accordance with local animal handling laws. Mice were sacrificed by CO_2 inhalation. Brain tissue was obtained from the $Grn^{-/-}$ mouse strain generated by Kayasuga and colleagues [42].

Isolation of adult primary microglia, neurons and astrocytes

Primary microglia were isolated from adult mouse brain using MACS Technology (Miltenyi Biotec) according to manufacturer's instructions. Briefly, brain cortices were dissected, and after removal of meninges dissociated by enzymatic digestion using the Neural Tissue Dissociation Kit P (Miltenyi Biotec). CD11b-positive microglia were magnetically labelled with CD11b MicroBeads, loaded onto a MACS Column (Miltenyi Biotec) and subjected to magnetic separation. Isolated microglia and the microglia depleted fraction were snap frozen in liquid nitrogen and stored at – 80 °C until further biochemical analysis. To determine PGRN expression in different brain cell types, microglial, neuronal and astrocytic cells, the dissected mouse brain, after removal of meninges, was dissociated by using the Adult Brain Dissociation Kit (Miltenyi Biotec). A single cell suspension was generated according to the manufactures instructions with the exception that the mouse brain was mechanically dissociated by using in sequence, three fire-polished Pasteur pipettes with decreasing tip diameters. The single cell suspension of five mice were combined and separated in three aliquots for isolating microglia cells (Anti-CD11b MicroBeads, Miltenyi Biotec), astrocytes (Anti-ACSA-2

Götzl *et al. Molecular Neurodegeneration* (2018) 13:48

Page 3 of 16

MicroBeads, Miltenyi Biotec) and neurons (Neuron Isolation Kit, Miltenyi Biotec) according to the manufactures instructions. Isolated cells were snap frozen in liquid nitrogen and stored at − 80 °C until further biochemical analysis.

Generation and culturing of mouse embryonic fibroblasts (MEF) lines

$Ctsd^{−/−}$ MEF were provided by Dr. Paul Saftig and generated from the *Ctsd* knockout mouse strain [43]. For $Grn^{−/−}$ MEF, timed pregnant female of a heterozygous *Grn* mating was sacrificed by CO_2 inhalation, the embryos (E15) were processed and MEF were separated by digestion with trypsin-EDTA [44]. MEF cells with the same genotype derived from littermates were pooled and immortalized by serial (3 T3) passaging [44]. From immortalized MEF either single cell clones were isolated or pools were generated. For rescue of PGRN deficiency, $Grn^{−/−}$ MEF were transfected with m*Grn* cloned into the HindIII and XhoI site of pcDNA3.1 (Hygro+) and selected with hygromycin B at 50 mg/mL (Invitrogen). Single cell clones were analyzed for PGRN expression. MEF were cultured in DMEM with Glutamax I (Invitrogen) supplemented with 10% fetal calf serum (Invitrogen) and penicillin/streptomycin (PAA Laboratories).

Quantitative NanoString nCounter gene expression assay

NanoString nCounter technology allows expression analysis of multiple genes from a single sample. We generated an nCounter panel for analyzing gene expression of 45 lysosomal and autophagy- related genes [45–48] and 5 housekeeping genes. Total RNA was extracted from aliquots of powdered mouse brain samples using QIAshredder and RNeasy Mini Kit (Qiagen). 100 ng RNA per brain was used for gene expression analysis. The NanoString panel measurement and evaluation was done at Proteros Biostructures GmbH, Martinsried, Germany. Gene expression levels in each sample were normalized against the geometric mean of four housekeeping genes including *Cltc, Hprt, Pgk1* and *Tubb5* using *nSolver™ Analysis Software, version 3.0* (NanoString Technologies, Inc.) *Gusb* was excluded because of significant changes of expression in $Grn^{−/−}$ mice. Based on the normalized gene expression levels of $Grn^{−/−}$ and $Grn^{+/+}$ ($n = 3$), statistical significance was determined by the unpaired, two-tailed student's t-test.

Quantitative real time PCR (qRT-PCR)

Approximately 10–20 mg of powdered mouse brain homogenates were subjected to total RNA preparation using the QIAshredder and RNeasy Mini Kit (Qiagen) according to manufacturer's instructions. 2 μg of RNA was reverse transcribed into cDNA using M-MLV reverse transcriptase (Promega) and oligo(dT) primers

(Life Technologies). The following primer sets from Integrated DNA Technologies were used: mouse *Ctsd* Mm.PT.53a.17202883 (Exon boundary 3 to 4), mouse *Ctsb* Mm.PT.53a.7639164 (Exon boundary 4 to 5), mouse *Ctsl* Mm.PT.58.9857472 (Exon boundary 7 to 8), mouse *App* Mm00431827_m1 (Applied Biosystems) and mouse *Gapdh* Mm.PT.39a.1 (Exon boundary 2 to 3). cDNA levels were quantitatively determined in triplicates using TaqMan assays on a 7500 Fast Real-Time-PCR System (Applied Biosystems). All cDNA levels were normalized to *Gapdh* cDNA and relative transcription levels of the respective sequences were analyzed using the comparative delta Ct method (7500 Software V2.0.5, Applied Biosystems, Life Technologies).

Antibodies

The following primary antibodies were used for immunoblotting: mouse monoclonal anti-β-actin antibody (Sigma-Aldrich; 1:10,000), mouse monoclonal anti-α-tubulin antibody (Sigma-Aldrich; 1:5,000), goat anti-cathepsin D (sc-20) antibody (Santa Cruz Biotechnology; 1:500), goat anti-cathepsin B (AF965) antibody (R&D Systems; 0,1 μg/ml), goat anti-cathepsin L (AF1515) antibody (R&D Systems; 1 μg/ml), goat anti-cathepsin S (M-19) antibody (Santa Cruz Biotechnology; 1:200), rat anti-PGRN (8H10) antibody (1:50) [18]; rabbit anti-GFAP antibody (Dako; 1:5,000), rabbit anti-Iba1 antibody (Dako; 1:1000), rabbit anti-neuronal class III ß-Tubulin (Tuj1) antibody (BioLegend; 1:10,000), rabbit anti-p62/SQSTM1 antibody (MBL; 1:1,000), mouse anti-ubiquitin (P4D1) antibody (Santa Cruz Biotechnology; 1:1000), rabbit anti-APP (Y188) antibody (Abcam, 1:2,000) rat monoclonal anti-mLamp1 antibody clone 1D4B (developed by J. Thomas August, distributed by Developmental Studies Hybridoma Bank, NICHD, maintained by the University of Iowa, Department of Biology; 1:200), goat polyclonal anti-saposin D antibody (1:1,000) [49], and rabbit anti-LC3BB/MAP1LC3B antibody (Novus Biologicals; 2 μg/ml). The following secondary antibodies were used: horseradish peroxidase-conjugated donkey anti-goat IgG (Santa Cruz Biotechnology; 1:5,000), anti-mouse IgG (Promega; 1:10,000), anti-rabbit IgG (Promega; 1:20,000), goat anti-rat IgG + IgM (L + M) (Dianova; 1:5,000) and generated mouse anti-rat IgG2c (1:1,000).

Protein analysis and immunoblotting

For microglia, neurons and astrocytes cell pellets were lysed in RIPA buffer [18] supplemented with protease inhibitor cocktail (Sigma-Aldrich) and phosphatase inhibitor (Roche Applied Science) and centrifuged for 30 min, 15,000 x g, 4 °C. MEF cells were lysed in RIPA buffer (150 mM NaCl, 50 mM TRIS pH 8.0; 0.1% SDS, 1% NP40, 0.5% Sodiumdeoxycholat) supplemented with Benzonase (Novagen), protease inhibitor cocktail (Sigma-Aldrich) and phosphatase inhibitor (Roche Applied

Götzl *et al. Molecular Neurodegeneration* (2018) 13:48

Page 3 of 16

MicroBeads, Miltenyi Biotec) and neurons (Neuron Isolation Kit, Miltenyi Biotec) according to the manufactures instructions. Isolated cells were snap frozen in liquid nitrogen and stored at − 80 °C until further biochemical analysis.

Generation and culturing of mouse embryonic fibroblasts (MEF) lines

$Ctsd^{-/-}$ MEF were provided by Dr. Paul Saftig and generated from the $Ctsd$ knockout mouse strain [43]. For $Grn^{-/-}$ MEF, timed pregnant female of a heterozygous Grn mating was sacrificed by CO_2 inhalation, the embryos (E15) were processed and MEF were separated by digestion with trypsin-EDTA [44]. MEF cells with the same genotype derived from littermates were pooled and immortalized by serial (3 T3) passaging [44]. From immortalized MEF either single cell clones were isolated or pools were generated. For rescue of PGRN deficiency, $Grn^{-/-}$ MEF were transfected with mGrn cloned into the HindIII and XhoI site of pcDNA3.1 (Hygro+) and selected with hygromycin B at 50 mg/mL (Invitrogen). Single cell clones were analyzed for PGRN expression. MEF were cultured in DMEM with Glutamax I (Invitrogen) supplemented with 10% fetal calf serum (Invitrogen) and penicillin/streptomycin (PAA Laboratories).

Quantitative NanoString nCounter gene expression assay

NanoString nCounter technology allows expression analysis of multiple genes from a single sample. We generated an nCounter panel for analyzing gene expression of 45 lysosomal and autophagy- related genes [45–48] and 5 housekeeping genes. Total RNA was extracted from aliquots of powdered mouse brain samples using QIAshredder and RNeasy Mini Kit (Qiagen). 100 ng RNA per brain was used for gene expression analysis. The NanoString panel measurement and evaluation was done at Proteros Biostructures GmbH, Martinsried, Germany. Gene expression levels in each sample were normalized against the geometric mean of four housekeeping genes including $Cltc, Hprt, Pgk1$ and $Tubb5$ using $nSolver^{™}$ *Analysis Software, version 3.0* (NanoString Technologies, Inc.) $Gusb$ was excluded because of significant changes of expression in $Grn^{-/-}$ mice. Based on the normalized gene expression levels of $Grn^{-/-}$ and $Grn^{+/+}$ ($n = 3$), statistical significance was determined by the unpaired, two-tailed student's t-test.

Quantitative real time PCR (qRT-PCR)

Approximately 10–20 mg of powdered mouse brain homogenates were subjected to total RNA preparation using the QIAshredder and RNeasy Mini Kit (Qiagen) according to manufacturer's instructions. 2 μg of RNA was reverse transcribed into cDNA using M-MLV reverse transcriptase (Promega) and oligo(dT) primers
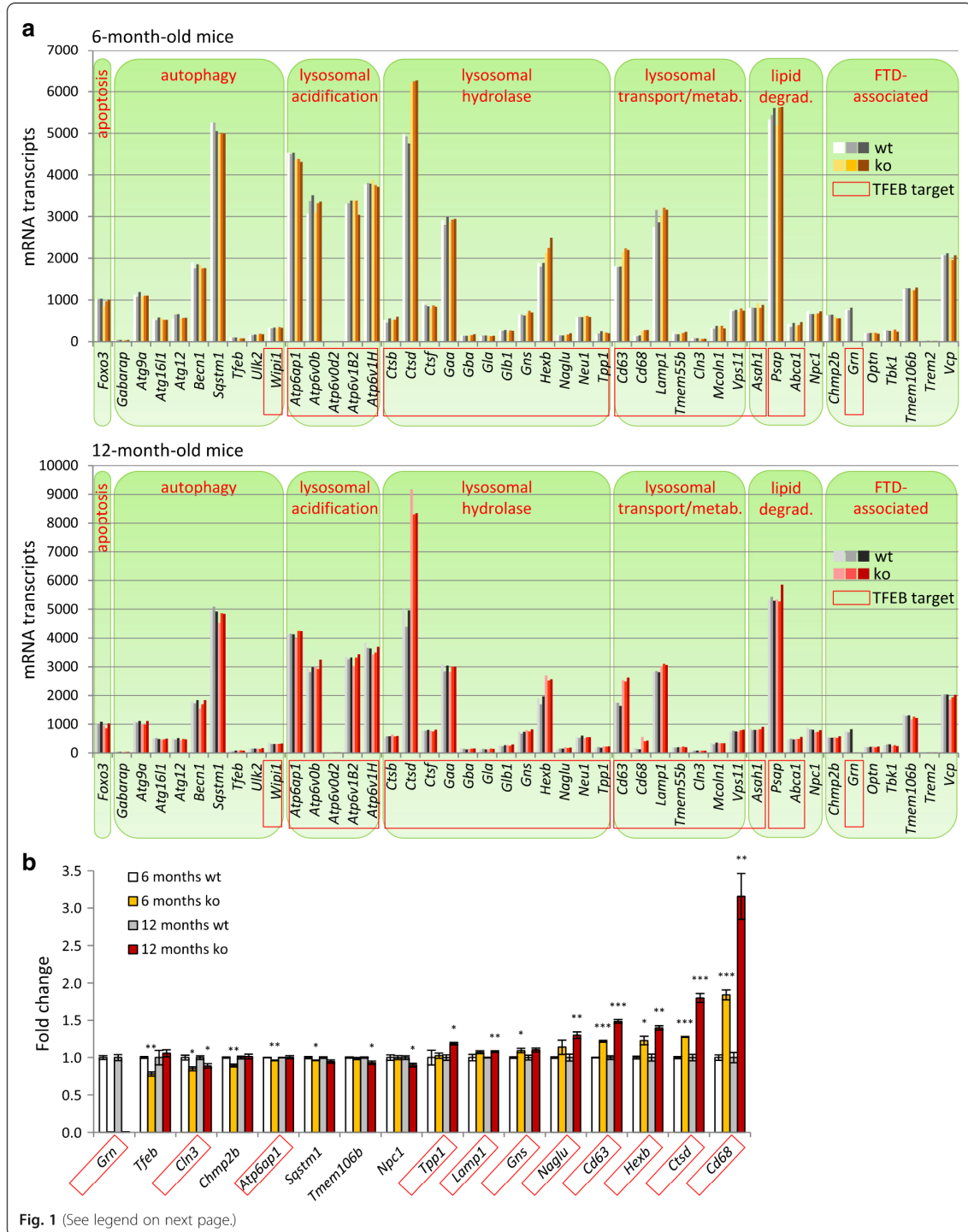
(Life Technologies). The following primer sets from Integrated DNA Technologies were used: mouse $Ctsd$ Mm.PT.53a.17202883 (Exon boundary 3 to 4), mouse $Ctsb$ Mm.PT.53a.7639164 (Exon boundary 4 to 5), mouse $Ctsl$ Mm.PT.58.9857472 (Exon boundary 7 to 8), mouse App Mm00431827_m1 (Applied Biosystems) and mouse $Gapdh$ Mm.PT.39a.1 (Exon boundary 2 to 3). cDNA levels were quantitatively determined in triplicates using TaqMan assays on a 7500 Fast Real-Time-PCR System (Applied Biosystems). All cDNA levels were normalized to $Gapdh$ cDNA and relative transcription levels of the respective sequences were analyzed using the comparative delta Ct method (7500 Software V2.0.5, Applied Biosystems, Life Technologies).

Antibodies

The following primary antibodies were used for immunoblotting: mouse monoclonal anti-β-actin antibody (Sigma-Aldrich; 1:10,000), mouse monoclonal anti-α-tubulin antibody (Sigma-Aldrich; 1:5,000), goat anti-cathepsin D (sc-20) antibody (Santa Cruz Biotechnology; 1:500), goat anti-cathepsin B (AF965) antibody (R&D Systems; 0,1 μg/ml), goat anti-cathepsin L (AF1515) antibody (R&D Systems; 1 μg/ml), goat anti-cathepsin S (M-19) antibody (Santa Cruz Biotechnology; 1:200), rat anti-PGRN (8H10) antibody (1:50) [18]; rabbit anti-GFAP antibody (Dako; 1:5,000), rabbit anti-Iba1 antibody (Dako; 1:1000), rabbit anti-neuronal class III ß-Tubulin (Tuj1) antibody (BioLegend; 1:10,000), rabbit anti-p62/SQSTM1 antibody (MBL; 1:1,000), mouse anti-ubiquitin (P4D1) antibody (Santa Cruz Biotechnology; 1:1000), rabbit anti-APP (Y188) antibody (Abcam, 1:2,000) rat monoclonal anti-mLamp1 antibody clone 1D4B (developed by J. Thomas August, distributed by Developmental Studies Hybridoma Bank, NICHD, maintained by the University of Iowa, Department of Biology; 1:200), goat polyclonal anti-saposin D antibody (1:1,000) [49], and rabbit anti-LC3BB/MAP1LC3B antibody (Novus Biologicals; 2 μg/ml). The following secondary antibodies were used: horseradish peroxidase-conjugated donkey anti-goat IgG (Santa Cruz Biotechnology; 1:5,000), anti-mouse IgG (Promega; 1:10,000), anti-rabbit IgG (Promega; 1:20,000), goat anti-rat IgG + IgM (L + M) (Dianova; 1:5,000) and generated mouse anti-rat IgG2c (1:1,000).

Protein analysis and immunoblotting

For microglia, neurons and astrocytes cell pellets were lysed in RIPA buffer [18] supplemented with protease inhibitor cocktail (Sigma-Aldrich) and phosphatase inhibitor (Roche Applied Science) and centrifuged for 30 min, 15,000 x g, 4 °C. MEF cells were lysed in RIPA buffer (150 mM NaCl, 50 mM TRIS pH 8.0; 0.1% SDS, 1% NP40, 0.5% Sodiumdeoxycholat) supplemented with Benzonase (Novagen), protease inhibitor cocktail (Sigma-Aldrich) and phosphatase inhibitor (Roche Applied

Götzl *et al. Molecular Neurodegeneration* (2018) 13:48

Page 4 of 16

Fig. 1 (See legend on next page.)

(See figure on previous page.)

Fig. 1 Minor alterations in expression of lysosomal and autophagy-related genes in brain of $Grn^{-/-}$ mice. **a** mRNA expression for 45 selected genes associated with the lysosome-autophagy degradation pathway [45, 46] in brain of $Grn^{+/+}$ (wt) and $Grn^{-/-}$ (ko) mice at 6 and 12 months of age (for original data see Additional file 2). Genes are grouped by their function within these pathways or by their FTLD-association. Previously identified TFEB targets are labeled by red boxes [46, 47]. $N = 3$ mice per group, notice the low expression differences between individual mice and between 6- and 12-month-old mice. *Trem2* and *Atp6v0d2* were below the detection limit. **b** Fold change of gene expression which show at least one significand change either at 6 or 12 months of age. Data were normalized to the corresponding mean value of $Grn^{+/+}$ (wt) mice and are shown as mean ± SD. For statistical analysis the unpaired, two-tailed student's t-test was used ($n = 3$) (*, $p < 0.05$; **, $p < 0.01$; ***, $p < 0.001$)

Science) and centrifuged for 30 min, 15,000 x g, 4 °C. The protein concentration of the supernatant was determined using the BCA protein assay (Pierce, Thermo Scientific) and equal amount of protein were separated by SDS-PAGE and transferred onto polyvinylidene difluoride membranes (Immobilon-P, Merck Millipore). For the detection of C-terminal fragments (CTF) of the amyloid precursor protein (APP) and saposin D the proteins were transferred onto nitrocellulose membranes (Protran BA85, GE Healthcare Lifesciences) and heated in PBS. Proteins of interest were detected by the indicated primary antibodies followed by horseradish peroxidase-conjugated secondary antibodies and ECL (Amersham Western Blotting Detection reagent, GE Healthcare Lifesciences) or ECL Plus (Pierce ECL Plus Western Blotting Substrates, Thermo Scientific). For the quantitatively analysis, images were taken by a Luminescent Image Analyzer LAS-4000 (Fujifilm Life Science, Tokyo, Japan) and evaluated with the Multi GaugeV3.0 software (Fujifilm Life Science, Tokyo, Japan).

Cathepsin activity assay

MEF cell pellets or aliquots of powdered mouse brain tissues were used for cathepsin D, B and L fluorescence based activity assays (Abnova). The samples were homogenized in the appropriate lysis buffer provided by the manufacturer and incubated for 10 min (MEF cell lysates) or 20 min (brain lysates) on ice, followed by a 5 min (MEF cell lysates) or 20 min (brain lysates) centrifugation at 15,000 x g, 4 °C. The protein concentration was determined by BCA protein assay (Pierce, Thermo Scientific) and equal amounts of protein were used for the activity assays. The assays were performed in black 96-well plates (FluoroNunc) at 37 °C for 20 min according to the manufacturer's protocol. Cleavage of the quenched fluorescence substrate was continuously measured as increase of fluorescence signal by Fluoroskan Ascent FL plate reader (Labsystems). The relative enzyme activity was calculated for a period of time with linear substrate turnover.

Metabolic labeling and protein turn over

To analyze protein turnover, MEF at 70–80% of confluency were starved for 1 h in methionine-, cysteine- and serum-free minimal essential medium (Invitrogen)

and subsequently metabolically pulse-labeled with 18.5 MBq ^{35}S-methionine/cysteine (Met-S35-label, Hartmann Analytic) in methionine-, cysteine- and serum free medium for 1 h, followed by indicated chase periods in the presence of a 5-fold excess of unlabeled methionine. Cell lysates were prepared and labeled proteins were precipitated with 5% TCA for 1 h at 4 °C, followed by 30 min centrifugation at 13,000 rpm, 4 °C. Pellets were washed twice with 80% acetone, dried at RT and resuspended in 50 µl sample buffer. Remaining radioactive-labeled proteins were measure in triplicates in liquid scintillation counter (Tri-Carb 2810, Perkin Elmer).

Statistical analysis

For statistical analysis the unpaired, two-tailed student's t-test was performed when two groups of samples (wt and ko) were compared, for comparison of more than two groups, one-way ANOVA with Dunnett's post hoc test was used and statistical significance was set at *, $p < 0.05$; **, $p < 0.01$; ***, $p < 0.001$; and ****, $p < 0.0001$.

Results

Subtle changes in lysosomal and autophagy-related gene expression in total brain of $Grn^{-/-}$ mice

Accumulating evidence indicates that PGRN plays a critical role for lysosomal integrity and function. To obtain insights into the role of PGRN in autophagic/lysosomal protein degradation pathways we performed on whole brain extract a NanoString based mRNA expression analysis of selected lysosomal and autophagy-related genes [45] (Fig. 1a). Surprisingly, expression of only very few genes was significantly altered in the brain of 6- and 12-month-old $Grn^{-/-}$ mice (Fig. 1a, b). Only eight genes, among which are three genes encoding the lysosomal membrane proteins *Cd68*, *Cd63* and *Lamp1*, show a significantly elevated expression in $Grn^{-/-}$ mice. Additionally, the lysosomal hydrolases *hexosaminidase subunit β* (*Hexb*) and *cathepsin D* (*Ctsd*) showed the strongest and age-dependent increase in $Grn^{-/-}$ mice (Fig. 1b). However, no general elevation of lysosomal and autophagy-related gene expression regulated by transcription factor EB (TFEB) [46, 50] was observed in $Grn^{-/-}$ mice brain. Thus, although $Grn^{-/-}$ mice recapitulate important pathological features of NCL, expression of lysosomal genes is not overtly affected.
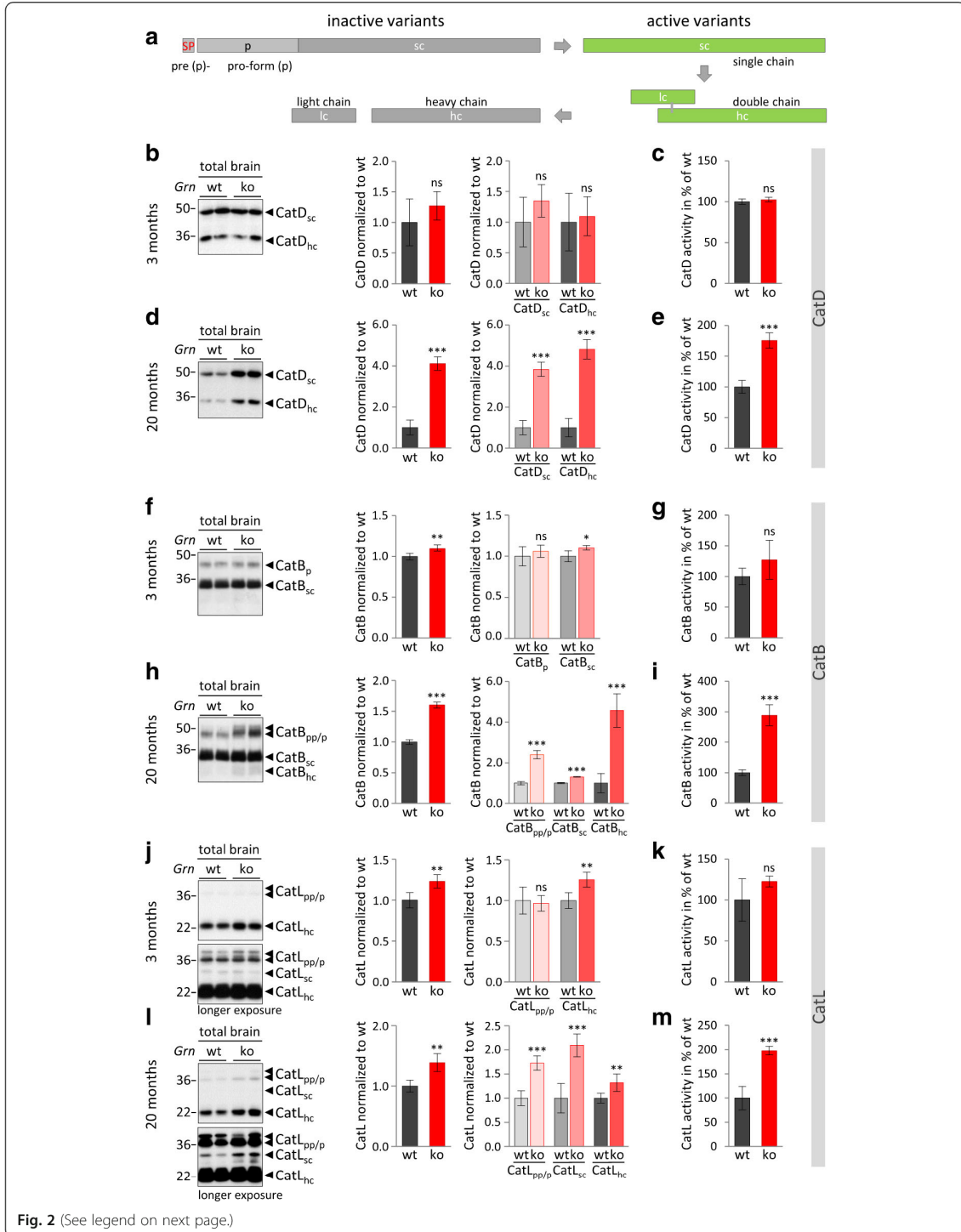
Götzl *et al. Molecular Neurodegeneration* (2018) 13:48

Page 6 of 16

Fig. 2 (See legend on next page.)

Götzl *et al. Molecular Neurodegeneration* (2018) 13:48

Page 7 of 16

(See figure on previous page.)

Fig. 2 Altered protein expression, maturation and activity of cathepsins in brain of $Grn^{-/-}$ mice. **a** Schematic presentation of cathepsin maturation [53]. Cathepsins (Cat) are synthesized as an inactive pre-pro-form (pp), translocated into the endoplasmic reticulum (ER) by signal peptide (SP). After SP removal the pro-form (p) becomes co-transitionally modified and is transported to lysosomes predominantly via the manose-6-phosphate pathway. With increasing acidification, the pro-peptide is removed, either autocatalytically or by other enzymes, leading to an active single chain variant (sc, green). For most cathepsins this sc-variant can be further proteolytically processed to a heavy (hc) and a light chain (lc), as long as hc and lc are linked by disulfide bridges or hydrophobic interaction the double chain variant remains active (green) but will be inactivated by separation of hc and lc. Representative blots of brain lysate from 3-month-old and 20-month-old $Grn^{+/+}$ (wt) and $Grn^{-/-}$ (ko) mice probed for cathepsin D (CatD) (**b, d**) cathepsin B (CatB) (**f, h**) and cathepsin L (CatL) (**j, l**). The molecular weight standards in kilo Daltons (kDa) are indicated on the left side of the blots. Quantification of blots for total cathepsin or maturation variants normalized to $Grn^{+/+}$ are shown as mean ± SD. $N = 5$ mice per genotype (**b, d, f, h, j, l**). Statistical significance was set at *, $p < 0.05$; **, $p < 0.01$; and ***, $p < 0.001$; ns, not significant using an unpaired, two-tailed student's t-test**.** In vitro enzyme activity of CatD, CatB and CatL in lysates of mouse brains used for immunoblot analysis. Equal amounts of enzyme optimized brain lysates from $Grn^{+/+}$ and $Grn^{-/-}$ ($n = 3–5$) mice were incubated with quenched fluorogenic substrate (**c, e, g, i, k, m**). The increase of fluorescence signal was continuously measured and for a linear turnover time period normalized to $Grn^{+/+}$ set as 100% activity, mean ± SD. Statistical significance was set at ***, $p < 0.001$ and ns, not significant using unpaired, two-tailed student's t-test
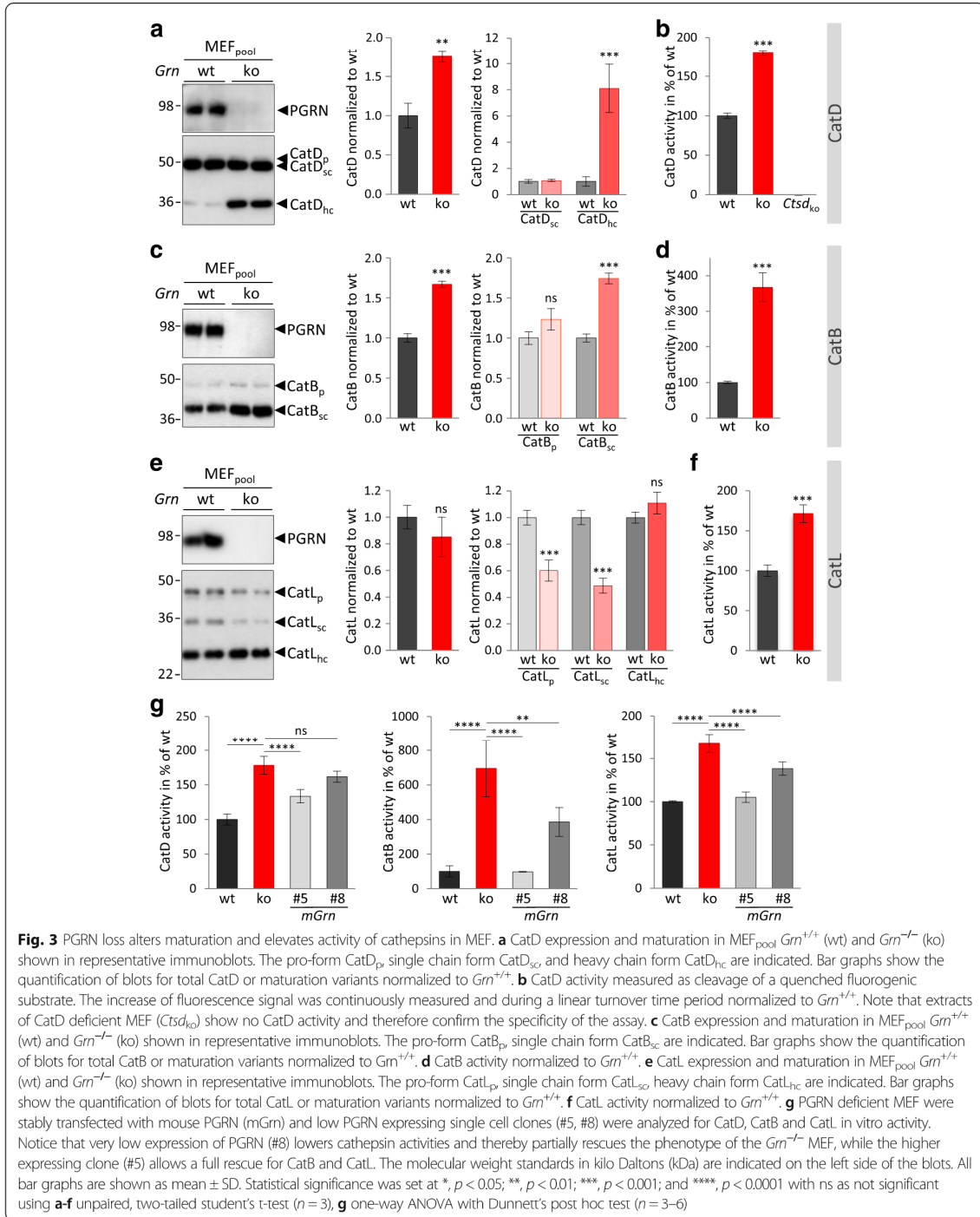
Elevated cathepsin maturation and activity in PGRN deficient mouse brain

We have previously shown that cathepsin D (CatD) is elevated in brain of young $Grn^{-/-}$ mice and that CatD accumulation further increases with age [18]. These findings have been confirmed [12, 51], but the origin of CatD increase remains mainly unclear and cannot simply be explained as a compensation phenomenon in response to general reduced expression of lysosomal enzymes (Fig. 1). To address whether elevated *Ctsd* mRNA levels (Fig. 1b; Additional file 1: Figure S1) translate into increased protein levels and result in enhanced enzyme activity, we analyzed protein expression, maturation and in vitro activity of CatD in brain of 3- and 20-month-old mice (Fig. 2b-e). To further monitor lysosomal activity in $Grn^{-/-}$ mice we also investigated protein expression, maturation and catalytic activity of two additional cathepsins, namely CatB (Fig. 2f-i) and CatL (Fig. 2j-m). Both lysosomal cysteine proteases have been associated with PGRN metabolism. CatL might be directly involved in lysosomal processing of PGRN into granulins [31] and CatL and CatB cleave and inactivate the secretory leucoprotease inhibitor (SLPI) which protects extracellular PGRN from processing [52]. Maturation and activation of most cathepsins follows a unified processing pathway generating active single and double chain variants (Fig. 2a) (reviewed in [53]). In 3-month-old $Grn^{-/-}$ mice, CatD expression, maturation and activity was unchanged (Fig. 2b, c; Additional file 1: Figure S1). In aged mice (20 months) active single chain CatD (CatD$_{sc}$) as well as further processed heavy chain CatD (CatD$_{hc}$) are about 4- to 5-fold increased (Fig. 2d). This is accompanied by a 1.75-fold elevated proteolytic activity in $Grn^{-/-}$ mice brain (Fig. 2e). In contrast to the robust increase of the CatD protein levels, we could only detect a 2-fold increase of mRNA (Additional file 1: Figure S1) suggesting posttranscriptional regulatory mechanisms. CatB and CatL are slightly elevated in young $Grn^{-/-}$ mice (Fig. 2f, j) but no significant change in their catalytic activity was observed (Fig. 2g, k). Their mRNA levels were not altered (CatB) or only slightly elevated (CatL)

(Additional file 1: Figure S1). In aged $Grn^{-/-}$ mice, CatB and CatL expression, processing and activity were elevated (Fig. 2h, i, l, m; Additional file 1: Figure S1). Thus, against the expectations that lysosomal activity might be decreased in $Grn^{-/-}$ mice, their proteolytic in vitro activity is elevated in total brain lysates.

Increased activity of cathepsins in mouse embryonic fibroblasts (MEF) lacking PGRN

MEF generated from $Grn^{+/+}$ show a robust localization of PGRN in lysosomes (Additional file 1: Figure S2a), while MEF generated from $Grn^{-/-}$ littermates show an increase of LAMP1 and an accumulation of saposin D, which is in line with our previous observations in brains of $Grn^{-/-}$ mice and FTLD/GRN patients [18] (Additional file 1: Figure S2b). We next examined the in vitro activity and maturation of CatD, CatB and CatL in $Grn^{-/-}$ and $Grn^{+/+}$ MEF (Fig. 3). In $Grn^{-/-}$ MEF the overall CatD level was 1.7-fold elevated. Moreover, CatD$_{hc}$ was increased about eight fold whereas CatD$_{sc}$ expression was not altered (Fig. 3a). The elevated protein level of CatD$_{hc}$ is in line with a significantly enhanced in vitro enzymatic activity (Fig. 3b). A second independent pool of MEF $Grn^{-/-}$ as well as single cell clones additionally confirmed altered maturation and elevated levels of CatD$_{hc}$ (Additional file 1: Figure S2c, d). Similar to mouse brain, CatB and CatL showed altered maturation (Fig. 3c, e) and a robust increase of in vitro activity (Fig. 3d, f). Low amounts of stably expressed PGRN were sufficient to rescue altered maturation of CatD and to lower hyperactivity of cathepsins (Fig. 3g, Additional file 1: Figure S3a, b). Thus, MEF, like total brain extract of $Grn^{-/-}$ mice, exhibit increased cathepsin expression, maturation and in vitro activity. To investigate the functional consequences of enhanced lysosomal activity we compared general protein degradation in $Grn^{-/-}$ and $Grn^{+/+}$ MEF. Newly synthesized proteins were metabolically pulse labeled for one hour and chased for indicated periods of time (Fig. 4a). The relative protein turnover calculated by the percentage of remaining radiolabeled protein was higher in $Grn^{-/-}$ MEF compared to

Götzl *et al. Molecular Neurodegeneration* (2018) 13:48

Page 8 of 16

Fig. 3 PGRN loss alters maturation and elevates activity of cathepsins in MEF. **a** CatD expression and maturation in MEF$_{pool}$ *Grn*$^{+/+}$ (wt) and *Grn*$^{-/-}$ (ko) shown in representative immunoblots. The pro-form CatD$_p$, single chain form CatD$_{sc}$, and heavy chain form CatD$_{hc}$ are indicated. Bar graphs show the quantification of blots for total CatD or maturation variants normalized to *Grn*$^{+/+}$. **b** CatD activity measured as cleavage of a quenched fluorogenic substrate. The increase of fluorescence signal was continuously measured and during a linear turnover time period normalized to *Grn*$^{+/+}$. Note that extracts of CatD deficient MEF (*Ctsd*$_{ko}$) show no CatD activity and therefore confirm the specificity of the assay. **c** CatB expression and maturation in MEF$_{pool}$ *Grn*$^{+/+}$ (wt) and *Grn*$^{-/-}$ (ko) shown in representative immunoblots. The pro-form CatB$_p$, single chain form CatB$_{sc}$ are indicated. Bar graphs show the quantification of blots for total CatB or maturation variants normalized to Grn$^{+/+}$. **d** CatB activity normalized to *Grn*$^{+/+}$. **e** CatL expression and maturation in MEF$_{pool}$ *Grn*$^{+/+}$ (wt) and *Grn*$^{-/-}$ (ko) shown in representative immunoblots. The pro-form CatL$_p$, single chain form CatL$_{sc}$, heavy chain form CatL$_{hc}$ are indicated. Bar graphs show the quantification of blots for total CatL or maturation variants normalized to *Grn*$^{+/+}$. **f** CatL activity normalized to *Grn*$^{+/+}$. **g** PGRN deficient MEF were stably transfected with mouse PGRN (mGrn) and low PGRN expressing single cell clones (#5, #8) were analyzed for CatD, CatB and CatL in vitro activity. Notice that very low expression of PGRN (#8) lowers cathepsin activities and thereby partially rescues the phenotype of the *Grn*$^{-/-}$ MEF, while the higher expressing clone (#5) allows a full rescue for CatB and CatL. The molecular weight standards in kilo Daltons (kDa) are indicated on the left side of the blots. All bar graphs are shown as mean ± SD. Statistical significance was set at *, $p < 0.05$; **, $p < 0.01$; ***, $p < 0.001$; and ****, $p < 0.0001$ with ns as not significant using **a-f** unpaired, two-tailed student's t-test ($n = 3$), **g** one-way ANOVA with Dunnett's post hoc test ($n = 3-6$)

Grn$^{+/+}$ MEF (Fig. 4a). In particular, during the first 24 h protein degradation is elevated in *Grn*$^{-/-}$ MEF (Fig. 4a). Elevated lysosomal protein turnover in PGRN deficient MEF was also indicated by lower steady state levels of proteins degraded by lysosomes such as APP and its CTF [54–57] (Fig. 4b), while the *App* mRNA level is not altered in *Grn*$^{-/}$
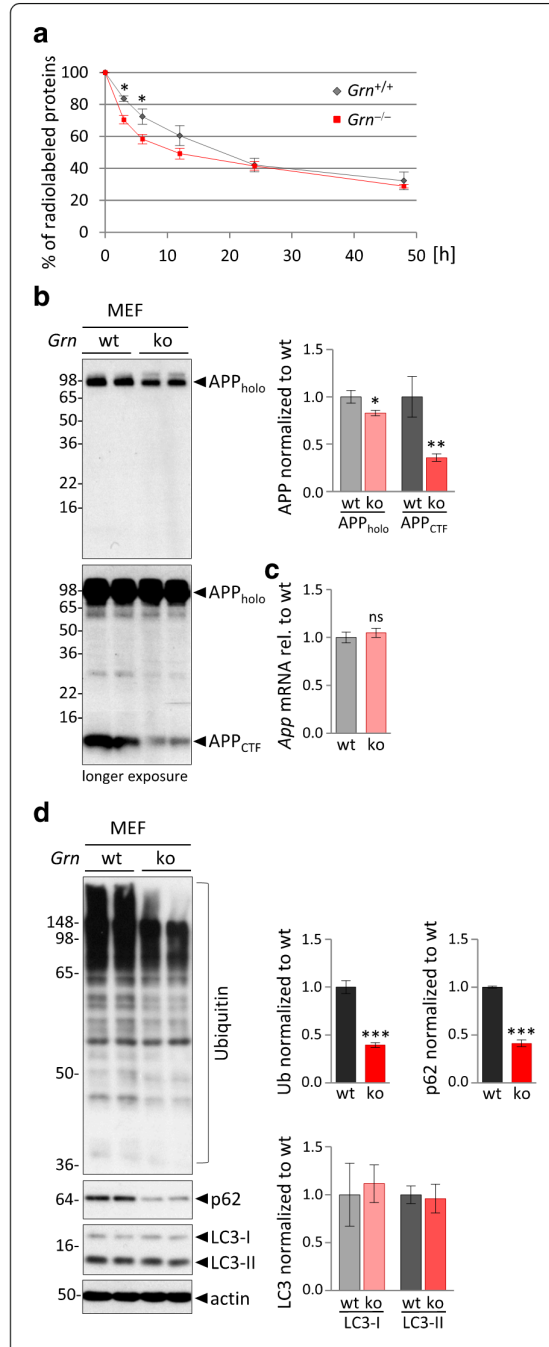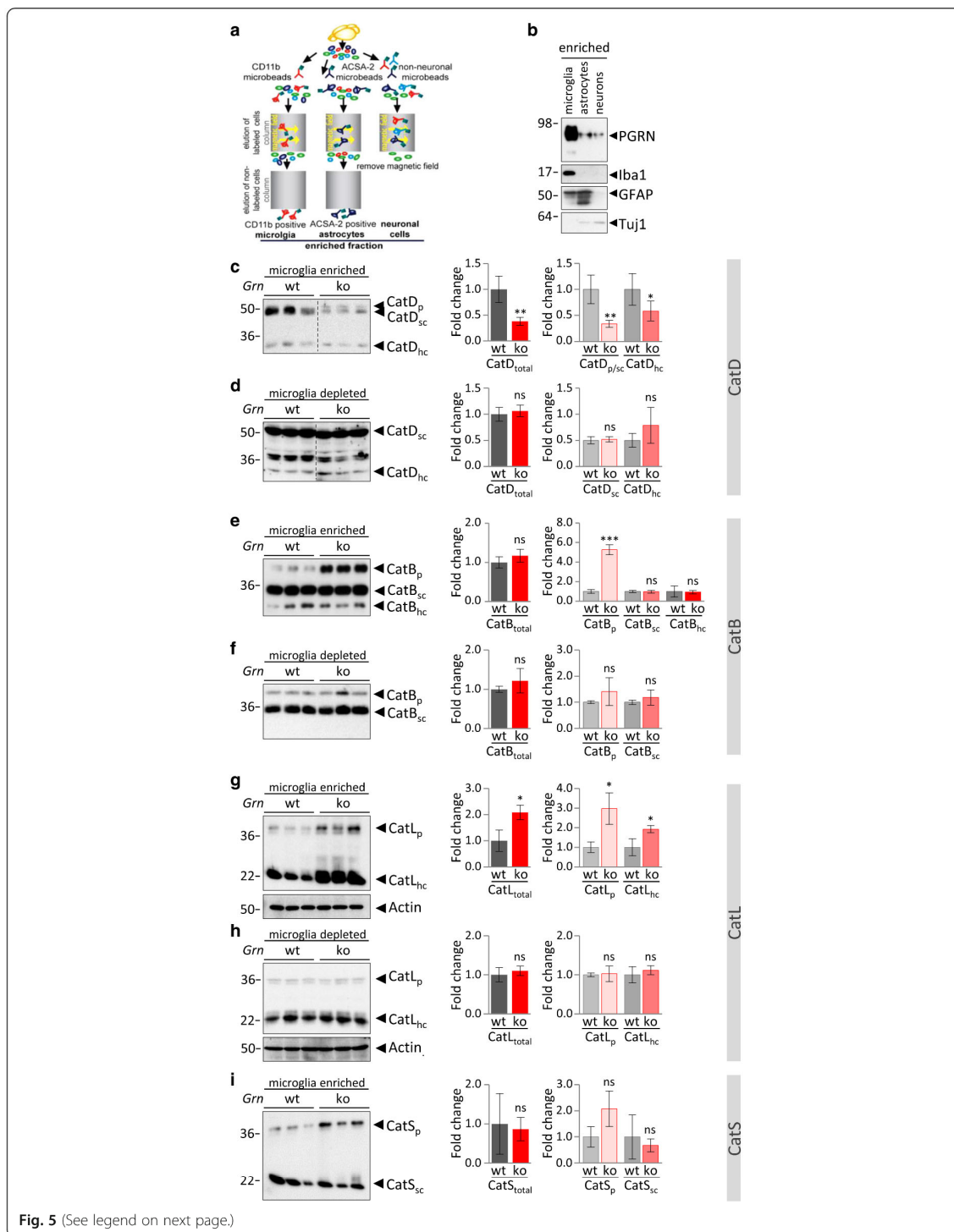
Götzl *et al. Molecular Neurodegeneration* (2018) 13:48

Page 9 of 16

Fig. 4 Elevated lysosomal activity results in enhanced fast protein degradation in $Grn^{-/-}$ MEF. **a** Turnover of ^{35}S-methionine radiolabeled proteins. MEF at 70–80% confluency were metabolically pulse-labeled with ^{35}S-methionine/cysteine for 1 h, followed by indicated chase periods. Radioactivity of ^{35}S-labeled proteins at chase time point 0 h was set to 100% and remaining radioactive-labeled proteins at later chase points were normalized to the initial radioactivity at time point 0 h. For statistical analysis the unpaired, two-tailed student's t-test was used to compare $Grn^{-/-}$ to $Grn^{+/+}$ MEF ($n = 5$), (*, $p < 0.05$). **b** APP holoprotein (APP$_{holo}$) and C-terminal fragments (APP$_{CTF}$) detected by immunoblotting of MEF$_{pool}$ $Grn^{+/+}$ (wt) and $Grn^{-/-}$ (ko) lysates. The molecular weight standards in kilo Daltons (kDa) are indicated on the left side of the blots. Bar graphs show the quantification of the blots for APP$_{holo}$ and APP$_{CTF}$ normalized to $Grn^{+/+}$ (wt) as mean ± SD. **c** Quantification of *App* mRNA of MEF$_{pool}$ $Grn^{-/-}$ (ko) normalized to $Grn^{+/+}$ (wt) as mean ± SD. **d** Ubiquitin (Ub), p62, LC3-I and LC3-II detected by immunoblotting of MEF$_{pool}$ $Grn^{+/+}$ (wt) and $Grn^{-/-}$ (ko) lysates. Bar graphs show the quantification of the blots normalized to wt as mean ± SD. **b-d** For statistical analysis the unpaired, two-tailed student's t-test was used to compare ko to wt cells (n = 3) (*, $p < 0.05$; **, $p < 0.01$; ***, $p < 0.001$; ns, not significant)

$^-$ MEF (Fig. 4c). To address the question whether autophagy is altered by PGRN deficiency, we analyzed ubiquitin and the adapter protein p62/SQSTM1 levels in $Grn^{-/-}$ MEF. Interestingly, we detect reduced levels of ubiquitinated proteins and p62 in $Grn^{-/-}$ MEF compared to $Grn^{+/+}$ MEF but no change in autophagy marker LC3I and LC3II (Fig. 4d). Thus, we do not find evidence that enhanced autophagosome formation contributes to the enhanced lysosomal degradation in $Grn^{-/-}$ MEF (Fig. 4a). Having observed an increased activity of cathepsins as well as enhanced lysosomal protein degradation in $Grn^{-/-}$ MEF, we asked whether PGRN or the proteolytically generated granulin peptides are direct inhibitors of lysosomal cathepsins. To do so, recombinant PGRN, granulin peptides generated by elastase digestion of PGRN or recombinant granulin E were added to in vitro cathepsin activity assays using lysates derived from $Grn^{-/-}$ MEF (Additional file 1: Figure S4). None of the PGRN variants added to the in vitro assays had a significant effect on proteolytic activity suggesting that cathepsins may not be directly inhibited by an interaction with PGRN or the granulin peptides.

Selective impairment of lysosomal processing of cathepsins in microglia upon PGRN deficiency

Enhanced lysosomal activity of cathepsins in $Grn^{-/-}$ MEF and total brain homogenates of $Grn^{-/-}$ mice is contradictory to impaired protein degradation and accumulation of lipofuscin and NCL storage components caused by PGRN deficiency. Therefore, we analyzed the consequence of PGRN deficiency in microglia, which are known to express more than 50-fold higher levels of *Grn* mRNA as compared to neurons [58, 59]. We hypothesized that PGRN depletion may cause cell autonomous
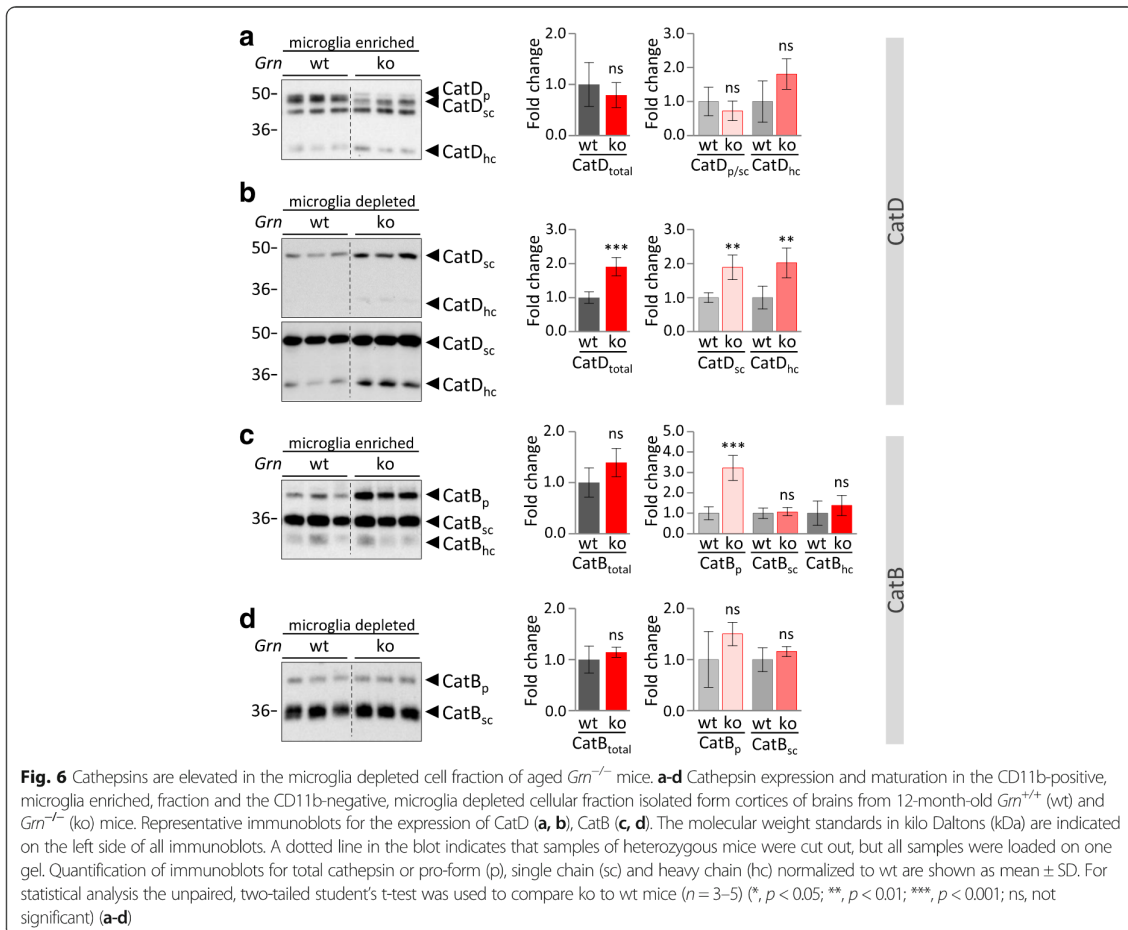
Götzl *et al. Molecular Neurodegeneration* (2018) 13:48

Page 10 of 16

Fig. 5 (See legend on next page.)

Götzl *et al. Molecular Neurodegeneration* (2018) 13:48

Page 11 of 16

(See figure on previous page.)

Fig. 5 Cathepsin maturation is selectively impaired in $Grn^{-/-}$ microglia. **a** Schematic representation of the brain cell isolation using MACS Technology (Miltenyi Biotec) **b** PGRN expression in acutely isolated microglia, astrocytes and neurons enriched fractions of 4- month-old wt mice detected by immunoblotting. The identity of neural cell types was verified by detection of Iba1 for microglia, GFAP for astrocytes and Tuj1 for neurons. **c-i** Cathepsin expression and maturation in the CD11b-positive, microglia enriched, fraction and the CD11b-negative, microglia depleted cellular fraction isolated form cortices of brain from 3-month-old $Grn^{+/+}$ (wt) and $Grn^{-/-}$ (ko) mice. Representative immunoblots for the cathepsin expression of CatD (**c, d**), CatB (**e, f**), CatL (**g, h**) and for CatS (**i**) (only microglia enriched fraction). The molecular weight standards in kilo Daltons (kDa) are indicated on the left side of all immunoblots. A dotted line in the blot indicates that samples of heterozygous mice were cut out, but all samples were loaded on one gel. Quantification of immunoblots for total cathepsin or maturation variants pro-form (p), single chain (sc) and heavy chain (hc) normalized to wt are shown as mean ± SD. For statistical analysis the unpaired, two-tailed student's t-test was used to compare ko to wt mice (n = 3–5) (*, $p < 0.05$; **, $p < 0.01$; ***, $p < 0.001$; ns, not significant) (**c-i**)

effects in microglia, which could be different to the majority of the non-microglial brain cell population. First, to confirm predominant PGRN protein expression in microglia, we performed immunoblots on lysates of acutely isolated microglia, astrocytes and neurons from adult wildtype mouse brain (Fig. 5a). This fully confirmed that PGRN is most robustly expressed in microglia (Fig. 5b). To address whether PGRN deficiency results in cell autonomous alterations of lysosomal function in microglia, we analyzed protein expression and maturation of selected cathepsins in acutely isolated microglia. Strikingly, microglia isolated from 3-month-old $Grn^{-/-}$ mice show impaired maturation of cathepsins and an accumulation of inactive pro-forms of CatD, CatB, CatL and CatS (Fig. 5c, e, g, i). For CatB and CatL, the pro-form is significantly elevated (Fig. 5e, g). The relative increase of
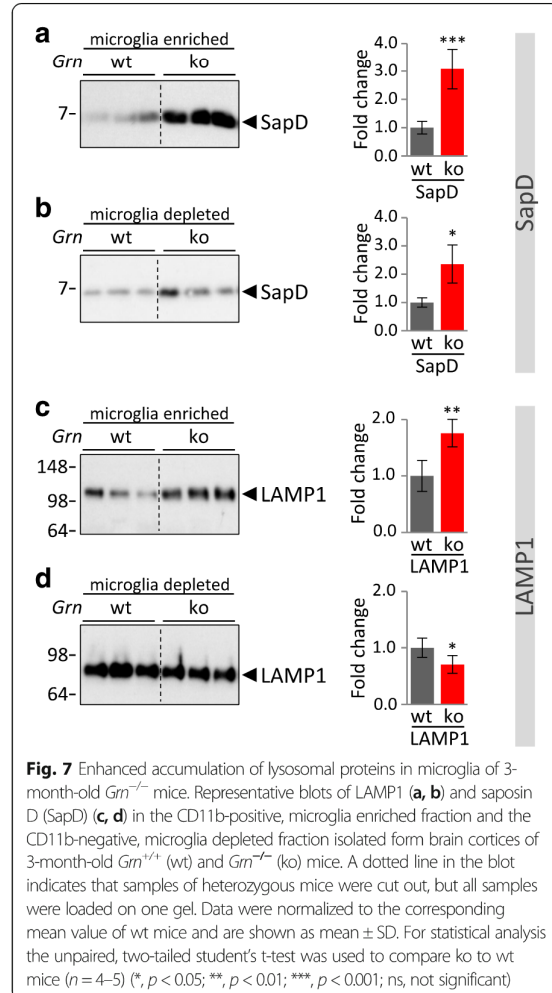

Fig. 6 Cathepsins are elevated in the microglia depleted cell fraction of aged $Grn^{-/-}$ mice. **a-d** Cathepsin expression and maturation in the CD11b-positive, microglia enriched, fraction and the CD11b-negative, microglia depleted cellular fraction isolated form cortices of brains from 12-month-old $Grn^{+/+}$ (wt) and $Grn^{-/-}$ (ko) mice. Representative immunoblots for the expression of CatD (**a, b**), CatB (**c, d**). The molecular weight standards in kilo Daltons (kDa) are indicated on the left side of all immunoblots. A dotted line in the blot indicates that samples of heterozygous mice were cut out, but all samples were loaded on one gel. Quantification of immunoblots for total cathepsin or pro-form (p), single chain (sc) and heavy chain (hc) normalized to wt are shown as mean ± SD. For statistical analysis the unpaired, two-tailed student's t-test was used to compare ko to wt mice (n = 3–5) (*, $p < 0.05$; **, $p < 0.01$; ***, $p < 0.001$; ns, not significant) (**a-d**)

Götzl *et al. Molecular Neurodegeneration* (2018) 13:48

Page 12 of 16

CatD$_p$ in $Grn^{-/-}$ could not be quantified since CatD$_p$ cannot be detected in $Grn^{+/+}$ microglia. Despite a general increase of pro-cathepsins, the levels of mature cathepsins are differentially affected by the loss of PGRN. Thus, the total protein level of CatD and the potentially active forms CatD$_{sc}$ and CatD$_{hc}$ are significantly reduced in microglia of $Grn^{-/-}$ (Fig. 5c). However a significantly reduced in vitro activity of CatD could not be detected (Additional file 1: Figure S5a). For the other analyzed cathepsins the total level is unchanged (CatB, CatS) (Fig. 5e, i) or even elevated (CatL) (Fig. 5g). In the microglia depleted fraction isolated from 3-month-old mice, no significant differences of cathepsin maturation, expression level or activity between $Grn^{-/-}$ and $Grn^{+/+}$ can be observed (Fig. 5d, f, h; Additional file 1: Figure S5a), whereas in the microglia depleted fraction of 12-month-old mice CatD is significantly elevated in $Grn^{-/-}$ (Fig. 6b) which results in enhanced CatD activity (Additional file 1: Figure S5b). However, in microglia of 12-month-old $Grn^{-/-}$ mice altered expression levels of CatD and CatB are not further enhanced but rather slightly reduced (Fig. 6a, c), e.g. immature CatB$_p$ shifts from an almost 6-fold increase in 3-month-old mice to an 3-fold increase in 12-month-old mice (Fig. 6c). In line with altered processed or reduced lysosomal cathepsins specifically in microglia, LAMP1 and saposin D accumulation occurred exclusively (LAMP1) or more robust (saposin D) in the microglia enriched fraction compared to the microglia depleted fraction isolated from 3-month-old mice (Fig. 7a-c).

Thus our data indicate that microglia and the remaining neural cell populations show fundamentally different lysosomal phenotypes upon PGRN deficiency.

Discussion

Accumulating evidence suggests that impaired lysosomal protein degradation plays a major role in FTLD-TDP [15]. Lysosomal dysfunction seems to be specifically associated with FTLD-TDP caused by *GRN* haploinsufficiency [18]. Furthermore total loss of PGRN leads to NCL (CLN11) [3], a lysosomal storage disease with severe neurodegeneration. However, it is still unknown if and how PGRN affects lysosomal homeostasis. Based on the selective expression of GRN in microglia (Fig. 5b) [51, 58, 59], we now searched for cell autonomous and non-cell autonomous deficits upon loss of PGRN.

We provide strong evidence that loss of PGRN selectively impairs lysosomal function in microglia. Microglia isolated from 3-month-old $Grn^{-/-}$ mice showed strongly reduced CatD levels compared to microglia isolated from $Grn^{+/+}$ mice, which surprisingly did not result in a significantly reduced in vitro activity. However, impaired maturation might not be reflected by the in vitro activity assay since defective CatD maturation and catalytic activity could be hidden by optimal in vitro conditions. In addition, maturation of CatB, CatL and CatS was
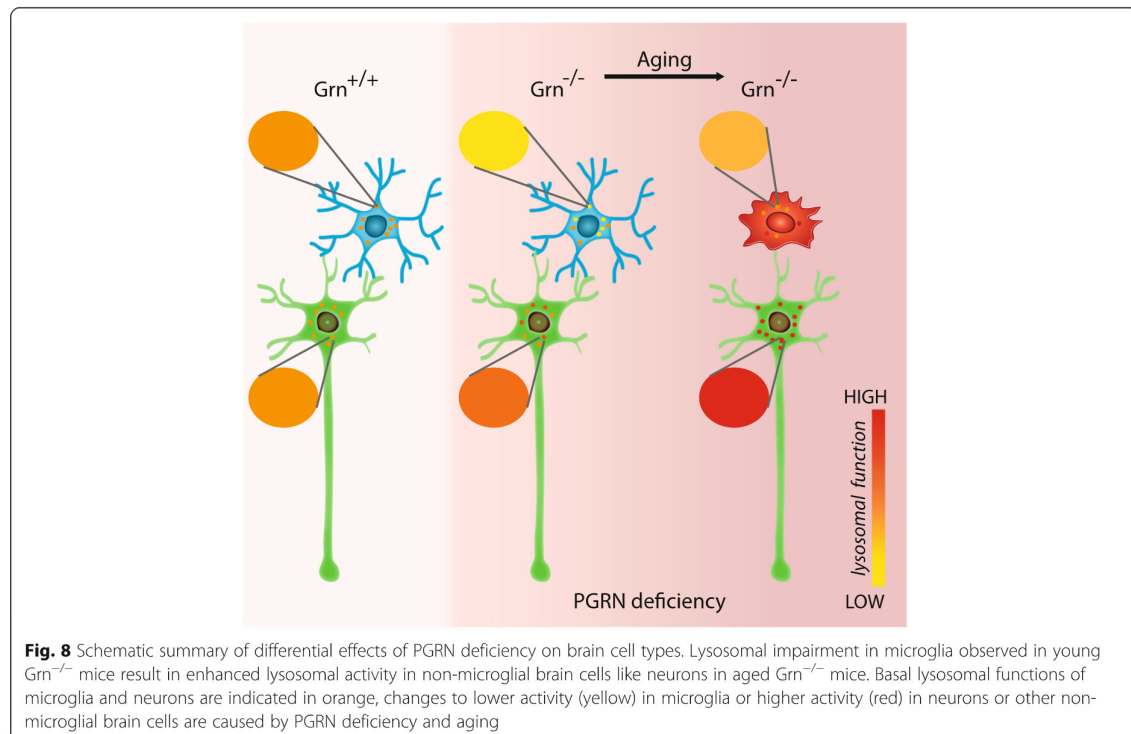

Fig. 7 Enhanced accumulation of lysosomal proteins in microglia of 3-month-old $Grn^{-/-}$ mice. Representative blots of LAMP1 (**a, b**) and saposin D (SapD) (**c, d**) in the CD11b-positive, microglia enriched fraction and the CD11b-negative, microglia depleted fraction isolated form brain cortices of 3-month-old $Grn^{+/+}$ (wt) and $Grn^{-/-}$ (ko) mice. A dotted line in the blot indicates that samples of heterozygous mice were cut out, but all samples were loaded on one gel. Data were normalized to the corresponding mean value of wt mice and are shown as mean ± SD. For statistical analysis the unpaired, two-tailed student's t-test was used to compare ko to wt mice (n = 4–5) (*, $p < 0.05$; **, $p < 0.01$; ***, $p < 0.001$; ns, not significant)

impaired. In contrast, in the microglia depleted fraction, isolated from the same 3-month-old $Grn^{-/-}$ mice, no altered cathepsin expression or maturation was observed. Furthermore, during ageing saposin D and LAMP1 accumulated earlier and to a higher extent in the microglia enriched fraction than in the microglia depleted fraction. Our finding that impaired maturation of lysosomal enzymes in microglia already occurs in early adulthood before other pathological hallmarks suggests that lysosomal dysfunction may be a primary consequence upon loss of PGRN expression. Thus, our findings suggest a cell autonomous reduction of lysosomal function caused by PGRN deficiency in microglia, which as a consequence appears to culminate during ageing in a compensatory upregulation of lysosomal activity selectively in non-microglial cells. Indeed, in the microglia depleted fraction isolated from aged $Grn^{-/-}$ mice CatD single and

Götzl *et al. Molecular Neurodegeneration* (2018) 13:48

Page 13 of 16

heavy chain are 2-fold and CatD in vitro activity is 2.5-fold elevated compared to $Grn^{+/+}$ mice. Our findings are supported by the observation that cultured neurons from $Grn^{-/-}$ mice show enhanced lysosomal proteolysis [51]. Moreover, in brain tissue of FTLD-TDP patients CatD is accumulating in neurons [21]. In line with enhanced cathepsin expression in non-microglial cells, mRNA, protein levels and in vitro activities of CatD, CatB, and CatL were increased in total brain of aged $Grn^{-/-}$ mice. Furthermore, in line with recent findings [21, 38, 40, 51, 59, 60], a subset of lysosomal proteases and membrane proteins were upregulated in 6- and 12-month-old $Grn^{-/-}$ mice. In addition to altered cathepsin levels, we demonstrate altered proteolytic processing and maturation of CatD, CatB, and CatL in the microglia enriched fraction, total brain lysates and MEF of $Grn^{-/-}$ mice. While in microglia proteolytic inactive pro-forms accumulate, potentially active single chain or heavy chain variants accumulate in total brain and MEF in accordance with increased in vitro activity. For example, robustly enhanced levels of the $CatD_{hc}$ variant are observed in $Grn^{-/-}$ MEF which is in line with findings by Tanaka et al. [21]. Previous research revealed enhanced [51, 59] as well reduced lysosomal enzyme activities [38, 39] in various $Grn^{-/-}$ cells types or tissue.

Based on our findings, these discrepancies may be explained by different cell types analyzed, difficulties with the determination of specific activities of lysosomal enzymes due to their complex proteolytic processing and consequences for their proteolytic activity [53, 61]. Single chain variants as well as dimeric variants of heavy and light chain are catalytically active whereas separated heavy and light chains are inactive [53, 61]. Since we cannot determine the amount of active species, we cannot calculate the specific activity. Indeed, in total brain of $Grn^{-/-}$ mice the increase of CatD protein is much stronger than the increase in enzyme activity which might indicate reduced specific activity as previously shown for CatD [38, 39]. However, it is unlikely that PGRN directly affects the specific activity of lysosomal proteases, because in our hands, adding PGRN, elastase digested PGRN, or granulin E to the in vitro activity assays of CatD, CatB, and CatL did not alter their activity. This might indicate that PGRN most likely modulates maturation and turnover of cathepsins.

In MEF, enhanced cathepsin activities are reversible by low expression levels of PGRN. Rescue of the lysosomal phenotype of $Grn^{-/-}$ by a very minor amount of PGRN is in line with recent data showing that low levels of AAV-expressed neuronal PGRN are sufficient to rescue

Fig. 8 Schematic summary of differential effects of PGRN deficiency on brain cell types. Lysosomal impairment in microglia observed in young $Grn^{-/-}$ mice result in enhanced lysosomal activity in non-microglial brain cells like neurons in aged $Grn^{-/-}$ mice. Basal lysosomal functions of microglia and neurons are indicated in orange, changes to lower activity (yellow) in microglia or higher activity (red) in neurons or other non-microglial brain cells are caused by PGRN deficiency and aging

Götzl *et al. Molecular Neurodegeneration* (2018) 13:48

Page 14 of 16

lysosomal phenotypes of *Grn* knockout mice [62]. Moreover, this also provides additional support for the lack of lysosomal abnormalities in heterozygous, neuronal or incomplete microglial *Grn* knockout mouse models [63, 64]. Finally, elevated catalytic activities of cathepsins result in enhanced protein turnover in $Grn^{-/-}$ MEF, which indicates enhanced protein degradation in lysosomes. In line with enhanced lysosomal degradation, levels of lysosomal targeted proteins such as mature APP and its CTF are significantly reduced in $Grn^{-/-}$ MEF while LC3I and LC3II levels are unchanged. Only under cellular stress impaired autophagy or altered autophagic flux has been reported for bone marrow derived macrophages (BMDM) [40].

The cell type dependent effects of PGRN deficiency in microglial and non-microglial cells could be caused by different lysosomal gene expression signatures in microglia/monocytes compared to other brain cells. Microglia not only express more and higher levels of lysosomal enzymes, they also express more and higher levels of lysosomal enzyme inhibitors. Thus regulation of lysosomal activity might be more complex in microglia. Further work needs to be done to elucidate how PGRN modulates cathepsin activities and which role lysosomal generated granulins play [31, 32]. With this work we provide strong evidence that PGRN plays a role as modulator of lysosomal activity by affecting maturation of lysosomal cathepsins. Such a function has been suggested for granulin-like domains located at the C-terminus of papain-like cysteine protease in plants [65–67]. Here, the granulin domain might slow maturation of the protease. Furthermore, the granulin domain must be proteolytically removed to allow full maturation [68, 69].

Finally, the divergent effects of PGRN deficiency in microglial and non-microglial cells not only provide evidence for differential cell autonomous and non-autonomous activities of PGRN, but also suggest a crosstalk of microglia with other cell types throughout the brain. Interestingly, we [70] and others [71] previously found that microglial loss-of-function mutations in *TREM2* affect energy metabolism throughout the entire brain. Again, a rather small percentage of brain cells seemed to influence metabolism throughout the entire brain.

Conclusions

We conclude that PGRN deficiency leads to cell autonomous altered maturation and turnover of lysosomal cathepsins with cell type dependent differences and consequences. In particular in microglia, PGRN deficiency results in accumulation of inactive cathepsin pro-forms, while in other brain cells and in MEF, variants with increased catalytic activities were found. We speculate that impaired lysosomal function in microglia caused by PGRN deficiency already in young adults is

likely responsible for impaired protein degradation and lipofuscin accumulation. With aging of $Grn^{-/-}$ mice, non-microglial brain cells try to compensate decreased protein degradation by microglia, with enhanced expression of selective cathepsins as shown for CatD, CatB and CatL (Fig. 8).

Additional files

Additional file 1: Figure S1. Elevated transcript levels of cathepsins in aged $Grn^{-/-}$ mice. **Figure S2.** PGRN loss results in accumulation of LAMP1 and saposin D in MEF. **Figure S3.** Altered maturation of CatD and activity of cathepsins can be rescued by stable PGRN expression. **Figure S4.** PGRN, elastase digested PGRN and granulin E do not affect in vitro activity of cathepsins. **Figure S5.** Selectively enhanced CatD in vitro activity in non-microglial brain cells of aged $Grn^{-/-}$ mice. (PPTX 1753 kb)

Additional file 2: Table S1. mRNA expression of selected genes associated with the lysosome-autophagy degradation pathway in brain of Grn+/+ and Grn−/− mice at 6 and 12 months of age. (XLSX 30 kb)

Götzl *et al. Molecular Neurodegeneration* (2018) 13:48

Page 15 of 16

Competing interests

C.H. collaborates with Denali Therapeutics. The authors declare that they have no competing interests.

Publisher's Note

Springer Nature remains neutral with regard to jurisdictional claims in published maps and institutional affiliations.

Author details

[1]Chair of Metabolic Biochemistry, Biomedical Center (BMC), Faculty of Medicine, Ludwig-Maximilians-Universität München, 81377 Munich, Germany. [2]German Center for Neurodegenerative Diseases (DZNE) Munich, 81377 Munich, Germany. [3]Munich Cluster for Systems Neurology (SyNergy), 81377 Munich, Germany.

References

1. Cruts M, Gijselinck I, van der Zee J, Engelborghs S, Wils H, Pirici D, Rademakers R, Vandenberghe R, Dermaut B, Martin JJ, et al. Null mutations in progranulin cause ubiquitin-positive frontotemporal dementia linked to chromosome 17q21. Nature. 2006;442(7105):920–4.
2. Baker M, Mackenzie IR, Pickering-Brown SM, Gass J, Rademakers R, Lindholm C, Snowden J, Adamson J, Sadovnick AD, Rollinson S, et al. Mutations in progranulin cause tau-negative frontotemporal dementia linked to chromosome 17. Nature. 2006;442(7105):916–9.
3. Smith KR, Damiano J, Franceschetti S, Carpenter S, Canafoglia L, Morbin M, Rossi G, Pareyson D, Mole SE, Staropoli JF, et al. Strikingly different clinicopathological phenotypes determined by progranulin-mutation dosage. Am J Hum Genet. 2012;90(6):1102–7.
4. Almeida MR, Macario MC, Ramos L, Baldeiras I, Ribeiro MH, Santana I. Portuguese family with the co-occurrence of frontotemporal lobar degeneration and neuronal ceroid lipofuscinosis phenotypes due to progranulin gene mutation. Neurobiol Aging. 2016;41:200 e1-5.
5. Finch N, Baker M, Crook R, Swanson K, Kuntz K, Surtees R, Bisceglio G, Rovelet-Lecrux A, Boeve B, Petersen RC, et al. Plasma progranulin levels predict progranulin mutation status in frontotemporal dementia patients and asymptomatic family members. Brain. 2009;132(3):583–91.
6. Sleegers K, Brouwers N, Van Damme P, Engelborghs S, Gijselinck I, van der Zee J, Peeters K, Mattheijssens M, Cruts M, Vandenberghe R, et al. Serum biomarker for progranulin-associated frontotemporal lobar degeneration. Ann Neurol. 2009;65(5):603–9.
7. Ghidoni R, Benussi L, Glionna M, Franzoni M, Binetti G. Low plasma progranulin levels predict progranulin mutations in frontotemporal lobar degeneration. Neurology. 2008;71(16):1235–9.
8. Carcel-Trullols J, Kovacs AD, Pearce DA. Cell biology of the NCL proteins: what they do and don't do. Biochim Biophys Acta. 2015;1852(10):2242–55.
9. Ahmed Z, Sheng H, Xu YF, Lin WL, Innes AE, Gass J, Yu X, Wuertzer CA, Hou H, Chiba S, et al. Accelerated lipofuscinosis and ubiquitination in granulin knockout mice suggest a role for progranulin in successful aging. Am J Pathol. 2010;177(1):311–24.
10. Wils H, Kleinberger G, Pereson S, Janssens J, Capell A, Van Dam D, Cuijt I, Joris G, De Deyn PP, Haass C, et al. Cellular ageing, increased mortality and FTLD-TDP-associated neuropathology in progranulin knockout mice. J Pathol. 2012;228(1):67–76.
11. Yin F, Banerjee R, Thomas B, Zhou P, Qian L, Jia T, Ma X, Ma Y, Iadecola C, Beal MF, et al. Exaggerated inflammation, impaired host defense, and neuropathology in progranulin-deficient mice. J Exp Med. 2010;207(1):117–28.
12. Tanaka Y, Chambers JK, Matsuwaki T, Yamanouchi K, Nishihara M. Possible involvement of lysosomal dysfunction in pathological changes of the brain in aged progranulin-deficient mice. Acta Neuropathol Commun. 2014;2:78.
13. Petkau TL, Neal SJ, Milnerwood A, Mew A, Hill AM, Orban P, Gregg J, Lu G, Feldman HH, Mackenzie IR, et al. Synaptic dysfunction in progranulin-deficient mice. Neurobiol Dis. 2012;45(2):711–22.
14. Ghoshal N, Dearborn JT, Wozniak DF, Cairns NJ. Core features of frontotemporal dementia recapitulated in progranulin knockout mice. Neurobiol Dis. 2012;45(1):395–408.
15. Gotzl JK, Lang CM, Haass C, Capell A. Impaired protein degradation in FTLD and related disorders. Ageing Res Rev. 2016;32:122–39.
16. Cairns NJ, Neumann M, Bigio EH, Holm IE, Troost D, Hatanpaa KJ, Foong C, White CL 3rd, Schneider JA, Kretzschmar HA, et al. TDP-43 in familial and sporadic frontotemporal lobar degeneration with ubiquitin inclusions. Am J Pathol. 2007;171(1):227–40.
17. Igaz LM, Kwong LK, Xu Y, Truax AC, Uryu K, Neumann M, Clark CM, Elman LB, Miller BL, Grossman M, et al. Enrichment of C-terminal fragments in TAR DNA-binding protein-43 cytoplasmic inclusions in brain but not in spinal cord of frontotemporal lobar degeneration and amyotrophic lateral sclerosis. Am J Pathol. 2008;173(1):182–94.
18. Gotzl JK, Mori K, Damme M, Fellerer K, Tahirovic S, Kleinberger G, Janssens J, van der Zee J, Lang CM, Kremmer E, et al. Common pathobiochemical hallmarks of progranulin-associated frontotemporal lobar degeneration and neuronal ceroid lipofuscinosis. Acta Neuropathol. 2014;127(6):845–60.
19. Ward ME, Chen R, Huang HY, Ludwig C, Telpoukhovskaia M, Taubes A, Boudin H, Minami SS, Reichert M, Albrecht P, et al. Individuals with progranulin haploinsufficiency exhibit features of neuronal ceroid lipofuscinosis. Sci Transl Med. 2017;9(385):eaah5642.
20. Terlizzi R, Valentino ML, Bartoletti-Stella A, Columbaro M, Piras S, Stanzani-Maserati M, Quadri M, Breedveld GJ, Bonifati V, Martinelli P, et al. Muscle ceroid lipofuscin-like deposits in a patient with corticobasal syndrome due to a progranulin mutation. Mov Disord. 2017;32(8):1259–60.
21. Tanaka Y, Suzuki G, Matsuwaki T, Hosokawa M, Serrano G, Beach TG, Yamanouchi K, Hasegawa M, Nishihara M. Progranulin regulates lysosomal function and biogenesis through acidification of lysosomes. Hum Mol Genet. 2017;26(5):969–88.
22. Capell A, Liebscher S, Fellerer K, Brouwers N, Willem M, Lammich S, Gijselinck I, Bittner T, Carlson AM, Sasse F, et al. Rescue of progranulin deficiency associated with frontotemporal lobar degeneration by alkalizing reagents and inhibition of vacuolar ATPase. J Neurosci. 2011;31(5):1885–94.
23. Belcastro V, Siciliano V, Gregoretti F, Mithbaokar P, Dharmalingam G, Berlingieri S, Iorio F, Oliva G, Polishchuck R, Brunetti-Pierri N, et al. Transcriptional gene network inference from a massive dataset elucidates transcriptome organization and gene function. Nucleic Acids Res. 2011;39(20):8677–88.
24. Zhou J, Gao G, Crabb JW, Serrero G. Purification of an autocrine growth factor homologous with mouse epithelin precursor from a highly tumorigenic cell line. J Biol Chem. 1993;268(15):10863–9.
25. Zhu J, Nathan C, Jin W, Sim D, Ashcroft GS, Wahl SM, Lacomis L, Erdjument-Bromage H, Tempst P, Wright CD, et al. Conversion of proepithelin to epithelins: roles of SLPI and elastase in host defense and wound repair. Cell. 2002;111(6):867–78.
26. He Z, Bateman A. Progranulin (granulin-epithelin precursor, PC-cell-derived growth factor, acrogranin) mediates tissue repair and tumorigenesis. J Mol Med. 2003;81(10):600–12.
27. Xu D, Suenaga N, Edelmann MJ, Fridman R, Muschel RJ, Kessler BM. Novel MMP-9 substrates in cancer cells revealed by a label-free quantitative proteomics approach. Mol Cell Proteomics. 2008;7(11):2215–28.
28. Butler GS, Dean RA, Tam EM, Overall CM. Pharmacoproteomics of a metalloproteinase hydroxamate inhibitor in breast cancer cells: dynamics of membrane type 1 matrix metalloproteinase-mediated membrane protein shedding. Mol Cell Biol. 2008;28(15):4896–914.
29. Bai XH, Wang DW, Kong L, Zhang Y, Luan Y, Kobayashi T, Kronenberg HM, Yu XP, Liu CJ. ADAMTS-7, a direct target of PTHrP, adversely regulates endochondral bone growth by associating with and inactivating GEP growth factor. Mol Cell Biol. 2009;29(15):4201–19.
30. Kessenbrock K, Frohlich L, Sixt M, Lammermann T, Pfister H, Bateman A, Belaaouaj A, Ring J, Ollert M, Fassler R, et al. Proteinase 3 and neutrophil elastase enhance inflammation in mice by inactivating antiinflammatory progranulin. J Clin Invest. 2008;118(7):2438–47.
31. Lee CW, Stankowski JN, Chew J, Cook CN, Lam YW, Almeida S, Carlomagno Y, Lau KF, Prudencio M, Gao FB, et al. The lysosomal protein cathepsin L is a progranulin protease. Mol Neurodegener. 2017;12(1):55.
32. Zhou X, Paushter DH, Feng T, Sun L, Reinheckel T, Hu F. Lysosomal processing of progranulin. Mol Neurodegener. 2017;12(1):62.
33. Hu F, Padukkavidana T, Vaegter CB, Brady OA, Zheng Y, Mackenzie IR, Feldman HH, Nykjaer A, Strittmatter SM. Sortilin-mediated endocytosis determines levels of the frontotemporal dementia protein, progranulin. Neuron. 2010;68(4):654–67.
34. Zhou X, Sun L, Bastos de Oliveira F, Qi X, Brown WJ, Smolka MB, Sun Y, Hu F. Prosaposin facilitates sortilin-independent lysosomal trafficking of progranulin. J Cell Biol. 2015;210(6):991–1002.
35. Gowrishankar S, Yuan P, Wu Y, Schrag M, Paradise S, Grutzendler J, De Camilli P, Ferguson SM. Massive accumulation of luminal protease-deficient

Götzl *et al. Molecular Neurodegeneration* (2018) 13:48

Page 16 of 16

axonal lysosomes at Alzheimer's disease amyloid plaques. Proc Natl Acad Sci U S A. 2015;112(28):E3699–708.

36. Tanaka Y, Matsuwaki T, Yamanouchi K, Nishihara M. Exacerbated inflammatory responses related to activated microglia after traumatic brain injury in progranulin-deficient mice. Neuroscience. 2013;231:49–60.

37. Tanaka Y, Matsuwaki T, Yamanouchi K, Nishihara M. Increased lysosomal biogenesis in activated microglia and exacerbated neuronal damage after traumatic brain injury in progranulin-deficient mice. Neuroscience. 2013;250:8–19.

38. Beel S, Moisse M, Damme M, De Muynck L, Robberecht W, Van Den Bosch L, Saftig P, Van Damme P. Progranulin functions as a cathepsin D chaperone to stimulate axonal outgrowth in vivo. Hum Mol Genet. 2017;26(15):2850–63.

39. Zhou X, Paushter DH, Feng T, Pardon CM, Mendoza CS, Hu F. Regulation of cathepsin D activity by the FTLD protein progranulin. Acta Neuropathol. 2017;134(1):151–3.

40. Chang MC, Srinivasan K, Friedman BA, Suto E, Modrusan Z, Lee WP, Kaminker JS, Hansen DV, Sheng M. Progranulin deficiency causes impairment of autophagy and TDP-43 accumulation. J Exp Med. 2017;214(9):2611–28.

41. Holler CJ, Taylor G, Deng Q, Kukar T. Intracellular proteolysis of Progranulin generates stable, lysosomal Granulins that are Haploinsufficient in patients with frontotemporal dementia caused by GRN mutations. eNeuro. 2017;4(4)

42. Kayasuga Y, Chiba S, Suzuki M, Kikusui T, Matsuwaki T, Yamanouchi K, Kotaki H, Horai R, Iwakura Y, Nishihara M. Alteration of behavioural phenotype in mice by targeted disruption of the progranulin gene. Behav Brain Res. 2007;185(2):110–8.

43. Saftig P, Hetman M, Schmahl W, Weber K, Heine L, Mossmann H, Koster A, Hess B, Evers M, von Figura K, et al. Mice deficient for the lysosomal proteinase cathepsin D exhibit progressive atrophy of the intestinal mucosa and profound destruction of lymphoid cells. EMBO J. 1995;14(15):3599–608.

44. Sharpless NE. Preparation and immortalization of primary murine cells. Cell Biology, Four-Volume Set. 2006:223–8.

45. Medina DL, Di Paola S, Peluso I, Armani A, De Stefani D, Venditti R, Montefusco S, Scotto-Rosato A, Prezioso C, Forrester A, et al. Lysosomal calcium signalling regulates autophagy through calcineurin and TFEB. Nat Cell Biol. 2015;17(3):288–99.

46. Sardiello M, Palmieri M, di Ronza A, Medina DL, Valenza M, Gennarino VA, Di Malta C, Donaudy F, Embrione V, Polishchuk RS, et al. A gene network regulating lysosomal biogenesis and function. Science. 2009;325(5939):473–7.

47. Palmieri M, Impey S, Kang H, di Ronza A, Pelz C, Sardiello M, Ballabio A. Characterization of the CLEAR network reveals an integrated control of cellular clearance pathways. Hum Mol Genet. 2011;20(19):3852–66.

48. Pena-Llopis S, Vega-Rubin-De-Celis S, Schwartz JC, Wolff NC, Tran TA, Zou L, Xie XJ, Corey DR, Brugarolas J. Regulation of TFEB and V-ATPases by mTORC1. EMBO J. 2011;30(16):3242–58.

49. Klein A, Henseler M, Klein C, Suzuki K, Harzer K, Sandhoff K. Sphingolipid activator protein D (sap-D) stimulates the lysosomal degradation of ceramide in vivo. Biochem Biophys Res Commun. 1994;200(3):1440–8.

50. Settembre C, Di Malta C, Polito VA, Garcia Arencibia M, Vetrini F, Erdin S, Erdin SU, Huynh T, Medina D, Colella P, et al. TFEB links autophagy to lysosomal biogenesis. Science. 2011;332(6036):1429–33.

51. Klein ZA, Takahashi H, Ma M, Stagi M, Zhou M, Lam TT, Strittmatter SM. Loss of TMEM106B ameliorates lysosomal and frontotemporal dementia-related phenotypes in Progranulin-deficient mice. Neuron. 2017;95(2):281–296 e6.

52. Taggart CC, Lowe GJ, Greene CM, Mulgrew AT, O'Neill SJ, Levine RL, McElvaney NG. Cathepsin B, L, and S cleave and inactivate secretory leucoprotease inhibitor. J Biol Chem. 2001;276(36):33345–52.

53. Erickson AH. Biosynthesis of lysosomal endopeptidases. J Cell Biochem. 1989;40(1):31–41.

54. Caporaso GL, et al. Chloroquine inhibits intracellular degradation but not secretion of Alzheimer beta/A4 amyloid precursor protein. Proc Natl Acad Sci. 1992;89(6):2252–6.

55. Golde TE, et al. Processing of the amyloid protein precursor to potentially amyloidogenic derivatives. Science. 1992;255(5045):728–30.

56. Haass C, et al. Targeting of cell-surface beta-amyloid precursor protein to lysosomes: alternative processing into amyloid-bearing fragments. Nature. 1992;357(6378):500–3.

57. Xiao Q, et al. Neuronal-Targeted TFEB Accelerates Lysosomal Degradation of APP, Reducing Abeta Generation and Amyloid Plaque Pathogenesis. J Neurosci. 2015;35(35):12137–51.

58. Zhang Y, Chen K, Sloan SA, Bennett ML, Scholze AR, O'Keeffe S, Phatnani HP, Guarnieri P, Caneda C, Ruderisch N, et al. An RNA-sequencing transcriptome and splicing database of glia, neurons, and vascular cells of the cerebral cortex. J Neurosci. 2014;34(36):11929–47.

59. Lui H, Zhang J, Makinson SR, Cahill MK, Kelley KW, Huang HY, Shang Y, Oldham MC, Martens LH, Gao F, et al. Progranulin deficiency promotes circuit-specific synaptic pruning by microglia via complement activation. Cell. 2016;165(4):921–35.

60. Evers BM, Rodriguez-Navas C, Tesla RJ, Prange-Kiel J, Wasser CR, Yoo KS, McDonald J, Cenik B, Ravenscroft TA, Plattner F, et al. Lipidomic and transcriptomic basis of lysosomal dysfunction in Progranulin deficiency. Cell Rep. 2017;20(11):2565–74.

61. Stoka V, Turk V, Turk B. Lysosomal cathepsins and their regulation in aging and neurodegeneration. Ageing Res Rev. 2016;32:22–37.

62. Arrant AE, Onyilo VC, Unger DE, Roberson ED. Progranulin gene therapy improves lysosomal dysfunction and microglial pathology associated with frontotemporal dementia and neuronal ceroid Lipofuscinosis. J Neurosci. 2018;38(9):2341–58.

63. Petkau TL, Blanco J, Leavitt BR. Conditional loss of progranulin in neurons is not sufficient to cause neuronal ceroid lipofuscinosis-like neuropathology in mice. Neurobiol Dis. 2017;106:14–22.

64. Petkau TL, Kosior N, de Asis K, Connolly C, Leavitt BR. Selective depletion of microglial progranulin in mice is not sufficient to cause neuronal ceroid lipofuscinosis or neuroinflammation. J Neuroinflammation. 2017;14(1):225.

65. Berti PJ, Storer AC. Alignment/phylogeny of the papain superfamily of cysteine proteases. J Mol Biol. 1995;246(2):273–83.

66. Butts CT, Zhang X, Kelly JE, Roskamp KW, Unhelkar MH, Freites JA, Tahir S, Martin RW. Sequence comparison, molecular modeling, and network analysis predict structural diversity in cysteine proteases from the cape sundew, Drosera capensis. Comput Struct Biotechnol J. 2016;14:271–82.

67. Richau KH, Kaschani F, Verdoes M, Pansuriya TC, Niessen S, Stuber K, Colby T, Overkleeft HS, Bogyo M, Van der Hoorn RA. Subclassification and biochemical analysis of plant papain-like cysteine proteases displays subfamily-specific characteristics. Plant Physiol. 2012;158(4):1583–99.

68. Gu C, Shabab M, Strasser R, Wolters PJ, Shindo T, Niemer M, Kaschani F, Mach L, van der Hoorn RA. Post-translational regulation and trafficking of the granulin-containing protease RD21 of Arabidopsis thaliana. PLoS One. 2012;7(3):e32422.

69. Yamada K, Matsushima R, Nishimura M, Hara-Nishimura I. A slow maturation of a cysteine protease with a granulin domain in the vacuoles of senescing Arabidopsis leaves. Plant Physiol. 2001;127(4):1626–34.

70. Kleinberger G, Brendel M, Mracsko E, Wefers B, Groeneweg L, Xiang X, Focke C, Deussing M, Suarez-Calvet M, Mazaheri F, et al. The FTD-like syndrome causing TREM2 T66M mutation impairs microglia function, brain perfusion, and glucose metabolism. EMBO J. 2017;36(13):1837–53.

71. Keren-Shaul H, Spinrad A, Weiner A, Matcovitch-Natan O, Dvir-Szternfeld R, Ulland TK, David E, Baruch K, Lara-Astaiso D, Toth B, et al. A unique microglia type associated with restricting development of Alzheimer's disease. Cell. 2017;169(7):1276–90.
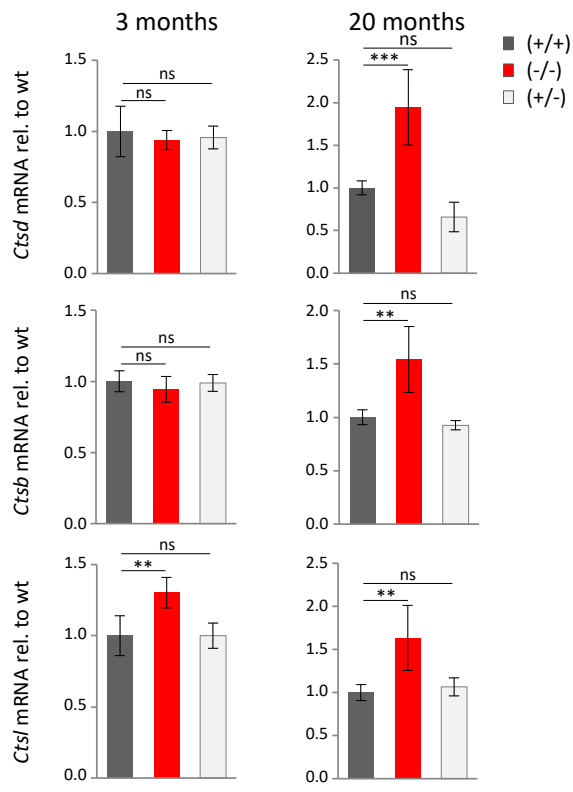
Götzl et al., Suppl. Fig. 1

Götzl et al., Suppl. Fig. 2

a

Grn wt

Grn ko

mGrn#5   mGrn#8

98 — ◄PGRN

98 — ◄PGRN

50 — ◄CatD$_{sc}$

36 — ◄CatD$_{hc}$

b

- ■ Grn wt
- ▲ Grn wt
- ■ Grn ko
- ▲ Grn ko
- ■ Grn rescue #5
- ▲ Grn rescue #5
- ■ Grn rescue #8
- ▲ Grn rescue #8
- — CatD ko
- — CatD ko

- ■ Grn wt
- ▲ Grn wt
- ■ Grn ko
- ▲ Grn ko
- ■ Grn rescue #5
- ▲ Grn rescue #5
- ■ Grn rescue #8
- ▲ Grn rescue #8
- — Grn wt CatB inh
- — Grn wt CatB inh

- ■ Grn wt
- ▲ Grn wt
- ■ Grn ko
- ▲ Grn ko
- ■ Grn rescue #5
- ▲ Grn rescue #5
- ■ Grn rescue #8
- ▲ Grn rescue #8
- — Grn wt CatL inh
- — Grn wt CatL inh

Götzl et al., Suppl. Fig. 3

48

-	+	-	-	-	NaOAc buffer
-	-	+	-	-	rhPGRN
-	-	-	+	-	ELAS rhPGRN
-	-	-	-	+	rhGRN E

Götzl et al., Suppl. Fig. 4

a

microglia enriched   microglia depleted

3 months

b

microglia enriched   microglia depleted

12 months
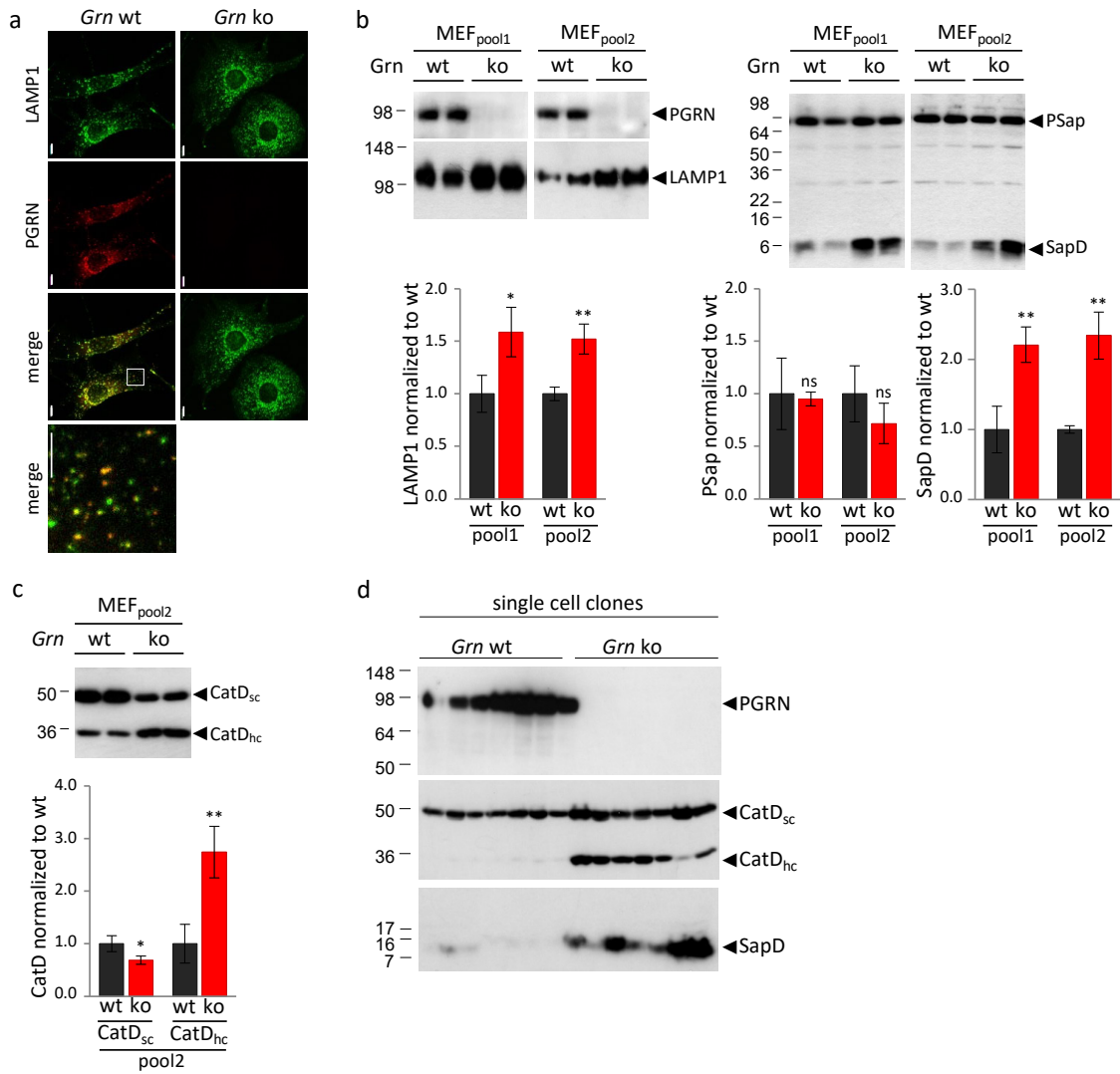
Götzl et al., Suppl. Fig. 5

1.1 Contribution to the publication

As a co-author of this publication, I isolated microglia for biochemical analysis and analyzed the effects of PGRN, elastase-digested PGRN and recombinant GRN E on the activity of Cat B, D and L on the activity of lysosomal proteases. This work is presented in Figure S4 and Figure S5. Additionally, I supported all primary authors during the time of revision.

Loss of TREM2 rescues hyperactivation of microglia, but not lysosomal deficits and neurotoxicity in models of progranulin deficiency

Anika Reifschneider, Sophie Robinson, Bettina van Lengerich, Johannes Gnörich, Todd Logan, Steffanie Heindl, Miriam A Vogt, Endy Weidinger, Lina Riedl, Karin Wind, Artem Zatcepin, Ida Pesämaa, Sophie Haberl, Brigitte Nuscher, Gernot Kleinberger, Julien Klimmt, Julia K. Götzl, Arthur Liesz, Katharina Bürger, Matthias Brendel, Johannes Levin, Janine Diehl-Schmid, Jung Suh, Gilbert Di Paolo, Joseph W Lewcock, Kathryn M Monroe, Dominik Paquet, Anja Capell and Christian Haass

SOURCE DATA TRANSPARENT PROCESS OPEN ACCESS

Loss of TREM2 rescues hyperactivation of microglia, but not lysosomal deficits and neurotoxicity in models of progranulin deficiency

Anika Reifschneider[1] , Sophie Robinson[2,3], Bettina van Lengerich[4], Johannes Gnörich[3,5], Todd Logan[4], Steffanie Heindl[2] , Miriam A Vogt[6], Endy Weidinger[7], Lina Riedl[8], Karin Wind[3,5], Artem Zatcepin[3,5] , Ida Pesämaa[3], Sophie Haberl[6], Brigitte Nuscher[1], Gernot Kleinberger[6], Julien Klimmt[2] , Julia K Götzl[1], Arthur Liesz[2,9] , Katharina Bürger[2,3], Matthias Brendel[3,5], Johannes Levin[3,5,7], Janine Diehl-Schmid[7,8], Jung Suh[4], Gilbert Di Paolo[4] , Joseph W Lewcock[4] , Kathryn M Monroe[4,*] , Dominik Paquet[2,9,**] , Anja Capell[1,***] & Christian Haass[1,3,9,****]

Abstract

Haploinsufficiency of the progranulin (PGRN)-encoding gene (*GRN*) causes frontotemporal lobar degeneration (*GRN*-FTLD) and results in microglial hyperactivation, TREM2 activation, lysosomal dysfunction, and TDP-43 deposition. To understand the contribution of microglial hyperactivation to pathology, we used genetic and pharmacological approaches to suppress TREM2-dependent transition of microglia from a homeostatic to a disease-associated state. *Trem2* deficiency in *Grn* KO mice reduced microglia hyperactivation. To explore antibody-mediated pharmacological modulation of TREM2-dependent microglial states, we identified antagonistic TREM2 antibodies. Treatment of macrophages from *GRN*-FTLD patients with these antibodies led to reduced TREM2 signaling due to its enhanced shedding. Furthermore, TREM2 antibody-treated PGRN-deficient microglia derived from human-induced pluripotent stem cells showed reduced microglial hyperactivation, TREM2 signaling, and phagocytic activity, but lysosomal dysfunction was not rescued. Similarly, lysosomal dysfunction, lipid dysregulation, and glucose hypometabolism of *Grn* KO mice were not rescued by TREM2 ablation. Synaptic loss and neurofilament light-chain (NfL) levels, a biomarker for neurodegeneration, were further elevated in the *Grn/Trem2* KO cerebrospinal fluid (CSF). These findings suggest that TREM2-dependent microglia hyperactivation in models of *GRN* deficiency does not promote neurotoxicity, but rather neuroprotection.

Introduction

Neurodegenerative diseases are currently incurable and novel therapeutic strategies are desperately required. Besides disease-defining protein deposits (Aguzzi & Haass, 2003), microgliosis is observed in almost all neurodegenerative diseases (Ransohoff, 2016). Microgliosis can be detrimental (Heneka *et al*, 2013; Hong *et al*, 2016a). However, recent findings strongly suggested that certain microglial responses to brain pathology may also be neuroprotective (Deczkowska *et al*, 2020; Lewcock *et al*, 2020). This is based on the identification of variants in genes predominantly or exclusively expressed in microglia within the brain that increase the risk for late-onset Alzheimer's disease (LOAD) and other neurodegenerative

1   Division of Metabolic Biochemistry, Faculty of Medicine, Biomedical Center (BMC), Ludwig-Maximilians-Universität München, Munich, Germany
2   Institute for Stroke and Dementia Research, University Hospital Munich, Ludwig-Maximilians-Universität München, Munich, Germany
3   German Center for Neurodegenerative Diseases (DZNE) Munich, Munich, Germany
4   Denali Therapeutics Inc., South San Francisco, CA, USA
5   Department of Nuclear Medicine, University Hospital, Ludwig-Maximilians-Universität München, Munich, Germany
6   ISAR Bioscience GmbH, Planegg, Germany
7   Department of Neurology, University Hospital, Ludwig-Maximilians-Universität München, Munich, Germany
8   Department of Psychiatry and Psychotherapy, School of Medicine, Technical University of Munich, Munich, Germany
9   Munich Cluster for Systems Neurology (SyNergy), Munich, Germany
    *Corresponding author. Tel: +1 650 4574910; E-mail: monroe@dnli.com
    **Corresponding author. Tel: +49 89 440046123; E-mail: dominik.paquet@med.uni-muenchen.de
    ***Corresponding author. Tel: +49 89 440046534; E-mail: anja.capell@med.uni-muenchen.de
    ****Corresponding author. Tel: +49 89 440046549; E-mail: christian.haass@dzne.de

disorders (Efthymiou & Goate, 2017). Protective microglial functions became particularly evident upon functional investigations of coding variants found within the triggering receptor expressed on myeloid cells 2 (TREM2) gene, which can increase the risk for LOAD and other neurogenerative disorders including frontotemporal dementia-like syndromes (Guerreiro *et al*, 2013; Jonsson *et al*, 2013). These TREM2 variants reduce lipid ligand binding, lipid and energy metabolism, chemotaxis, survival/proliferation, phagocytosis of cellular debris, and potentially other essential microglial functions (Deczkowska *et al*, 2020; Lewcock *et al*, 2020). Moreover, a loss of TREM2 function locks microglia in a dysfunctional homeostatic state (Keren-Shaul *et al*, 2017; Krasemann *et al*, 2017; Mazaheri *et al*, 2017; Nugent *et al*, 2020), in which they are unable to respond to pathological challenges by inducing a disease-associated mRNA signature.

Disease-associated microglia (DAM) respond to amyloid pathology by clustering around amyloid plaques where they exhibit a protective function by encapsulating the protein deposits via a barrier function (Yuan *et al*, 2016) that promotes amyloid plaque compaction (Ulrich *et al*, 2014; Wang *et al*, 2016; Meilandt *et al*, 2020) and reduces *de novo* seeding of amyloid plaques (Parhizkar *et al*, 2019). TREM2 is therefore believed to be a central target for therapeutic modulation of microglial functions (Deczkowska *et al*, 2020; Lewcock *et al*, 2020). A number of agonistic anti-TREM2 antibodies were recently developed (Cheng *et al*, 2018; Cignarella *et al*, 2020; Price *et al*, 2020; Schlepckow *et al*, 2020; Wang *et al*, 2020; Ellwanger *et al*, 2021; Fassler *et al*, 2021), which either enhance cell surface levels of signaling-competent TREM2 by blocking TREM2 shedding and/or crosslinking TREM2 receptors to stimulate downstream signaling via Syk phosphorylation. In preclinical studies, these antibodies boost protective functions of microglia as shown by enhanced amyloid β-peptide and myelin clearance, reduced amyloid plaque load, improved memory in models of amyloidosis, and supported axon regeneration and remyelination in models of demyelinating disorders such as multiple sclerosis (Cheng *et al*, 2018; Cignarella *et al*, 2020; Lewcock *et al*, 2020; Price *et al*, 2020; Schlepckow *et al*, 2020; Wang *et al*, 2020; Bosch-Queralt *et al*, 2021; Ellwanger *et al*, 2021).

Although increased TREM2 may be protective in AD patients (Ewers *et al*, 2019), in other neurodegenerative diseases, microglia may be overactivated and become dysfunctional (Heneka *et al*, 2013; Hong *et al*, 2016a; Ransohoff, 2016). Therefore, in these contexts, antagonistic TREM2 antibodies may display therapeutic benefit through dampening microglial hyperactivation. A well-described example of a neurodegenerative disorder where microglia are hyperactivated is *GRN*-associated frontotemporal lobar degeneration (*GRN*-FTLD) with TDP-43 (transactive response DNA-binding protein 43 kDa) deposition caused by progranulin (PGRN) deficiency (Baker *et al*, 2006; Cruts *et al*, 2006; Gotzl *et al*, 2019). In models of *GRN*-FTLD-associated haploinsufficiency, hyperactivation of microglia is evident, as demonstrated by an increased disease-associated mRNA signature as well as strongly increased 18-kDa translocator protein positron emission-tomography ((TSPO)-PET) signals in mouse models (Martens *et al*, 2012; Lui *et al*, 2016; Krabbe *et al*, 2017; Gotzl *et al*, 2019; Huang *et al*, 2020; Marschallinger *et al*, 2020; Zhang *et al*, 2020). This is the opposite phenotype of *Trem2* knockout (KO) microglia, which are locked in a homeostatic state (Keren-Shaul *et al*, 2017; Kleinberger *et al*, 2017;

Krasemann *et al*, 2017; Mazaheri *et al*, 2017; Gotzl *et al*, 2019; Nugent *et al*, 2020). Hyperactivation of microglia is also observed in the brain of *GRN*-FTLD patients (Lui *et al*, 2016; Woollacott *et al*, 2018; Gotzl *et al*, 2019). PGRN is a secreted protein, which is also transported to lysosomes (Hu *et al*, 2010; Zhou *et al*, 2015), where it appears to control activity of hydrolases, such as cathepsins and glucocerebrosidase (GCase) (Gotzl *et al*, 2016, 2018; Beel *et al*, 2017; Ward *et al*, 2017; Paushter *et al*, 2018; Arrant *et al*, 2019; Butler *et al*, 2019b; Logan *et al*, 2021). Total loss of PGRN results in a lysosomal storage disorder (Smith *et al*, 2012; Almeida *et al*, 2016). A potential synergistic contribution of lysosomal dysfunction and hyperactivated microglia to the disease pathology and specifically to the deposition of TDP-43 in neurons is likely but currently not understood (Kao *et al*, 2017; Ward *et al*, 2017; Huang *et al*, 2020; Logan *et al*, 2021).

To determine whether hyperactivation of microglia and its pathological consequences in *Grn* KO mice are dependent on aberrant TREM2 signaling, we sought to reduce the microglial activation status by crossing them to *Trem2* KO mice. This reduced the expression of DAM genes, suggesting that negative modulation of TREM2 signaling may be exploited to lower microglial activation in neuroinflammatory disorders. In analogy to the agonistic 4D9 TREM2 antibody developed earlier in our laboratory (Schlepckow *et al*, 2020), we therefore generated monoclonal antibodies with opposite, namely antagonistic, properties. Such antibodies blocked lipid ligand-induced TREM2 signaling, reduced signaling-competent cell surface TREM2 in *GRN*-FTLD patient-derived macrophages, and concomitantly increased shedding of TREM2, which resulted in enhanced release of soluble TREM2 (sTREM2). Therefore, TREM2 antagonist antibodies inhibit receptor function via multiple mechanisms of action. In genetically engineered human-induced pluripotent stem cell-derived (iPSC) microglia-lacking PGRN, the antagonistic antibodies reduced expression of the majority of candidate genes of the DAM signature, however, they failed to restore lysosomal function. Similarly, in *Grn/Trem2* double-knockout (*Double* KO) mice, lysosomal dysfunction was not rescued. Moreover, pathological features such as reduced 2-deoxy-2-[18F]fluoro-d-glucose (FDG) uptake, disturbed lipid metabolism, and abnormal microglial morphology were not ameliorated. Strikingly, synapse loss was exacerbated, and neurofilament light chain (NfL), a sensitive fluid biomarker of neurodegeneration (Meeter *et al*, 2016; Rohrer *et al*, 2016; Preische *et al*, 2019), was also not reduced but unexpectedly increased in the cerebrospinal fluid (CSF). These findings therefore suggest that against common expectations, hyperactivated microglia may retain at least some TREM2-dependent neuroprotective activities.

Results

Trem2 KO dampens hyperactivation of microglia in PGRN-deficient mice

PGRN and TREM2 deficiency results in opposite microglial activation states (Gotzl *et al*, 2019). To determine if reduction in TREM2 signaling can ameliorate hyperactivation of PGRN-deficient microglia, we crossed *Grn* KO mice (Kayasuga *et al*, 2007) to *Trem2* KO mice (Turnbull *et al*, 2006) and performed TSPO-PET imaging using

54

established protocols (Liu *et al*, 2015; Kleinberger *et al*, 2017). TSPO-PET imaging in mice is rather specific for microglial activation, as plexin treatment and ablation of TREM2, both of which reduce microglia numbers, strongly reduce the TSPO signal (Xiang *et al*, 2021). In line with our earlier findings (Gotzl *et al*, 2019), we confirmed a strong increase in the TSPO-PET signal in the brains of *Grn* KO mice when compared to WT ($P < 0.01$) (Figs 1A and B, and EV5A). We also confirmed reduced TSPO expression in the brain of *Trem2* KO mice ($P < 0.03$) (Figs 1A and B, and EV5A), consistent with our initial findings in TREM2 loss-of-function models (Kleinberger *et al*, 2017; Gotzl *et al*, 2019). Consistent with the above-described goal to dampen hyperactivation of microglia, investigation of *Double* KO mice (Figs 1A and B, and EV5A) indicated a balanced TSPO expression without a significant difference when compared to WT ($P = 0.945$) and a reduction in TSPO expression relative to *Grn* KO mice ($P < 0.05$) (Figs 1A and B, and EV5A).

These findings suggest that DAM gene expression patterns as observed in *Grn* KO mice may be partially rescued in *Double* KO mice. To test this, we isolated microglia from adult mouse brains. Microglial mRNA of all three mouse lines was analyzed using a customized nCounter panel (NanoString Technologies), which includes 65 genes that previously showed opposite expression levels in *Grn* and *Trem2* KO mice (Mazaheri *et al*, 2017; Gotzl *et al*, 2019). Gene expression levels were normalized against the geometric mean of four housekeeping genes, including *Asb10*, *Cltc*, *Hprt1*, and *Tubb5*. In accordance with our previous findings (Gotzl *et al*, 2019), candidate genes of the DAM signature such as *ApoE*, *Cd22*, *Ly9*, *Clec7a*, *Spp1*, and *Olfr110* were massively upregulated in *Grn* KO microglia while these genes were suppressed in the *Trem2* KO microglia (Fig 2A–E). In the *Double* KO microglia, expression of the DAM signature genes *Olfr110*, *Spp1*, and *Clec7a* is fully rescued to WT expression levels and others, such as *Ly9*, *Cd22*, and *ApoE*, are at least partially reduced compared to the *Grn* KO (Fig 2D and E). These data thus provide direct evidence that in *Double* KO mice, the molecular signature of microglia is shifted away from a DAM state toward a homeostatic state.

Antagonistic TREM2 antibodies decrease cell surface TREM2 and reduce ligand-induced Syk signaling in monocyte-derived patient macrophages

Antagonist TREM2 antibodies were generated by immunizing rodents with human TREM2 extracellular domain (ECD)-Fc fusion protein and performing single B-cell sequencing on peripheral lymphoid tissues. Antibodies that bound specifically to human TREM2 were evaluated for functional impact to TREM2 signaling. Antagonistic antibodies were identified by their ability to block TREM2-dependent lipid ligand-induced activation of p-Syk on HEK293 cells overexpressing TREM2/DAP12 (Fig EV1). Cells were dosed with three different concentrations of liposomes, and antagonistic antibody 1 (Ab1) and antagonistic antibody 2 (Ab2), which were found to block phosphatidylserine (PS)-induced p-Syk activity (Fig EV1A). Both antibodies bind to an epitope in the IgV domain between amino acids 30 and 63 of human TREM2 (Figs 3A and EV1B). These selected antibodies were reformatted onto an effector-less human hIgG1-LALAPG backbone, and demonstrated high affinity for cell surface TREM2 (0.38 nM EC50 Ab1 and 0.18 nM EC50
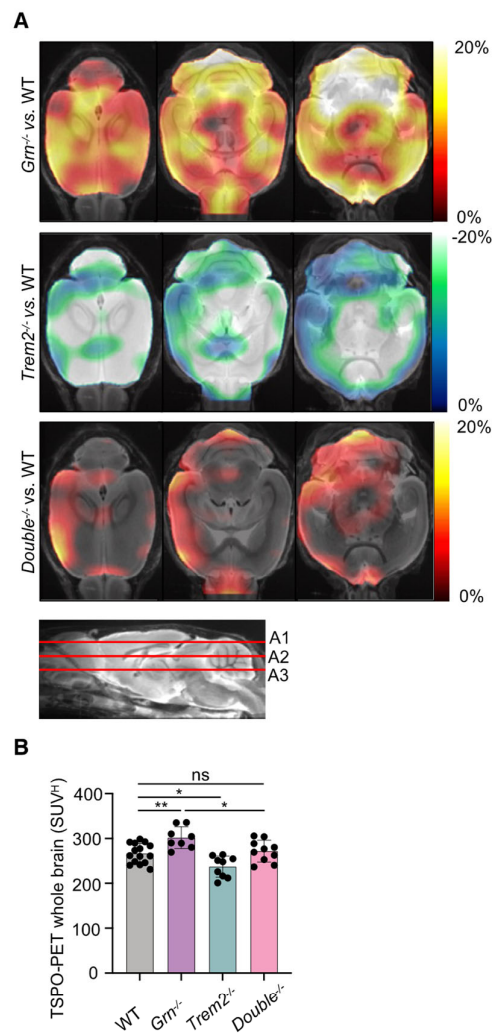
Figure 1. TSPO-PET imaging indicates rescue of microglial hyperactivation in *Double*$^{-/-}$ mice.

A Axial slices as indicated below (A1, A2, and A3) show %-TSPO-PET differences between *Grn*$^{-/-}$, *Trem2*$^{-/-}$, or *Double*$^{-/-}$ mice and WT at the group level. Images adjusted to an MRI template indicate increased microglial activity in the brain of *Grn*$^{-/-}$ mice (hot color scale), compensated microglial activity in the brain of *Double*$^{-/-}$ mice, and decreased microglial activity in the brain of *Trem2*$^{-/-}$ mice (cold color scale), each in contrast against age-matched WT mice.

B Scatter plot illustrates individual mouse TSPO-PET values derived from a whole-brain volume of interest. A total of 8–15 female mice per group at an average age of 11.1 ± 1.6 months (*Grn*$^{-/-}$ ($n = 8$), *Trem2*$^{-/-}$ ($n = 9$), *Double*$^{-/-}$ ($n = 10$), and WT ($n = 15$)). Data represent mean ± SD. For statistical analysis, one-way ANOVA with Tukey *post hoc* test was used. Statistical significance was set at *$P < 0.05$; **$P < 0.01$; ns, not significant.
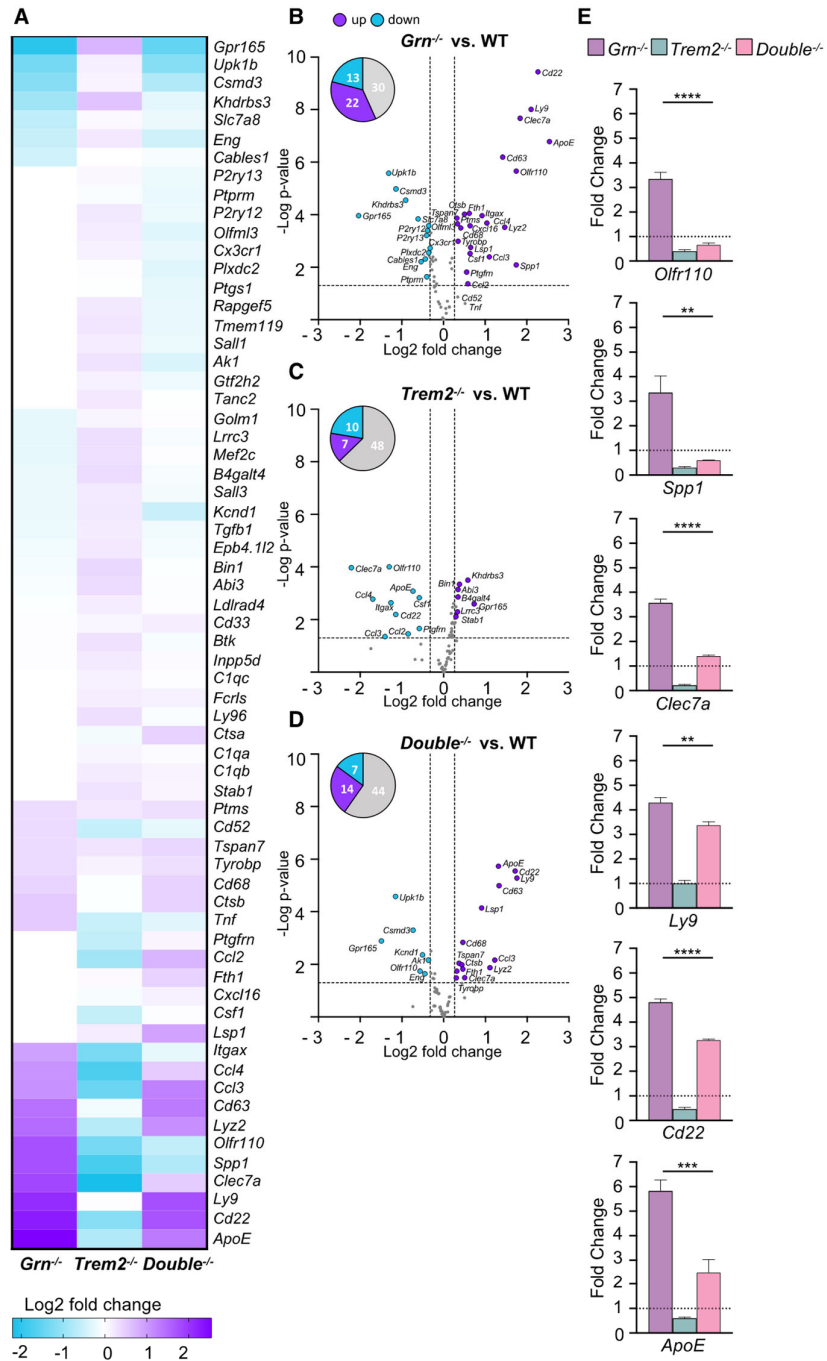
Source data are available online for this figure.

Figure 2.

◀

Figure 2. Loss of TREM2 reduces the DAM signature of $Grn^{-/-}$ mice.

A   Heatmap of 65 DAM-associated gene transcripts analyzed by NanoString in FCRLS- and CD11b-positive $Grn^{-/-}$ ($n = 6$), $Trem2^{-/-}$ ($n = 5$), and $Double^{-/-}$ ($n = 6$) microglia in comparison to WT ($n = 7$) microglia isolated from 6-month-old male mice. The expression-corrected and housekeeping gene normalized RNA counts for each gene and sample were normalized to the mean value of WT followed by a log2 transformation.

B   Volcano plot presentation of the differently expressed transcripts in FCRLS- and CD11b-positive $Grn^{-/-}$ ($n = 6$) in comparison to WT ($n = 6$) microglia isolated from 6-month-old male mice. A total of 35 of 65 analyzed genes are significantly changed more than 20%, with 22 genes upregulated (purple) and 13 genes downregulated (blue).

C   Volcano plot presentation of the differently expressed transcripts in FCRLS- and CD11b-positive $Trem2^{-/-}$ ($n = 5$) in comparison to WT ($n = 6$) microglia isolated from 6-month-old male mice. A total of 17 of 65 analyzed genes are significantly changed more than 20%, with 7 genes upregulated (purple) and 10 genes downregulated (blue).

D   Volcano plot presentation of the differently expressed transcripts in FCRLS- and CD11b-positive $Double^{-/-}$ ($n = 6$) in comparison to WT ($n = 6$) microglia isolated from 6-month-old male mice. A total of 21 of 65 analyzed genes are significantly changed more than 20%, with 14 genes upregulated (purple) and 7 genes downregulated (blue).

E   Expression profiles of selected DAM genes, whose mRNA levels are rescued in $Double^{-/-}$ ($n = 6$) versus $Grn^{-/-}$ ($n = 6$) microglia. mRNA expression normalized to the mean of the WT cohort. Data represent mean ± SEM.

Data information: For statistical analysis in B–D, the unpaired, two-tailed student's *t*-test was performed, and in E, one-way ANOVA with Dunnett's *post hoc* test was used to compare $Grn^{-/-}$, $Trem2^{-/-}$, and $Double^{-/-}$ microglia. Statistical significance was set at **$P < 0.01$; ***$P < 0.001$; ****$P < 0.0001$.
Source data are available online for this figure.

Ab2 in cell binding) and high affinity to human TREM2 ECD protein binding via surface plasmon resonance (0.21 nM Ab1 and 4.5 nM Ab2) (Fig EV1C–G). Ligand blocking activity was further validated in human monocyte-derived macrophages, which were treated in a dose–response format with antibodies in the presence of PS-containing liposomes to determine the potency of Ab1 and Ab2 to block liposome-induced TREM2-mediated p-Syk signaling (Figs 3B and EV1C).

Next, we tested if antagonistic TREM2 antibodies are capable of reducing TREM2 signaling in *GRN*-FTLD patient-derived macrophages. To do so, we identified four patients with low PGRN plasma levels (Fig 3C) and confirmed heterozygous *GRN* loss-of-function mutation (Fig EV2A and B). We then generated monocyte-derived macrophages from peripheral blood samples of these patients and healthy volunteers. Western blot analysis revealed that macrophages of *GRN* mutation carriers show significantly enhanced levels of mature TREM2 as compared to healthy controls (Fig 3D and E). Although *GRN* mutation carriers express more mature TREM2 than healthy controls, sTREM2 in the conditioned media was not significantly altered (Fig 3D and F). Since evidence exists that shedding of TREM2 terminates cell autonomous signaling in myeloid cells (Kleinberger *et al*, 2014; Schlepckow *et al*, 2017, 2020; Thornton *et al*, 2017), these findings suggest that macrophages from *GRN*-FTLD patients exhibit increased TREM2 signaling, which occurs in conjunction with the microglial hyperactivation phenotype observed *in vitro* and *in vivo* (Gotzl *et al*, 2019).

Macrophages from *GRN*-FTLD patients and healthy controls were then treated with Ab1 and Ab2 for 24 h. TREM2 levels in cell lysates revealed that both antibodies reduced mature TREM2, whereas an isotype control antibody had no effect (Figs 3G and H, and EV2C). The reduction in mature membrane-bound TREM2 was accompanied by an increase in sTREM2 in conditioned media (Fig 3G and I). Thus, in line with the data shown in Figs 3A and B, and EV1A–G, both antibodies reduce signaling-competent mature TREM2 and increase TREM2 shedding. To further demonstrate that TREM2 signaling can be modulated by TREM2 antagonistic antibodies in patient-derived macrophages, we quantified Syk signaling. This demonstrated that both antagonistic antibodies reduce p-Syk in liposome-stimulated macrophages, suggesting that antagonistic TREM2 antibodies may be capable of modulating TREM2 hypersignaling in microglia in a beneficial manner (Fig 3J).

Antagonistic TREM2 antibodies reduce hyperactivation of PGRN-deficient human microglia

To corroborate and extend our findings in human myeloid cells, we aimed to test modulation of TREM2 via the antagonistic antibodies in human-induced pluripotent stem cell (iPSC)-derived microglia (hiMGL). For this purpose, we generated *GRN* KO iPSC by targeting exon 2 using our established CRISPR genome-editing pipeline (Weisheit *et al*, 2020; see methods for details). We deeply phenotyped *GRN* KO iPSC to confirm loss of PGRN protein expression, maintenance of pluripotency, clonality, as well as absence of unintended on- and off-target effects and chromosomal abnormalities (Weisheit *et al*, 2021) (Figs 4A and EV3A–G; Appendix Fig S1). As expected, *GRN* KO hiMGL increased expression of TREM2 (Fig 4B and C) and showed consequently elevated levels of sTREM2 (Fig 4D). PGRN-deficient hiMGL were treated with the antagonistic TREM2 antibodies as described above. Consistent with the antibody mechanism of action, antagonistic antibodies increased secretion of sTREM2 (Fig 4E). In line with this finding, both antagonistic antibodies reduced p-Syk signaling (Fig 4F). Moreover, both antibodies not only reduced the phagocytic activity of WT hiMGL (Fig 4G), but also ameliorated the pathologically increased phagocytic activity of PGRN-deficient hiMGL (Fig 4H), indicating that they dampen the activation state of PGRN-deficient hiMGL. To further extend these findings, we asked if the antagonistic antibodies could also correct the transcriptional signature of hyperactivated hiMGL. Therefore, we used a customized nCounter panel (NanoString Technologies) analyzing gene expression of 82 microglia-related genes and 8 housekeeping genes of WT and PGRN-deficient hiMGL treated with the two antagonistic antibodies or isotype control (Fig 5A). Gene expression levels in each sample were normalized against the geometric mean of five housekeeping genes including *CLTC*, *HPRT1*, *RPL13A*, *TBP* and *PPIA*. DAM genes, such as *APOE*, *SPP1*, *GPNMB*, *CSF1*, *LGALS3*, *CCL3*, *LPL*, *TREM2*, *ITGAX* and *CD68*, were all significantly upregulated in PGRN-deficient hiMGL compared to WT hiMGL (Fig 5A and B). In addition, expression of genes associated with lysosomal dysfunction was also significantly upregulated (*CTSD*, *NPC2*, and *CD68*). Both antagonistic TREM2 antibodies significantly modulated the mRNA signature of PGRN-deficient hiMGL toward a

more homeostatic state (Fig 5A–D). Upregulation of TREM2 in PGRN-deficient hiMGL was completely corrected by treating the cells with either antagonist antibody (Fig 5E). Upregulation of DAM genes was completely (*GPNMB*, *LGALS3*, *SPP1*, *CSF1*, *CCL3*, *LPL*, and *ITGAX*) or at least partially (*APOE* and *CCL2*) rescued, while downregulation of the homeostatic marker *P2RY12* was reversed by antibody treatment (Fig 5E). Thus, TREM2 modulation with antagonistic antibodies ameliorates hyperactivation of microglia.

Reduced TREM2 signaling does not rescue lysosomal dysfunction

Next, we searched for a rescue of lysosomal phenotypes in PGRN-deficient hiMGL. In contrast to the profound rescue of the homeostatic and disease-associated mRNA signatures upon treatment with the two antagonistic antibodies (Fig 5A–E), we did not observe a significant rescue of increased gene expression patterns associated with lysosomal dysfunction upon PGRN deficiency, like *CTSD*, *NPC2*, and *CD68* mRNA expression (Fig 5A–D and F). Antagonistic
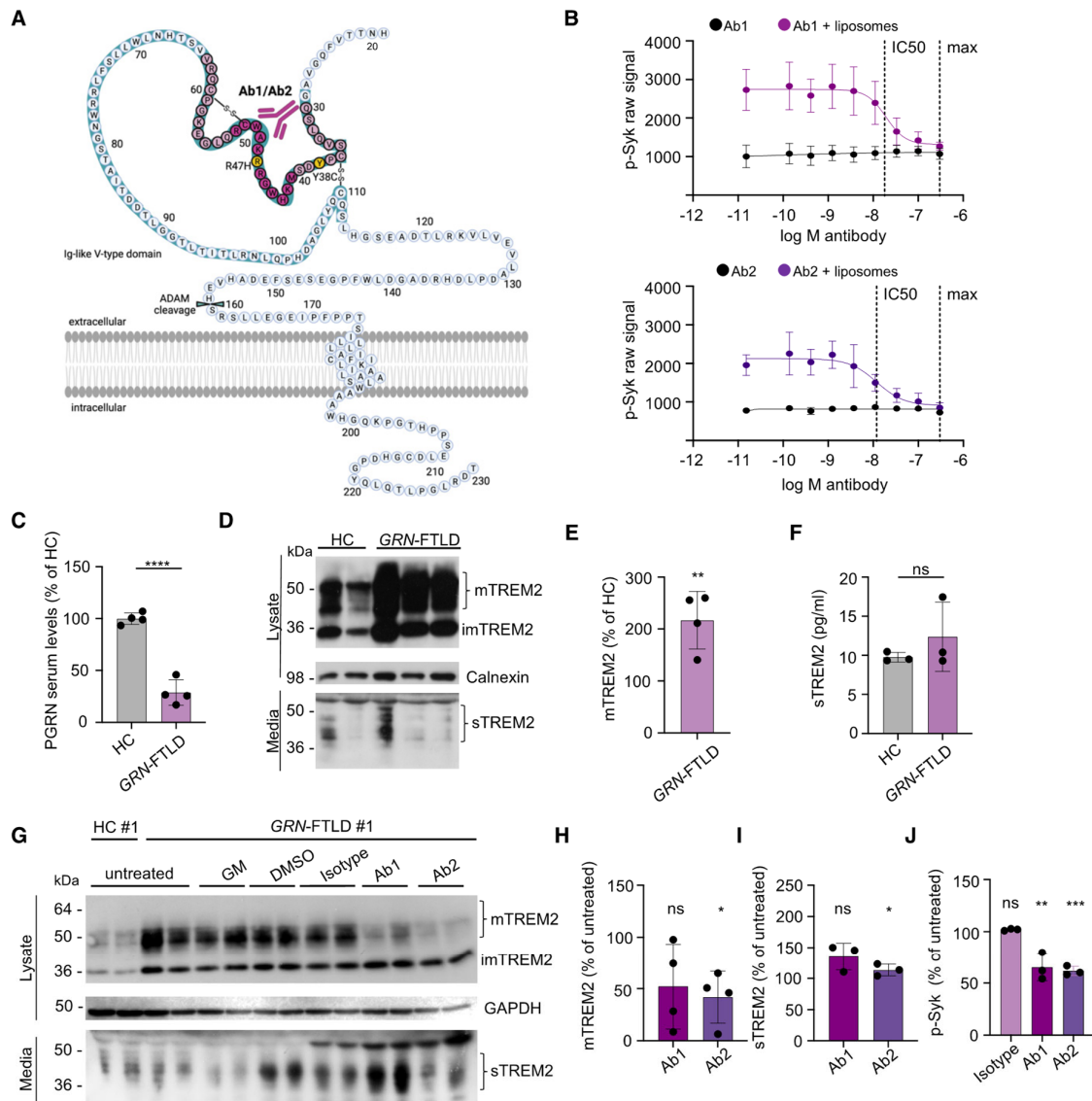

Figure 3.

Figure 3. Human antagonistic TREM2 antibodies rescue elevated membrane-bound TREM2 levels and reduce p-Syk in primary human macrophages isolated from PGRN mutation carriers.

A Schematic presentation of human TREM2 with the identified binding site of antagonistic antibodies Ab1 and Ab2 (purple) in the Ig-like V-type domain. Light purple indicates the overlapping amino acid sequence of the two peptides, which are bound by Ab1 and Ab2 (see also EV1B). The disease-associated Y38C and R47H mutations are indicated in yellow. Created with BioRender.com.

B AlphaLISA-mediated quantification of p-Syk in human macrophages with a dose titration treatment of Ab1 and Ab2 with or without liposomes for 5 min. IC50 and maximal inhibition (max) are indicated by a dotted line. Data represent the mean ± SEM ($n = 3$ independent experiments).

C ELISA-mediated quantification confirms reduced PGRN serum levels in *GRN* mutation carriers versus healthy controls. PGRN was measured by ELISA in technical triplicates and normalized to serum levels of healthy controls. Data points indicate individual patients (*GRN*-FTLD) and healthy controls (HC).

D Western blot of TREM2 in lysates and conditioned media of cultured human macrophages isolated from *GRN*-FTLD patients and HC. Mature (mTREM2), immature (imTREM2), and soluble TREM2 (sTREM2) are indicated. Calnexin was used as loading control.

E Quantification of mTREM2 expression levels in lysates of cultured human macrophages isolated from *GRN*-FTLD patients (data shown in D). mTREM2 levels were normalized to HC ($n = 4$). Data points indicate individual patients.

F ELISA-mediated quantification of sTREM2 in conditioned media of human macrophages isolated from *GRN*-FTLD patients and HC ($n = 3$). sTREM2 could not be measured in conditioned media of human macrophages isolated from patient #3 due to low overall cell yield. Data points indicate individual patients and HC.

G Western blot of TREM2 in lysates and media of cultured human macrophages isolated from *GRN*-FTLD #1 and HC #1 upon treatment with Ab1 and Ab2. An isotype antibody was used as a negative control. ADAM protease inhibition (GM) does not further increase mTREM2 levels in *GRN*-FTLD patients. Equal amounts of protein were loaded. GAPDH was used as loading control.

H Quantification of mTREM2 expression normalized to HC ($n = 4$) (data shown in G). Data points indicate individual patients.

I ELISA-mediated quantification of sTREM2 in conditioned media of human macrophages isolated from *GRN*-FTLD patients ($n = 3$). sTREM2 could not be measured in conditioned media of human macrophages isolated from patient #3 due to low overall cell yield. Data points indicate individual patients.

J AlphaLISA-mediated quantification of p-Syk levels in human macrophages upon treatment with Ab1 and Ab2 with liposomes for 60 min ($n = 3$). An isotype antibody was used as a negative control. Data points indicate individual patients. Isolated material from patient #3 did not yield enough cells to perform this experiment.

Data information: Data represent mean ± SEM. For statistical analysis of patient samples in comparison to HC, the unpaired, two-tailed student's *t*-test was performed. Statistical significance was set at *$P < 0.05$; **$P < 0.01$; ***$P < 0.001$; ****$P < 0.0001$; ns, not significant

Source data are available online for this figure.

antibodies also failed to rescue elevated cathepsin D (CatD) activity in PGRN-deficient hiMGL (Fig 5G).

In total brain lysates of 14-month-old *Grn* KO and *Double* KO mice, CatD single chain (sc) and heavy chain (hc) were both increased without a reduction in *Double* KO mice (Fig 6A–C). Furthermore, the catalytic activity of CatD, which was increased in *Grn* KO mice in an age-dependent manner (Fig 6D and E), was also not rescued by the additional loss of TREM2 (Fig 6E), suggesting that lysosomal dysfunction of *Grn* KO mice cannot be rescued by TREM2 modulation. To further support this, we investigated *Double* KO brains for the accumulation of lipofuscin, an autofluorescent lipopigment, found in *Grn* KO and several lysosomal storage disorders (Gotzl *et al*, 2014). In line with the failure of the *Double* KO to rescue lysosomal hyperactivity, lipofuscin accumulation was not reduced upon loss of TREM2 in *Grn* KO mice, although remarkably almost no lipofuscin was observed in single *Trem2* KO mice via mechanisms that have yet to be investigated (Fig 6F and G).

Loss of TREM2 does not rescue lysosomal lipid dyshomeostasis in *Grn* KO mice

Previous studies have examined the impact of either *Trem2* or *Grn* deletion on the lipidome of mouse brain. In the case of *Trem2*, no significant lipid changes were observed in *Trem2* KO mouse brain at baseline, although upon cuprizone challenge, a striking accumulation of cholesterol esters and various sphingolipids was revealed (Nugent *et al*, 2020). In *Grn* KO mice, lipid metabolism is altered (Evers *et al*, 2017; Marschallinger *et al*, 2020) and a recent study described an age-independent deficit in levels of the lysosomal lipid bis(monoacylglycerol)phosphate (BMP) that was accompanied by an age-dependent accumulation of the GCase substrate glucosylsphingosine (GlcSph) (Logan *et al*, 2021). To determine whether

deletion of *Trem2* on the *Grn* KO background has any effect on the composition of the brain lipidome, we performed targeted lipidomic analysis using LCMS on 6-month-old WT, *Grn* KO, *Trem2* KO, and *Double* KO mouse brain homogenates (Fig 7). As previously described (Nugent *et al*, 2020), the *Trem2* KO showed no significant differences in brain lipid content relative to WT mice (Fig 7B), while the *Grn* KO as well as the *Double* KO showed a significant decrease in several BMP species as well as an increase in GlcSph (Fig 7A, C and E–G), which is consistent with previous data (Logan *et al*, 2021). Consistent with previous findings (Jian *et al*, 2016; Arrant *et al*, 2019; Zhou *et al*, 2019; Logan *et al*, 2021) and the increased accumulation of the GCase substrate GlcSph, we found a significant decrease in the GCase activity in *Grn* KO mice and *Double* KO (Fig 7H). Importantly, genetic interaction analysis demonstrated no statistically significant difference in the levels of any analyte in the *Double* KO brain compared to the *Grn* KO alone (Fig 7D). Thus, ablation of TREM2 fails to correct abnormal lysosomal function and lipid metabolism in PGRN-deficient mice.

Enhanced brain pathology in *Double* KO mice suggests a neuroprotective function of hyperactivated microglia

Aged *Grn* KO mice show enhanced synaptic pruning (Lui *et al*, 2016; Zhang *et al*, 2020). To investigate if abolishing TREM2 signaling mitigates a neurodegenerative phenotype in 14-month-old *Grn* KO mice, we analyzed the thalamic synaptic density using synaptophysin (SPH) and the vesicular GABA transporter (VGAT) as a marker for presynaptic density (Fig 8A–C). Interestingly, immunohistochemical staining of the thalamic region revealed a reduction in SPH in *Trem2* KO, which was even more robust in *Double* KO mice (Fig 8A and B). Western blot analysis confirmed reduced total SPH levels in *Trem2* KO (Jadhav *et al*, 2020) and *Double* KO mice (Fig 8D and E). Similarly, immunostainings against VGAT revealed

a further reduction in *Double* KO mice compared to WT, *Grn* KO, and *Trem2* KO (Fig 8A and C).

To obtain additional information on the activation status of *Double* KO microglia, we determined microglial morphology. We extracted morphological features in WT, *Grn* KO, *Trem2* KO, and *Double* KO animals after 3D reconstruction of IBA1+ microglia from confocal *z*-stack images (Fig 8F and G). Microglial cells from *Grn* KO and *Double* KO animals showed a significantly decreased score for "branch volume," "number of branch nodes," and less pronounced for "branch length," as well as a significantly increased score for "sphericity," which is associated with an increased activation state of microglia (Heindl *et al*, 2018). In contrast, the morphological scores for *Trem2* KO animals were comparable to WT. Thus,

although the transcriptional signature of hyperactivated PGRN-deficient microglia is partially rescued by the loss of TREM2, the morphological and immunohistochemical analysis indicates that *Double* KO microglia neither rescue *Grn* KO microglial morphology nor synapse loss.

To further test if reduction in microglial hyperactivation fails to ameliorate secondary neurodegeneration, we analyzed the concentrations of NfL, a fluid biomarker for neuronal damage (Meeter *et al*, 2016; Rohrer *et al*, 2016; Preische *et al*, 2019), in the CSF of 6-month-old (Fig 9A) and 14-month-old mice (Fig 9B). In line with previous findings (Zhang *et al*, 2020), NfL was increased in PGRN-deficient mice, whereas no change was observed in *Trem2* KO animals as compared to WT mice (Fig 9A and B). Surprisingly, we
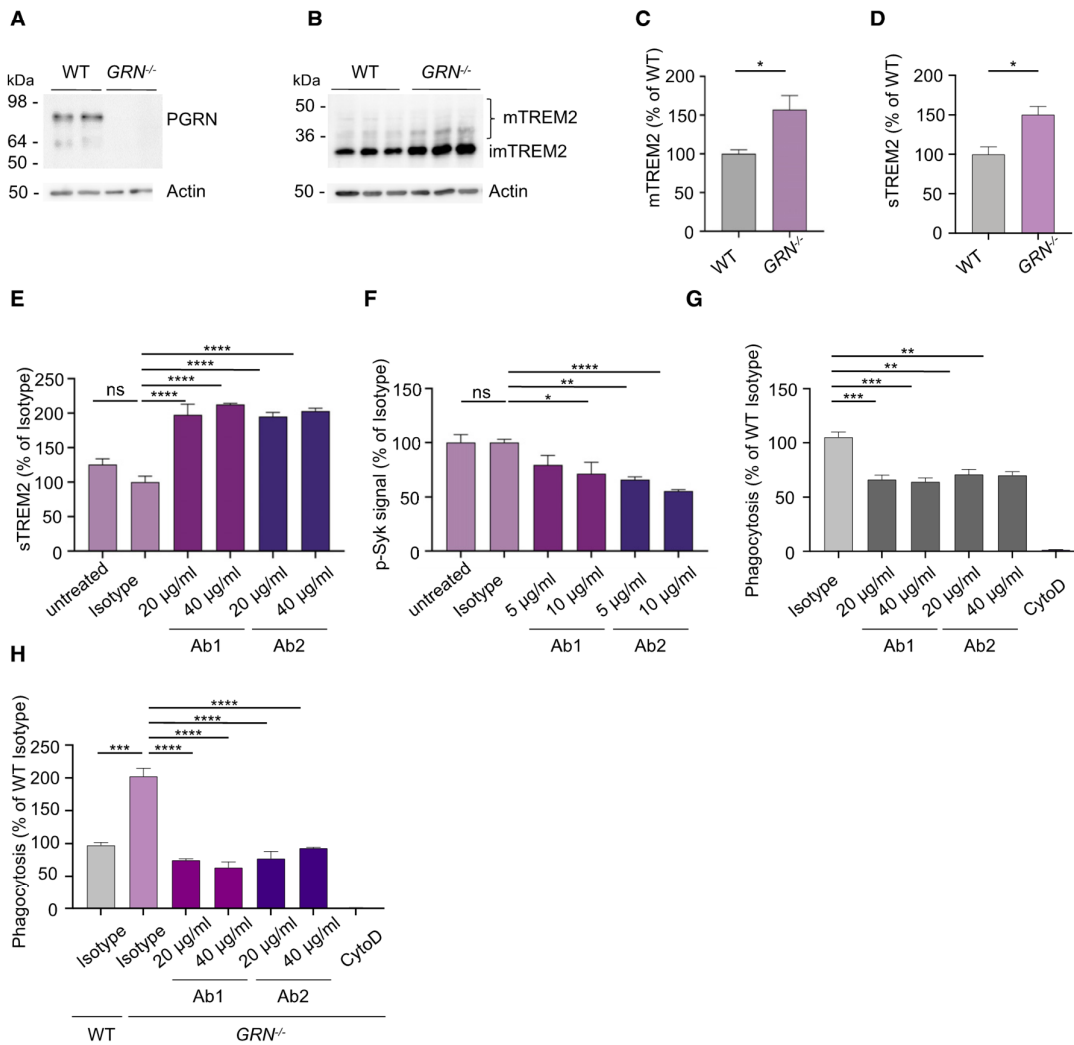

Figure 4.

60

◀

Figure 4. Antagonistic TREM2 antibodies enhance TREM2 shedding and reduce TREM2-dependent signaling and phagocytosis in PGRN-deficient iPSC-derived human microglia (hiMGL).

A   Western blot of PGRN in whole-cell lysates of WT and $GRN^{-/-}$ hiMGL. Actin was used as loading control.

B   Western blot of TREM2 in whole-cell lysates of WT and $GRN^{-/-}$ hiMGL. Mature (mTREM) and immature TREM2 (imTREM2) are indicated. Actin was used as loading control.

C   Quantification of mTREM2 expression in whole-cell lysates of WT and $GRN^{-/-}$ hiMGL (data shown in B). mTREM2 levels were normalized to WT ($n = 3$, biological replicates).

D   ELISA-mediated quantification of sTREM2 in conditioned media of WT and $GRN^{-/-}$ hiMGL ($n = 3$, biological replicates).

E   ELISA-mediated quantification of sTREM2 in conditioned media during $GRN^{-/-}$ hiMGL upon treatment with Ab1 and Ab2 (20 μg/ml, 40 μg/ml) ($n = 3$, biological replicates). An isotype antibody (10 μg/ml) was used as a negative control.

F   AlphaLISA-mediated quantification of p-Syk levels in $GRN^{-/-}$ hiMGL upon treatment with Ab1 and Ab2 (5 μg/ml, 10 μg/ml) with liposomes (1 mg/ml) for 5 min. ($n = 8$, biological replicates).

G   Uptake assay for fluorescent myelin in WT hiMGL. Phagocytosis of myelin significantly decreased upon treatment with TREM2 antagonistic antibodies Ab1 and Ab2 ($n = 4$, biological replicates).

H   Uptake assay for fluorescent myelin. $GRN^{-/-}$ hiMGL phagocytose significantly more myelin as compare to WT hiMGL. This is reversed upon treatment with TREM2 antagonistic antibodies Ab1 and Ab2 ($n = 4$, biological replicates).

Data information: Data represent mean ± SEM. For statistical analysis in C and D, the unpaired, two-tailed student's t-test was performed, in E and F, one-way ANOVA with Dunnett's post hoc test, and in G and H, one-way ANOVA with Tukey's post hoc was used to compare untreated, Ab1, and Ab2 (20 μg/ml and 40μg/ml) conditions to the isotype-treated condition. Statistical significance was set at *$P < 0.05$; **$P < 0.01$; ***$P < 0.001$; ****$P < 0.0001$; and ns, not significant.
Source data are available online for this figure.

found a striking increase in NfL in the 14-month-old *Double* KO mice (Fig 9B), suggesting a protective role of TREM2-dependent microglial hyperactivation in PGRN-deficient mice. To further elucidate which genes and pathological pathways may be affected by eliminating TREM2 in *Grn* KO mice, we isolated mRNA from total brain of all three mouse models after 6 and 14 months of age and searched for changes in mRNA expression using the nCounter Neuropathology panel (NanoString Technologies) (Werner *et al*, 2020). The Neuropathology panel with 770 genes included was specifically designed to analyze neurodegenerative phenotypes in mouse models and allows investigating six fundamental themes of neurodegeneration, namely neurotransmission, neuron–glia interaction, neuroplasticity, cell structure integrity, neuroinflammation, and metabolism. Analysis of total brain mRNA confirmed rescue of the age-dependent *Grn* KO-associated DAM signature in the *Double* KO mice (Fig EV4A–G, Appendix Fig S2A and B) and revealed no significant upregulation of genes associated with neuroinflammation like *Gfap*, *Tnf*, or *Tnfrsf11b* or genes associated with synaptic pruning, such as the complement factors (*C1qc*, *C1qa*, and *C1qb*) compared to WT mice (Fig EV4G). Although differences in the transcriptomic signature of male and female microglia were overserved, as described earlier (Villa *et al*, 2018), rescue of gene expression associated with neuroinflammation and synaptic pruning was evident in both sexes (Fig EV4G, Appendix Fig S3). Pathway analysis in *Grn* KO mice revealed the highest increases in "autophagy," "activated microglia," "angiogenesis," and "disease association" associated clusters with further increase during aging (Fig 9C). These four pathways score very low in *Trem2* KO mice, again confirming opposite effects of the two single-gene deletions. In the 6-month-old and in the 14-month-old cohort, all four pathways score is lower in the *Double* KO than in the single *Grn* KO. Three of these pathways, namely "activated microglia," "angiogenesis," and "disease association," are even downregulated in the 6-month-old *Double* KO cohort compared to WT. However, other pathways like "neuronal cytoskeleton," "tissue integrity," and "transmitter synthesis and storage" and "transmitter response and uptake," are most heavily affected in the 6-month-old *Double* KO, which is consistent with enhanced neuropathological phenotypes.

When looking into individual genes, we found that strikingly, compared to single *Grn* KO and WT mice, only two genes were significantly altered and in fact downregulated more than 20% in the 6-month-old *Double* KO. These include the transcription factor *Npas4* (Neuronal PAS domain protein 4), which regulates activation of genes involved in the excitatory–inhibitory balance and is known to exert neuroprotective activities (Spiegel *et al*, 2014; Fu *et al*, 2020) (Figs 9D and EV4C), and *Grin3b* (Perez-Otano *et al*, 2016), a glutamate receptor subunit (Figs 9D and EV4C). In the 14-month-old cohort *Npas4* expression is not significantly altered in *Double* KO mice compared to WT or *Grn* KO mice, although still reduced in single *Grn* KO mice (Fig 9D). In comparison to single *Grn* KO and WT mice, only four genes were significantly downregulated more than 20% in the *Double* KO mice. Interestingly, three of these, namely *Ninj2*, *Ugt8a*, and *Plnxb3*, are exclusively expressed in oligodendrocytes, suggesting major deficits in myelination in *Double* KO mice (Fig 9E) as recently reported for *Trem2* KO (Wu *et al*, 2021).

Although gene expression analysis of the *Double* KO suggests dampening of the pathological DAM signature, enhanced synaptic loss and increased NfL in CSF of *Double* KO indicate that neurodegeneration of PGRN-deficient mice may not be improved by the additional knockout of TREM2 but instead increased even further. We therefore investigated if the additional loss of TREM2 in PGRN-deficient mice affects deficits in glucose uptake *in vivo*. To determine brain cerebral uptake rates of glucose in *Double* KO *in vivo*, we performed 2-[18F]fluoro-d-glucose PET (FDG-PET). We confirmed a reduced cerebral glucose uptake in *Grn* KO ($P < 0.05$) and *Trem2* KO ($P < 0.0001$) mice compared to WT (Figs 9E and F, and EV5B), as described in previous studies (Kleinberger *et al*, 2017; Gotzl *et al*, 2019). However, we still observed similar decreased glucose uptake in *Double* KO mice when compared to WT ($P < 0.0001$) (Figs 9E and F, and EV5B), revealing a consistently decreased glucose uptake between *Grn* KO, *Trem2* KO, or *Double* KO mice and WT mice. Together, all our findings indicate that reducing hyperactivation of microglia does not ameliorate lysosomal dysfunction of PGRN-deficient mice but may even promote neurodegeneration.
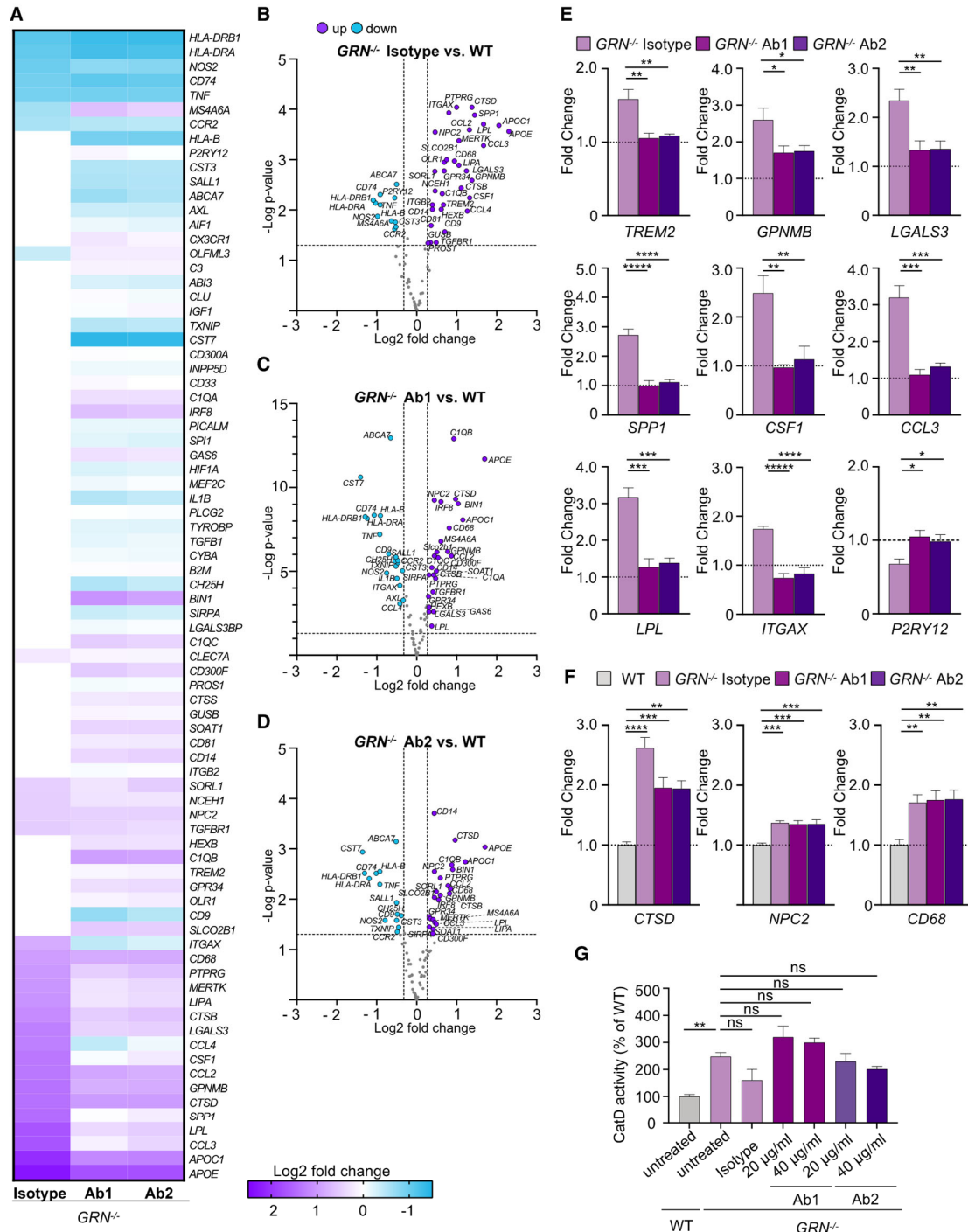
Figure 5.

◀

Figure 5.   Antagonistic TREM2 antibodies reduce hyperactivation of PGRN-deficient hiMGL.

A   Expression of all analyzed gene transcripts in $GRN^{-/-}$ hiMGL treated with control isotype antibody, Ab1, or Ab2 in comparison to WT hiMGL. Data show the mean of four individual treatments and NanoString measurements. The mRNA counts for each gene were normalized to the mean value of all WT samples followed by a log2 transformation.

B   Volcano plot presentation of the differently expressed transcripts in $GRN^{-/-}$ hiMGL treated with isotype compared to WT hiMGL. Genes with more than 20% significantly changed expression are marked in purple (upregulated) or blue (downregulated).

C   Volcano plot presentation of the differently expressed transcripts in $GRN^{-/-}$ hiMGL treated with Ab1 comparison to WT hiMGL. Genes with more than 20% significantly changed expression are marked in purple (upregulated) or blue (downregulated).

D   Volcano plot presentation of the differently expressed transcripts in $GRN^{-/-}$ hiMGL treated with Ab2 comparison to WT hiMGL. Genes with more than 20% significantly changed expression are marked in purple (upregulated) or blue (downregulated).

E   Transcript levels of DAM gene transcripts significantly altered in $GRN^{-/-}$ hiMGL, treated with Ab1 or Ab2 in comparison to isotype treatment from the data set in A, and normalized to the mean of the WT hiMGL samples ($n = 4$, biological replicates).

F   Transcript levels of *CTSD*, *NPC2*, and *CD68* of WT and $GRN^{-/-}$ hiMGL untreated, treated with isotype control, and Ab1 or Ab2 in comparison to WT hiMGL from the data set in A normalized to the mean of the WT hiMGL samples ($n = 4$, biological replicates).

G   Catalytic activity of cathepsin D (CatD) in untreated WT and $GRN^{-/-}$ hiMGL or $GRN^{-/-}$ hiMGL treated with isotype control, Ab1 or Ab2 (20 μg/ml, 40 μg/ml), as measured by a CatD *in vitro* activity assay ($n = 3$, biological replicates).

Data information: Data represent mean ± SEM. For statistical analysis in B–D, the unpaired, two-tailed student's *t*-test was performed, in E, one-way ANOVA with Dunnett's *post hoc* test was used to compare Ab1 and Ab2 (20 μg/ml and 40 μg/ml) conditions to the isotype-treated condition, and in F and G, one-way ANOVA with Dunnett`s *post hoc* test was used to compare Ab1-, Ab2- (20 μg/ml and 40 μg/ml), and isotype-treated condition to WT cells. Statistical significance was set at *$P < 0.05$; **$P < 0.01$; ***$P < 0.001$; ****$P < 0.0001$, *****$P < 0.00001$, and ns, not significant.
Source data are available online for this figure.

Discussion

PGRN and the proteolytically derived granulin peptides may have important lysosomal functions, as exemplified by the identification of homozygous loss-of-function *GRN* mutations, which are causative for NCL (Smith *et al*, 2012). Accumulating evidence suggests that PGRN /granulins directly or indirectly regulate the activity of lysosomal enzymes such as CatD (Beel *et al*, 2017; Valdez *et al*, 2017; Zhou *et al*, 2017; Butler *et al*, 2019a, 2019b; Huang *et al*, 2020), GCase (Jian *et al*, 2016; Arrant *et al*, 2019; Zhou *et al*, 2019), and HexA (Chen *et al*, 2018). The last two enzymes are involved in sphingolipid degradation, a process regulated by the lysosomal phospholipid BMP, which is stabilized by PGRN (Logan *et al*, 2021). PGRN may affect lysosome acidification and thereby lysosomal enzyme activity (Tanaka *et al*, 2017; Logan *et al*, 2021). We and others have shown that PGRN deficiency results in upregulation of several lysosomal enzymes (Gotzl *et al*, 2014, 2018; Klein *et al*, 2017; Huang *et al*, 2020; Root *et al*, 2021). However, it remained unclear if microglial hyperactivation observed in PGRN-deficient microglia contributes to or is a consequence of lysosomal dysfunction. Activated microglia are found in late stages of many neurodegenerative diseases including AD and FTLD, and are believed to be deleterious by promoting synaptic pruning and neuronal cell death (Heneka *et al*, 2013; Hong *et al*, 2016a, 2016b). Specifically, FTLD patients suffering from *GRN* haploinsufficiency show pathological hyperactivation of microglia as measured by TSPO-PET (Martens *et al*, 2012; Gotzl *et al*, 2019; Marschallinger *et al*, 2020; Zhang *et al*, 2020). Similarly, mice lacking PGRN exhibit hyperactivation of microglia as indicated by an enhanced DAM signature including TREM2 and galectin 3, an increased TSPO signal, and increased phagocytic and synaptic pruning activity (Lui *et al*, 2016; Gotzl *et al*, 2019; Zhang *et al*, 2020). We therefore asked if the pathological outcome of PGRN deficiency may be promoted by TREM2-dependent microglial overaction. To address this question, we sought to reduce TREM2-dependent signaling by two independent strategies: genetic loss-of-function and pharmacological inhibition with antagonist antibodies. To achieve the former, we crossed

Trem2 KO mice to the *Grn* KO to generate a *Double* KO model. For the latter approach, we identified TREM2 antagonistic antibodies, which negatively regulate TREM2 by increasing surface receptor shedding and preventing lipid ligand-induced signaling of the co-receptor DAP12. Both approaches successfully dampened several aspects of TREM2-dependent microglial activation. However, although reduction in TREM2 signaling by two independent approaches rescued microglial hyperactivation to some extent, this was not sufficient to ameliorate lysosomal deficits, dysregulation of lysosomal lipids, synapse loss/neurodegeneration, and reduced glucose uptake. These findings demonstrate in this model that microglial hyperactivation is secondary to the primary loss of lysosomal function caused by PGRN deficiency. Surprisingly, inhibition of TREM2 function results in elevated markers for neurodegeneration and synapse loss in *Double* KO animals. Our extensive gene expression analyses do not suggest that the total loss of TREM2 function in *Grn* KO mice causes additional neurotoxicity, for example, by supporting pro-inflammatory microglial responses. Instead, the fact that the additional loss of TREM2 leads to increased brain pathology indicates that TREM2-regulated microglial activation states may not necessarily be deleterious but protective. We suggest that hyperactivated microglia, for example, in *Grn* KO mice, resemble the previously described DAM2 microglia or may develop into them by even further increasing their DAM signature (Keren-Shaul *et al*, 2017). Consistently, fully activated DAM2 microglia were recently described to be particularly protective in a mouse model for amyloidosis and tau pathology (Lee *et al*, 2021). This is very surprising since chronically activated microglia, as observed in PGRN loss-of-function models and mouse models for amyloid and tau pathology, would have been expected to exert significant damage within the brain, for example, by induction of the inflammasome (Heneka *et al*, 2018). However, our findings together with those by Lee *et al* (2021) rather suggest that TREM2-dependent chronic activation is protective, which may have implications for therapeutic attempts employing modulation of TREM2 activity by agonistic antibodies (Deczkowska *et al*, 2020; Lewcock *et al*, 2020). In that regard, the nomenclature used for describing diverse microglial states, namely
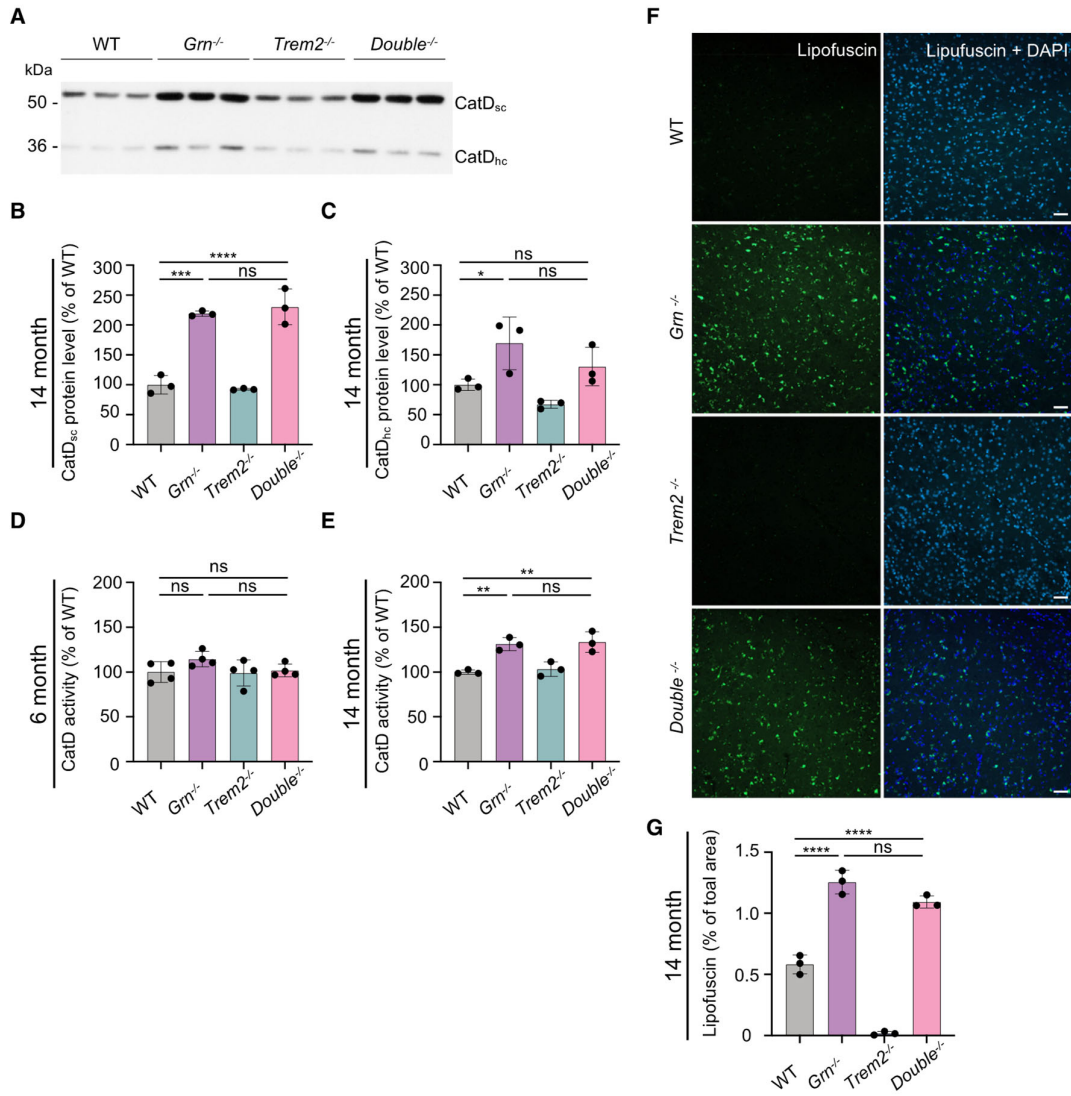
Figure 6. Abolishing TREM2 signaling does not rescue lysosomal dysfunction in *Grn*^{−/−} mice.

A   Western blot of CatD in total brain lysates from 14-month-old female WT, *Grn*^{−/−}, *Trem2*^{−/−}, and *Double*^{−/−} mice. CatD maturation variants are indicated (sc: single chain; hc: heavy chain; $n = 3$).

B, C   Quantification of CatD variants in A normalized to WT ($n = 3$ per genotype).

D, E   Catalytic activity of CatD in brain lysates from female 6-month-old ($n = 4$ per genotype) (D) or 14-month-old ($n = 3$ per genotype) (E) *Grn*^{−/−}, *Trem2*^{−/−}, and *Double*^{−/−} mice normalized to WT.

F   Immunohistochemical analysis of lipofuscin (green) in coronal brain sections. Representative images of thalamus are shown. Scalebars = 50 μm.

G   Quantification of lipofuscin autofluorescence. Five images per mouse were taken, and means were normalized to WT samples ($n = 3$ per genotype, female).

Data information: Data represent mean ± SEM. For statistical analysis, one-way ANOVA with Tukey's *post hoc* test of *Grn*^{−/−}, *Trem2*^{−/−}, and *Double*^{−/−} was used. Statistical significance was set at *$P < 0.05$; **$P < 0.01$; ***$P < 0.001$; ****$P < 0.0001$, and ns, not significant.
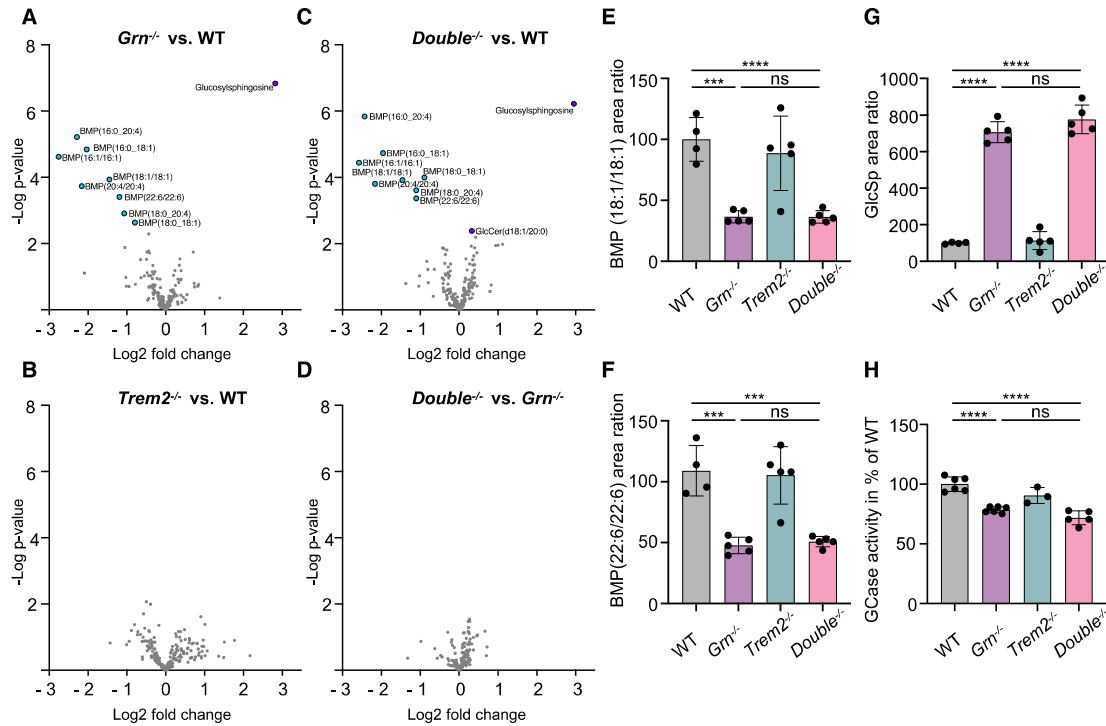Source data are available online for this figure.

64

Figure 7. Reduced TREM2 signaling does not rescue dysregulated lipids in *Grn*−/− mice.

A–D Volcano plot presentation of lipids and metabolites upregulated (purple) or downregulated (blue) in total brain homogenates from 6-month-old male *Grn*−/− (A, *n* = 5), *Trem2*−/− (B, *n* = 5), and *Double*−/− (C, *n* = 5) mice in comparison to WT (*n* = 4), and *Double*−/− in comparison to *Grn*−/− mice (D). Counts for each sample were normalized to the mean value of WT followed by a log2 transformation (*n* = 4–5 per genotype). Analyte values were adjusted with an FDR < 10% to exclude type I errors in null hypothesis testing.

E–G Abundance of BMP species and glucosylsphingosine (GlcSph) in total brain of 6-month-old *Grn*−/−, *Trem2*−/−, *Double*−/−, and WT mice (*n* = 4–5 per genotype).

H Glucocerebrosidase (GCase) activity in whole-brain lysates from 6-month-old male *Grn*−/−, *Trem2*−/−, *Double*−/−, and WT mice. The linear increase in fluorescence signal was measured and then normalized to WT mice (*n* = 3–6 per genotype).

Data information: Data represent mean ± SEM. For statistical analysis, one-way ANOVA with Tukey's *post hoc* test of *Grn*−/−, *Trem2*−/−, and *Double*−/− was used. Statistical significance was set at ***$P < 0.001$; ****$P < 0.0001$, and ns, not significant.
Source data are available online for this figure.

Figure 8. Loss of TREM2 does not prevent synapse loss and activated microglia morphology.

A Immunohistochemical analysis of synaptophysin (SPH, pink) and VGAT (yellow) in coronal brain sections. Representative images of thalamus are shown. Scalebars = 50 μm.

B Quantification of SPH-positive area. Three images per mouse were taken, and means were normalized to WT samples (*n* = 3 per genotype, female).

C Quantification of VGAT-positive area. Three images per mouse were taken, and means were normalized to WT samples (*n* = 3 per genotype, female).

D Western blot of SPH in RIPA lysates from 14-month-old female WT, *Grn*−/−, *Trem2*−/−, and *Double*−/− mice. Actin was used as loading control.

E Quantification of SPH protein levels in D normalized to WT (*n* = 3).

F Morphological analysis of cortical microglia. Representative maximum-intensity projections of confocal *z*-stack images showing IBA1+ microglial cells of female WT, *Grn*−/−, *Trem2*−/−, and *Double*−/− mice (scalebar = 50 μm). Arrows point to individual microglia, which are shown as three-dimensional reconstruction, scalebar = 10 μm.

G Morphological differences in cortical microglia from WT, *Grn*−/−, *Trem2*−/−, and *Double*−/− mice shown by branch volume, sphericity score, branch length, and the number of branch nodes. Statistical analysis of group difference for the morphological scores "Branch volume" (auc = 0.72), "Sphericity score" (auc = 0.82), "Branch length" (auc = 0.69), and "Number of branch nodes" (auc = 0.80) was performed using the Wilcoxon rank-sum test with continuity correction and Bonferroni *post hoc* correction for multiple testing in R (version 4.0.3). Two images per mouse (*n* = 3 per genotype, female) were analyzed, each data point represents one microglia cell. Median and interquartile range are displayed.

Data information: Data represent mean ± SEM. For statistical analysis in B-C and E, one-way ANOVA with Tukey's *post hoc* test of *Grn*−/−, *Trem2*−/−, and *Double*−/− was used. Statistical significance was set at *$P < 0.05$; **$P < 0.01$; ***$P < 0.001$; ****$P < 0.0001$, and ns, not significant.
Source data are available online for this figure.

Figure 8.

66

Figure 9.

67
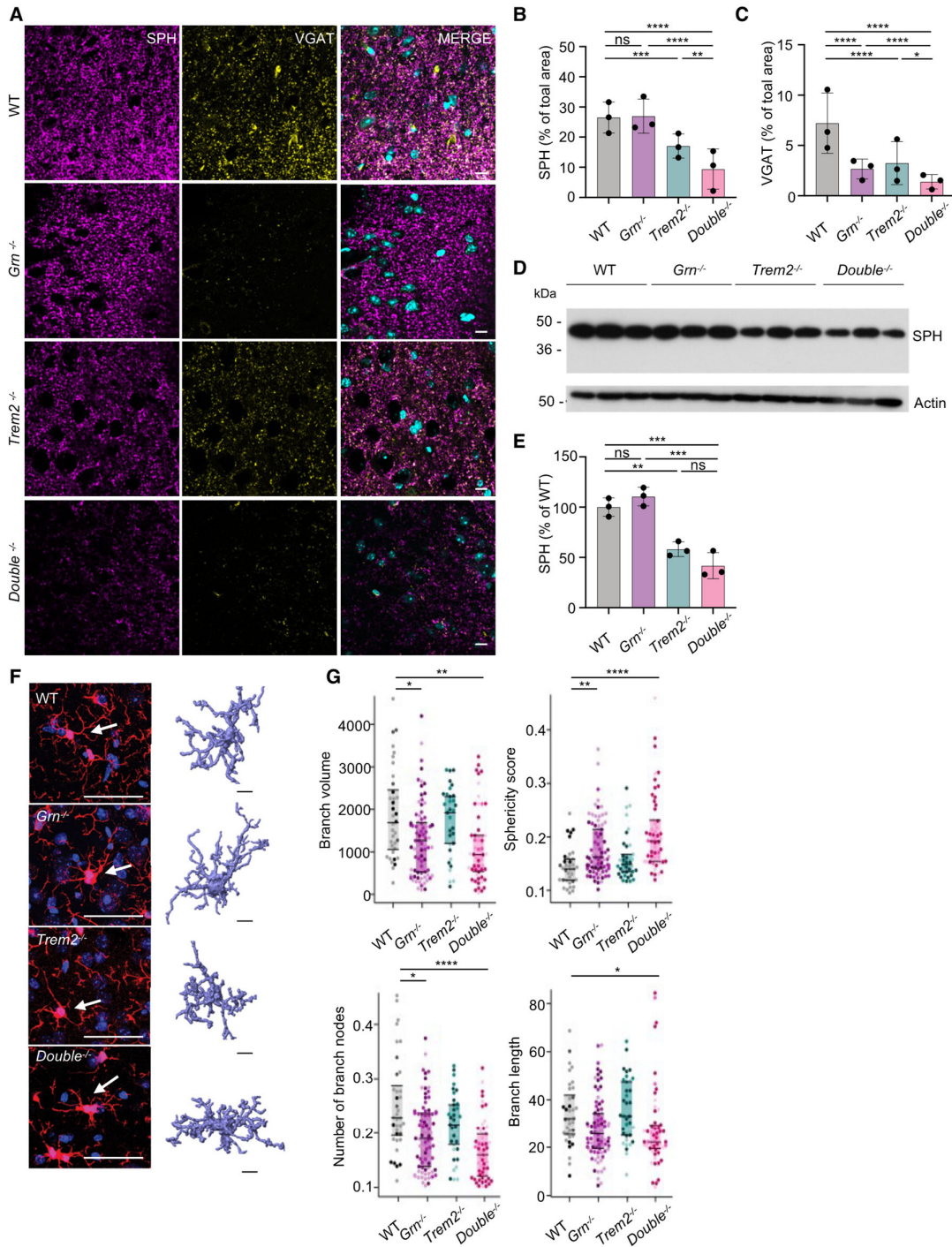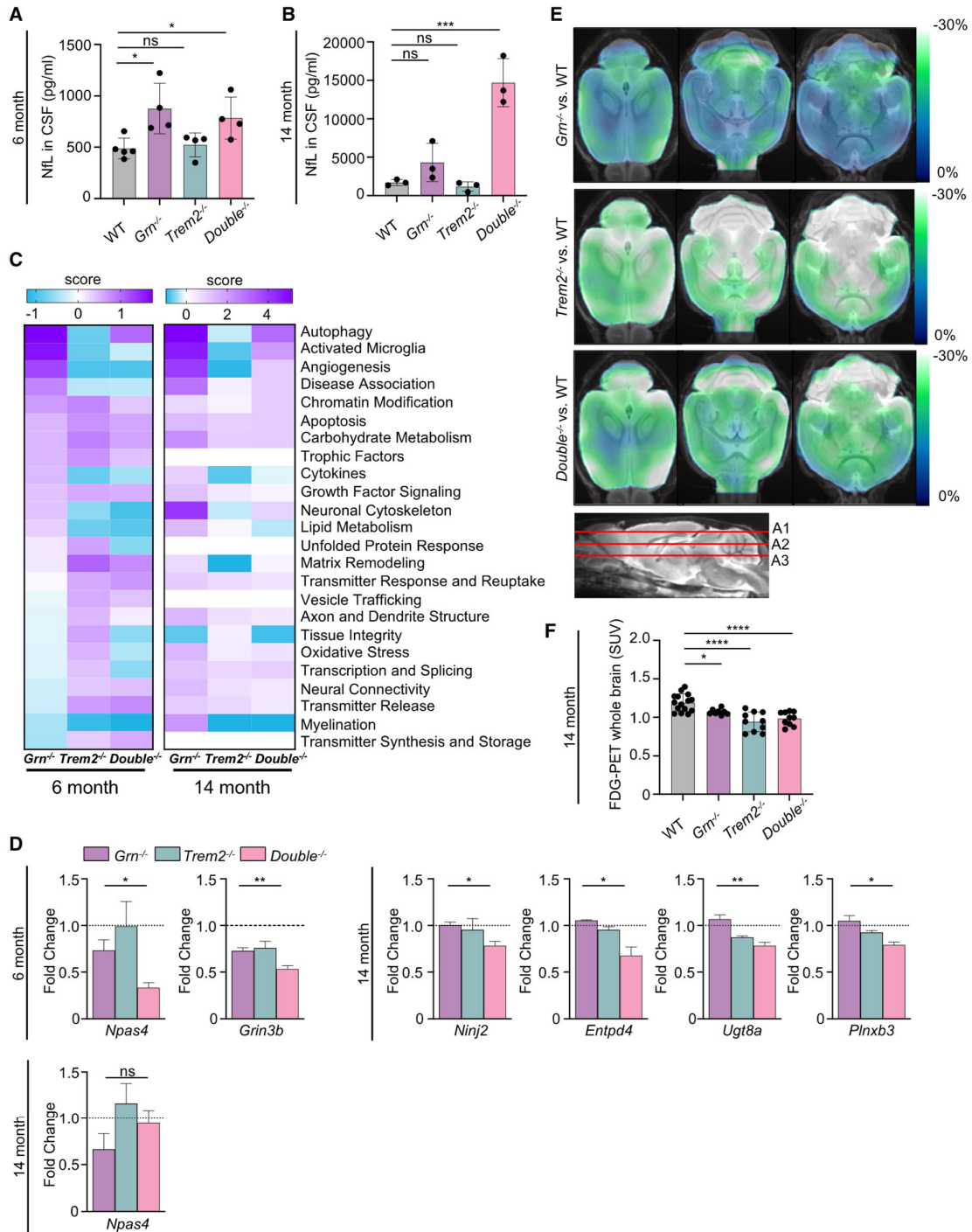
Figure 9. Hyperactivation of microglia in *Grn⁻ᐟ⁻* mice is not deleterious.

A   Immunoassay-based quantification of neurofilament light-chain (NfL) protein levels in CSF of 6-month-old *Grn⁻ᐟ⁻* (*n* = 4), *Trem2⁻ᐟ⁻* (*n* = 4), *Double⁻ᐟ⁻* (*n* = 4), and WT (*n* = 5) male mice.

B   Immunoassay-based quantification of NfL levels in CSF of 14-month-old *Grn⁻ᐟ⁻*, *Trem2⁻ᐟ⁻*, *Double⁻ᐟ⁻*, and WT female mice (*n* = 3 per genotype).

C   Neuropathology NanoString panel analysis of total brain mRNA expression of 6-month-old and 14-month-old *Grn⁻ᐟ⁻*, *Trem2⁻ᐟ⁻*, *Double⁻ᐟ⁻*, and WT male mice based on NanoString advanced analysis R-script included in the panel (6-month-old mice: *n* = 4, 14-month-old mice: *n* = 3).

D   Transcript levels of all significantly changed genes in *Double⁻ᐟ⁻* versus *Grn⁻ᐟ⁻* brain mRNA of 6-month-old and 14-month-old mice analyzed in C. *Grin3b* were under detection limit in the 14-month-old cohort. Transcript expression is normalized to the mean of the WT cohort.

E   The same cohort of mice scanned for TSPO-PET was additionally scanned for FDG-PET. Axial slices as indicated show %-FDG-PET differences among *Grn⁻ᐟ⁻*, *Trem2⁻ᐟ⁻*, and *Double⁻ᐟ⁻* (all cold color scales) when compared to WT at the group level. Images were adjusted to an MRI template.

F   Bar graph illustrates individual FDG-PET values derived from a whole-brain volume of interest. Data represent mean ± SD. A total of 8–15 female mice per group at an average age of 10.7 ± 1.5 months (*Grn⁻ᐟ⁻* *n* = 8, *Trem2⁻ᐟ⁻* *n* = 10, *Double⁻ᐟ⁻* *n* = 10, WT *n* = 15) were used.

Data information: Data in A, B, and D represent mean ± SEM. For statistical analysis in A–B, two-way ANOVA with Dunnett's *post hoc* test was used, in D, F, the unpaired, two-tailed student's *t*-test was performed. Statistical significance was set at *P < 0.05; **P < 0.01; ***P < 0.001; ****P < 0.0001, and ns, not significant. Source data are available online for this figure.

homeostatic, disease associated, and hyperactivated, may need to be reconsidered. We find these terms misleading, as they indicate that homeostatic microglia are beneficial, whereas disease-associated or - hyperactivated microglia are deleterious. Importantly, the brain environment and pathological context is important for ascribing microglial state and associated functions and requires a deeper understanding beyond transcriptional characterization to elucidate the overall impact to brain function and disease. However, one may describe these fundamentally different states of microglia as "surveilling" versus "responding" microglia to capture activities that occur during normal versus pathological contexts. The term "responding" would implicate that these microglia exert protective effects.

Protective microglial functions are promoted by enhancing TREM2 signaling with agonist TREM2 antibodies (Lewcock *et al*, 2020). All currently described agonistic TREM2 antibodies act via similar mechanisms by inhibiting shedding and directly activating TREM2, and therefore increasing functional receptor on the cell surface (Lewcock *et al*, 2020). Notably, all known agonistic TREM2 antibodies bind to the stalk region close to the cleavage site by ADAM10/17 (Schlepckow *et al*, 2017; Lewcock *et al*, 2020). In contrast, the two antagonistic antibodies described here bind in the IgV-fold between amino acids 30 and 63 (Fig EV1A). Interestingly, this domain of TREM2 harbors a number of AD- and FTLD-associated sequence variants (Colonna & Wang, 2016). The R47H variant increases AD risk and affects TREM2-dependent microglial proliferation, lipid metabolism, and microgliosis. Similarly, the FTLD-associated Y38C variant causes a loss of function by misfolding and retention of TREM2 within the endoplasmic reticulum (Kleinberger *et al*, 2014). Antagonistic antibodies therefore appear to bind at a functionally critical region and may displace natural ligands (e.g., lipids), thus preventing induction of TREM2 signaling, in addition to promoting TREM2 shedding.

Finally, our findings also contribute to addressing the long-standing question of whether microglia can dynamically reverse their activation state in both directions, from homeostatic to DAM and back again. Our findings strongly indicate that even hyperactivated microglia can switch back to homeostatic microglia. The fact that one can influence microglial activation in both directions with TREM2-modulating antibodies is another example for the tremendous dynamics of microglia, and offers the opportunity for therapeutic fine tuning of microglial activity.

Taken together, eliminating TREM2 function and thus reducing hyperactivation by two independent approaches do not rescue lysosomal dysfunction caused by GRN deficiency, but rather exacerbates pathological endpoints characteristic for neurodegeneration, including elevation of CSF NfL and reduced transcription of the neuroprotective transcription factor *Npas*. Thus, despite common assumptions, these results suggest that hyperactivated microglia can retain TREM2-dependent protective functions.

Materials and Methods

Animal experiments and mouse brain tissue

All animal experiments were performed in accordance with German animal welfare law and approved by the government of upper Bavaria. Mice were kept under standard housing conditions including standard pellet food and water provided *ad libitum*. Mice were sacrificed by CO_2 inhalation or deep/lethal anesthesia followed by PBS perfusion. Brain tissue was obtained from male and female of the following mouse strains: C57BL/6J *Grn* (Kayasuga *et al*, 2007) and *Trem2* knockout line (Turnbull *et al*, 2006). To minimize mouse numbers and to reduce variability due to sex differences, both male and female cohorts were used but separately analyzed. PET scans and CSF withdrawal were performed under the animal license: ROB 55.2-2532. Vet_02-18-32.

Isolation, differentiation, and culture of human primary monocytes

Human primary monocytes were isolated from whole blood using Sepmate tubes (StemCell Technologies, #85450) in combination with RosetteSep Human Monocyte Enrichment Cocktail (StemCell Technologies, #15068) according to the manufacturer's protocol. Briefly, fresh blood was collected into EDTA-coated collection tubes and stored at room temperature (RT) until further processing for maximal 6 h. EDTA was added to a final concentration of 1 mM and tubes were mixed by inversion. Fifty μl/ml blood of RosetteSep cocktail was added and samples for incubated for 20 min at RT. Cells were separated on a density gradient using Ficoll-Paque PLUS (ThermoFisher, #11768538). After centrifugation isolated cells were washed with PBS supplemented with 2% FCS. Leftover red blood

cells were lysed using ACK lysing buffer (ThermoFisher, #11509876) for 2 min at RT. Subsequently, cells were washed two times with PBS supplemented with 2% FCS. Cells were counted using Trypan blue as a viability dye and 1×10^6 cells were plated in 10 cm dishes in 10-ml RPMI medium supplemented with 10% FCS, 10% NEAA, 10% L-glutamine, 10% sodium pyruvate, and M-CSF with a final concentration of 50 ng/ml. Forty-eight hours after isolation, 1-ml medium with 500 ng/ml M-CSF was added to the cells. Five days after isolation, cells were washed with PBS and scraped. Cells were counted as described above and plated in either 96-well plates at a density of 5×10^4 cells/well in 100 μl or in 12-well plates at a density of 3×10^5 cells/well in 600 μl RPMI medium supplemented with 10% FCS, 10% NEAA, 10% L-glutamine, 10% sodium pyruvate, and M-CSF with a final concentration of 50 ng/ml.

Generation and maintenance of *GRN* KO iPSC lines

iPSC experiments were performed in accordance with all relevant guidelines and regulations. Female iPSC line A18944 was purchased from ThermoFisher (#A18945). iPSCs were grown in Essential 8 Flex Medium (ThermoFisher, #A2858501) on VTN-coated (Thermo-Fisher, #A14700) cell culture plates at 37°C with 5% CO_2 and split twice a week as small clumps after a 5 min incubation in PBS/ EDTA. Prior to electroporation, iPSCs were split to single cells after a 10 min incubation in PBS/EDTA to Geltrex-coated (ThermoFisher, #A1413302) plates and cultured in StemFlex Medium (Thermo-Fisher, #A3349401) containing 10 mM ROCK inhibitor (Selleck-chem S1049) for 2 days. iPSCs were transfected by electroporation as described earlier (Kwart *et al*, 2017) with modifications. Briefly, 2 million cells were harvested with Accutase (ThermoFisher, #A1110501), resuspended in 100 ml cold BTXpress electroporation solution (VWR International GmbH, #732-1285) with 20 mg Cas9 (pSpCas9(BB)-2A-Puro (PX459) V2.0 (gift from Feng Zhang; Addgene plasmid #62988; http://n2t.net/addgene:62988; RRID: Addgene_62988 (Ran *et al*, 2013)) and 5 mg sgRNA cloned into the BsmBI restriction site of the MLM3636 plasmid (gift from Keith Joung, Addgene plasmid #43860; http://n2t.net/addgene:48360; RRID: Addgene_43860). Cells were electroporated with two pulses at 65 mV for 20 ms in a 1 mm cuvette (ThermoFisher, #15437270). After electroporation, cells were transferred to Geltrex-coated 10 cm plates and grown in StemFlex Medium containing 10 mM ROCK inhibitor until visible colonies appeared. Cells expressing Cas9 were selected by 350 ng/ml Puromycin dihydrochloride (VWR International GmbH, #J593) for 3 consecutive days starting 1 day after electroporation (Steyer *et al*, 2018). Single-cell clone colonies were then picked and analyzed by RFLP assay, using NEB enzyme MwoI for the *GRN* KO, and Sanger sequencing as previously described (Kwart *et al*, 2017).

CRISPR/Cas9 genome editing
Design and preparation of editing reagents and quality control of edited iPSCs was performed as described previously (Weisheit *et al*, 2020, 2021). Briefly, we used CRISPOR (http://crispor.tefor.net (Concordet & Haeussler, 2018)) to select guide RNAs and determine putative off-target loci. We chose gRNAs targeting exon 2 of *GRN*, as it is present in most splice isoforms and a frameshift would affect large parts of the coding region. We also ensured presence of nearby stop codons in alternate reading frames in the sequence after the cut

site. Successful knockout was confirmed on mRNA level by qPCR, and on protein level by Western blot using RIPA lysate and ELISA using conditioned media, respectively. For quality control of edited iPSC clones, we checked absence of off-target effects by PCR amplifying and Sanger sequencing the top five hits based on MIT and CFD scores on CRISPOR. We also confirmed absence of on-target effects such as large deletions and loss of heterozygosity using qgPCR and nearby SNP sequencing (Weisheit *et al*, 2021). Finally, we also ensured pluripotency by immunofluorescence staining for typical markers OCT4, NANOG, SSEA4, and TRA160, and chromosomal integrity by molecular karyotyping (LIFE & BRAIN GmbH). One clonal cell line passed the described quality controls and was further differentiated into hiMGL.

Differentiation of human iPSC-derived Microglia (hiMGL)
We differentiated hiMGL from iPSCs as described (Abud *et al*, 2017) with modifications to improve efficiency and yield: When iPSCs were 70–90% confluent, they were split 1:100–200 onto GelTrex-coated six-well plates for the HPC differentiation using EDTA to get around ~20 small colonies per well. Cells were fed with 2 ml of HemA medium (HPC differentiation kit, StemCell Technologies) on day 0 and half-fed with 1 ml on day 2. Media were switched to 2 ml of HemB on day 3 with half-feeds on days 5 and 7 and 1 ml added on top on day 10. On day 12, HPCs were collected as non-adherent cells to either freeze or continue with the microglia differentiation. HPCs were frozen at 1 million cells per ml in BamBanker (FUJIFILM Wako Chemicals). They were then thawed directly onto GelTrex-coated six-well plates with 1 million cells evenly distributed among six wells in 2-ml iMGL media with 25 ng/ml M-CSF, 100 ng/ml IL-34, and 50 ng/ml TGF-β added fresh. One milliliter of media was added every other day. During the microglia differentiation, the cells were split 1:2 every 6–8 days depending on confluency. We did not use CD200 and CX3CL1 for final differentiation, as this did not alter hiMGL gene expression in NanoString analysis. hiMGL were used for experiments on day 16 of the differentiation. A very similar differentiation protocol was published recently (McQuade *et al*, 2018).

Antagonist antibody generation and verification

Antibody generation was carried out by performing single B-cell sequencing on lymphoid tissues from rodents immunized full-length human TREM2 ectodomaine (ECD)-Fc protein (AbCellera Inc.). Antibodies were screened based on binding to human TREM2, and clones of interest were reformatted onto human effectorless human IgG1-LALAPG backbones for material generation and further evaluation of cell-binding potency and functional impact to TREM2 signaling. Antagonists were identified by their ability to block lipid ligand-induced activation of p-Syk on HEK293 cells overexpressing TREM2-DAP12.

Affinity determination and binding kinetics
Human TREM2-binding affinities of anti-TREM2 antibodies were determined by surface plasmon resonance using a Biacore 8K instrument. Biacore Series S CM5 sensor chip was immobilized with a mixture of two monoclonal mouse anti-Fab antibodies (Human Fab capture kit from GE Healthcare) to capture antibodies for binding measurements. In order to measure human TREM2-binding affinities of anti-TREM2 antibodies, serial threefold dilutions of

recombinant human TREM2-ECD protein were injected at a flow rate of 30 μl/min for 300 s followed by 600 s dissociation in HBS-EP$^+$ running buffer (GE, #BR100669). A 1:1 Languir model of simultaneous fitting of k_{on} and k_{off} was used for antigen-binding kinetics analysis.

Epitope mapping of antagonist TREM2 antibodies

Biotinylated polypeptides for human Trem2 IgV domain (Sequences in Fig EV1B) were purchased from Elim Biopharmaceuticals, Inc. N-terminal cysteine was added to peptides to enable maleimide–thiol conjugation of biotin. The lyophilized biotinylated peptides were reconstituted in 20 mM Tris buffer at pH 8.0. Antibody binding to TREM2 IgV domain peptides was detected using a sandwich ELISA. Briefly, a 96-well half-area ELISA plate was coated with streptavidin overnight at 4°C. The following day, biotinylated TREM2 IgV peptides diluted to 1 μM in 1% BSA/PBS were added to the plate and incubated for 1 h. Antibodies diluted to 120 nM in 1% BSA/PBS were then added and incubated for 1 h. Antibodies bound to peptide were detected with anti-Human IgG-HRP secondary antibody diluted in 1% BSA/PBS. Plates were developed with the addition of TMB substrate and stopped by the addition of 2N sulfuric acid. Absorbance at 450 nm was measured on the Synergy Neo2 plate reader (Biotek). A positive signal was identified as an absorbance value above twofold of lower limit of detection (defined as average of blank + threefold SD of blank).

Detection of anti-TREM2 antibody cell binding by flow cytometry

HEK293-overexpressing human TREM2 (HEK293-H6) and HEK293-overexpressing GFP were harvested using 0.05% trypsin and incubated at 37°C for 2 h. All cells were centrifuged and washed in FACS buffer (PBS + 0.5% BSA) twice. Mixed cells were resuspended in FACS buffer at a density of 10^6 cells/ml per cell line. The mixed cell lines were seeded at 100,000 cells per well in a 96-well V-bottom plate and incubated for 20 min at RT. After incubation, the cells were centrifuged and incubated with anti-TREM2 antibodies in a dose titration from 0 to 300 nM for 45 min on ice. After incubation, cells were centrifuged and washed with FACS buffer three times. The cells were then incubated with secondary antibody (Alexa Fluor 647 AffiniPure F(ab')2 fragment goat anti-human IgG (H + L), Jackson ImmunoResearch Laboratories, #109-606-088, 1:800 dilution), for 30 min on ice without exposure to light. After incubation, the cells were washed with FACS buffer three times, resuspended in 100 μl of FACS buffer, and analyzed by flow cytometry (BD FACS-Canto II, San Jose, CA), for which 50,000 events were obtained for each sample. Mean fluorescence intensity (MFI) per cell was calculated by FLowJO software and used for generation of dose–response binding curve.

Antibody treatment

Eight hours after seeding the cells, they were treated with anti-human TREM2 antibodies (Fig EV1C). Antibodies were diluted in RPMI medium and added to the cells with a final concentration of 20 μg/ml. As control for TREM2 shedding, cells were treated with GM6001 (25 μM, Enzo Life Sciences), or DMSO as a vehicle control. hiMGL were seeded in six-well plates with 400,000 cells/well. Eight hours after seeding, antibodies were diluted in iMGL media and added at a concentration of either 20 or 40 μg/ml. Isotype or TREM2

antibodies were added at a concentration of 40 μg/ml and 24 h after antibody treatment, medium and cells were harvested as previously described.

Small animal PET/MRI

All rodent PET procedures followed an established standardized protocol for radiochemistry, acquisition times, and post-processing (Brendel *et al*, 2016; Overhoff *et al*, 2016), which was transferred to a novel PET/MRI system.

All mice were scanned with a 3T Mediso nanoScan PET/MR scanner (Mediso Ltd) with a single-mouse imaging chamber. A 15-min anatomical T1 MR scan was performed at 15 min after [^{18}F]-FDG injection or at 45 min after [^{18}F]-GE180 injection (head receive coil, matrix size 96 × 96 × 22, voxel size 0.24 × 0.24 × 0.80 mm³, repetition time 677 ms, echo time 28.56 ms, and flip angle 90°). PET emission was recorded at 30–60 min p.i. ([^{18}F]-FDG) or at 60–90 min p.i. ([^{18}F]-GE-180). PET list-mode data within 400–600 keV energy window were reconstructed using a 3D iterative algorithm (Tera-Tomo 3D, Mediso Ltd) with the following parameters: matrix size 55 × 62 × 187 mm³, voxel size 0.3 × 0.3 × 0.3 mm³, eight iterations, six subsets. Decay, random, and attenuation correction were applied. The T1 image was used to create a body–air material map for the attenuation correction. We studied PET images of *Grn* KO mice ($n = 8$), *Trem2* KO mice ($n = 10$ or $n = 9$), Double KO mice ($n = 10$), and WT mice ($n = 15$), all female at an average age of 10.9 ± 1.6 months or 11.1 ± 1.6 months, as indicated in the figure legends. Normalization of injected activity was performed by the previously validated myocardium correction method (Deussing *et al*, 2018) for [^{18}F]-GE-180 TSPO-PET and by standardized uptake value (SUV) normalization for [^{18}F]-FDG-PET. Groups of *Grn* KO, *Trem2* KO, and Double KO mice were compared against WT mice by calculation of %-differences in each cerebral voxel. Finally, [^{18}F]-TSPO-PET and [^{18}F]-FDG-PET values deriving from a whole-brain VOI (Kleinberger *et al*, 2017) were extracted and compared between groups of different genotypes by a one-way ANOVA including Tukey *post hoc* correction.

CSF collection

Mice were fully anesthetized via an intraperitoneal injection of medetomidine (0.5 mg/kg) + midazolam (5 mg/kg) + fentanyl (0.05 mg/kg). CSF was collected as described previously (Lim *et al*, 2018). Briefly, subcutaneous tissue and musculature were removed to expose the meninges overlying the cisterna magna. A glass capillary with a trimmed tip (inner diameter is approximately 0.75 mm) was used to puncture the membrane, and CSF was allowed to flow into the capillary for approximately 10 min. After collection, CSF was centrifuged at 1,000 *g* for 10 min, assessed macroscopically for blood contamination, aliquoted (5 μl) in propylene tubes, snap-frozen in liquid nitrogen, and stored at −80°C until use.

CSF neurofilament light-chain analysis

NfL levels were quantitatively determined in CSF samples using the Simoa NF-light Advantage kit (Quanterix, #103186) following the manufacturer's instructions. CSF samples were diluted 1:10 in sample dilution buffer and mixed with Simoa detector reagent and bead reagent, following an incubation at 30°C for 30 min, shaking

at 800 rpm. Plates were washed with Simoa washing buffer A and SBG reagent from the kit was added. Following a 10 min incubation at 30°C and shaking at 800 rpm, plates were washed twice and sample beads were resuspended in Simoa wash buffer B. NfL concentrations were measured after a 10 min drying at RT using the Simoa DH-1 analyzer (Quanterix).

Gene expression profiling of total brain

Adult mice were perfused transcardially with PBS and dissected brains were snap frozen in liquid nitrogen. Snap frozen brains were mechanically powdered in liquid nitrogen. Total RNA was isolated using the RNeasy Mini kit (Qiagen, #74104) and 60 ng of total RNA per sample was subjected to gene expression profiling using the nCounter® Neuropathology panel from NanoString (NanoString Technologies). Gene expression levels in each sample were normalized against the geometric mean of four housekeeping genes including *Asb10*, *Cltc*, *Hprt1*, and *Tubb5* using the *nSolver Analysis Software*, version 4.0. *Gusb* was excluded because of significant changes in *Grn* KO and *Double* KO mice.

Gene expression profiling of primary microglia

CD11b$^+$ and FCRL$^+$ primary microglia were isolated from adult mouse brain. Mice were perfused transcardially and brains were collected into ice-cold HBSS (ThermoFisher, #14175095). Brain tissue was mechanically dissociated into single-cell suspension using Potter-Elvehjem homogenizers with PTFE Pestle. Microglia cell pellets were resuspended in 70% Percoll and overlayed with equal volumes of 40% Percoll. Microglia were enriched at the interface of 70% (v/v) to 40% (v/v) Percoll after centrifugation (at 18°C, 300g for 30 min; slow acceleration and deceleration: 3) (Mazaheri *et al*, 2017). Microglia were collected, filtered through 100 μm cell strainers, and washed with blocking buffer (0.2% BSA in HBSS). Cells were then consecutively stained with FCRLs monoclonal rat antibody (Butovsky *et al*, 2014) (30 min), goat anti-rat APC antibody (Biogegend, # 405407) (20 min), and Cd11b PeCy7 antibody (BD, #553142) (20 min) on ice. Cells were then washed and resuspended in 0.5 ml blocking buffer and subjected to cell sorting. Sorted CD11b$^+$ and FCRL$^+$ cells were pelleted by centrifugation and snap frozen in liquid nitrogen, stored at −80°C until further use. Following total cell lysis in 1:3 diluted RLT buffer (Quiagen, RNeasy Mini Kit), 10,000 cells in 4 μl volume were subjected to gene expression profiling with the nCounter® customized panel from NanoString (NanoString Technologies). We generated an nCounter panel for analyzing gene expression of 65 microglial activation-related genes including five (*Asb10*, *Cltc*, *Hprt1 Tubb5*, and *Gusb*) housekeeping genes. Gene expression levels in each sample were normalized against the geometric mean of four housekeeping genes using the *nSolver Analysis Software*, version 4.0. *Gusb* was excluded because of significant changes in *Grn* KO and *Double* KO mice.

Gene expression profiling of human hiMGL

hiMGL were seeded into 12-well plates and incubated for 3 h at 37°C (5% CO$_2$). Thereafter, microglia were treated with TREM2 antagonistic antibodies and isotype control for 24 h. After treatment, cells were collected and RNA was isolated using the E.Z.N.A

HP Total RNA kit (Omega Bio-Tek) according to the manufacturer's instructions. Following isolation, RNA quality was determined using a 4200 TapeStation (Agilent) and gene expression profiling with the nCounter® customized panel from NanoString (NanoString Technologies) was performed. We generated an nCounter panel for analyzing gene expression of 82 microglial-related genes and 8 housekeeping genes. Gene expression levels in each sample were normalized against the geometric mean of five housekeeping genes including *CLTC*, *HPRT1*, *RPL13A*, *TBP*, and *PPIA* using the *nSolver Analysis Software*, version 4.0. *CALR*, *TUBB5*, and *YWAHZ* were excluded because of significant changes in *Grn* KO and WT microglia.

Lipid analysis by liquid chromatography-mass spectrometry (LCMS)

Sample preparation for LCMS

For LCMS sample preparation, 10 mg of brain powder prepared from whole-brain–powered homogenates was mixed with 400 ml of methanol spiked with internal standards and homogenized with a 3 mm tungsten carbide bead (shaken at 25 Hz for 30 s). The methanol fraction was then isolated via centrifugation (20 min at 4°C, 14,000 g, followed by transfer of supernatant to a 96-well plate, and 1 h incubation at −20°C followed by an additional 20 min centrifugation (4,000 g at 4°C)) and transferred to glass vials for LCMS analysis. For analysis of a GlcCer/GalCer panel, an aliquot of the methanol fraction was dried under N$_2$ gas and then resuspended in 100 ml of 92.5/5/2.5 CAN/IPA/H2 (MS grade) with 5 mM ammonium formate (MS grade) and 0.5% formic acid (MS grade).

Unless otherwise noted, relative quantification of lipids and metabolites was performed using the Shimadzu Nexera X2 LC system (Shimadzu Scientific Instrument) coupled to Sciex QTRAP 6500+ mass spectrometer (Sciex).

Lipidomic analysis

For each analysis, 5 μl of sample was injected on a BEH C18 1.7 μm, 2.1 × 100 mm column (Waters Corporation), using a flow rate of 0.25 ml/min at 55°C. Mobile phase A consisted of 60:40 acetonitrile/water (v/v); and mobile phase B consisted of 90:10 isopropyl alcohol/acetonitrile (v/v). These buffers were fortified with 10 mM ammonium formate with 0.1% formic acid (positive ionization) or with 10 mM ammonium acetate (negative ionization). The gradient was programmed as follows: 0.0–8.0 min from 45% B to 99% B, 8.0–9.0 min at 99% B, 9.0–9.1 min to 45% B, and 9.1–10.0 min at 45% B. Source settings were as follows: curtain gas at 30 psi; collision gas was set at medium; ion spray voltage at 5,500 V (positive mode) or 4,500 V (negative mode); temperature at 250°C (positive mode) or 600°C (negative mode); ion source gas 1 at 55 psi; and ion source gas 2 at 60 psi. Data acquisition was performed using Analyst 1.6.3 (Sciex) in multiple reaction monitoring mode (MRM). Area ratios of endogenous metabolites and surrogate internal standards were quantified using MultiQuant 3.02 (Sciex).

Protein analysis and Western blotting

Cell pellets obtained from human primary monocytes, cultured hiMGL, or aliquots of powdered frozen brains were lysed in Triton lysis buffer (150 mM NaCl, 50 mM Tris-HCL, pH 7.6, 2 mM EDTA,

1% Triton X-100) supplemented with protease inhibitor (Sigma-Aldrich). Lysates were incubated on ice for 30 min and then centrifuged at 17,000 *g* for 15 min at 4°C. For sequential biochemical protein extraction of soluble, less soluble, and insoluble proteins, brain powder was lysed in high salt (HS) buffer (0.5 M NaCl, 10 mM Tris-HCL pH 7.5, 5 mM EDTA, 1 mM DTT, 10% sucrose), then RIPA buffer (150 mM NaCl, 20 mM Tris-HCL pH7.4, 1% NP-40, 0.05% Triton X-100, 0.5% sodium-desoxycholate, 2.5 mM EDTA), followed by urea buffer (30 mM Tris-HCL pH 8.5, 7 M urea, 2 M thiourea) as described previously (Gotzl *et al*, 2014). For membrane preparation of hiMG, pellets were resuspended with hypotonic buffer (10 mM Tris, pH 7.4, 1 mM EDTA, pH 8.0, 1 mM EGTA, pH 8.0) and incubated on ice for 30 min, vortexed every 10 min, followed by a freeze–thaw cycle, and centrifuged at 17,000 *g* for 45 min at 4°C. The supernatants were collected (cytosolic fraction) and the pellet (membrane fraction) resuspended in STEN lysis buffer and incubated on ice for 20 min. Insoluble proteins were pelleted at 17,000 *g* for 20 min at 4°C and the supernatant (membrane fraction) was collected and used for further analysis. Protein concentrations were determined using the BCA protein assay (Pierce, ThermoFisher). Equal amounts of protein adjusted to lysis buffer were mixed with Laemmli sample buffer supplemented with β-mercaptoethanol. Proteins were separated by SDS–PAGE and transferred onto polyvinylidene difluoride membranes (Immobilon-P, Merck Millipore). Proteins of interest were detected using the following primary antibodies: goat anti-TREM2 (R&D Systems, Inc., #AF1828), rabbit anti-PGRN (ThermoFisher, #40-3400), goat anti-CatD (R&D, #AF1029), mouse anti-SPH (abcam, # ab8049), mouse anti-βActin (Sigma, #A5316), mouse anti-GAPDH (Invitrogen, #AM4300), and rabbit anti-Calnexin (Stressgene, #SPA-860) followed by incubation with horseradish peroxidase-conjugated secondary antibodies and ECL Plus substrate (Thermo-Fisher, Pierce ECL Plus Western Blotting Substrates). For quantification, images were taken with a Luminescent Image Analyzer LAS-4000 (Fujifilm Life Science, Tokyo, Japan) and evaluated with the Multi GaugeV3.0 software (Fujifilm Life Science, Tokyo, Japan).

ELISA-based quantification of sTREM2 and PGRN

sTREM2 in conditioned media was quantitated using the Meso Scale Discovery Platform as described previously (Schlepckow *et al*, 2020). Briefly, streptavidin-coated small-spot 96-well plates were blocked overnight at 4°C, incubated with 0.125 μg/ml biotinylated polyclonal goat anti-human TREM2 capture antibody (R&D, #BAF1828). After washing, plates were incubated with samples and standards for 2 h at RT. If cells were antibody treated, samples and standards were previously mixed 9:1 with denaturing buffer (200 mM Tris-HCL pH 6.8, 4% (w/v) SDS, 40% (v/v) glycerol, 2% (v/v) β-mercaptoethanol, 50 mM EDTA), and boiled at 95°C for 5 min to dissociate and denature TREM2 antibodies-bound antibodies. Plates were washed before incubation for 1 h at RT with 1 μg/ml mouse anti-human TREM2 antibody (SantaCruz Biotechnology, B-3 SCBT-373828). After washing, plates were incubated with a SULFO-TAG-labeled anti-mouse secondary antibody (MesoScaleDiscovery, R32AC-5) for 1 h at RT. After additional washing steps, 1× Meso Scale Discovery Read buffer was added and the light emission at 620 nm after electrochemical stimulation as measured with a Meso Scale Discovery Sector Imager 2400 reader.

PGRN levels were determined using a previously described protocol (Gotzl *et al*, 2019) using the following antibodies: a biotinylated polyclonal goat anti-human PGRN antibody (R&D, #BAF2420) at 0.2 μg/ml as capture antibody, a mouse anti-human PGRN antibody (R&D, #MAB2420) as detection antibody, and a SULFO-TAG-labeled anti-mouse (MesoScaleDiscovery, #R32AC-5) as secondary antibody.

GRN gene sequencing

All 12 coding exons including intron boundaries of the *GRN gene* were amplified by PCR. For PCR reaction, the Q5 polymerase was used according to the manufacturer's protocol. PCR products were then subjected to Sanger sequencing and sequences were compared to the healthy control sequence. A two base pair deletion in exon 6 was detected using forward primer GGGCCTCATTGACTCCAAG and reverse primer GTGGTGTAAGCGGTACCCTC.

p-Syk AlphaLISA

Phosphorylated SYK (p-Syk) was measured using the AlphaLISA SureFire Ultra p-Syk Assay kit (PerkinElmer, #ALSU-PSYK-A-HV) following the manufacturer's instructions. Briefly, differentiated human macrophages were plated in 100 μl media at a density of 50,000 cells/well. hiMGL were plated in iMGL media at a density of 30,000 cells/well, in 96-well plates, and incubated overnight at 37°C in a cell culture incubator. Plates were then washed three times with HBSS and 50 μl of liposome (1 mg/ml)/antibody (20 μg/ml) mix was added to the cells. Following an incubation at 37°C for 1 h for macrophages, or 5 min for hiMGL, treatment solutions were removed and cells were lysed with 40 μl lysis buffer supplemented with protease inhibitor mix (Sigma) and phosphatase inhibitor (PhosSTOP, Roche) for 30 min at 4°C. Equal volumes of lysate were then subjected to analysis using an EnSpire Multimode Plate Reader (PerkinElmer).

Liposome preparation

POPC/POPS (7:3) liposomes at 10 mg/ml were prepared as follows: 7 mg POPC and 3 mg POPS were dissolved in chloroform followed by thorough evaporation of solvent. The lipid mixture was then resuspended in 1 ml HBSS, and suspensions were extruded using 100 nm polycarbonate membranes (Whatman, #800309) and a LiposoFast extruder device (Sigma-Aldrich) to generate large unilamellar vesicles.

Cathepsin activity assay

hiMGL cell pellets or powdered mouse brain tissue was used for cathepsin D fluorescence-based activity assays (Abnova) as described previously (Gotzl *et al*, 2018). Mouse brain tissue was homogenized using precellys lysing kit (Bertin Instruments, #P000933-LYSK0-A).

GCase activity assay

Brain powder was lysed in GCase lysis buffer (150 mM NaCl, 20 mM Tris-HCl (pH 7.5), 1% Triton X-100, 1 mM EDTA, and

1 mM EGTA) and protein concentrations were determined using the BCA assay. Lysates were adjusted to 2 mg/ml. Lysates were diluted 12.5-fold in GCase activity buffer (100 mM Phosphate Citrate buffer pH 5.2, 0.5% Sodium Taurocholate, 0.25% Triton-X 100) and 4-Methylumbelliferyl β-D-glucopyranoside stock solution (30 mM; Sigma-Aldrich, M3633-1G, stock solution in DMF) was diluted three-fold in the GCase activity buffer. Ninety microliter of the diluted lysates and 10 µl of the diluted 4-Methylumbelliferyl β-D-glucopyranoside were added to a 96-well plate. Plates were incubated for 15 min at 37°C. Signal intensities were measured continuously for 1 h (Ex 365 nm/Em 455 nm).

Phagocytosis assays

Microglial phagocytosis was determined using the IncuCyte S3 Live-Cell Analysis System (Sartorius). hiMGL cells were plated in 96-well plates at 30% confluency. Cells were incubated at 37°C and the confluency (pre-treatment) of each well was determined with the IncuCyte S3 3 h after seeding. Thereafter, TREM2 antagonistic antibodies and isotype control were added at 20 and 40 µg/ml. Eighteen hours after antibody treatment, pHrodo-labeled myelin (5 µg/ml) was added to the hiMGL cells and images of fluorescence and phase were captured at 4× in the IncuCyte S3 live cell imager every 15 min. Using IncuCyte 2020B software (Satorius), image masks for phase and fluorescent signal (phagocytosis of pHrodo-labelled myelin) were acquired, and the fluorescent signal was normalized to cell confluency (cell body area), which was measured before the antibody treatment.

pHrodo labeling of myelin

Myelin was labeled with amine reactive pHrodo™ Red succinimidyl ester (ThermoFisher) for 45 min at RT (protected from light). Labeled myelin was washed with PBS and either directly used or stored in aliquots at −80°C.

Immunohistochemistry and image acquisition

Mice were transcardially perfused with PBS and brains were dissected into two hemispheres. One hemisphere was snap frozen and stored at −80°C until further use. The other hemisphere was immersion fixed for 24 h in 4% paraformaldehyde, washed with PBS, and incubated 30% sucrose for 48 h for cryoprotection. After freezing, brains were cut into 50 µm or 100 µm coronal sections using a vibratome (Leica Biosystems), collected in PBS, and stored at 4°C until further use. For visualizing lipofuscin, SPH or VGAT, 50 µm free-floating sections were stained with primary antibodies (mouse anti-VGAT (Synaptic Systems, #131011C3, or rabbit anti-SPH (Abcam, #ab32594)) in 5% donkey serum in PBS overnight at 4°C with slow agitation. After washing, tissue sections were incubated with corresponding secondary antibodies for 3 h at RT. After washing, tissue sections were stained with DAPI for 10 min at RT and mounted onto slides using ProlongTM Gold Antifade reagent (ThermoFisher, #P36961). For morphological analysis of microglia, 100 µm sections were blocked with goat serum blocking buffer (2% goat serum, 0.05% Tween 20 in 0.01 M PBS, pH 7.2–7.4) and stained with anti-IBA1 in primary antibody buffer (1% bovine serum albumin, 0.1% gelatin from cold water fish skin, 0.5% Triton

X-100 in 0.01 M PBS, pH 7.2–7.4) and anti-rabbit IgG-coupled Alexa Flour 555 in secondary antibody buffer (0.05% Tween 20 in 0.01 M PBS, pH 7.2–7.4). After washing, tissue sections were stained with DAPI for 10 min at RT and mounted onto slides using ProlongTM Gold Antifade reagent. Images were acquired using a LSM800 Zeiss confocal microscope and the ZEN 2011 software package (blue edition). For lipofuscin analysis, five images were taken per slide using a 20× objective at 2,048 × 2,048 pixel resolution. For SPH and VGAT analysis, three images were taken per slide using a 20× objective at 2,048 × 2,048 pixel resolution. Total fluorescence above background was quantified using the Fiji software (ImageJ, Version 1.0).

Automated analysis of microglia morphology

For morphological analysis of microglia, two z-stack images per animal (n = 3) were recorded with a 40× objective in a resolution of 1,024 × 1,024 pixels (x–y-pixel size = 0.15598 µm) and a slice distance (z) of 0.4 µm. The raw confocal z-stacks were then analyzed using the Microglia Morphology Quantification Tool (MMQT) for automated analysis of microglial morphology as previously described (Heindl *et al*, 2018). The algorithm was run in MATLAB (Version R2016b). To identify the most discriminating features, a receiver operating characteristic (ROC) analysis was performed in R (version 4.0.3) for calculating the area under the curve (auc) between the groups "WT" and "*Double* KO." Statistical analysis of group difference for the morphological scores, "Branch volume" (auc = 0.72), "Sphericity score" (auc = 0.82), "Branch length" (auc = 0.69), and "Number of branch nodes" (auc = 0.80) was performed using the Wilcoxon rank-sum test with continuity correction and Bonferroni *post hoc* correction for multiple testing in R (version 4.0.3).

Statistical analysis

Data were analyzed using GraphPad Prism 9. If no other test of significance is indicated, for statistical analysis of two groups of samples, the unpaired, two-tailed student's *t*-test was performed. For comparison of more than two groups, one-way ANOVA and Dunnett's or Tukey's *post hoc* test were used. Statistical significance was set at $*P < 0.05$; $**P < 0.01$; $***P < 0.001$; and $****P < 0.0001$.

Data availability

The accession number for the Neuropathology NanoString data reported in this paper is Gene Expression Omnibus GSE181135 http://www.ncbi.nlm.nih.gov/geo/query/acc.cgi?acc = GSE181135 (6-month-old cohort) and GSE185510 http://www.ncbi.nlm.nih.gov/geo/query/acc.cgi?acc = GSE185510 (14-month-old cohort).

Expanded View for this article is available online.

Author contributions

CH, AC, and AR conceived the study and analyzed the results. CH wrote the manuscript with further input from AR, AC, GDP, KMM, JWL, SR, and DP. AR performed and analyzed Western Blots, ELISAs, enzyme activity assays, mRNA isolation, NanoString experiments, and immunofluorescence on all mouse samples. AR isolated and performed all experiments of human-derived macrophages and analyzed hiMGL NanoString data. With supervision of DP, SR generated and validated *GRN* KO hiPSC, differentiated into hiMGL, and performed and analyzed Western Blots, ELISAs, and enzyme activity assays. JK and GK helped to establish hiMGL cell differentiation. KMM and BVL discovered, generated, and validated antagonistic TREM2 antibodies. TL and JS performed lipidomic analysis. MAV and SHa performed NanoString and phagocytosis assays on hiMGL cells. JGn, KW, AZ, and MB conducted, performed, and analyzed PET imaging. SHe performed automated analysis on microglia morphology, with supervision of AL. IP performed CSF isolation. JKG helped to establish mouse lines. JL, KB, JD-S, EW, and LR identified FTLD patients and performed sequencing analysis. BN performed NfL measurements. The synopsis image was created with BioRender.com.

Disclosure statement and competing interests

CH collaborates with Denali Therapeutics, participated on one advisory board meeting of Biogen, and received a speaker honorarium from Novartis and Roche. CH is chief advisor of ISAR Bioscience. KMM, BVL, TL, JS, JWL, and GDP are employees and shareholders of Denali Therapeutics. DP is a scientific advisor of ISAR Bioscience. MB received speaker honoraria from GE healthcare, Roche, and LMI and is an advisor of LMI.

References

Abud EM, Ramirez RN, Martinez ES, Healy LM, Nguyen CHH, Newman SA, Yeromin AV, Scarfone VM, Marsh SE, Fimbres C *et al* (2017) iPSC-derived human microglia-like cells to study neurological diseases. *Neuron* 94: 278 – 293.e9

Aguzzi A, Haass C (2003) Games played by rogue proteins in prion disorders and Alzheimer's disease. *Science* 302: 814 – 818

Almeida MR, Macario MC, Ramos L, Baldeiras I, Ribeiro MH, Santana I (2016) Portuguese family with the co-occurrence of frontotemporal lobar degeneration and neuronal ceroid lipofuscinosis phenotypes due to progranulin gene mutation. *Neurobiol Aging* 41: 200 e201 – 200 e205

Arrant AE, Roth JR, Boyle NR, Kashyap SN, Hoffmann MQ, Murchison CF, Ramos EM, Nana AL, Spina S, Grinberg LT *et al* (2019) Impaired beta-glucocerebrosidase activity and processing in frontotemporal dementia due to progranulin mutations. *Acta Neuropathol Commun* 7: 218

Baker M, Mackenzie IR, Pickering-Brown SM, Gass J, Rademakers R, Lindholm C, Snowden J, Adamson J, Sadovnick AD, Rollinson S *et al* (2006) Mutations in progranulin cause tau-negative frontotemporal dementia linked to chromosome 17. *Nature* 442: 916 – 919

Beel S, Moisse M, Damme M, De Muynck L, Robberecht W, Van Den Bosch L, Saftig P, Van Damme P (2017) Progranulin functions as a cathepsin D chaperone to stimulate axonal outgrowth in vivo. *Hum Mol Genet* 26: 2850 – 2863

Bosch-Queralt M, Cantuti-Castelvetri L, Damkou A, Schifferer M, Schlepckow K, Alexopoulos I, Lutjohann D, Klose C, Vaculciakova L, Masuda T *et al* (2021) Diet-dependent regulation of TGFbeta impairs reparative innate immune responses after demyelination. *Nat Metab* 3: 211 – 227

Brendel M, Probst F, Jaworska A, Overhoff F, Korzhova V, Albert NL, Beck R, Lindner S, Gildehaus F-J, Baumann K *et al* (2016) Glial activation and glucose metabolism in a transgenic amyloid mouse model: a triple-tracer PET study. *J Nucl Med* 57: 954 – 960

Butler VJ, Cortopassi WA, Argouarch AR, Ivry SL, Craik CS, Jacobson MP, Kao AW (2019a) Progranulin stimulates the in vitro maturation of pro-cathepsin D at acidic pH. *J Mol Biol* 431: 1038 – 1047

Butler VJ, Cortopassi WA, Gururaj S, Wang AL, Pierce OM, Jacobson MP, Kao AW (2019b) Multi-granulin domain peptides bind to pro-cathepsin D and stimulate its enzymatic activity more effectively than progranulin in vitro. *Biochemistry* 58: 2670 – 2674

Butovsky O, Jedrychowski MP, Moore CS, Cialic R, Lanser AJ, Gabriely G, Koeglsperger T, Dake B, Wu PM, Doykan CE *et al* (2014) Identification of a unique TGF-beta-dependent molecular and functional signature in microglia. *Nat Neurosci* 17: 131 – 143

Chen Y, Jian J, Hettinghouse A, Zhao X, Setchell KDR, Sun Y, Liu CJ (2018) Progranulin associates with hexosaminidase A and ameliorates GM2 ganglioside accumulation and lysosomal storage in Tay-Sachs disease. *J Mol Med* 96: 1359 – 1373

Cheng Q, Danao J, Talreja S, Wen P, Yin J, Sun N, Li C-M, Chui D, Tran D, Koirala S *et al* (2018) TREM2-activating antibodies abrogate the negative pleiotropic effects of the Alzheimer's disease variant Trem 2(R47H) on murine myeloid cell function. *J Biol Chem* 293: 12620 – 12633

Cignarella F, Filipello F, Bollman B, Cantoni C, Locca A, Mikesell R, Manis M, Ibrahim A, Deng LI, Benitez BA *et al* (2020) TREM2 activation on microglia promotes myelin debris clearance and remyelination in a model of multiple sclerosis. *Acta Neuropathol* 140: 513 – 534

Colonna M, Wang Y (2016) TREM2 variants: new keys to decipher Alzheimer disease pathogenesis. *Nat Rev Neurosci* 17: 201 – 207

Concordet JP, Haeussler M (2018) CRISPOR: intuitive guide selection for CRISPR/Cas9 genome editing experiments and screens. *Nucleic Acids Res* 46: W242 – W245

Cruts M, Gijselinck I, van der Zee J, Engelborghs S, Wils H, Pirici D, Rademakers R, Vandenberghe R, Dermaut B, Martin J-J *et al* (2006) Null mutations in progranulin cause ubiquitin-positive frontotemporal dementia linked to chromosome 17q21. *Nature* 442: 920 – 924

Deczkowska A, Weiner A, Amit I (2020) The physiology, pathology, and potential therapeutic applications of the TREM2 signaling pathway. *Cell* 181: 1207–1217

Deussing M, Blume T, Vomacka L, Mahler C, Focke C, Todica A, Unterrainer M, Albert NL, Lindner S, von Ungern-Sternberg B *et al* (2018) Coupling between physiological TSPO expression in brain and myocardium allows stabilization of late-phase cerebral [(18)F]GE180 PET quantification. *NeuroImage* 165: 83–91

Efthymiou AG, Goate AM (2017) Late onset Alzheimer's disease genetics implicates microglial pathways in disease risk. *Mol Neurodegener* 12: 43

Ellwanger DC, Wang S, Brioschi S, Shao Z, Green L, Case R, Yoo D, Weishuhn D, Rathanaswami P, Bradley J *et al* (2021) Prior activation state shapes the microglia response to antihuman TREM2 in a mouse model of Alzheimer's disease. *Proc Natl Acad Sci USA* 118: e2017742118

Evers BM, Rodriguez-Navas C, Tesla RJ, Prange-Kiel J, Wasser CR, Yoo KS, McDonald J, Cenik B, Ravenscroft TA, Plattner F *et al* (2017) Lipidomic and transcriptomic basis of lysosomal dysfunction in progranulin deficiency. *Cell Rep* 20: 2565–2574

Ewers M, Franzmeier N, Suárez-Calvet M, Morenas-Rodriguez E, Caballero MAA, Kleinberger G, Piccio L, Cruchaga C, Deming Y, Dichgans M *et al* (2019) Increased soluble TREM2 in cerebrospinal fluid is associated with reduced cognitive and clinical decline in Alzheimer's disease. *Sci Transl Med* https://doi.org/10.1126/scitranslmed.aav6221

Fassler M, Rappaport MS, Cuno CB, George J (2021) Engagement of TREM2 by a novel monoclonal antibody induces activation of microglia and improves cognitive function in Alzheimer's disease models. *J Neuroinflammation* 18: 19

Fu J, Guo O, Zhen Z, Zhen J (2020) Essential functions of the transcription factor Npas4 in neural circuit development, plasticity, and diseases. *Front Neurosci* 14: 603373

Gotzl JK, Brendel M, Werner G, Parhizkar S, Sebastian Monasor L, Kleinberger G, Colombo AV, Deussing M, Wagner M, Winkelmann J *et al* (2019) Opposite microglial activation stages upon loss of PGRN or TREM2 result in reduced cerebral glucose metabolism. *EMBO Mol Med* 11: 1–15

Gotzl JK, Colombo AV, Fellerer K, Reifschneider A, Werner G, Tahirovic S, Haass C, Capell A (2018) Early lysosomal maturation deficits in microglia triggers enhanced lysosomal activity in other brain cells of progranulin knockout mice. *Mol Neurodegener* 13: 48

Gotzl JK, Lang CM, Haass C, Capell A (2016) Impaired protein degradation in FTLD and related disorders. *Ageing Res Rev* 32: 122–139

Götzl JK, Mori K, Damme M, Fellerer K, Tahirovic S, Kleinberger G, Janssens J, van der Zee J, Lang CM, Kremmer E *et al* (2014) Common pathobiochemical hallmarks of progranulin-associated frontotemporal lobar degeneration and neuronal ceroid lipofuscinosis. *Acta Neuropathol* 127: 845–860

Guerreiro R, Wojtas A, Bras J, Carrasquillo M, Rogaeva E, Majounie E, Cruchaga C, Sassi C, Kauwe JS, Younkin S *et al* (2013) TREM2 variants in Alzheimer's disease. *N Engl J Med* 368: 117–127

Heindl S, Gesierich B, Benakis C, Llovera G, Duering M, Liesz A (2018) Automated morphological analysis of microglia after stroke. *Front Cell Neurosci* 12: 106

Heneka MT, Kummer MP, Stutz A, Delekate A, Schwartz S, Vieira-Saecker A, Griep A, Axt D, Remus A, Tzeng T-C *et al* (2013) NLRP3 is activated in Alzheimer's disease and contributes to pathology in APP/PS1 mice. *Nature* 493: 674–678

Heneka MT, McManus RM, Latz E (2018) Inflammasome signalling in brain function and neurodegenerative disease. *Nat Rev Neurosci* 19: 610–621

Hong S, Beja-Glasser VF, Nfonoyim BM, Frouin A, Li S, Ramakrishnan S, Merry KM, Shi Q, Rosenthal A, Barres BA *et al* (2016a) Complement and microglia mediate early synapse loss in Alzheimer mouse models. *Science* 352: 712–716

Hong S, Dissing-Olesen L, Stevens B (2016b) New insights on the role of microglia in synaptic pruning in health and disease. *Curr Opin Neurobiol* 36: 128–134

Hu F, Padukkavidana T, Vaegter CB, Brady OA, Zheng Y, Mackenzie IR, Feldman HH, Nykjaer A, Strittmatter SM (2010) Sortilin-mediated endocytosis determines levels of the frontotemporal dementia protein, progranulin. *Neuron* 68: 654–667

Huang M, Modeste E, Dammer E, Merino P, Taylor G, Duong DM, Deng Q, Holler CJ, Gearing M, Dickson D *et al* (2020) Network analysis of the progranulin-deficient mouse brain proteome reveals pathogenic mechanisms shared in human frontotemporal dementia caused by GRN mutations. *Acta Neuropathol Commun* 8: 163

Jadhav VS, Lin PBC, Pennington T, Di Prisco GV, Jannu AJ, Xu G, Moutinho M, Zhang J, Atwood BK, Puntambekar SS *et al* (2020) Trem2 Y38C mutation and loss of Trem2 impairs neuronal synapses in adult mice. *Mol Neurodegener* 15: 62

Jian J, Zhao S, Tian Q-Y, Liu H, Zhao Y, Chen W-C, Grunig G, Torres PA, Wang BC, Zeng B *et al* (2016) Association between progranulin and gaucher disease. *EBioMedicine* 11: 127–137

Jonsson T, Stefansson H, Steinberg S, Jonsdottir I, Jonsson PV, Snaedal J, Bjornsson S, Huttenlocher J, Levey AI, Lah JJ *et al* (2013) Variant of TREM2 associated with the risk of Alzheimer's disease. *N Engl J Med* 368: 107–116

Kao AW, McKay A, Singh PP, Brunet A, Huang EJ (2017) Progranulin, lysosomal regulation and neurodegenerative disease. *Nat Rev Neurosci* 18: 325–333

Kayasuga Y, Chiba S, Suzuki M, Kikusui T, Matsuwaki T, Yamanouchi K, Kotaki H, Horai R, Iwakura Y, Nishihara M (2007) Alteration of behavioural phenotype in mice by targeted disruption of the progranulin gene. *Behav Brain Res* 185: 110–118

Keren-Shaul H, Spinrad A, Weiner A, Matcovitch-Natan O, Dvir-Szternfeld R, Ulland TK, David E, Baruch K, Lara-Astaiso D, Toth B *et al* (2017) A Unique microglia type associated with restricting development of Alzheimer's disease. *Cell* 169: 1276–1290.e17

Klein ZA, Takahashi H, Ma M, Stagi M, Zhou M, Lam TT, Strittmatter SM (2017) Loss of TMEM106B ameliorates lysosomal and frontotemporal dementia-related phenotypes in progranulin-deficient mice. *Neuron* 95: 281–296.e6

Kleinberger G, Brendel M, Mracsko E, Wefers B, Groeneweg L, Xiang X, Focke C, Deussing M, Suarez-Calvet M, Mazaheri F *et al* (2017) The FTD-like syndrome causing TREM2 T66M mutation impairs microglia function, brain perfusion, and glucose metabolism. *EMBO J* 36: 1837–1853

Kleinberger G, Yamanishi Y, Suárez-Calvet M, Czirr E, Lohmann E, Cuyvers E, Struyfs H, Pettkus N, Wenninger-Weinzierl A, Mazaheri F *et al* (2014) TREM2 mutations implicated in neurodegeneration impair cell surface transport and phagocytosis. *Sci Transl Med* 6: 243ra286

Krabbe G, Minami SS, Etchegaray JI, Taneja P, Djukic B, Davalos D, Le D, Lo I, Zhan L, Reichert MC *et al* (2017) Microglial NFkappaB-TNFalpha hyperactivation induces obsessive-compulsive behavior in mouse models of progranulin-deficient frontotemporal dementia. *Proc Natl Acad Sci USA* 114: 5029–5034

Krasemann S, Madore C, Cialic R, Baufeld C, Calcagno N, El Fatimy R, Beckers L, O'Loughlin E, Xu Y, Fanek Z *et al* (2017) The TREM2-APOE pathway drives the transcriptional phenotype of dysfunctional microglia in neurodegenerative diseases. *Immunity* 47: 566–581.e9

Kwart D, Paquet D, Teo S, Tessier-Lavigne M (2017) Precise and efficient scarless genome editing in stem cells using CORRECT. *Nat Protoc* 12: 329−354

Lee SH, Meilandt WJ, Xie L, Gandham VD, Ngu H, Barck KH, Rezzonico MG, Imperio J, Lalehzadeh G, Huntley MA *et al* (2021) Trem2 restrains the enhancement of tau accumulation and neurodegeneration by beta-amyloid pathology. *Neuron* 109: 1283−1301 e1286

Lewcock JW, Schlepckow K, Di Paolo G, Tahirovic S, Monroe KM, Haass C (2020) Emerging microglia biology defines novel therapeutic approaches for Alzheimer's disease. *Neuron* 108: 801−821

Lim NK, Moestrup V, Zhang X, Wang WA, Moller A, Huang FD (2018) An improved method for collection of cerebrospinal fluid from anesthetized mice. *J Vis Exp* https://doi.org/10.3791/56774

Liu B, Le KX, Park MA, Wang S, Belanger AP, Dubey S, Frost JL, Holton P, Reiser V, Jones PA *et al* (2015) In vivo detection of age- and disease-related increases in neuroinflammation by 18F-GE180 TSPO MicroPET imaging in wild-type and Alzheimer's transgenic mice. *J Neurosci* 35: 15716−15730

Logan T, Simon JS, Rana A, Cherf GM, Srivastava A, Davis SS, Yoon Low RL, Chiu C, Fang M, Huang F *et al* (2021) Rescue of a lysosomal storage disorder caused by BMP deficiency in Grn loss-of-function with a brain penetrant progranulin biologic. *Cell* 184: 4651−4668.e25

Lui H, Zhang J, Makinson S, Cahill M, Kelley K, Huang H-Y, Shang Y, Oldham M, Martens L, Gao F *et al* (2016) Progranulin Deficiency Promotes Circuit-Specific Synaptic Pruning By Microglia Via Complement Activation. *Cell* 165: 921−935

Marschallinger J, Iram T, Zardeneta M, Lee SE, Lehallier B, Haney MS, Pluvinage JV, Mathur V, Hahn O, Morgens DW *et al* (2020) Lipid-droplet-accumulating microglia represent a dysfunctional and proinflammatory state in the aging brain. *Nat Neurosci* 23: 194−208

Martens LH, Zhang J, Barmada SJ, Zhou P, Kamiya S, Sun B, Min S-W, Gan LL, Finkbeiner S, Huang EJ *et al* (2012) Progranulin deficiency promotes neuroinflammation and neuron loss following toxin-induced injury. *J Clin Invest* 122: 3955−3959

Mazaheri F, Snaidero N, Kleinberger G, Madore C, Daria A, Werner G, Krasemann S, Capell A, Trumbach D, Wurst W *et al* (2017) TREM2 deficiency impairs chemotaxis and microglial responses to neuronal injury. *EMBO Rep* 18: 1186−1198

McQuade A, Coburn M, Tu CH, Hasselmann J, Davtyan H, Blurton-Jones M (2018) Development and validation of a simplified method to generate human microglia from pluripotent stem cells. *Mol Neurodegener* 13: 67

Meeter LH, Dopper EG, Jiskoot LC, Sanchez-Valle R, Graff C, Benussi L, Ghidoni R, Pijnenburg YA, Borroni B, Galimberti D *et al* (2016) Neurofilament light chain: a biomarker for genetic frontotemporal dementia. *Ann Clin Transl Neurol* 3: 623−636

Meilandt WJ, Ngu H, Gogineni A, Lalehzadeh G, Lee SH, Srinivasan K, Imperio J, Wu T, Weber M, Kruse AJ *et al* (2020) Trem2 deletion reduces late-stage amyloid plaque accumulation, elevates the Abeta42:Abeta40 ratio, and exacerbates axonal dystrophy and dendritic spine loss in the PS2APP Alzheimer's mouse model. *J Neurosci* 40: 1956−1974

Nugent AA, Lin K, van Lengerich B, Lianoglou S, Przybyla L, Davis SS, Llapashtica C, Wang J, Kim DJ, Xia D *et al* (2020) TREM2 regulates microglial cholesterol metabolism upon chronic phagocytic challenge. *Neuron* 105: 837−854.e9

Overhoff F, Brendel M, Jaworska A, Korzhova V, Delker A, Probst F, Focke C, Gildehaus F-J, Carlsen J, Baumann K *et al* (2016) Automated spatial brain normalization and hindbrain white matter reference tissue give improved

[(18)F]-Florbetaben PET quantitation in Alzheimer's model mice. *Front Neurosci* 10: 45

Parhizkar S, Arzberger T, Brendel M, Kleinberger G, Deussing M, Focke C, Nuscher B, Xiong M, Ghasemigharagoz A, Katzmarski N *et al* (2019) Loss of TREM2 function increases amyloid seeding but reduces plaque-associated ApoE. *Nat Neurosci* 22: 191−204

Paushter DH, Du H, Feng T, Hu F (2018) The lysosomal function of progranulin, a guardian against neurodegeneration. *Acta Neuropathol* 136: 1−17

Perez-Otano I, Larsen RS, Wesseling JF (2016) Emerging roles of GluN3-containing NMDA receptors in the CNS. *Nat Rev Neurosci* 17: 623−635

Preische O, Schultz SA, Apel A, Kuhle J, Kaeser SA, Barro C, Gräber S, Kuder-Buletta E, LaFougere C, Laske C *et al* (2019) Serum neurofilament dynamics predicts neurodegeneration and clinical progression in presymptomatic Alzheimer's disease. *Nat Med* 25: 277−283

Price BR, Sudduth TL, Weekman EM, Johnson S, Hawthorne D, Woolums A, Wilcock DM (2020) Therapeutic Trem2 activation ameliorates amyloid-beta deposition and improves cognition in the 5XFAD model of amyloid deposition. *J Neuroinflammation* 17: 238

Ran FA, Hsu PD, Wright J, Agarwala V, Scott DA, Zhang F (2013) Genome engineering using the CRISPR-Cas9 system. *Nat Protoc* 8: 2281−2308

Ransohoff RM (2016) How neuroinflammation contributes to neurodegeneration. *Science* 353: 777−783

Rohrer JD, Woollacott IOC, Dick KM, Brotherhood E, Gordon E, Fellows A, Toombs J, Druyeh R, Cardoso MJ, Ourselin S *et al* (2016) Serum neurofilament light chain protein is a measure of disease intensity in frontotemporal dementia. *Neurology* 87: 1329−1336

Root J, Merino P, Nuckols A, Johnson M, Kukar T (2021) Lysosome dysfunction as a cause of neurodegenerative diseases: lessons from frontotemporal dementia and amyotrophic lateral sclerosis. *Neurobiol Dis* 154: 105360

Schlepckow K, Kleinberger G, Fukumori A, Feederle R, Lichtenthaler SF, Steiner H, Haass C (2017) An Alzheimer-associated TREM2 variant occurs at the ADAM cleavage site and affects shedding and phagocytic function. *EMBO Mol Med* 9: 1356−1365

Schlepckow K, Monroe KM, Kleinberger G, Cantuti-Castelvetri L, Parhizkar S, Xia D, Willem M, Werner G, Pettkus N, Brunner B *et al* (2020) Enhancing protective microglial activities with a dual function TREM2 antibody to the stalk region. *EMBO Mol Med* 12: e11227

Smith K, Damiano J, Franceschetti S, Carpenter S, Canafoglia L, Morbin M, Rossi G, Pareyson D, Mole S, Staropoli J *et al* (2012) Strikingly different clinicopathological phenotypes determined by progranulin-mutation dosage. *Am J Hum Genet* 90: 1102−1107

Spiegel I, Mardinly AR, Gabel HW, Bazinet JE, Couch CH, Tzeng CP, Harmin DA, Greenberg ME (2014) Npas4 regulates excitatory-inhibitory balance within neural circuits through cell-type-specific gene programs. *Cell* 157: 1216−1229

Steyer B, Bu Q, Cory E, Jiang K, Duong S, Sinha D, Steltzer S, Gamm D, Chang Q, Saha K (2018) Scarless genome editing of human pluripotent stem cells via transient puromycin selection. *Stem Cell Rep* 10: 642−654

Tanaka Y, Suzuki G, Matsuwaki T, Hosokawa M, Serrano G, Beach TG, Yamanouchi K, Hasegawa M, Nishihara M (2017) Progranulin regulates lysosomal function and biogenesis through acidification of lysosomes. *Hum Mol Genet* 26: 969−988

Thornton P, Sevalle J, Deery MJ, Fraser G, Zhou Y, Stahl S, Franssen EH, Dodd RB, Qamar S, Gomez Perez-Nievas B *et al* (2017) TREM2 shedding by cleavage at the H157−S158 bond is accelerated for the Alzheimer's disease-associated H157Y variant. *EMBO Mol Med* 9: 1366−1378

76

Turnbull IR, Gilfillan S, Cella M, Aoshi T, Miller M, Piccio L, Hernandez M, Colonna M (2006) Cutting edge: TREM-2 attenuates macrophage activation. *J Immunol* 177: 3520−3524

Ulrich JD, Finn MB, Wang Y, Shen A, Mahan TE, Jiang H, Stewart FR, Piccio L, Colonna M, Holtzman DM (2014) Altered microglial response to Abeta plaques in APPPS1-21 mice heterozygous for TREM2. *Mol Neurodegener* 9: 20

Valdez C, Wong YC, Schwake M, Bu G, Wszolek ZK, Krainc D (2017) Progranulin-mediated deficiency of cathepsin D results in FTD and NCL-like phenotypes in neurons derived from FTD patients. *Hum Mol Genet* 26: 4861−4872

Villa A, Gelosa P, Castiglioni L, Cimino M, Rizzi N, Pepe G, Lolli F, Marcello E, Sironi L, Vegeto E *et al* (2018) Sex-specific features of microglia from adult mice. *Cell Rep* 23: 3501−3511

Wang S, Mustafa M, Yuede CM, Salazar SV, Kong P, Long H, Ward M, Siddiqui O, Paul R, Gilfillan S *et al* (2020) Anti-human TREM2 induces microglia proliferation and reduces pathology in an Alzheimer's disease model. *J Exp Med* https://doi.org/10.1084/jem.20200785

Wang Y, Ulland TK, Ulrich JD, Song W, Tzaferis JA, Hole JT, Yuan P, Mahan TE, Shi Y, Gilfillan S *et al* (2016) TREM2-mediated early microglial response limits diffusion and toxicity of amyloid plaques. *J Exp Med* 213: 667−675

Ward ME, Chen R, Huang H-Y, Ludwig C, Telpoukhovskaia M, Taubes A, Boudin H, Minami SS, Reichert M, Albrecht P *et al* (2017) Individuals with progranulin haploinsufficiency exhibit features of neuronal ceroid lipofuscinosis. *Sci Transl Med* https://doi.org/10.1126/scitranslmed.aah5642

Weisheit I, Kroeger JA, Malik R, Klimmt J, Crusius D, Dannert A, Dichgans M, Paquet D (2020) Detection of deleterious on-target effects after HDR-mediated CRISPR editing. *Cell Rep* 31: 107689

Weisheit I, Kroeger JA, Malik R, Wefers B, Lichtner P, Wurst W, Dichgans M, Paquet D (2021) Simple and reliable detection of CRISPR-induced on-target effects by qgPCR and SNP genotyping. *Nat Protoc* 16: 1714−1739

Werner G, Damme M, Schludi M, Gnorich J, Wind K, Fellerer K, Wefers B, Wurst W, Edbauer D, Brendel M *et al* (2020) Loss of TMEM106B potentiates lysosomal and FTLD-like pathology in progranulin-deficient mice. *EMBO Rep* 21: e50241

Woollacott IOC, Bocchetta M, Sudre CH, Ridha BH, Strand C, Courtney R, Ourselin S, Cardoso MJ, Warren JD, Rossor MN *et al* (2018) Pathological correlates of white matter hyperintensities in a case of progranulin mutation associated frontotemporal dementia. *Neurocase* 24: 166−174

Wu Y, Shao W, Todd TW, Tong J, Yue M, Koga S, Castanedes-Casey M, Librero AL, Lee CW, Mackenzie IR *et al* (2021) Microglial lysosome dysfunction contributes to white matter pathology and TDP-43 proteinopathy in GRN-associated FTD. *Cell Rep* 36: 109581

Xiang X, Wind K, Wiedemann T, Blume T, Shi Y, Briel N, Beyer L, Biechele G, Eckenweber F, Zatcepin A *et al* (2021) Microglial activation states drive glucose uptake and FDG-PET alterations in neurodegenerative diseases. *Sci Transl Med* 13: eabe5640

Yuan P, Condello C, Keene CD, Wang Y, Bird TD, Paul SM, Luo W, Colonna M, Baddeley D, Grutzendler J (2016) TREM2 haplodeficiency in mice and humans impairs the microglia barrier function leading to decreased amyloid compaction and severe axonal dystrophy. *Neuron* 92: 252−264

Zhang J, Velmeshev D, Hashimoto K, Huang Y-H, Hofmann JW, Shi X, Chen J, Leidal AM, Dishart JG, Cahill MK *et al* (2020) Neurotoxic microglia promote TDP-43 proteinopathy in progranulin deficiency. *Nature* 588: 459−465

Zhou X, Paushter DH, Feng T, Pardon CM, Mendoza CS, Hu F (2017) Regulation of cathepsin D activity by the FTLD protein progranulin. *Acta Neuropathol* 134: 151−153

Zhou X, Paushter DH, Pagan MD, Kim D, Nunez Santos M, Lieberman RL, Overkleeft HS, Sun Y, Smolka MB, Hu F (2019) Progranulin deficiency leads to reduced glucocerebrosidase activity. *PLoS One* 14: e0212382

Zhou X, Sun L, Bastos de Oliveira F, Qi X, Brown WJ, Smolka MB, Sun Y, Hu F (2015) Prosaposin facilitates sortilin-independent lysosomal trafficking of progranulin. *J Cell Biol* 210: 991−1002

Expanded View Figures

A

B

Peptide Sequence	Ab1	Ab2	Isotype
NTTVFQGVAGQSLQVSCPYDSM	-	-	-
QSLQVSCPYDSMKHWGRRKAWCR	+	+	-
MKHWGRRKAWCRQLGEKGPCQRV	+	+	-
QLGEKGPCQRVVSTHNLWLLSF	-	-	-
VSTHNLWLLSFLRRWNGSTAIT	-	-	-
LRRWNGSTAITDDTLGGTLTITL	-	-	-
DDTLGGTLTITLRNLQPHDAGL	-	-	-
RNLQPHDAGLYQCQSLHGSEAD	-	-	-
YQCQSLHGSEADTLRKVLVEVL	-	-	-
TLRKVLVEVLADPLDHRDAGDL	-	-	-
ADPLDHRDAGDLWFPGESESFE	-	-	-
WFPGESESFEDAHVEHSISRSL	-	-	-

C

DC Number	Functional Class	Biacore Affinity (K_D) Human Specific No Mouse XR (nM)	H6 binding EC50 / FOB (200 nM)	Human Macrophage p-Syk IC_{50} (nM)	Human Macrophage pSyk max inhibition in %
Ab1	Antagonist	0.21	0.38 / 22.37	18.0	92
Ab2	Antagonist	4.5	0.18 / 26.28	11.9	98

D

E

F

$K_{on} = 1.4 \times 10^6 \, M^{-1}s^{-1}$
$K_{off} = 3.0 \times 10^{-4} \, s^{-1}$
$K_D = 210 \, pM$

G

$K_{on} = 1.1 \times 10^6 \, M^{-1}s^{-1}$
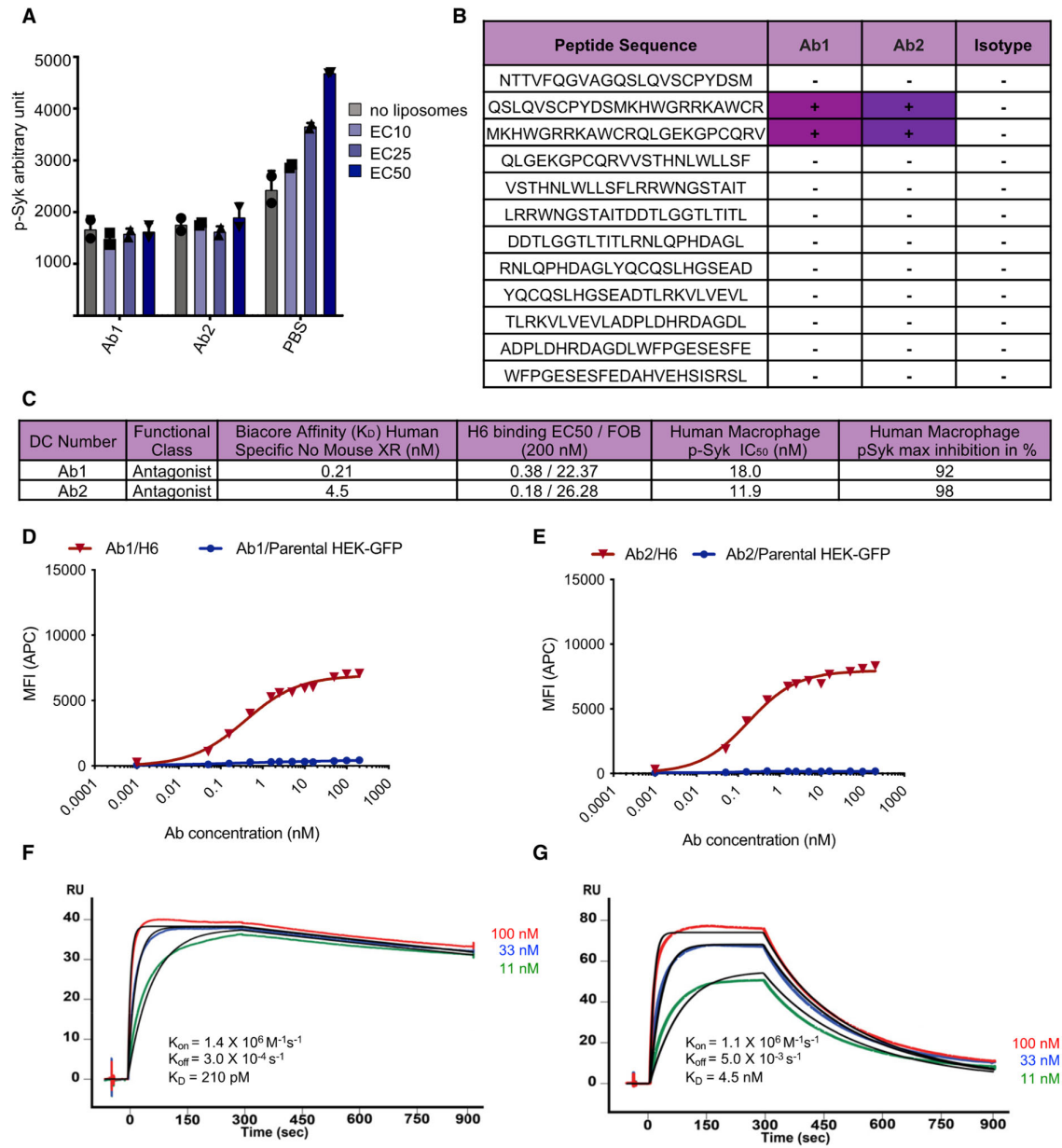$K_{off} = 5.0 \times 10^{-3} \, s^{-1}$
$K_D = 4.5 \, nM$

Figure EV1.

78

**Figure EV1. Generation and characterization of TREM2 antagonistic antibodies.**

A AlphaLISA quantification of p-Syk levels in HEK293 cells overexpressing TREM2-DAP12 upon treatment with Ab1 or Ab2 with three doses of liposomes (EC10: 0.0189527 mg/ml, EC25: 0.0633607 mg/ml, or EC50: 0.211731 mg/ml). PBS was used as a negative control. Individual data points are shown (n = 2 independent experiments).

B Biochemical binding data of TREM2 IgV peptides to antagonistic antibodies Ab1 and Ab2, as well as isotype control. Positive data represent binding level above a threshold of 2*LLOD (lower limit of detection), from an average of three independent experiments.

C Table of Ab1 and Ab2 with Biacore binding affinities, cell binding affinities, and liposome signaling (p-Syk) inhibition (EC50 and maximal inhibition) in human macrophage (n = 3 independent experiments).

D, E Cell-binding dose–response curves generated by FACS in HEK293 cells overexpressing TREM2/DAP12 versus parental lines shown as mean fluorescence intensity (MFI).

F, G Biacore binding measurements of immobilized antagonist antibody to three concentrations of recombinant hTREM2-ECD.

A

patient #	sex	Age of onset	Clinical diagnosis	*GRN* mutation	PGRN serum levels (in % of HC)
1	f	57	bvFTD	c.759_760del	26,7
2	f	61	dementia (PNFA/SD)	c.328C>T	16,9
3	f	65	bvFTD	c.709-2A>G	46,0
4	f	57	PNFA	c.675-676del	25,7

B

HC #	gender	Age
1	f	59
2	f	53
3	f	64
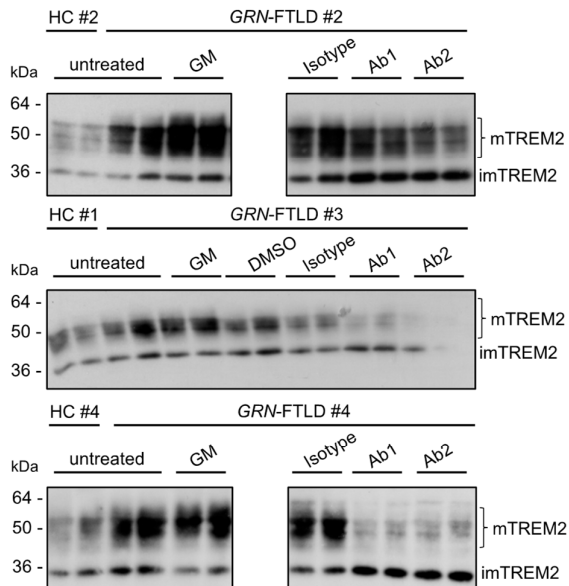
Figure EV2. *GRN*-FTLD patients.

A Clinical data and mutation status of the four identified *GRN* mutation carriers and healthy controls. Mutation status of patients #1–3 was already confirmed before. The mutation status of patient #4 was detected by sequencing of exons including flanking sequences.

B Clinical data of healthy controls (HC).

C Western blot analysis of TREM2 using lysates of cultured human macrophages isolated from *GRN* mutation carriers (patients #2 to #4) (A) and healthy control upon treatment with Ab1 and Ab2. An isotype antibody was used as a negative control. ADAM protease inhibition (GM) does not further increase mTREM2 levels in PGRN mutation carriers. Equal amounts of protein were loaded.
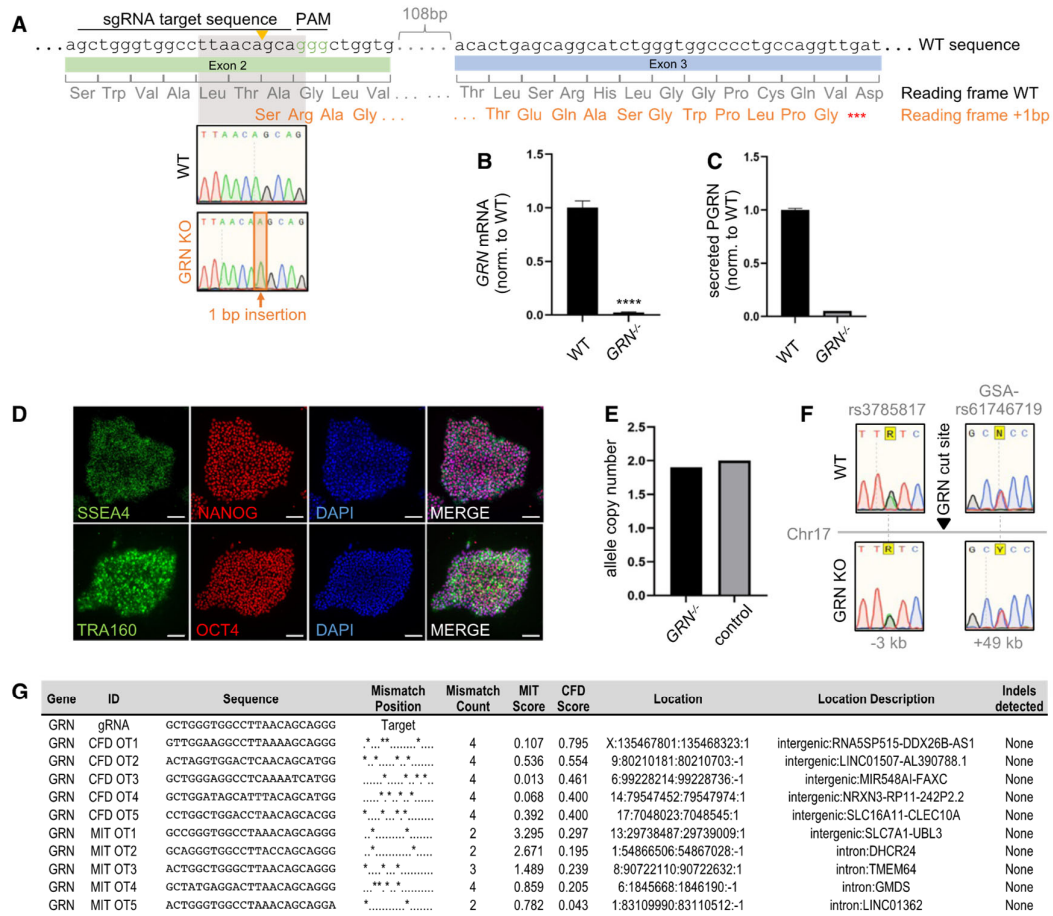
C

Figure EV3. Generation and characterization of $GRN^{-/-}$ iPSC line.

A GRN knockout generation strategy: GRN was targeted in exon 2 by a sgRNA (target and PAM sequence indicated), leading to a one base pair insertion in the $GRN^{-/-}$ line. The resulting frameshift exposes a nearby stop codon.

B GRN mRNA transcript levels in WT and $GRN^{-/-}$ hiMGL normalized to WT, as measured by qPCR (n = 3, biological replicates).

C   ELISA-mediated quantification of secreted PGRN in conditioned media of WT and $GRN^{-/-}$ hiMGL (n = 3, biological replicates).

D   Immunofluorescence analysis of pluripotency markers SSEA4, NANOG, TRA160, and OCT 4 with DAPI in $GRN^{-/-}$ iPSCs. Scalebars = 100 μm.

E, F   Analysis of CRISPR-mediated on-target effects by qgPCR quantitation of allele copy number (E) and Sanger sequencing of SNPs near the edited locus in WT and $GRN^{-/-}$ iPSC lines (F) shows maintenance of both alleles after editing.

G   List of top five most similar off-target sites ranked by the CFD and MIT prediction scores, respectively. No off-target editing was detected by Sanger sequencing.

Data information: Data represent the mean ± SD. For statistical analysis, the unpaired, two-tailed student's t-test was performed. Statistical significance was set at ****P < 0.0001, and ns, not significant.

Figure EV4. Differential gene expression in *Grn*$^{-/-}$ and *Trem2*$^{-/-}$ is partially rescued in *Double* KO mice.

A Volcano plot presentation of the differently expressed transcripts in brains of 6-month-old male *Grn*$^{-/-}$ mice compared to WT brain mRNA ($n = 4$ per genotype). A total of 17 of 752 analyzed genes are significantly changed more than 20%, with 11 genes upregulated (purple) and 6 genes downregulated (blue).

B Volcano plot presentation of the differently expressed genes in brain mRNA of 6-month-old male *Trem2*$^{-/-}$ mice in comparison to WT brain mRNA ($n = 4$ per genotype). A total of 16 of 752 analyzed genes are significantly changed by more than 20%, with 4 genes upregulated (purple) and 12 genes downregulated (blue).

C Volcano plot presentation of the differently expressed genes in brain mRNA of 6-month-old male *Double*$^{-/-}$ mice in comparison to WT brain mRNA ($n = 4$ per genotype). A total of 25 of 752 analyzed genes are significantly changed by more than 20%, with 8 genes upregulated (purple) and 17 genes downregulated (blue).

D Volcano plot presentation of the differently expressed transcripts in brains of 14-month-old male *Grn*$^{-/-}$ mice compared to WT brain mRNA ($n = 3$ per genotype). A total of 49 of 752 analyzed genes are significantly changed more than 20%, with 44 genes upregulated (purple) and 5 genes downregulated (blue).

E Volcano plot presentation of the differently expressed genes in brain mRNA of 14-month-old male *Trem2*$^{-/-}$ mice in comparison to WT brain mRNA ($n = 3$ per genotype). A total of 7 of 752 analyzed genes are significantly changed by more than 20%, with 7 downregulated (blue).

F Volcano plot presentation of the differently expressed genes in brain mRNA of 14-month-old male *Double*$^{-/-}$ mice in comparison to WT brain mRNA ($n = 3$ per genotype). A total of 21 of 752 analyzed genes are significantly changed by more than 20%, with 8 genes upregulated (purple) and 13 genes downregulated (blue).

G Transcript levels of selected significantly rescued genes in *Double*$^{-/-}$ versus *Grn*$^{-/-}$ brain mRNA of 6-month-old ($n = 4$ per genotype) and 14-month-old mice ($n = 3$ per genotype). Transcript expression is normalized to the mean of the WT cohort.

Data information: Data represent mean $\pm$ SEM. For statistical analysis in G, the unpaired, two-tailed student's *t*-test was performed to compare *Grn*$^{-/-}$, *Trem2*$^{-/-}$, and *Double*$^{-/-}$ whole-brain mRNA expression. Statistical significance was set at *$P < 0.05$; **$P < 0.01$; ***$P < 0.001$; ****$P < 0.0001$, and ns, not significant.
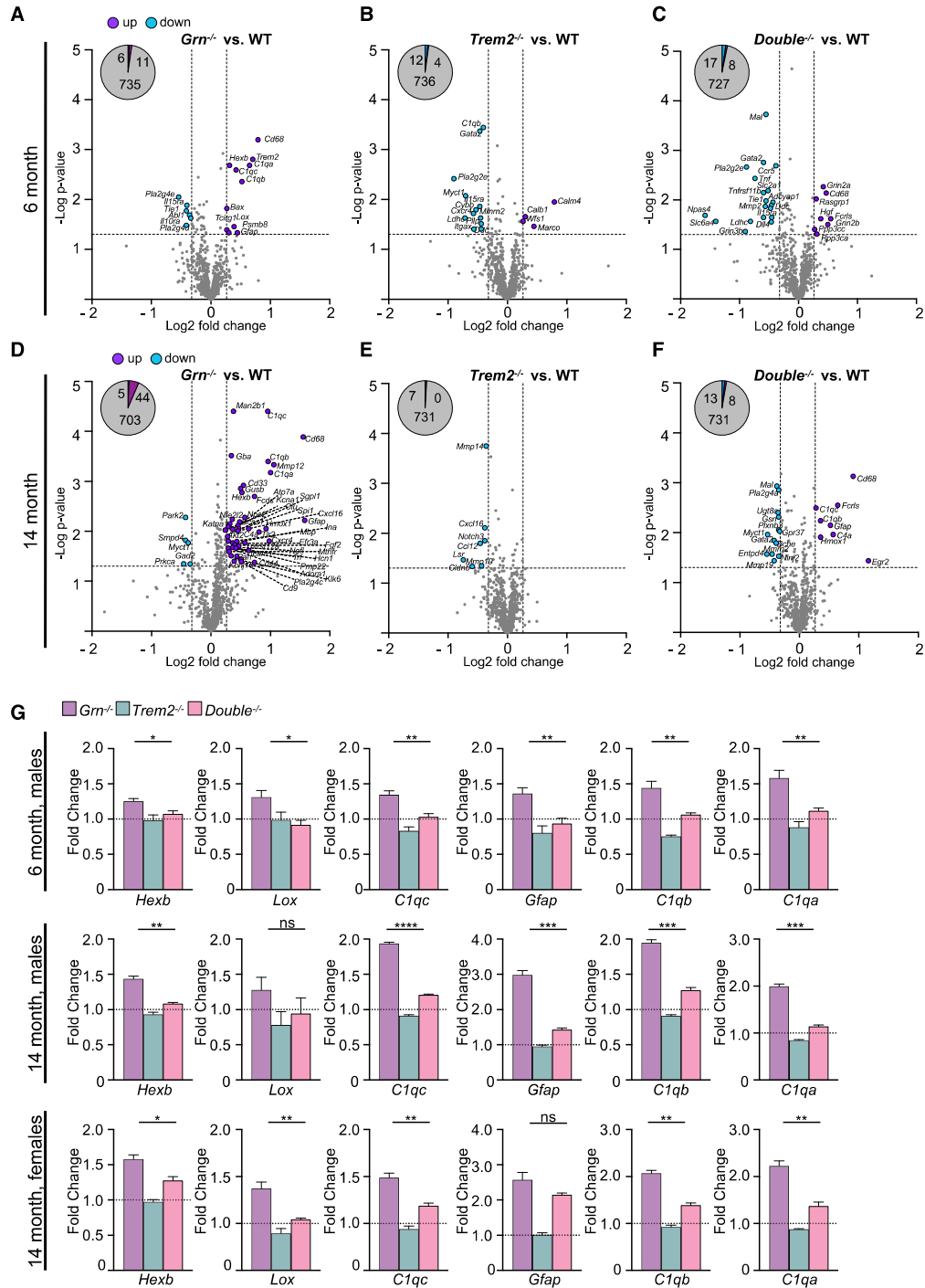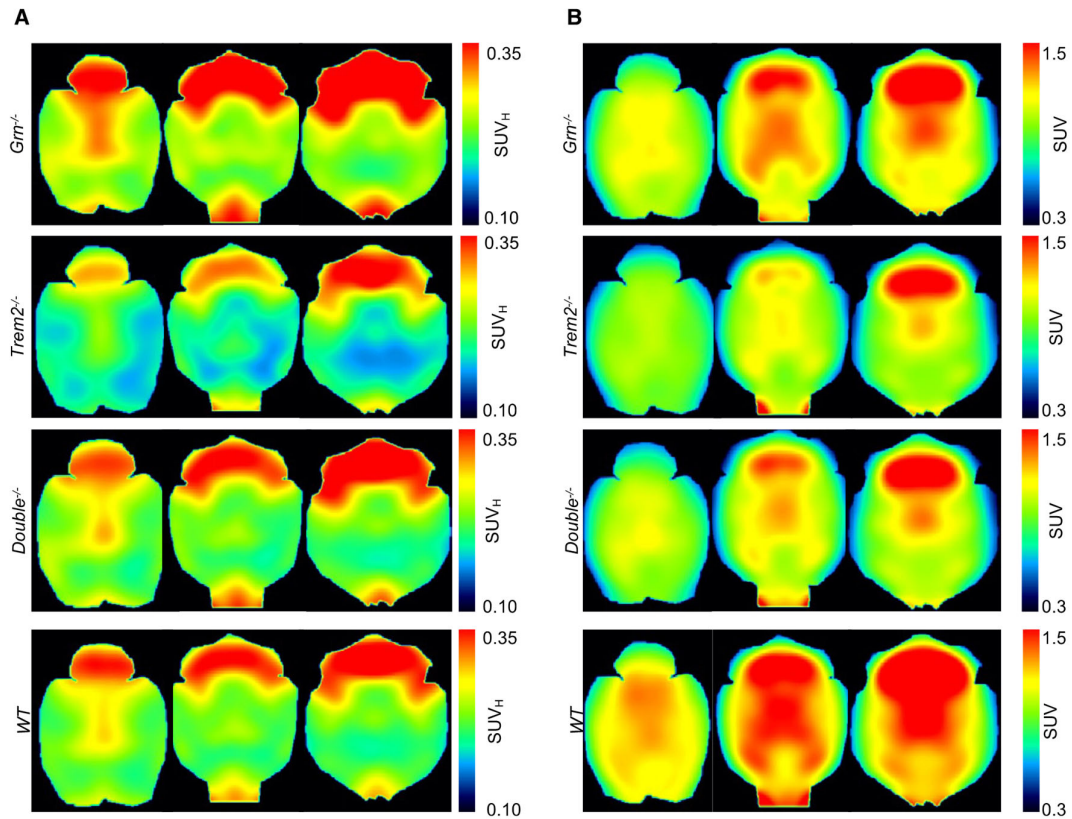
Figure EV4.

Figure EV5.   Group-level PET images without MRI template overlay.

Group-averaged axial slices of TSPO-PET (SUV_H scaling) and FDG-PET (SUV scaling) show microglia activity and glucose metabolism in comparison of $Grn^{-/-}$, $Trem2^{-/-}$, $Double^{-/-}$, and WT-type mice. Images represent the raw PET data used for calculation of %-differences in Figs 1A and 9E.

A   TSPO-PET images depict increased microglial activity in $Grn^{-/-}$ mice, reduced microglial activity in $Trem2^{-/-}$ mice, and similar levels of microglial activity in $Double^{-/-}$ and WT mice.

B   FDG-PET images indicate similar reduction in glucose uptake in $Grn^{-/-}$, $Trem2^{-/-}$, and $Double^{-/-}$ in comparison to WT mice.

2.1 Contribution to the publication

As the first author of this paper, I conceived the study and analyzed the results with the help of Prof. Christian Haass and Anja Capell. I majorly contributed to the writing process, coordinated the process and put together all displayed figures.

Figure 1:

TSPO-PET imaging was performed by Johannes Gnörich, Karin Wind, Artem Zatcepin and Matthias Brendel. I organized and genotyped all necessary mice.

Figure 2:

I performed all isolations of mouse microglia, mRNA isolation, NanoString experiments and analyzed the results.

Figure 3, Figure EV1 and Figure EV2:

Human TREM2 antagonistic antibodies were generated and validated by Denali Therapeutics. PGRN mutation carriers were identified by Endy Weidinger, Lina Riedl, Katharina Bürger, Johannes Levin and Janine Diehl-Schmid. I isolated and performed all experiments of human-derived macrophages.

Figure 4 and Figure EV3:

Sophie Robinson generated and performed all experiments on hiMGL.

Figure 5:

NanoString experiments on hiMGL cells were performed by Miriam A Vogt and Sophie Haberl. I analyzed the results.

Figure 6:

I performed and analyzed all Western Blots, enzyme activity assays and immunofluorescence assays of all mouse samples.

Figure 7:

Todd Logan and Jung Suh performed lipidomic analysis. I provided all brain samples.

Figure 8:

I performed and analyzed all Western Blots, enzyme activity assays and immunofluorescence assays of all mouse samples. Steffanie Heindl performed automated analysis of microglia morphology.

Figure 9 and Figure EV4:

I performed all isolations of mouse brain, mRNA isolation, NanoString experiments and analyzed the results. I assisted Ida Pesäama in collecting cerebrospinal fluid and Brigitte Nuscher performed Nfl measurements. FDG-PET imaging was performed by Johannes Gnörich, Karin Wind, Artem Zatcepin and Matthias Brendel. I organized and genotyped all necessary mice.

X. References

Van Acker, Zoë P., Anika Perdok, Marine Bretou, and Wim Annaert. 2021. "The Microglial Lysosomal System in Alzheimer's Disease: Guardian against Proteinopathy." *Ageing Research Reviews* 71(April).

Ajami, Bahareh, Jami L. Bennett, Charles Krieger, Wolfram Tetzlaff, and Fabio M. V. Rossi. 2007. "Local Self-Renewal Can Sustain CNS Microglia Maintenance and Function throughout Adult Life." *Nature Neuroscience* 10(12):1538–43.

Allcock, Richard J. N., Alexander D. Barrow, Simon Forbes, Stephan Beck, and John Trowsdale. 2003. "The Human TREM Gene Cluster at 6p21.1 Encodes Both Activating and Inhibitory Single LgV Domain Receptors and Includes NKp44." *European Journal of Immunology* 33(2):567–77.

Amarante-Mendes, Gustavo P., Sandy Adjemian, Laura Migliari Branco, Larissa C. Zanetti, Ricardo Weinlich, and Karina R. Bortoluci. 2018. "Pattern Recognition Receptors and the Host Cell Death Molecular Machinery." *Frontiers in Immunology* 9(OCT):1–19.

Arrant, Andrew E., Jonathan R. Roth, Nicholas R. Boyle, Shreya N. Kashyap, Madelyn Q. Hoffmann, Charles F. Murchison, Eliana Marisa Ramos, Alissa L. Nana, Salvatore Spina, Lea T. Grinberg, Bruce L. Miller, William W. Seeley, and Erik D. Roberson. 2019. "Impaired β-Glucocerebrosidase Activity and Processing in Frontotemporal Dementia Due to Progranulin Mutations." *Acta Neuropathologica Communications* 7(1).

Asai, Hirohide, Seiko Ikezu, Satoshi Tsunoda, Maria Medalla, Jennifer Luebke, Benjamin Wolozin, Oleg Butovsky, Tsuneya Ikezu, and Experimental Therapeutics. 2015. "Depletion of Microglia and Inhibition of Exosome Synthe." *Nature Neuroscience* 18(11):1584–93.

Askew, Katharine, Kaizhen Li, Adrian Olmos-Alonso, Fernando Garcia-Moreno, Yajie Liang, Philippa Richardson, Tom Tipton, Mark A. Chapman, Kristoffer Riecken, Sol Beccari, Amanda Sierra, Zoltán Molnár, Mark S. Cragg, Olga Garaschuk, V. Hugh Perry, and Diego Gomez-Nicola. 2017. "Coupled Proliferation and Apoptosis Maintain the Rapid Turnover of Microglia in the Adult Brain." *Cell Reports* 18(2):391–405.

Baker, Matt, Ian R. Mackenzie, Stuart M. Pickering-Brown, Jennifer Gass, Rosa Rademakers, Caroline Lindholm, Julie Snowden, Jennifer Adamson, a Dessa Sadovnick, Sara Rollinson, Ashley Cannon, Emily Dwosh, David Neary, Stacey Melquist, Anna Richardson, Dennis Dickson, Zdenek Berger, Jason Eriksen, Todd Robinson, Cynthia Zehr, Chad a Dickey, Richard Crook, Eileen McGowan, David Mann, Bradley Boeve, Howard Feldman, and Mike Hutton. 2006. "Mutations in Progranulin Cause Tau-Negative Frontotemporal Dementia Linked to Chromosome 17." *Nature* 442(7105):916–19.

Ball, M. 1977. "Neuronal Loss, Neurofibrillary Tangles and Granulovacuolar Degeneration in the Hippocampus with Aging and Dementia." *Acta Neuropathologica* 37:111–18.

Bateman, A., and H. P. J. Bennett. 1998. "Granulins: The Structure and Function of an Emerging Family of Growth Factors." *Journal of Endocrinology* 158(2):145–51.

Bateman, RJ, TL Benzinger, S. Berry, DB Clifford, C. Duggan, AM Fagan, K. Fanning, MR Farlow, J. Hassenstab, EM McDade, S. Mills, K. Paumier, M. Quintana, SP Salloway, A. Santacruz, LS Schneider, G. Wang, C. Xiong, and DIAN-TU Pharma Consortium for the Dominantly Inherited Alzheimer Network. 2017. "Adaptive Design and Disease Progression Model." *Alzheimer's and Dementia* 13(1):8–19.

Beel, Sander, Matthieu Moisse, Markus Damme, Louis De Muynck, Wim Robberecht, Ludo Van Den Bosch, Paul Saftig, and Philip Van Damme. 2017. "Progranulin Functions as a Cathepsin D Chaperone to Stimulate Axonal Outgrowth in Vivo." *Human Molecular Genetics* 26(15):2850–63.

Belcastro, Vincenzo, Velia Siciliano, Francesco Gregoretti, Pratibha Mithbaokar, Gopuraja Dharmalingam, Stefania Berlingieri, Francesco Iorio, Gennaro Oliva, Roman Polishchuck, Nicola Brunetti-Pierri, and Diego Di Bernardo. 2011. "Transcriptional Gene Network Inference from a Massive Dataset Elucidates Transcriptome Organization and Gene Function." *Nucleic Acids Research* 39(20):8677–88.

Bertram, Lars, Christoph Lange, Kristina Mullin, Michele Parkinson, Monica Hsiao, Meghan F. Hogan, Brit M. M. Schjeide, Basavaraj Hooli, Jason DiVito, Iuliana Ionita, Hongyu Jiang, Nan Laird, Thomas Moscarillo, Kari L. Ohlsen, Kathryn Elliott, Xin Wang, Diane Hu-Lince, Marie Ryder, Amy Murphy, Steven L. Wagner, Deborah Blacker, K. David

Becker, and Rudolph E. Tanzi. 2008. "Genome-Wide Association Analysis Reveals Putative Alzheimer's Disease Susceptibility Loci in Addition to APOE." *American Journal of Human Genetics* 83(5):623–32.

Bhandari, V., R. Daniel, P. S. Lim, and A. Bateman. 1996. "Structural and Functional Analysis of a Promoter of the Human Granulin/Epithelin Gene." *The Biochemical Journal* 319 (Pt 2:441–47.

Block, Michelle L., Luigi Zecca, and Jau Shyong Hong. 2007. "Microglia-Mediated Neurotoxicity: Uncovering the Molecular Mechanisms." *Nature Reviews Neuroscience* 8(1):57–69.

Bolós, Marta, Maria Llorens-Martín, Jeronimo Jurado-Arjona, Felix Hernández, Alberto Rábano, and Jesús Avila. 2016. "Direct Evidence of Internalization of Tau by Microglia in Vitro and in Vivo." *Journal of Alzheimer's Disease* 50(1):77–87.

Brady, Owen A., Yanqiu Zheng, Kira Murphy, Marshall Huang, and Fenghua Hu. 2013. "The Frontotemporal Lobar Degeneration Risk Factor, TMEM106B, Regulates Lysosomal Morphology and Function." *Human Molecular Genetics* 22(4):685–95.

Brouwers, Nathalie, Karen Nuytemans, Julie van der Zee, Ilse Gijselinck, Sebastiaan Engelborghs, Jessie Theuns, Samir Kumar-Singh, Barbara a Pickut, Philippe Pals, Bart Dermaut, Veerle Bogaerts, Tim De Pooter, Sally Serneels, Marleen Van den Broeck, Ivy Cuijt, Maria Mattheijssens, Karin Peeters, Raf Sciot, Jean-Jacques Martin, Patrick Cras, Patrick Santens, Rik Vandenberghe, Peter P. De Deyn, Marc Cruts, Christine Van Broeckhoven, and Kristel Sleegers. 2007. "Alzheimer and Parkinson Diagnoses in Progranulin Null Mutation Carriers in an Extended Founder Family." *Archives of Neurology* 64(10):1436–46.

Bruttger, Julia, Khalad Karram, Simone Wörtge, Tommy Regen, Federico Marini, Nicola Hoppmann, Matthias Klein, Thomas Blank, Simon Yona, Yochai Wolf, Matthias Mack, Emmanuel Pinteaux, Werner Müller, Frauke Zipp, Harald Binder, Tobias Bopp, Marco Prinz, Steffen Jung, and Ari Waisman. 2015. "Genetic Cell Ablation Reveals Clusters of Local Self-Renewing Microglia in the Mammalian Central Nervous System." *Immunity* 43(1):92–106.

Butler, Victoria J., Wilian A. Cortopassi, Olivia M. Pierce, Matthew P. Jacobson, and Aimee W. Kao. 2019. "Multi-Granulin Domain Peptides Bind to pro-Cathepsin D and Stimulate Its Enzymatic Activity in Vitro." *Biochemistry* 58(23):2670–74.

Butovsky, Oleg, Mark P. Jedrychowski, Craig S. Moore, Ron Cialic, Amanda J. Lanser, Galina Gabriely, Thomas Koeglsperger, Ben Dake, Pauline M. Wu, Camille E. Doykan, Zain Fanek, Liping Liu, Zhuoxun Chen, Jeffrey D. Rothstein, Richard M. Ransohoff, Steven P. Gygi, Jack P. Antel, and Howard L. Weiner. 2014. "Identification of a Unique TGF-β-Dependent Molecular and Functional Signature in Microglia." *Nature Neuroscience* 17(1):131–43.

Campbell-Taylor, Irene. 2014. "Contribution Of Alzheimer Disease to Mortality in the United States." *Neurology* 83(14):1302.

Chang, Andrew, Xinyu Xiang, Jing Wang, Carolyn Lee, Tamta Arakhamia, Marija Simjanoska, Chi Wang, Yari Carlomagno, Guoan Zhang, Shikhar Dhingra, Manon Thierry, Jolien Perneel, Bavo Heeman, Lauren M. Forgrave, Michael DeTure, Mari L. DeMarco, Casey N. Cook, Rosa Rademakers, Dennis W. Dickson, Leonard Petrucelli, Michael H. B. Stowell, Ian R. A. Mackenzie, and Anthony W. P. Fitzpatrick. 2022. "Homotypic Fibrillization of TMEM106B across Diverse Neurodegenerative Diseases." *Cell* 185(8):1346-1355.e15.

Chang, Michael C., Karpagam Srinivasan, Brad A. Friedman, Eric Suto, Zora Modrusan, Wyne P. Lee, Joshua S. Kaminker, David V. Hansen, and Morgan Sheng. 2017. "Progranulin Deficiency Causes Impairment of Autophagy and TDP-43 Accumulation." *Journal of Experimental Medicine* 214(9):2611–28.

Chen, Yuehong, Jiniong Jian, Aubryanna Hettinghouse, Xueheng Zhao, Kenneth D. R. Setchell, Ying Sun, and Chian-ju Liu. 2018. "Progranulin Associates with Hexosaminidase A and Ameliorates GM2 Ganglioside Accumulation and Lysosomal Storage in Tay-Sachs Disease." *J Mol Biol* 176(12):139–48.

Chen, Zhihong, and Bruce D. Trapp. 2016. "Microglia and Neuroprotection." *Journal of Neurochemistry* 136:10–17.

Cheng, Qingwen, Jean Danao, Santosh Talreja, Paul Wen, Jun Yin, Ning Sun, Chi Ming Li, Danny Chui, David Tran, Samir Koirala, Hang Chen, Ian N. Foltz, Songli Wang, and

Shilpa Sambashivan. 2018. "TREM2-Activating Antibodies Abrogate the Negative Pleiotropic Effects of the Alzheimer's Disease Variant Trem2R47H on Murine Myeloid Cell Function." *Journal of Biological Chemistry* 293(32):12620–33.

Cignarella, Francesca, Fabia Filipello, Bryan Bollman, Claudia Cantoni, Alberto Locca, Robert Mikesell, Melissa Manis, Adiljan Ibrahim, Li Deng, Bruno A. Benitez, Carlos Cruchaga, Danilo Licastro, Kathie Mihindukulasuriya, Oscar Harari, Michael Buckland, David M. Holtzman, Arnon Rosenthal, Tina Schwabe, Ilaria Tassi, and Laura Piccio. 2020. "TREM2 Activation on Microglia Promotes Myelin Debris Clearance and Remyelination in a Model of Multiple Sclerosis." *Acta Neuropathologica* 140(4):513–34.

Cockram, Tom O. J., Mar Puigdellívol, and Guy C. Brown. 2019. "Calreticulin and Galectin-3 Opsonise Bacteria for Phagocytosis by Microglia." *Frontiers in Immunology* 10(November):1–12.

Colonna, Marco, and Yaming Wang. 2016. "TREM2 Variants: New Keys to Decipher Alzheimer Disease Pathogenesis." *Nature Reviews. Neuroscience* 17(4):201–7.

Conde, Jessica R., and Wolfgang J. Streit. 2006. "Microglia in the Aging Brain." *Journal of Neuropathology and Experimental Neurology* 65(3):199–203.

Condello, Carlo, Peng Yuan, Aaron Schain, and Jaime Grutzendler. 2015. "Microglia Constitute a Barrier That Prevents Neurotoxic Protofibrillar Aβ42 Hotspots around Plaques." *Nature Communications* 6(May 2014).

Corder, E. H., A. M. Saunders, W. J. Strittmatter, D. E. Schmechel, P. C. Gaskell, G. W. Small, A. D. Roses, J. L. Haines, and M. A. Pericak-Vance. 1993. "Gene Dose of Apolipoprotein E Type 4 Allele and the Risk of Alzheimer's Disease in Late Onset Families." *Science* 261(5123):921–23.

Cruts, M., I. Gijselinck, J. van der Zee, S. Engelborghs, H. Wils, D. Pirici, R. Rademakers, R. Vandenberghe, B. Dermaut, J. J. Martin, C. van Duijn, K. Peeters, R. Sciot, P. Santens, T. De Pooter, M. Mattheijssens, M. Van den Broeck, I. Cuijt, K. Vennekens, P. P. De Deyn, S. Kumar-Singh, and C. Van Broeckhoven. 2006. "Null Mutations in Progranulin Cause Ubiquitin-Positive Frontotemporal Dementia Linked to Chromosome 17q21." *Nature* 442(7105):920–24.

Dagher, Nabil N., Allison R. Najafi, Kara M. Neel. Kayala, Monica R. P. Elmore, Terra E. White, Rodrigo Medeiros, Brian L. West, and Kim N. Green. 2015. "Colony-Stimulating Factor 1 Receptor Inhibition Prevents Microglial Plaque Association and Improves Cognition in 3xTg-AD Mice." *Journal of Neuroinflammation* 12(1):1–14.

Dailey, Michael E., Ukpong Eyo, Leah Fuller, John Hass, and Dana Kurpius. 2013. "Imaging Microglia in Brain Slices and Slice Cultures."

Damani, Mausam R., Lian Zhao, Aurora M. Fontainhas, Juan Amaral, Robert N. Fariss, and Wai T. Wong. 2011. "Age-Related Alterations in the Dynamic Behavior of Microglia." *Aging Cell* 10(2):263–76.

Davalos, Dimitrios, Jaime Grutzendler, Guang Yang, Jiyun V. Kim, Yi Zuo, Steffen Jung, Dan R. Littman, Michael L. Dustin, and Wen Biao Gan. 2005. "ATP Mediates Rapid Microglial Response to Local Brain Injury in Vivo." *Nature Neuroscience* 8(6):752–58.

Deczkowska, Aleksandra, Hadas Keren-Shaul, Assaf Weiner, Marco Colonna, Michal Schwartz, and Ido Amit. 2018. "Disease-Associated Microglia: A Universal Immune Sensor of Neurodegeneration." *Cell* 173(5):1073–81.

Deczkowska, Aleksandra, Assaf Weiner, and Ido Amit. 2020. "The Physiology, Pathology, and Potential Therapeutic Applications of the TREM2 Signaling Pathway." *Cell* 181(6):1207–17.

Doens, Deborah, and Patricia L. Fernández. 2014. "Microglia Receptors and Their Implications in the Response to Amyloid β for Alzheimer's Disease Pathogenesis." *Journal of Neuroinflammation* 11:1–14.

Donat, Cornelius K., Gregory Scott, Steve M. Gentleman, and Magdalena Sastre. 2017. "Microglial Activation in Traumatic Brain Injury." *Frontiers in Aging Neuroscience* 9(JUN):1–20.

Efthymiou, Anastasia G., and Alison M. Goate. 2017. "Late Onset Alzheimer's Disease Genetics Implicates Microglial Pathways in Disease Risk." *Molecular Neurodegeneration* 12(1):1–12.

Elmore, Monica Renee Pittman, Allison Rachel Najafi, Maya Allegra Koike, Nabil Nazih, Elizabeth Erin Spangenberg, Rachel Anne Rice, Masashi Kitazawa, Hoa Nguyen, Brian Lee West, and Kim Nicholas Green. 2015. "CSF1 Receptor Signaling Is Necessary for

Microglia Viability, Which Unmasks a Cell That Rapidly Repopulates the Microglia-Depleted Adult Brain." *Neuron* 82(2):380–97.

Fellner, Lisa, Regina Irschick, Kathrin Schanda, Markus Reindl, Lars Klimaschewski, Werner Poewe, Gregor K. Wenning, and Nadia Stefanova. 2013. "Toll-like Receptor 4 Is Required for α-Synuclein Dependent Activation of Microglia and Astroglia." *Glia* 61(3):349–60.

Felsky, Daniel, Tina Roostaei, Kwangsik Nho, Shannon L. Risacher, Elizabeth M. Bradshaw, Vlad Petyuk, Julie A. Schneider, Andrew Saykin, David A. Bennett, and Philip L. De Jager. 2019. "Neuropathological Correlates and Genetic Architecture of Microglial Activation in Elderly Human Brain." *Nature Communications* 10(1).

Friedman, Brad A., Karpagam Srinivasan, Gai Ayalon, William J. Meilandt, Han Lin, Melanie A. Huntley, Yi Cao, Seung Hye Lee, Patrick C. G. Haddick, Hai Ngu, Zora Modrusan, Jessica L. Larson, Joshua S. Kaminker, Marcel P. van der Brug, and David V. Hansen. 2018. "Diverse Brain Myeloid Expression Profiles Reveal Distinct Microglial Activation States and Aspects of Alzheimer's Disease Not Evident in Mouse Models." *Cell Reports* 22(3):832–47.

Ginhoux, Florent, Melanie Greter, Marylene Leboeuf, Sayan Nandi, Peter See, Solen Gokhan, Mark F. Mehler, Simon J. Conway, Lai Guan Ng, E. Richard Stanley, Igor M. Samokhvalov, and Miriam Merad. 2010. "Fate Mapping Analysis Reveals That Adult Microglia Derive from Primitive Macrophages." *Science* 701(November):841–45.

Gitik, Miri, Sigal Liraz-Zaltsman, Per Arne Oldenborg, Fanny Reichert, and Shlomo Rotshenker. 2011. "Myelin Down-Regulates Myelin Phagocytosis by Microglia and Macrophages through Interactions between CD47 on Myelin and SIRPα (Signal Regulatory Protein-α) on Phagocytes." *Journal of Neuroinflammation* 8(March).

Gitler, Aaron D., and Hitomi Tsuiji. 2016. "There Has Been an Awakening: Emerging Mechanisms of C9orf72 Mutations in FTD/ALS." *Brain Research* 1647:19–29.

Gómez-Isla, Teresa, Joseph L. Price, Daniel W. McKeel, John C. Morris, John H. Growdon, and Bradley T. Hyman. 1996. "Profound Loss of Layer II Entorhinal Cortex Neurons Occurs in Very Mild Alzheimer's Disease." *Journal of Neuroscience* 16(14):4491–4500.

Gosselin, David, Verena Link, Casey E. Romanoski, Gregory J. Fonseca, Z. Dawn, Nathaneal J. Spann, Joshua D. Stender, Hyun B. Chun, Hannah Garner, Frederic Geissmann, and Christopher K. Glass. 2014. "Environment Drives Selection and Function of Enhancers Controlling Tissue-Specific Macrophage Identities." *Cell* 159(6):1327–40.

Götzl, Julia K., Matthias Brendel, Georg Werner, Samira Parhizkar, Laura Sebastian Monasor, Gernot Kleinberger, Alessio-Vittorio Colombo, Maximilian Deussing, Matias Wagner, Juliane Winkelmann, Janine Diehl-Schmid, Johannes Levin, Katrin Fellerer, Anika Reifschneider, Sebastian Bultmann, Peter Bartenstein, Axel Rominger, Sabina Tahirovic, Scott T. Smith, Charlotte Madore, Oleg Butovsky, Anja Capell, and Christian Haass. 2019. "Opposite Microglial Activation Stages upon Loss of PGRN or TREM2 Result in Reduced Cerebral Glucose Metabolism." *EMBO Molecular Medicine* 11(6):e9711.

Götzl, Julia K., Alessio-vittorio Colombo, Katrin Fellerer, Anika Reifschneider, Georg Werner, Sabina Tahirovic, Christian Haass, and Anja Capell. 2018. "Early Lysosomal Maturation Deficits in Microglia Triggers Enhanced Lysosomal Activity in Other Brain Cells of Progranulin Knockout Mice." 1–16.

Götzl, Julia K., Christina M. Lang, Christian Haass, and Anja Capell. 2016. "Impaired Protein Degradation in FTLD and Related Disorders." *Ageing Research Reviews*.

Götzl, Julia K., Kohji Mori, Markus Damme, Katrin Fellerer, Sabina Tahirovic, Gernot Kleinberger, Jonathan Janssens, Julie Van Der Zee, Christina M. Lang, Elisabeth Kremmer, Jean Jacques Martin, Sebastiaan Engelborghs, Hans A. Kretzschmar, Thomas Arzberger, Christine Van Broeckhoven, Christian Haass, and Anja Capell. 2014. "Common Pathobiochemical Hallmarks of Progranulin-Associated Frontotemporal Lobar Degeneration and Neuronal Ceroid Lipofuscinosis." *Acta Neuropathologica* 127(6):845–60.

Graeber, Manuel B., Bernd W. Scheithauer, and Georg W. Kreutzberg. 2002. "Microglia in Brain Tumors." *Glia* 40(2):252–59.

Grathwohl, Stefan a, Roland E. Kälin, Tristan Bolmont, Stefan Prokop, Stephan a Kaeser, Jörg Odenthal, Rebecca Radde, Therese Eldh, Sam Gandy, Adriano Aguzzi, Matthias

Staufenbiel, and Paul M. Mathews. 2009. "Formation and Maintenance of Alzheimer`s Disease Beta-Amyloid Plaques in the Absence of Microglia." *Nature Neuroscience* 12(11):1361–63.

Gratuze, Maud, Cheryl E. G. Leyns, and David M. Holtzman. 2018. "New Insights into the Role of TREM2 in Alzheimer's Disease." *Molecular Neurodegeneration* 13(1):1–16.

Guerreiro, Rita, Ebba Lohmann, Jose Bras, Jesse Gibbs, Jonathan D. Rohrer, Nicole Gurunlian, Burcu Dursun, Basar Bilgic, Hasmet Hanagasi, Hakan Gurvit, Murat Emre, Andrew Singleton, and John Hardy. 2013. "Using Exome Sequencing to Reveal Mutations in TREM2 Presenting as a Frontotenporal Dementia-like Syndrome without Bone Involvment." *JAMA Neurology* 70(1):78–84.

Guerreiro, Rita, Aleksandra Wojtas, Jose Bras, Minerva Carrasquillo, Ekaterina Rogaeva, Elisa Majounie, Carlos Cruchaga, Celeste Sassi, John S. K. Kauwe, Steven Younkin, Lilinaz Hazrati, John Collinge, Jennifer Pocock, Tammaryn Lashley, Julie Williams, Jean-Charles Lambert, Philippe Amouyel, Alison Goate, Rosa Rademakers, Kevin Morgan, John Powell, Peter St. George-Hyslop, Andrew Singleton, and John Hardy. 2013. "TREM2 Variants in Alzheimer's Disease." *New England Journal of Medicine* 368(2):117–27.

Guerrero, Brooke L., and Nancy L. Sicotte. 2020. "Microglia in Multiple Sclerosis: Friend or Foe?" *Frontiers in Immunology* 11(March):1–8.

Haass, Christian, and Dennis Selkoe. 2022 *(in press)*. "If Amyloid Drives Alzheimer Disease , Why Have Anti-Amyloid Therapies Not yet Slowed Cognitive Decline ?" *PLoS Biology* 1–16.

Hamerman, Jessica A., Jessica R. Jarjoura, Mary Beth Humphrey, Mary C. Nakamura, William E. Seaman, and Lewis L. Lanier. 2006. "Cutting Edge: Inhibition of TLR and FcR Responses in Macrophages by Triggering Receptor Expressed on Myeloid Cells (TREM)-2 and DAP12." *The Journal of Immunology* 177(4):2051–55.

Hammond, Timothy R., Connor Dufort, Lasse Dissing-Olesen, Stefanie Giera, Adam Young, Alec Wysoker, Alec J. Walker, Frederick Gergits, Michael Segel, James Nemesh, Samuel E. Marsh, Arpiar Saunders, Evan Macosko, Florent Ginhoux, Jinmiao Chen, Robin J. M. Franklin, Xianhua Piao, Steven A. McCarroll, and Beth Stevens. 2019. "Single-Cell RNA Sequencing of Microglia throughout the Mouse Lifespan and in the Injured Brain Reveals Complex Cell-State Changes." *Immunity* 50(1):253-271.e6.

Han, Xiaoping, Ziming Zhou, Lijiang Fei, Huiyu Sun, Renying Wang, Yao Chen, Haide Chen, Jingjing Wang, Huanna Tang, Wenhao Ge, Yincong Zhou, Fang Ye, Mengmeng Jiang, Junqing Wu, Yanyu Xiao, Xiaoning Jia, Tingyue Zhang, Xiaojie Ma, Qi Zhang, Xueli Bai, Shujing Lai, Chengxuan Yu, Lijun Zhu, Rui Lin, Yuchi Gao, Min Wang, Yiqing Wu, Jianming Zhang, Renya Zhan, Saiyong Zhu, Hailan Hu, Changchun Wang, Ming Chen, He Huang, Tingbo Liang, Jianghua Chen, Weilin Wang, Dan Zhang, and Guoji Guo. 2020. "Construction of a Human Cell Landscape at Single-Cell Level." *Nature* 581(7808):303–9.

Hansen, David V, Jesse E. Hanson, and Morgan Sheng. 2014. "Microglia in Alzheimer ' s Disease." *Journal of Cell Biology* 2014(2):1–14.

Hart, Adam D., Andreas Wyttenbach, V. Hugh Perry, and Jessica L. Teeling. 2012. "Age Related Changes in Microglial Phenotype Vary between CNS Regions: Grey versus White Matter Differences." *Brain, Behavior, and Immunity* 26(5):754–65.

Hashimoto, Daigo, Andrew Chow, Clara Noizat, Pearline Teo, Mary Beth Beasley, Marylene Leboeuf, Christian D. Becker, Peter See, Jeremy Price, Daniel Lucas, Melanie Greter, Arthur Mortha, Scott W. Boyer, E. Camilla Forsberg, Masato Tanaka, Nico van Rooijen, Adolfo García-Sastre, E. Richard Stanley, Florent Ginhoux, Paul S. Frenette, and Miriam Merad. 2013. "Tissue-Resident Macrophages Self-Maintain Locally throughout Adult Life with Minimal Contribution from Circulating Monocytes." *Immunity* 38(4):792–804.

Hefendehl, Jasmin K., Jonas J. Neher, Rafael B. Sühs, Shinichi Kohsaka, Angelos Skodras, and Mathias Jucker. 2014. "Homeostatic and Injury-Induced Microglia Behavior in the Aging Brain." *Aging Cell* 13(1):60–69.

Heneka, Michael T., Douglas T. Golenbock, and Eicke Latz. 2015. "Innate Immunity in Alzheimer's Disease." *Nature Immunology* 16(3):229–36.

Heneka, Michael T., Markus P. Kummer, Andrea Stutz, Andrea Delekate, Stephanie Schwartz, Ana Vieira-Saecker, Angelika Griep, Daisy Axt, Anita Remus, Te Chen

Tzeng, Ellen Gelpi, Annett Halle, Martin Korte, Eicke Latz, and Douglas T. Golenbock. 2013. "NLRP3 Is Activated in Alzheimer's Disease and Contributes to Pathology in APP/PS1 Mice." *Nature* 493(7434):674–78.

Heneka, Michael T., Róisín M. McManus, and Eicke Latz. 2018. "Inflammasome Signalling in Brain Function and Neurodegenerative Disease." *Nature Reviews Neuroscience* 19(10):610–21.

Hickman, Suzanne E., Elizabeth K. Allison, and Joseph El Khoury. 2008. "Microglial Dysfunction and Defective β-Amyloid Clearance Pathways in Aging Alzheimer's Disease Mice." *Journal of Neuroscience* 28(33):8354–60.

Hickman, Suzanne, Saef Izzy, Pritha Sen, Liza Morsett, and Joseph El Khoury. 2018. "Microglia in Neurodegeneration." *Nature Neuroscience* 21(10):1359–69.

Holler, Christopher J., Georgia Taylor, Qiudong Deng, and Thomas Kukar. 2017. "Intracellular Proteolysis of Progranulin Generates Stable, Lysosomal Granulins That Are Haploinsufficient in Patients with Frontotemporal Dementia Caused by GRN Mutations." *ENeuro* 4(4).

Hong, Soyon, Victoria F. Beja-glasser, Bianca M. Nfonoyim, Arnaud Frouin, Saranya Ramakrishnan, Katherine M. Merry, Qiaoqiao Shi, Arnon Rosenthal, A. Barres, Cynthia A. Lemere, Dennis J. Selkoe, and Beth Stevens. 2016. "Complement and Microglia Mediate Early Synapse Loss in Alzheimer Mouse Models." *Science* 352(6286):712–16.

Hopp, Sarah C., Yang Lin, Derek Oakley, Allyson D. Roe, Sarah L. DeVos, David Hanlon, and Bradley T. Hyman. 2018. "The Role of Microglia in Processing and Spreading of Bioactive Tau Seeds in Alzheimer's Disease." *Journal of Neuroinflammation* 15(1):1–15.

Hsieh, Christine L., Maya Koike, Steve C. Spusta, Erene C. Niemi, Midori Yenari, Mary C. Nakamura, and William E. Seaman. 2009. "A Role for TREM2 Ligands in the Phagocytosis of Apoptotic Neuronal Cells by Microglia." *Journal of Neurochemistry* 109(4):1144–56.

Hu, Fenghua, Thihan Padukkavidana, Christian B. Vaegter, Owen A. Brady, Yanqiu Zheng, Ian R. Mackenzie, Howard H. Feldman, Anders Nykjaer, and Stephen M. Strittmatter. 2010. "Sortilin-Mediated Endocytosis Determines Levels of the Frontotemporal Dementia Protein, Progranulin." *Neuron* 68(4):654–67.

Huang, E. J., and L. F. Reichardt. 2001. "Neurotrophins: Roles in Neuronal Development and Function." *Annual Review of Neuroscience* 24:677–736.

Huang, Youtong, Kaisa E. Happonen, Patrick G. Burrola, Carolyn O'Connor, Nasun Hah, Ling Huang, Axel Nimmerjahn, and Greg Lemke. 2021. "Microglia Use TAM Receptors to Detect and Engulf Amyloid β Plaques." *Nature Immunology* 22(5):586–94.

Huang, Yubin, Zhen Xu, Shanshan Xiong, Fangfang Sun, Guangrong Qin, Guanglei Hu, Jingjing Wang, Lei Zhao, Yu Xiang Liang, Tianzhun Wu, Zhonghua Lu, Mark S. Humayun, Kwok Fai So, Yihang Pan, Ningning Li, Ti Fei Yuan, Yanxia Rao, and Bo Peng. 2018. "Repopulated Microglia Are Solely Derived from the Proliferation of Residual Microglia after Acute Depletion." *Nature Neuroscience* 21(4):530–40.

Ising, Christina, Carmen Venegas, Shuangshuang Zhang, Hannah Scheiblich, Susanne V. Schmidt, Ana Vieira-Saecker, Stephanie Schwartz, Shadi Albasset, Róisín M. McManus, Dario Tejera, Angelika Griep, Francesco Santarelli, Frederic Brosseron, Sabine Opitz, James Stunden, Maximilian Merten, Rakez Kayed, Douglas T. Golenbock, David Blum, Eicke Latz, Luc Buée, and Michael T. Heneka. 2019. "NLRP3 Inflammasome Activation Drives Tau Pathology." *Nature* 575(7784):669–73.

Ito, Hiroaki, and Jessica A. Hamerman. 2012. "TREM-2, Triggering Receptor Expressed on Myeloid Cell-2, Negatively Regulates TLR Responses in Dendritic Cells." *European Journal of Immunology* 42(1):176–85.

Jaitin, Diego Adhemar, Lorenz Adlung, Christoph A. Thaiss, Assaf Weiner, Baoguo Li, Hélène Descamps, Patrick Lundgren, Camille Bleriot, Zhaoyuan Liu, Aleksandra Deczkowska, Hadas Keren-Shaul, Eyal David, Niv Zmora, Shai Meron Eldar, Nir Lubezky, Oren Shibolet, David A. Hill, Mitchell A. Lazar, Marco Colonna, Florent Ginhoux, Hagit Shapiro, Eran Elinav, and Ido Amit. 2019. "Lipid-Associated Macrophages Control Metabolic Homeostasis in a Trem2-Dependent Manner." *Cell* 178(3):686-698.e14.

Jian, Jinlong, Qing Yun Tian, Aubryanna Hettinghouse, Shuai Zhao, Helen Liu, Jianlu Wei, Gabriele Grunig, Wujuan Zhang, Kenneth D. R. Setchell, Ying Sun, Herman S. Overkleeft, Gerald L. Chan, and Chuan ju Liu. 2016. "Progranulin Recruits HSP70 to β-

Glucocerebrosidase and Is Therapeutic Against Gaucher Disease." *EBioMedicine* 13:212–24.

Jiang, Yi Xiao, Qin Cao, Michael R. Sawaya, Romany Abskharon, Peng Ge, Michael DeTure, Dennis W. Dickson, Janine Y. Fu, Rachel R. Ogorzalek Loo, Joseph A. Loo, and David S. Eisenberg. 2022. "Amyloid Fibrils in Disease FTLD-TDP Are Composed of TMEM106B Not TDP-43." *Nature*.

Jonsson, Thorlakur, Hreinn Stefansson, Stacy Steinberg, Ingileif Jonsdottir, Palmi V. Jonsson, Jon Snaedal, Sigurbjorn Bjornsson, Johanna Huttenlocher, Allan I. Levey, James J. Lah, Dan Rujescu, Harald Hampel, Ina Giegling, Ole A. Andreassen, Knut Engedal, Ingun Ulstein, Srdjan Djurovic, Carla Ibrahim-Verbaas, Albert Hofman, M. Arfan Ikram, Cornelia M. van Duijn, Unnur Thorsteinsdottir, Augustine Kong, and Kari Stefansson. 2013. " Variant of TREM2 Associated with the Risk of Alzheimer's Disease ." *New England Journal of Medicine* 368(2):107–16.

Kam, Tae In, Jared T. Hinkle, Ted M. Dawson, and Valina L. Dawson. 2020. "Microglia and Astrocyte Dysfunction in Parkinson's Disease." *Neurobiology of Disease* 144(July):105028.

Kang, Silvia S., Mark T. W. Ebbert, Kelsey E. Baker, Casey Cook, Xuewei Wang, Jonathon P. Sens, Jeanne Pierre Kocher, Leonard Petrucelli, and John D. Fryer. 2018. "Microglial Translational Profiling Reveals a Convergent APOE Pathway from Aging, Amyloid, and Tau." *Journal of Experimental Medicine* 215(9):2235–45.

Kelley, Brendan J., Wael Haidar, Bradley F. Boeve, Matt Baker, Maria Shiung, David S. Knopman, Rosa Rademakers, Mike Hutton, Jennifer Adamson, Karen M. Kuntz, Dennis W. Dickson, Joseph E. Parisi, Glenn E. Smith, and Ronald C. Petersen. 2010. "Alzheimer Disease-like Phenotype Associated with the c.154delA Mutation in Progranulin." *Archives of Neurology* 67(2):171–77.

Keren-Shaul, Hadas, Amit Spinrad, Assaf Weiner, Orit Matcovitch-Natan, Raz Dvir-Szternfeld, Tyler K. Ulland, Eyal David, Kuti Baruch, David Lara-Astaiso, Beata Toth, Shalev Itzkovitz, Marco Colonna, Michal Schwartz, and Ido Amit. 2017. "A Unique Microglia Type Associated with Restricting Development of Alzheimer's Disease." *Cell* 169(7):1276-1290.e17.

Kerschensteiner, Martin, Christine Stadelmann, Georg Dechant, Hartmut Wekerle, and Reinhard Hohlfeld. 2003. "Neurotrophic Cross-Talk between the Nervous and Immune Systems: Implications for Neurological Diseases." *Annals of Neurology* 53(3):292–304.

El Khoury, Joseph B., Kathryn J. Moore, Terry K. Means, Josephine Leung, Kinya Terada, Michelle Toft, Mason W. Freeman, and Andrew D. Luster. 2003. "CD36 Mediates the Innate Host Response to β-Amyloid." *Journal of Experimental Medicine* 197(12):1657–66.

Kleinberger, Gernot, Matthias Brendel, Eva Mracsko, Benedikt Wefers, Linda Groeneweg, Xianyuan Xiang, Carola Focke, Maximilian Deußing, Marc Suárez-Calvet, Fargol Mazaheri, Samira Parhizkar, Nadine Pettkus, Wolfgang Wurst, Regina Feederle, Peter Bartenstein, Thomas Mueggler, Thomas Arzberger, Irene Knuesel, Axel Rominger, and Christian Haass. 2017. "The FTD-like Syndrome Causing TREM2 T66M Mutation Impairs Microglia Function, Brain Perfusion, and Glucose Metabolism." *The EMBO Journal* 36(13):1837–53.

Kleinberger, Gernot, Anja Capell, Nathalie Brouwers, Katrin Fellerer, Kristel Sleegers, Marc Cruts, Christine Van Broeckhoven, and Christian Haass. 2016. "Reduced Secretion and Altered Proteolytic Processing Caused by Missense Mutations in Progranulin." *Neurobiology of Aging* 39:220.e17-220.e26.

Kleinberger, Gernot, Anja Capell, Christian Haass, and Christine Van Broeckhoven. 2013. "Mechanisms of Granulin Deficiency: Lessons from Cellular and Animal Models." *Molecular Neurobiology* 47(1):337–60.

Kleinberger, Gernot, Yoshinori Yamanishi, Marc Suárez-calvet, Eva Czirr, Ebba Lohmann, Elise Cuyvers, Hanne Struyfs, Nadine Pettkus, Andrea Wenninger-weinzierl, Fargol Mazaheri, Sabina Tahirovic, Alberto Lleó, Daniel Alcolea, Juan Fortea, Michael Willem, Sven Lammich, José L. Molinuevo, Asli Demirtas-tatlidede, Henrik Zetterberg, Christine Van Broeckhoven, and Hakan Gurvit. 2014. "TREM2 Mutations Implicated in Neurodegeneration Impair Cell Surface Transport and Phagocytosis." *Science Translational Medicine* 6(243).

Kober, Daniel L., Jennifer M. Alexander-Brett, Celeste M. Karch, Carlos Cruchaga, Marco

Colonna, Michael J. Holtzman, and Thomas J. Brett. 2016. "Neurodegenerative Disease Mutations in TREM2 Reveal a Functional Surface and Distinct Loss-of-Function Mechanisms." *ELife* 5(DECEMBER2016):1–24.

Krasemann, Susanne, Charlotte Madore, Ron Cialic, Caroline Baufeld, Narghes Calcagno, Rachid El Fatimy, and Lien Beckers. 2017. "The TREM2-APOE Pathway Drives the Transcriptional Phenotype of Dysfunctional Microglia in Neurodegenerative Diseases." *Immunity* 47(3):215–26.

Kreutzberg, Georg W. 1996. "Microglia: A Sensor for Pathological Events in the CNS." *Trends in Neurosciences* 19(8):312–18.

Kwon, Hyuk Sung, and Seong Ho Koh. 2020. "Neuroinflammation in Neurodegenerative Disorders: The Roles of Microglia and Astrocytes." *Translational Neurodegeneration* 9(1):1–12.

Lang, Christina M., Katrin Fellerer, Benjamin M. Schwenk, Peer Hendrik Kuhn, Elisabeth Kremmer, Dieter Edbauer, Anja Capell, and Christian Haass. 2012. "Membrane Orientation and Subcellular Localization of Transmembrane Protein 106B (TMEM106B), a Major Risk Factor for Frontotemporal Lobar Degeneration." *Journal of Biological Chemistry* 287(23):19355–65.

Lee, C. Y. Danie., and Gary E. Landreth. 2010. "The Role of Microglia in Amyloid Clearance from the AD Brain." *Journal of Neural Transmission* 117(8):949–60.

Lee, Sunjun, and Won-Seok Choi. 2022. "Protective Role of Microglia on Neuronal Survival after Exposure to Amyloid Beta." *Chonnam Medical Journal* 58(1):13.

Lewandowska, Eliza, Teresa Wierzba-Bobrowicz, Elzbieta Kosno-Kruszewska, Waldemar Lechowicz, Bogna Schmidt-Sidor, Grazyna M. Szpak, Ewa Bertrand, Elzbieta Pasennik, and Elzbieta Gwiazda. 2004. "Ultrastructural Evaluation of Activated Forms of Microglia in Human Brain in Selected Neurological Diseases (SSPE, Wilson's Disease and Alzheimer's Disease)." *Folia Neuropathologica* 42(2):81–91.

Lewcock, Joseph W., Kai Schlepckow, Gilbert Di Paolo, Sabina Tahirovic, Kathryn M. Monroe, and Christian Haass. 2020. "Emerging Microglia Biology Defines Novel Therapeutic Approaches for Alzheimer's Disease." *Neuron* 108(5):801–21.

Leyns, Cheryl E G, Maud Gratuze, Sneha Narasimhan, Nimansha Jain, Lauren J. Koscal, Hong Jiang, Melissa Manis, Marco Colonna, Virginia M. Y. Lee, Jason D. Ulrich, and David M. Holtzman. 2019. "TREM2 Function Impedes Tau Seeding in Neuritic Plaques." *Nature Neuroscience* 22(8):1217–22.

Leyns, Cheryl E.G., Maud Gratuze, Sneha Narasimhan, Nimansha Jain, Lauren J. Koscal, Hong Jiang, Melissa Manis, Marco Colonna, Virginia M. Y. Lee, Jason D. Ulrich, and David M. Holtzman. 2019. "TREM2 Function Impedes Tau Seeding in Neuritic Plaques." *Nature Neuroscience* 22(8):1217–22.

Leyns, Cheryl E. G., and David M. Holtzman. 2017. "Glial Contributions to Neurodegeneration in Tauopathies." *Molecular Neurodegeneration* 12(1):1–16.

Logan, Todd, Matthew J. Simon, Anil Rana, Gerald M. Cherf, Ankita Srivastava, Sonnet S. Davis, Ray Lieh Yoon Low, Chi Lu Chiu, Meng Fang, Fen Huang, Akhil Bhalla, Ceyda Llapashtica, Rachel Prorok, Michelle E. Pizzo, Meredith E. K. Calvert, Elizabeth W. Sun, Jennifer Hsiao-Nakamoto, Yashas Rajendra, Katrina W. Lexa, Devendra B. Srivastava, Bettina van Lengerich, Junhua Wang, Yaneth Robles-Colmenares, Do Jin Kim, Joseph Duque, Melina Lenser, Timothy K. Earr, Hoang Nguyen, Roni Chau, Buyankhishig Tsogtbaatar, Ritesh Ravi, Lukas L. Skuja, Hilda Solanoy, Howard J. Rosen, Bradley F. Boeve, Adam L. Boxer, Hilary W. Heuer, Mark S. Dennis, Mihalis S. Kariolis, Kathryn M. Monroe, Laralynne Przybyla, Pascal E. Sanchez, Rene Meisner, Dolores Diaz, Kirk R. Henne, Ryan J. Watts, Anastasia G. Henry, Kannan Gunasekaran, Giuseppe Astarita, Jung H. Suh, Joseph W. Lewcock, Sarah L. DeVos, and Gilbert Di Paolo. 2021. "Rescue of a Lysosomal Storage Disorder Caused by Grn Loss of Function with a Brain Penetrant Progranulin Biologic." *Cell* 184(18):4651-4668.e25.

Long, Justin M., and David M. Holtzman. 2019. "Alzheimer Disease: An Update on Pathobiology and Treatment Strategies." *Cell* 179(2):312–39.

Lu, Tao, Ying Pan, Shyan Yuan Kao, Cheng Li, Isaac Kohane, Jennifer Chan, and Bruce A. Yankner. 2004. "Gene Regulation and DNA Damage in the Ageing Human Brain." *Nature* 429(6994):883–91.

Lucin, Kurt M., and Tony Wyss-Coray. 2009. "Immune Activation in Brain Aging and Neurodegeneration: Too Much or Too Little?" *Neuron* 83(4):255–62.

Lui, Hansen, Jiasheng Zhang, Stefanie R. Makinson, Michelle K. Cahill, Kevin W. Kelley, Hsin Yi Huang, Yulei Shang, Michael C. Oldham, Lauren Herl Martens, Fuying Gao, Giovanni Coppola, Steven A. Sloan, Christine L. Hsieh, Charles C. Kim, Eileen H. Bigio, Sandra Weintraub, Marek Marsel Mesulam, Rosa Rademakers, Ian R. Mackenzie, William W. Seeley, Anna Karydas, Bruce L. Miller, Barbara Borroni, Roberta Ghidoni, Robert V. Farese, Jeanne T. Paz, Ben A. Barres, and Eric J. Huang. 2015. "Progranulin Deficiency Promotes Circuit-Specific Synaptic Pruning by Microglia via Complement Activation." *Cell* 1–15.

Lynch, Marina A. 2009. "The Multifaceted Profile of Activated Microglia." *Molecular Neurobiology* 40(2):139–56.

Mackenzie, Ian R. A., Rosa Rademakers, and Manuela Neumann. 2010. "TDP-43 and FUS in Amyotrophic Lateral Sclerosis and Frontotemporal Dementia." *The Lancet Neurology* 9(10):995–1007.

Madore, Charlotte, Zhuoran Yin, Jeffrey Leibowitz, and Oleg Butovsky. 2020. "Microglia, Lifestyle Stress, and Neurodegeneration." *Immunity* 52(2):222–40.

Maezawa, Izumi, Pavel I. Zimin, Heike Wulff, and Lee Way Jin. 2011. "Amyloid-β Protein Oligomer at Low Nanomolar Concentrations Activates Microglia and Induces Microglial Neurotoxicity." *Journal of Biological Chemistry* 286(5):3693–3706.

Marioni, Riccardo E., Sarah E. Harris, Qian Zhang, Allan F. McRae, Saskia P. Hagenaars, W. David Hill, Gail Davies, Craig W. Ritchie, Catharine R. Gale, John M. Starr, Alison M. Goate, David J. Porteous, Jian Yang, Kathryn L. Evans, Ian J. Deary, Naomi R. Wray, and Peter M. Visscher. 2018. "GWAS on Family History of Alzheimer's Disease." *Translational Psychiatry* 8(1):0–6.

Masuda, Takahiro, Roman Sankowski, Ori Staszewski, Chotima Böttcher, Lukas Amann, Sagar, Christian Scheiwe, Stefan Nessler, Patrik Kunz, Geert van Loo, Volker Arnd Coenen, Peter Christoph Reinacher, Anna Michel, Ulrich Sure, Ralf Gold, Dominic Grün, Josef Priller, Christine Stadelmann, and Marco Prinz. 2019. "Spatial and Temporal Heterogeneity of Mouse and Human Microglia at Single-Cell Resolution." *Nature* 566(7744):388–92.

Matcovitch-Natan, Orit, Deborah R. Winter, Amir Giladi, Stephanie Vargas Aguilar, Amit Spinrad, Sandrine Sarrazin, Hila Ben-Yehuda, Eyal David, Fabiola Zelada González, Pierre Perrin, Hadas Keren-Shaul, Meital Gury, David Lara-Astaiso, Christoph A. Thaiss, Merav Cohen, Keren Bahar Halpern, Kuti Baruch, Aleksandra Deczkowska, Erika Lorenzo-Vivas, Shalev Itzkovitz, Eran Elinav, Michael H. Sieweke, Michal Schwartz, and Ido Amit. 2016. "Microglia Development Follows a Stepwise Program to Regulate Brain Homeostasis." *Science* 353(6301).

Matsubara, Toshiya, Ayako Mita, Kohtaro Minami, Tetsuya Hosooka, Sohei Kitazawa, Kenichi Takahashi, Yoshikazu Tamori, Norihide Yokoi, Makoto Watanabe, Ei Ichi Matsuo, Osamu Nishimura, and Susumu Seino. 2012. "PGRN Is a Key Adipokine Mediating High Fat Diet-Induced Insulin Resistance and Obesity through IL-6 in Adipose Tissue." *Cell Metabolism* 15(1):38–50.

Mazaheri, Fargol, Nicolas Snaidero, Gernot Kleinberger, Charlotte Madore, Anna Daria, Georg Werner, Susanne Krasemann, Anja Capell, Dietrich Trümbach, Wolfgang Wurst, Bettina Brunner, Sebastian Bultmann, Sabina Tahirovic, Martin Kerschensteiner, Thomas Misgeld, Oleg Butovsky, and Christian Haass. 2017. "TREM2 Deficiency Impairs Chemotaxis and Microglial Responses to Neuronal Injury." *EMBO Reports* 18(7):1186–98.

Meilandt, Wiliam J., Hai Ngi, Alvin Gogineni, Guita Lalehzadeh, Seung-Hye Lee, Karpagam Srinivasan, Jose Imperio, Tiffany Wu, Martin Weber, Agatha J. Kruse, Kimberly L. Stark, Pamelka Chan, Mandy Kwong, Zora Modrusan, Brad A. Friedman, Justin Elstrott, Oded Foreman, Amy Easton, Morgan Sheng, and David V. Hansen. 2020. "Trem2 Deletion Reduces Late-Stage Amyloid Plaque Accumulation, Elevates the Aβ42:Aβ40 Ratio, and Exacerbates Axonal Dystrophy and Dendritic Spine Loss in the PS2APP Alzheimer's Mouse Model." *The Jorunal of Neuroscience* (9):1956–74.

Morenas-Rodríguez, Estrella, Yan Li, Brigitte Nuscher, Nicolai Franzmeier, Chengjie Xiong, Marc Suárez-calvet, Anne M. Fagan, Stephanie Schultz, Brian A. Gordon, Tammie L. S. Benzinger, Jason Hassenstab, Eric Mcdade, Regina Feederle, Celeste M. Karch, Kai Schlepckow, John C. Morris, Gernot Kleinberger, Bengt Nellgard, Jonathan Vöglein, Kaj Blennow, Henrik Zetterberg, Michael Ewers, Mathias Jucker, and Johannes Levin.

2022. "Soluble TREM2 in CSF and Its Association with Other Biomarkers and Cognition in Autosomal-Dominant Alzheimer´s Disease : A Longitudinal Observational Study." *Lancet Neurology* 21:329–41.

Mrdjen, Dunja, Anto Pavlovic, Felix J. Hartmann, Bettina Schreiner, Sebastian G. Utz, Brian P. Leung, Iva Lelios, Frank L. Heppner, Jonathan Kipnis, Doron Merkler, Melanie Greter, and Burkhard Becher. 2018. "High-Dimensional Single-Cell Mapping of Central Nervous System Immune Cells Reveals Distinct Myeloid Subsets in Health, Aging, and Disease." *Immunity* 48(2):380-395.e6.

Muzio, Luca, Alice Viotti, and Gianvito Martino. 2021. "Microglia in Neuroinflammation and Neurodegeneration: From Understanding to Therapy." *Frontiers in Neuroscience* 15(September).

Neumann, Harald, Bettina Linnartz, and Yiner Wang. 2010. "Microglial Immunoreceptor Tyrosine-Based Activation and Inhibition Motif Signaling in Neuroinflammation." *International Journal of Alzheimer's Disease* 2010.

Neumann, Manuela, DM Sampathu, LK Kwong, AC Truax, MC Micsenyi, TT Chou, J. Bruce, T. Schuck, M. Grossman, CM Clark, LF McCluskey, Bruce L. Miller, E. Masliah, IR Mackenzie, H. Feldman, W. Feiden, HA Kretzschmar, JQ Trojanowski, and VM Lee. 2006. "Ubiquitinated TDP-43 in Frontotemporal Lobar Degeneration and Amyotrophic Lateral Sclerosis." *Science (New York, N.Y.)* 314(6 OCTOBER 2006):130–33.

Nugent, Alicia A., Karin Lin, Bettina van Lengerich, Steve Lianoglou, Laralynne Przybyla, Sonnet S. Davis, Ceyda Llapashtica, Junhua Wang, Do Jin Kim, Dan Xia, Anthony Lucas, Sulochanadevi Baskaran, Patrick C. G. Haddick, Melina Lenser, Timothy K. Earr, Ju Shi, Jason C. Dugas, Benjamin J. Andreone, Todd Logan, Hilda O. Solanoy, Hang Chen, Ankita Srivastava, Suresh B. Poda, Pascal E. Sanchez, Ryan J. Watts, Thomas Sandmann, Giuseppe Astarita, Joseph W. Lewcock, Kathryn M. Monroe, and Gilbert Di Paolo. 2020. "TREM2 Regulates Microglial Cholesterol Metabolism upon Chronic Phagocytic Challenge." *Neuron* 105(5):837-854.e9.

Oxford, Alexandra E., Erica S. Stewart, and Troy T. Rohn. 2020. "Clinical Trials in Alzheimer's Disease: A Hurdle in the Path of Remedy." *International Journal of Alzheimer's Disease* 2020.

Paloneva, Juha, Tuula Manninen, Grant Christman, Karine Hovanes, Jami Mandelin, Rolf Adolfsson, Marino Bianchin, Thomas Bird, Roxana Miranda, Andrea Salmaggi, Lisbeth Tranebjærg, Yrjö Konttinen, and Leena Peltonen. 2002. "Mutations in Two Genes Encoding Different Subunits of a Receptor Signaling Complex Result in an Identical Disease Phenotype." *American Journal of Human Genetics* 71(3):656–62.

Paolicelli, Rosa C., Giulia Bolasco, Francesca Pagani, Laura Maggi, Maria Scianni, Patrizia Panzanelli, Maurizio Giustetto, Tiago Alves Ferreira, Eva Guiducci, Laura Dumas, Davide Ragozzino, and Cornelius T. Gross. 2011. "Synaptic Pruning by Microglia Is Necessary for Normal Brain Development." *Science* 333(6048):1456–58.

Parhizkar, Samira, Thomas Arzberger, Matthias Brendel, Gernot Kleinberger, Maximilian Deussing, Carola Focke, Brigitte Nuscher, Monica Xiong, Natalie Katzmarski, Susanne Krasemann, F. Stefan, Stephan A. Müller, Alessio Colombo, Laura Sebastian Monasor, Peter Bartenstein, Dieter Edbauer, Axel Rominger, and Ali Ertürk. 2019. "Loss of TREM2 Function Increases Amyloid Seeding but Decreases Plaque Associated ApoE." *Nat Methods* 22(2):191–204.

Penadés, Rafael, Nicolas Franck, Laura González-Vallespí, and and Marie Dekerle. 2019. *Reviews on Biomarker Studies in Psychiatric and Neurodegenerative Disorders*. Vol. 1118.

Peng, Qisheng, Shikha Malhotra, James A. Torchia, William G. Kerr, K. Mark Coggeshall, and Mary Beth Humphrey. 2010. "TREM2-and DAP12-Dependent Activation of PI3K Requires DAP10 and Is Inhibited by SHIP1 Previously Uncharacterized Interaction of SHIP1 with DAP12 That Functionally Limits TREM2-and DAP12-Dependent Signaling and Identify a Mechanism through Which SHIP1 Regu." *Sci Signal* 3(122):38.

Perdiguero, Elisa Gomez, Kay Klapproth, Christian Schulz, Katrin Busch, Emanuele Azzoni, Lucile Crozet, Hannah Garner, Celine Trouillet, Marella De Bruijn, Frederic Geissmann, and Hans-Reimer Rodewald. 2015. "Tissue-Resident Macrophages Originate from Yolk Sac-Derived Erythro-Myeloid Progenitors." *Experimental Hematology* 43(9):S64.

Price, Brittani R., Tiffany L. Sudduth, Erica M. Weekman, Sherika Johnson, Danielle Hawthorne, Abigail Woolums, and Donna M. Wilcock. 2020. "Therapeutic Trem2

Activation Ameliorates Amyloid-Beta Deposition and Improves Cognition in the 5XFAD Model of Amyloid Deposition." *Journal of Neuroinflammation* 17(1):1–13.

Rabinovici, Gd, and Bl Miller. 2010. *Frontotemporal Lobar Degeneration: Epidemiology, Pathophysiology, Diagnosis and Management*. Vol. 24.

Reifschneider, Anika, Sophie Robinson, Bettina van Lengerich, Johannes Gnörich, Todd Logan, Steffanie Heindl, Miriam A. Vogt, Endy Weidinger, Lina Riedl, Karin Wind, Artem Zatcepin, Ida Pesämaa, Sophie Haberl, Brigitte Nuscher, Gernot Kleinberger, Julien Klimmt, Julia K. Götzl, Arthur Liesz, Katharina Bürger, Matthias Brendel, Johannes Levin, Janine Diehl-Schmid, Jung Suh, Gilbert Di Paolo, Joseph W. Lewcock, Kathryn M. Monroe, Dominik Paquet, Anja Capell, and Christian Haass. 2022. "Loss of TREM2 Rescues Hyperactivation of Microglia, but Not Lysosomal Deficits and Neurotoxicity in Models of Progranulin Deficiency." *The EMBO Journal* 41(4):1–25.

Riedl, Lina, Ian R. Mackenzie, Hans Förstl, Alexander Kurz, and Janine Diehl-Schmid. 2014. "Frontotemporal Lobar Degeneration: Current Perspectives." *Neuropsychiatric Disease and Treatment* 10:297–310.

Rio-Hortega, Pio D. 1919. "El 'Tercer Elemento' de Los Centros Nerviosos." *Boletin de La Sociedad Espanola de Biologia* 9:68–166.

Sakae, Nobutaka, Shanu F. Roemer, Kevin F. Bieniek, Melissa E. Murray, Matthew C. Baker, Koji Kasanuki, Neill R. Graff-Radford, Leonard Petrucelli, Marka Van Blitterswijk, Rosa Rademakers, and Dennis W. Dickson. 2019. "Microglia in Frontotemporal Lobar Degeneration with Progranulin or C9ORF72 Mutations." *Annals of Clinical and Translational Neurology* 6(9):1782–96.

Schafer, Dorothy P., E. Lehrmann, Amanda G. Kautzman, Ryuta Koyama, Alan R. Mardinly, Ryo Yamasaki, Richard M. Ranshoff, Michael E. Greenberg, Ben A. Barres, and Beth Stevens. 2012. "Microglia Sculpt Postnatal Neural Circuits in an Activity and Complement-Dependent Manner." *Neuron* 74(4):691–705.

Schlepckow, Kai, Gernot Kleinberger, Akio Fukumori, Regina Feederle, Stefan F. Lichtenthaler, Harald Steiner, and Christian Haass. 2017. " An Alzheimer-associated TREM2 Variant Occurs at the ADAM Cleavage Site and Affects Shedding and Phagocytic Function ." *EMBO Molecular Medicine* 9(10):1356–65.

Schlepckow, Kai, Kathryn M. Monroe, Gernot Kleinberger, Ludovico Cantuti-Castelvetri, Samira Parhizkar, Dan Xia, Michael Willem, Georg Werner, Nadine Pettkus, Bettina Brunner, Alice Sülzen, Brigitte Nuscher, Heike Hampel, Xianyuan Xiang, Regina Feederle, Sabina Tahirovic, Joshua I. Park, Rachel Prorok, Cathal Mahon, Chun-Chi Liang, Ju Shi, Do Jin Kim, Hanna Sabelström, Fen Huang, Gilbert Di Paolo, Mikael Simons, Joseph W. Lewcock, and Christian Haass. 2020. " Enhancing Protective Microglial Activities with a Dual Function TREM 2 Antibody to the Stalk Region ." *EMBO Molecular Medicine*.

Schulz, Christian, Elisa Gomez Perdiguero, Laurent Chorro, Heather Szabo-Rogers, Nicolas Cagnard, Katrin Kierdorf, Marco Prinz, Bishan Wu, Sten Eirik W. Jacobsen, Jeffrey W. Pollard, Jon Frampton, Karen J. Liu, and Frederic Geissmann. 2012. "A Lineage of Myeloid Cells Independent of Myb and Hematopoietic Stem Cells." *Science* 335(6077):86–90.

Schweighauser, Manuel, Diana Arseni, Mehtap Bacioglu, Melissa Huang, Sofia Lövestam, Yang Shi, Yang Yang, Wenjuan Zhang, Abhay Kotecha, Holly J. Garringer, Ruben Vidal, Grace I. Hallinan, Kathy L. Newell, Airi Tarutani, Shigeo Murayama, Masayuki Miyazaki, Yuko Saito, Mari Yoshida, Kazuko Hasegawa, Tammaryn Lashley, Tamas Revesz, Gabor G. Kovacs, John van Swieten, Masaki Takao, Masato Hasegawa, Bernardino Ghetti, Maria Grazia Spillantini, Benjamin Ryskeldi-Falcon, Alexey G. Murzin, Michel Goedert, and Sjors H. W. Scheres. 2022. "Age-Dependent Formation of TMEM106B Amyloid Filaments in Human Brains." *Nature*.

Sevigny, Jeff, Ping Chiao, Thierry Bussière, Paul H. Weinreb, Leslie Williams, Marcel Maier, Robert Dunstan, Stephen Salloway, Tianle Chen, Yan Ling, John O'Gorman, Fang Qian, Mahin Arastu, Mingwei Li, Sowmya Chollate, Melanie S. Brennan, Omar Quintero-Monzon, Robert H. Scannevin, H. Moore Arnold, Thomas Engber, Kenneth Rhodes, James Ferrero, Yaming Hang, Alvydas Mikulskis, Jan Grimm, Christoph Hock, Roger M. Nitsch, and Alfred Sandrock. 2016. "The Antibody Aducanumab Reduces Aβ Plaques in Alzheimer's Disease." *Nature* 537(7618):50–56.

Shankaran, Sunita S., Anja Capell, Alexander T. Hruscha, Katrin Fellerer, Manuela

Neumann, Bettina Schmid, and Christian Haass. 2008. "Missense Mutations in the Progranulin Gene Linked to Frontotemporal Lobar Degeneration with Ubiquitin-Immunoreactive Inclusions Reduce Progranulin Production and Secretion." *Journal of Biological Chemistry* 283(3):1744–53.

Shen, Yong, Rena Li, Edith G. McGeer, and Patrick L. McGeer. 1997. "Neuronal Expression of MRNAs for Complement Proteins of the Classical Pathway in Alzheimer Brain." *Brain Research* 769(2):391–95.

Sheng, Jianpeng, Christiane Ruedl, and Klaus Karjalainen. 2015. "Most Tissue-Resident Macrophages Except Microglia Are Derived from Fetal Hematopoietic Stem Cells." *Immunity* 43(2):382–93.

Sheng, Jin G., Robert E. Mrak, and W. S. T. Griffin. 1998. "Enlarged and Phagocytic, but Not Primed, Interleukin-1α-Immunoreactive Microglia Increase with Age in Normal Human Brain." *Acta Neuropathologica* 95(3):229–34.

Sierra, Amanda, Oihane Abiega, Anahita Shahraz, and Harald Neumann. 2013. "Janus-Faced Microglia: Beneficial and Detrimental Consequences of Microglial Phagocytosis." *Frontiers in Cellular Neuroscience* 7(JANUARY 2013):1–22.

Smith, Katherine R., John Damiano, Silvana Franceschetti, Stirling Carpenter, Laura Canafoglia, Michela Morbin, Giacomina Rossi, Davide Pareyson, Sara E. Mole, John F. Staropoli, Katherine B. Sims, Jada Lewis, Wen Lang Lin, Dennis W. Dickson, Hans Henrik Dahl, Melanie Bahlo, and Samuel F. Berkovic. 2012. "Strikingly Different Clinicopathological Phenotypes Determined by Progranulin-Mutation Dosage." *American Journal of Human Genetics* 90(6):1102–7.

Song, W., B. Hooli, K. Mullin, S. Jin, M. Cella, Tyler K. Ulland, Rudolph E. Tanzi, and Marco Colonna. 2017. "Alzheimer´s Disease-Associated TREM2 Variants Exhibit Either Decreased or Increased Ligand-Dependent ActivATION." *Alzheimers Demetia* 176(10):139–48.

Stephan, Alexander H., Ben A. Barres, and Beth Stevens. 2012. "The Complement System: An Unexpected Role in Synaptic Pruning during Development and Disease." *Annual Review of Neuroscience* 35:369–89.

Stevens, Beth, Nicola J. Allen, Luis E. Vazquez, Gareth R. Howell, Karen S. Christopherson, Navid Nouri, Kristina D. Micheva, Adrienne K. Mehalow, Andrew D. Huberman, Benjamin Stafford, Alexander Sher, Alan M. M. Litke, John D. Lambris, Stephen J. Smith, Simon W. M. John, and Ben A. Barres. 2007. "The Classical Complement Cascade Mediates CNS Synapse Elimination." *Cell* 131(6):1164–78.

Streit, Wolfgang J., Kelly R. Miller, Kryslaine O. Lopes, and Emalick Njie. 2008. "Microglia Degeneration in the Aging Brain - Bad News for Neurons?" *Frontiers in Bioscience* 13(3):3423–38.

Strohmeyer, Ron, Yong Shen, and Joseph Rogers. 2000. "Detection of Complement Alternative Pathway MRNA and Proteins in the Alzheimer's Disease Brain." *Molecular Brain Research* 81(1–2):7–18.

Suárez-Calvet, Marc, MA. Araque Caballero, Gernot Kleinberger, RJ Bateman, Anne M. Fagan, John C. Morris, Johannes Levin, Adrian Danek, Michael Ewers, and Christian Haass. 2016. "Early Changes in CSF STREM2 in Dominantly Inherited Alzheimer´s Disease Occur after Amyloid Deposition and Neuronal Injury." *Science Translational Medicine* 369(8).

Suárez-Calvet, Marc, Gernot Kleinberger, Miguel Ángel Araque Caballero, Matthias Brendel, Axel Rominger, Daniel Alcolea, Juan Fortea, Alberto Lleó, Rafael Blesa, Juan Domingo Gispert, Raquel Sánchez-Valle, Anna Antonell, Lorena Rami, José L. Molinuevo, Frederic Brosseron, Andreas Traschütz, Michael T. Heneka, Hanne Struyfs, Sebastiaan Engelborghs, Kristel Sleegers, Christine Van Broeckhoven, Henrik Zetterberg, Bengt Nellgård, Kaj Blennow, Alexander Crispin, Michael Ewers, and Christian Haass. 2016. " STREM 2 Cerebrospinal Fluid Levels Are a Potential Biomarker for Microglia Activity in Early-stage Alzheimer's Disease and Associate with Neuronal Injury Markers ." *EMBO Molecular Medicine* 8(5):466–76.

Syková, Eva, Tomáš Mazel, and Zuzana Šimonová. 1998. "Diffusion Constraints and Neuron-Glia Interaction during Aging." *Experimental Gerontology* 33(7–8):837–51.

Takahashi, Kazuya, Christian D. P. Rochford, and Harald Neumann. 2005. "Clearance of Apoptotic Neurons without Inflammation by Microglial Triggering Receptor Expressed on Myeloid Cells-2." *Journal of Experimental Medicine* 201(4):647–57.

Tanaka, Yoshinori, James K. Chambers, Takashi Matsuwaki, Keitaro Yamanouchi, and Masugi Nishihara. 2014. "Possible Involvement of Lysosomal Dysfunction in Pathological Changes of the Brain in Aged Progranulin-Deficient Mice." *Acta Neuropathologica Communications* 2(1):1–15.

Tang, Yu, and Weidong Le. 2016. "Differential Roles of M1 and M2 Microglia in Neurodegenerative Diseases." *Molecular Neurobiology* 53(2):1181–94.

Tremblay, Marie Ěve, Rebecca L. Lowery, and Ania K. Majewska. 2010. "Microglial Interactions with Synapses Are Modulated by Visual Experience." *PLoS Biology* 8(11).

Trzeciak, Alissa, Yelena V. Lerman, Tae-Hyoun Kim, Ma Rie Kim, Nguyen Mai, Marc W. Halterman, and Minsoo Kim. 2019. "Long-Term Microgliosis Driven by Acute Systemic Inflammation." *The Journal of Immunology* 203(11):2979–89.

Udan, Maria L. D., Deepa Ajit, Nikkilina R. Crouse, and Michael R. Nichols. 2008. "Toll-like Receptors 2 and 4 Mediate Aβ(1-42) Activation of the Innate Immune Response in a Human Monocytic Cell Line." *Journal of Neurochemistry* 104(2):524–33.

Ulland, Tyler K., and Marco Colonna. 2018. "TREM2 — a Key Player in Microglial Biology and Alzheimer Disease." *Nature Reviews Neurology* 14(11):667–75.

Ulland, Tyler K., Wilbur M. Song, Stanley Ching-cheng Huang, Jason D. Ulrich, Alexey Sergushichev, Wandy L. Beatty, Alexander A. Loboda, Yingyue Zhou, J. Nigel, Amal Kambal, Ekaterina Loginicheva, Susan Gilfillan, Marina Cella, W. Virgin, Emil R. Unanue, Yaming Wang, Maxim N. Artyomov, David M. Holtzman, and Marco Colonna. 2017. "TREM2 Maintains Microglual Metabolic Fitness in Alzheimer`s Disease." *Cell* 170(4):649–63.

Ulrich, Jason D., Mary Beth Finn, Yaming Wang, Alice Shen, Thomas E. Mahan, Hong Jiang, Floy R. Stewart, Laura Piccio, Marco Colonna, and David M. Holtzman. 2014. "Altered Microglial Response to Abeta Plaques in APPPS1-21 Mice Heterozygous for TREM2." *Molecular Neurodegeneration* 9(1):20.

Varvel, Nicholas H., Stefan A. Grathwohl, Frank Baumann, Christian Liebig, Andrea Bosch, Bianca Brawek, Dietmar R. Thal, Israel F. Charo, Frank L. Heppner, Adriano Aguzzi, Olga Garaschuk, Richard M. Ransohoff, and Mathias Jucker. 2012. "Microglial Repopulation Model Reveals a Robust Homeostatic Process for Replacing CNS Myeloid Cells." *Proceedings of the National Academy of Sciences of the United States of America* 109(44):18150–55.

Venegas, Carmen, Sathish Kumar, Bernardo S. Franklin, Tobias Dierkes, Rebecca Brinkschulte, Dario Tejera, Ana Vieira-Saecker, Stephanie Schwartz, Francesco Santarelli, Markus P. Kummer, Angelika Griep, Ellen Gelpi, Michael Beilharz, Dietmar Riedel, Douglas T. Golenbock, Matthias Geyer, Jochen Walter, Eicke Latz, and Michael T. Heneka. 2017. "Microglia-Derived ASC Specks Crossseed Amyloid-β in Alzheimer's Disease." *Nature* 552(7685):355–61.

Villegas-Llerena, Claudio, Alexandra Phillips, Pablo Garcia Reitboeck, John Hardy, and Jennifer M. Pocock. 2016. "Microglial Genes Regulating Neuroinflammation in the Progression of Alzheimer's Disease." *Current Opinion in Neurobiology* 36:74–81.

Volpicelli-daley, Laura, Johanna I. Busch, Sebastian Akle, and Murray Grossman. 2013. "Pathways." 32(33):11213–27.

Walker, Douglas G., Lih Fen Lue, and Thomas G. Beach. 2001. "Gene Expression Profiling of Amyloid Beta Peptide-Stimulated Human Post-Mortem Brain Microglia." *Neurobiology of Aging* 22(6):957–66.

Wang, Jun, Philip Van Damme, Carlos Cruchaga, Michael A. Gitcho, Jose Manuel Vidal, Manuel Seijo-Martinez, Lei Wang, Jane Y. Wu, Wim Robberecht, and Goa. 2010. "Pathogenic Cysteine Mutations Affect Progranulin Function and Production of Mature Granulins." *J Neurochem* 112(5):1305–15.

Wang, Shoutang, Meer Mustafa, Carla M. Yuede, Santiago Viveros Salazar, Philip Kong, Hua Long, Michael Ward, Omer Siddiqui, Robert Paul, Susan Gilfillan, Adiljan Ibrahim, Hervé Rhinn, Ilaria Tassi, Arnon Rosenthal, Tina Schwabe, and Marco Colonna. 2020. "Anti-Human TREM2 Induces Microglia Proliferation and Reduces Pathology in an Alzheimer's Disease Model." *Journal of Experimental Medicine* 217(9).

Wang, Yaming, Tyler K. Ulland, Jason D. Ulrich, Wilbur Song, John A. Tzaferis, Justin T. Hole, Peng Yuan, Thomas E. Mahan, Yang Shi, Susan Gilfillan, Marina Cella, Jaime Grutzendler, Ronald B. DeMattos, John R. Cirrito, David M. Holtzman, and Marco Colonna. 2016. "TREM2-Mediated Early Microglial Response Limits Diffusion and

Toxicity of Amyloid Plaques." *Journal of Experimental Medicine* 213(5):667–75.

Weuve, Jennifer, Liesi E. Hebert, Paul A. Scherr, and Denis A. Evans. 2014. "Deaths in the United States among Persons with Alzheimer ' s Disease PubMed Commons." *Alzheimer's & Dementia* 10(2):1–2.

Woollacott, Ione O. C., Christina E. Toomey, Catherine Strand, Robert Courtney, Bridget C. Benson, Jonathan D. Rohrer, and Tammaryn Lashley. 2020. "Microglial Burden, Activation and Dystrophy Patterns in Frontotemporal Lobar Degeneration." *Journal of Neuroinflammation* 17(1):1–27.

Wunderlich, Patrick, Konstantin Glebov, Nadja Kemmerling, Nguyen T. Tien, Harald Neumann, and Jochen Walter. 2013. "Sequential Proteolytic Processing of the Triggering Receptor Expressed on Myeloid Cells-2 (TREM2) Protein by Ectodomain Shedding and γ-Secretase- Dependent Intramembranous Cleavage." *Journal of Biological Chemistry* 288(46):33027–36.

Yeh, Felix L., Yuanyuan Wang, Irene Tom, Lino C. Gonzalez, and Morgan Sheng. 2016. "TREM2 Binds to Apolipoproteins, Including APOE and CLU/APOJ, and Thereby Facilitates Uptake of Amyloid-Beta by Microglia." *Neuron* 91(2):328–40.

Yeo, Weeteck, and Jean Gautier. 2004. "Early Neural Cell Death: Dying to Become Neurons." *Developmental Biology* 274(2):233–44.

Yuan, Peng, Carlo Condello, C. Dirk Keene, Yaming Wang, Thomas D. Bird, Steven M. Paule, Marco Colonna, David Baddeley, and Jaime Grutzendler. 2016. "TREM2 Haplodeficiency in Mice and Humans Impairs the Microglia Barrier Function Leading to Decreased Amyloid Compaction and Severe Axonal Dystrophy." *Neuron* 4(33):9557–61.

Zahid, Ayesha, Bofeng Li, Arnaud John Kombe Kombe, Tengchuan Jin, and Jinhui Tao. 2019. "Pharmacological Inhibitors of the Nlrp3 Inflammasome." *Frontiers in Immunology* 10(OCT):1–10.

Zhang, Jiasheng, Dmitry Velmeshev, Kei Hashimoto, Yu-hsin Huang, W. Jeffrey, Kevin W. Kelley, Shane A. Liddelow, William W. Seeley, and Bruce L. Miller. 2021. "Neurotoxic Microglia Promote TDP-43 Proteinopathy in Progranulin Deficiency." *Nature* 588(7838):459–65.

Zhang, Y., K. Chen, S. A. Sloan, M. L. Bennett, A. R. Scholze, S. O'Keeffe, H. P. Phatnani, P. Guarnieri, C. Caneda, N. Ruderisch, S. Deng, S. A. Liddelow, C. Zhang, R. Daneman, T. Maniatis, B. A. Barres, and J. Q. Wu. 2014. "An RNA-Sequencing Transcriptome and Splicing Database of Glia, Neurons, and Vascular Cells of the Cerebral Cortex." *Journal of Neuroscience* 34(36):11929–47.

Zhong, Li, Xiao Fen Chen, Tingting Wang, Zhe Wang, Chunyan Liao, Zongqi Wang, Ruizhi Huang, Daxin Wang, Xinxiu Li, Linbei Wu, Lin Jia, Honghua Zheng, Meghan Painter, Yuka Atagi, Chia Chen Liu, Yun Wu Zhang, John D. Fryer, Huaxi Xu, and Guojun Bu. 2017. "Soluble TREM2 Induces Inflammatory Responses and Enhances Microglial Survival." *Journal of Experimental Medicine* 214(3):597–607.

Zhong, Li, Ying Xu, Rengong Zhuo, Tingting Wang, Kai Wang, Ruizhi Huang, Daxin Wang, Yue Gao, Yifei Zhu, Xuan Sheng, Kai Chen, Na Wang, Lin Zhu, Dan Can, Yuka Marten, Mitsuru Shinohara, Chia Chen Liu, Dan Du, Hao Sun, Lei Wen, Huaxi Xu, Guojun Bu, and Xiao Fen Chen. 2019. "Soluble TREM2 Ameliorates Pathological Phenotypes by Modulating Microglial Functions in an Alzheimer's Disease Model." *Nature Communications* 10(1):1–16.

Zhou, Xiaolai, Daniel H. Paushter, Tuacheng Feng, Cara M. Pardon, Christina S. Mendoza, and Fenghua Hu. 2017. "Regulation of Cathepsin D Activity by the FTLD Protein Progranulin." *Acta Neuropathologica* 134(1):151–53.

Zhou, Xiaolai, Lirong Sun, Francisco Bastos de Oliveira, Xiaoyang Qi, William J. Brown, Marcus B. Smolka, Ying Sun, and Fenghua Hu. 2015. "Prosaposin Facilitates Sortilin-Independent Lysosomal Trafficking of Progranulin." *The Journal of Cell Biology* 210(6):991–1002.

Zuchero, J. Bradley, and Ben A. Barres. 2015. "Glia in Mammalian Development and Disease." *Development (Cambridge)* 142(22):3805–9.

All figures were created with BioRender.com

XI. Acknowledgements

The past five years have been an incredible ride. I am tremendously blessed to have had the possibility to spent these years in a laboratory full of supportive team members, collaborators and supervisors.

First, I would like to thank my supervisor Christian Haass. During the time of my PhD you have guided me even through difficult times, with a tremendous amount of encouragement and support. You have not only provided me with an incredible amount of knowledge, but also encouraged me to find my own confidence and space in the scientific world. I am extremely grateful that I had the chance to do my PhD in your laboratory.

A very special thanks to Anja Capell. I want to thank you for all your support, guidance, encouragement and personal advice. No matter if I had good or bad news – you always took the time and listened to me. I do admire your passion for science and your endless patience with PhD students.

Christan and Anja - you both have guided me even through the most difficult time of my life, the scientific but more important, my personal life. I do not have the words to express how thankful I am that in the most difficult time of my personal life, you gave me every space and support that I needed. And I can say for sure, that I would not have continued my studies without the trust and understanding that you gave me!

In a laboratory you can never be successful alone. I want to especially thank all AC-lab members: Katrin Buschman (Fellerer), Julia Götzl, Georg Werner, Claudia Thiel, Ramona Rodde and Marvin Reich. A warm thanks to all my colleagues from the Haass-lab: Kai Schlepckow, Samira Parhizkar, Brigitte Nuscher, Xianyuan Xiang, Gernot Kleinberger, Yoshihiro Nihei, Ida Pesämaa, Bettina Brunner, Nadine Pettkus, Estrella Morenas-Rodriguez, Marc Suarez-Calvet, Jane Hettinger, Fargol Mazaheri, Maryam Khojasteh-Fard, Alice Sülzen, Michael Willem, Sven Lammich, Heike Hampel, Johannes Trammbauer, Harald Steiner, Ann-Katrin Bergmann, Nicole Exner and Sabine Odoy. Thanks a lot to everyone from our animal facility: Manuela Schneider, Anne von Haden, Elena Drutskaya, Krystyna Kantor, Ekrem Göcmenoglu, Stefanie Wurster and Claudia Ihbe.

I would like to especially thank all my collaborators. Without you, none of my projects would have ended as successfully as they did: Benedikt Wefers, Sophie Robinson, Alessio-Vittorio Colombo, Sabina Tahirovoc, Johannes Gnörich, Steffanie Heindl, Miriam A Vogt, Endy Weidinger, Lina Riedl, Karin Wind, Artem Zatcepin, Sophie Haberl, Julien Klimmt, Arthur Liesz,

Katharina Bürger, Matthias Brendel, Johannes Levin, Janine Diehl-Schmid and Dominik Paquet.
I would also like to thank Dorothee Dormann and Michael Simons for encouraging and supporting me during the last years.

A special thanks to every of my collaborators working at Denali therapeutics – it was a pleasure to work with you: Bettina van Lengerich, Todd Logan, Jung Suh, Gilbert Di Paolo, Joseph W Lewcock and Kathryn M Monroe.

Finally, I would like to thank my family and friends. I am grateful to have every one of you in my life. You have been on my side in all the good, but also bad and stressful times. Mum and Dad, you have always supported every wish or dream I had. You have encouraged me to pursue every goal of mine – no matter if it was moving to the other side of the world or achieving my career goals.

Und weil ich mir nichts mehr wünschen würde, als dass du dieses besondere Ereignis noch mit mir erleben könntest, gehören die allerletzten Zeilen dir Papa. Wie sehr ich dich vermisse kann ich gar nicht ausdrücken und ich weiß du bist mehr als Stolz auf mich. Das ist für dich.